Galerkin-truncated dynamics of ideal fluids and superfluids: cascades, thermalization and dissipative effects

Giorgio Krstulovic

École Normale Supérieure
Département de Physique
Laboratoire de Physique Statistique

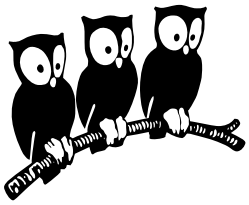

Thèse de doctorat de
l'Université Pierre et Marie Curie (Paris VI)

UFR de Physique

Spécialité : Physique des liquides

présentée par

Giorgio KRSTULOVIC M.

pour obtenir le titre de
Docteur de l'Université Pierre et Marie Curie (Paris VI)

Galerkin-truncated dynamics of ideal fluids and superfluids: cascades, thermalization and dissipative effects

---

Soutenue le 19 de Mars 2010 devant le jury composé de :

M. Marc BRACHET	Directeur
M. Carlo BARENGHI	Rapporteur
M. Sergey NAZARENKO	Rapporteur
M. Michel MOREAU	Examinateur
M. Stéphane FAUVE	Examinateur
M. Christophe JOSSERAND ...	Examinateur

REMERCIEMENTS

J'ai effectué ma thèse de septembre 2006 à janvier 2010 au Laboratoire de Physique Statistique de l'École Normale Supérieure, dont je tiens à remercier le directeur Éric PEREZ, pour son accueil au sein de son unité.

Cette thèse a été dirigée par Marc-Étienne BRACHET, que je remercie pour le constant intérêt, le soutien et la présence dont il a fait preuve pendant tout mon travail de recherche. En plus de m'accorder sa confiance dans le cadre de ma thèse, il s'est montré disponible pour échanger avec moi sur une infinité de sujets de différents domaines de la physique, et a ainsi réussi à me transmettre au cours de ces presque quatre ans, une partie de ses vastes connaissances scientifiques.

Je voudrais également remercier les professeurs du Departamento de Ciencias Físicas y Matemáticas de la Universidad de Chile, en particulier Enrique TIRAPEGUI, grâce à qui j'ai pu me rendre en France pour poursuivre mes études. Je remercie le Gouvernement du Chili, pour son soutien économique par le biais d'une bourse du CONICYT.

J'exprime ma plus profonde reconnaissance à Carlo BARENGHI et Sergey NAZARENKO qui m'ont fait l'honneur d'accepter d'être rapporteurs de la présente thèse (thank you Prof. C. BARENGHI and Prof. S. NAZARENKO to have accepted to be the examiners of this thesis). J'associe à ces remerciements les autres membres du jury : Michel MOREAU, Stéphan FAUVE et Christophe JOSSERAND.

Pendant ce travail de thèse j'ai eu l'occasion de profiter de la grande expertise de Carlos CARTES, Fabrice DEBBASCH, Annick POUQUET, Pablo MININNI et Enrique TIRAPEGUI. Je les remercie pour leur innombrables conseils.

Mon séjour au LPS aurait été extrêmement difficile sans la disponibilité et la sympathie des secrétaires Marie-Christine GEFFLOT, Annie RIBAUDEAU et Nora SADAOUI. Je remercie également Frédéric AYRAULT, Zaïre DISSI et Rémy PORTIER pour leur assistance en informatique.

Pendant mon travail de thèse, j'ai d'abord partagé mon bureau avec Mokhtar ADDA-BEDIA, que je remercie pour son esprit convivial et la patience dont il a fait preuve au cours de mes discussions avec Marc. Pendant le reste de mon séjour au LPS, j'ai aussi eu le plaisir de partager le bureau DC21 avec Laetitia GAUVIN, Antoine GERSCHENFELD, Sébastian GIRAUD, Hervé ROUAULT, Marc SANTOLLINI, Nestor SEPULVEDA et Miguel TREJO qui ont participé à une ambiance de travail très agréable.

Je souhaite également remercier Marc-Etienne et Edith HANTZ pour m'avoir accueilli lors de mon séjour à Boulder, Colorado. Je les remercie aussi pour leur sympathie,

leur soutien au moment de mon arrivée en France et l'amitié qu'ils m'ont montrée au cours de ces dernières années.

Je tiens aussi à exprimer toute ma gratitude à mes amis qui m'ont accompagné et qui ont fait de mon séjour en France une incroyable expérience. Je remercie spécialement les chiliens qui ont vécu la même expérience que moi et qui ont toujours été présents, même dans les moments les plus difficiles. Un très grand merci à mes amis les grimpeurs, toujours disponibles pour m'aider à contrôler le stress, parfois si intense.

Je remercie plus particulièrement ma mère, mon frère et mes sœurs qui m'ont toujours encouragé à distance. Toute ma gratitude à Francisca, qui m'a apporté le plus grand soutien et qui a rendu possible l'aboutissement de cette thèse. Gracias Pancha por todo el apoyo que me has dado y tu paciencia infinita.

CONTENTS

1. INTRODUCTION

This thesis is devoted to the study of the thermalization dynamics of several Galerkin-truncated conservatives systems related to the dynamics of ideal fluids and superfluid. A Galerkin truncation is simply obtained (in the homogeneous case) by performing a Fourier transform of a partial differential equation (PDE) and then keeping only a finite number of Fourier modes. If the truncation is correctly performed the finite-dimensional system inherits a number of conservation laws from the original PDE. These finite-dimensional dynamical systems are interesting in themself because they possess statistically stationary solutions, known as absolute equilibria [1, 2, 3, 4], that are exact solution of the associated Liouville equation.

Perhaps the simplest of such truncated systems corresponds to the three-dimensional Euler equation [1, 2, 3, 4, 5, 6]. The Fourier modes at the highest wavenumbers are known to rapidly thermalize through a mechanism first discovered by TD. Lee [1] in the 50's and further studied by RH. Kraichnan [2, 3] in the 60's. However, the first work attempting to study in detail the thermalization was done by Cichowlas et al. [5] in 2005. They studied, by using direct numerical simulations at high resolutions, the relaxation dynamics of the truncated Euler equation. Long-lasting transients which behave just as those of high Reynolds-number viscous-flows were reported. In particular they found an approximately $k^{-5/3}$ Kolmogorov inertial range followed by a dissipative range. The most striking result of this work is that a clear scale separation is exhibited. At high wavenumbers, the Fourier modes thermalize following a k^2 equipartition energy spectrum and this thermalized zone progressively extends to lower wavenumbers and finally covers the whole spectrum. At intermediate times a very rich behavior was observed: the thermalized modes playing the role of a thermostat create a fictitious microworld that generates an effective dissipation at large scales. Posteriorly, Bos and Bertoglio [6] studied that problem using the eddy damped quasi-normal Markovian (EDQNM) closure theory. By simple dimensional analysis and making use of the concept of eddy-viscosity [7] they gave an estimate of the dissipation wavenumber that corresponds to the Kolmogorov dissipation scale based on this eddy-viscosity. They found the same estimate that Cichowlas et al. [5] had found using a fluctuation dissipation theorem [8].

The fact that the EDQNM closure well reproduces the dynamics of truncated Euler equation was numerically exploited by Frisch et al. [9] to relate the bottlenecks observed in (viscous) turbulence [10, 11, 12, 13] to an incomplete thermalization of the type of Cichowlas et al. [5]. Frisch et al. [9] studied the hyperviscous limit of the Navier-Stoke equation, that consists on taking higher and higher power of the diffusive term (the Laplacian). The system obtained in this limits corresponds (at least intuitively) to the

truncated Euler equation. They found by performing numerical integration of EDQNM equations that the bottleneck observed with the usual diffusion drastically increases in the hyperviscous limit. At very high powers of the Laplacian a large scale $k^{-5/3}$ Kolmogorov spectrum followed by a k^2 power-law at small scales was observed, giving a possible explanation of bottlenecks in turbulence as an incomplete thermalization.

It is important to remark that a truncated system is not always equivalent to the original PDE. Both system, the truncated and original PDE, coincide as long as the spectral convergence of the numerical scheme is ensured [14]. For spectral convergence we understand that energy the spectrum needs to rapidly fall down (at least exponentially) at a wavenumber much smaller than the truncation wavenumber $k_{\max}$. If this condition is not verified the system is thus influenced by the truncation. In most cases, thermalization is achieved only in a truncated system. One exception is the partial thermalization reported by Frisch et al. [9] in the hyperviscous limit. Other exceptions occur when a very inefficient energy transfer is present in the system. In this context, V.S. L'Vov et al. [15] proposed in superfluid turbulence, a scenario where a Kolmogorov energy cascade and a Kelvin waves cascade are joined by a thermalized intermediate zone. In this thesis we present two new systems where a partial thermalization is observed in an intermediate range. The first one corresponds to the two-dimensional magnetohydrodynamics (MHD), where a strong constant magnetic field can slowdown the nonlinear transfer to produce a partial thermalization. The other one corresponds to the Gross-Pitaevskii equation (GPE) where dispersive effects can also induce a partial thermalization in an intermediate range.

We turn now to the problem of finite-time singularities. At a fixed resolution, the spectral convergence is typically ensured only until a finite time t^*. Beyond this time, the truncation becomes relevant and the truncated system only is well defined as a finite dimensional dynamical system because the fields typically become not differentiable at any point, as is the case of absolute equilibrium. The relation between t^* and the spectral cut-off $k_{\max}$ can be extremely complex because it is closely related to the finite-time singularity problem. Typically, t^* is an increasing function of $k_{\max}$. However if there is a finite-time singularity in the system, the spectral convergence will be lost at that time independently of the resolution. In the context of hydrodynamics it is known that the one-dimensional inviscid Burgers equation presents a finite-time singularity [16] and the two-dimensional Euler equation does not [17]. For the three-dimensional Euler equation there does not yet exist a mathematical proof or even a consistent numerical evidence in favor of the existence or not of a finite-time singularity (see [18, 19, 20, 21] and reference therein). Nevertheless, the truncated version of these three systems reach the thermodynamical equilibrium after a long and interesting transient.

The property that a conservative truncated system relaxes toward the equilibrium with a rich dynamics is very general. In this thesis we characterize the relaxation dynamics of several systems. We study the truncated compressible and incompressible $3D$ Euler, the $2D$ Euler, the $2D$ MHD and the $3D$ Gross-Pitaevskii (GP) equations. In all those systems the thermalized modes generate an effective dissipation that acts at large scales. In particular, in the truncated GP equation (TGPE) we show that

effects that are physically present in superfluids at finite temperature, such as mutual friction and counterflow (effects that are not included in the untruncated GPE), are naturally present in the truncated system. The richness of the dynamics produced by the interaction between the thermalized small scales and the pseudo-dissipative large scales motivates the present thesis.

In this thesis we first look for a quantitative understanding of the effective dissipation generated by the thermalized modes. Using EDQNM theory and Monte-Carlo simulations we are able to obtain a time and scale dependent effective viscosity. Using this result we introduce a phenomenological two-fluid model of the truncated Euler equation.

The previous results on the truncated Euler equation and its respective EDQNM version were restricted to flows with a vanishing mean helicity. The helicity, that plays a relevant role in many atmospheric processes [22] and in strongly rotating turbulence [23], is also conserved by the Euler equation [24, 25]. The conservation of the helicity modifies the absolute equilibrium and the corresponding spectra were found by Kraichnan [3].

We thus also present here a study of the dynamics of the truncated Euler equations with helical initial conditions. We find a behavior similar to that of Cichowlas et al. [5] but with mixed direct energy and helicity cascades and a small scales thermalization exhibiting the Kraichnan helical absolute equilibrium.

We also investigate the cascades and thermalization in the case of $2D$ truncated Euler equation and truncated magnetohydrodynamics. Several similarities and differences with the thee-dimensional case are observed.

In a second part of this thesis we study the GPE equation that describes superfluids at very low temperatures. The GPE was known to posses a Kolmogorov turbulent behavior [26, 27, 28]. Nore et al [26, 27] reported that during the turbulent regime an energy transfer from the incompressible kinetic energy to sound waves is observed. The Fourier TGPE was first introduced in the context of Bose condensation by Davis et al.[29], as a description of the classical modes of a finite-temperature partially-condensed homogeneous Bose gas. They showed that the thermodynamic equilibrium presents a condensation transition at finite energy. The same condensation transition was later interpreted as a condensation of classical non-linear waves [30, 31]. Berloff and Svistunov [32] used a finite difference version of TGPE and obtained a finite temperature vortex rings contraction that they related it to a mutual friction effect.

We show that the thermalization under the TGPE can also be achieved by a direct energy cascade, similar to that one of truncated Euler flows, with a vortex annihilation as a prelude to final thermalization. We also show that increasing the amount of dispersion a clear bottleneck in a intermediate range is observed leading to a partially thermalized zone.

We introduce then a stochastic Ginzburg-Landau equation (SGLE) to obtain the absolute equilibrium of the TGPE. We show that the condensation transition that was previously observed in [29, 30, 31] corresponds to a standard second-order transition described by the $\lambda - \phi^4$ theory.

Using equilibrium states generated with the SGLE we study its interaction with

vortex rings under the TGPE dynamics. We observe that Kelvin waves are naturally present due to thermal fluctuations and that the ring velocity strongly depends on the temperature.

It was previously known [33, 34] that finite-amplitude Kelvin waves in a vortex ring induce an anomalous translational velocity. This astonishing result was first analytically obtained within the local induction approximation (LIA) by Kiknadze and Mamaladze [33] and then numerically by Barenghi et al. [34] using the Biot-Savart equation. By assuming equipartition of the energy of the Kelvin waves with the heat bath we obtain a good estimate of the effect.

Finally, we study the problem of sound radiation produced by GP vortices. The energy radiated, that is carried to infinity by sound propagation, can be considered as a mechanism of slow relaxation to thermodynamic equilibrium.

This thesis is organized in two main parts, the first is devoted to the ideal flows described by Euler and MHD equations and the second one to superfluid flows of the GPE type. In each chapter a general overview is given that covers some basics concepts and references needed to introduce the respective publications presented in their original forms at the end of the chapters.

The first part contains four chapters. The first chapter concerns the dynamics of the $3D$ truncated Euler equation. The basic concepts on turbulence theory are recalled Then we present a two-fluid model of the truncated Euler equations [35] and we extend the thermalization results to the case with helical initial conditions [36]. In chapter 3 the cascades and the thermalization of two-dimensional truncated Euler and MHD equation are studied. In chapter 4 we study the thermalization of compressible truncated Euler flows [37].

The second part of this starts with chapter 5 where we review some basics of statistical mechanics related to truncated systems. In chapter 6 we review some basic properties of the GPE. We then introduce our new results on the TGPE [38]. Finally, chapter 6 is concerned to the radiation of sound by point GP vortices [39].

There is three appendices in this thesis. In appendix A a two-fluid model version of TGPE, that use the extended thermodynamic that was introduced in chapter 6, is presented. Then in appendix B the numerical methods used in this thesis are detailed. Finally, a comment submitted to *Phys. Rev. Letter* is included in appendix C.

LIST OF PUBLICATIONS

During this thesis the following works have been published, submitted or are in preparation:

- *Two-fluid model of the Truncated Euler Equations.* G. Krstulovic et M.E. Brachet. Physica D 237,2015-2019 (2008)
- *Cascades, thermalization and eddy viscosity in helical Galerkin truncated Euler flows.* G. Krstulovic, P.D. Mininni, M.E. Brachet, et A. Pouquet. Phys. Rev. E 79, 056304 (2009).
- *Generation and Characterization of Absolute Equilibrum of Compressible Flows.* G.Krstulovic, C. Cartes, M. Brachet and E. Tirapegui. International Journal of Bifurcation and Chaos (IJBC). Vol 19 (10). 2009.
- *Energy cascade with small-scales thermalization, counter flow metastability and anomalous velocity of vortex rings in Fourier-truncated Gross-Pitaevskii equation.* G. Krstulovic and M.E. Brachet, to be submitted.
- *Radiation and Vortex Dynamics in Non Linear Schrödinger Equation.* G.Krstulovic, M. Brachet and E. Tirapegui. Phys. Rev E 78, 026601, (2008)
- *Comment on "Superfluid turbulence from quantum Kelvin wave to classical Kolmogorov cascade" (Phys. Rev. Lett. 103, 084501 (2009)).* Submitted to PRL. (2009)

LIST OF ACRONYMES

DNS:	Direct numerical simulation
FFT:	Fast Fourier transform
PDE:	Partial differential equation
MHD:	Magnetohydrodynamics
NLSE:	Non-linear Schrödinger equation
GPE:	Gross-Pitaevskii equation
TGPE:	Tuncated Gross-Pitaevskii equation
EDQNM:	Eddy damped quasi-normal Markovian
SGLE:	Stochastic Ginzburg-Landau equation
ARGLE:	Advected real Stochastic Ginzburg-Landau equation

Part I

IDEAL FLUIDS

2. CASCADES AND THERMALIZATION IN TRUNCATED EULER EQUATION

This chapter is basically made of two main parts, the first one is devoted to give a brief overview which will permit to discus the two publications that are presented in the second part. More specifically, in the first section some basic concepts of turbulence theory are reviewed. Then, the truncated Euler equation is defined and its statistical stationary solution, known as absolute equilibrium, are discussed. Some of the literature related to the thermalization of truncated Euler flows is reviewed, together with a brief introduction to the Eddy-Damped Quasi-Normal Markovian theory. Finally the last two sections correspond to two published works. In the first one, a phenomenological two-fluid model which takes in account the large-scale dissipative effects of truncated Euler flows is presented. The second work is concerned by the role of helicity on the thermalization of truncated Euler flows.

Turbulence is a subject of scientific study with a long history. Leonardo da Vinci (April 15, 1452 - May 2, 1519) was already interested studying the eddies formed behind the pillars of a bridge. About 250 years ago Leonhard Paul Euler (15 April 1707 - 18 September 1783) proposed the now famous Euler equation that governs the dynamics of perfect fluids. Seventy years later Claude-Louis Navier (10 February 1785 - 21 August 1836) modified this equation to include viscosity. Taking into account the work of Sir George Gabriel Stokes (13 August 1819-1 February 1903) this equation is now known as the Navier-Stokes equation.

The Navier-Stokes equation has a fundamental importance for both the physics and mathematics communities. From a mathematical point of view, the existence and smoothness of the solutions of this equation is still a complex and unsolved problem, considered as one of the seven Millennium Prize Problems in mathematics [1].

Many tentative theoretical models have been developed in the physics community to further the understanding of turbulence. Since the end of the 70's, using the development of super-computers a lot of progress has been achieved. Nowadays most of the theoretical works are based on numerical computations.

Among all the studies on turbulence, some remarkable results were obtained by the mathematician Andrey Nikolaevich Kolmogorov (April 25, 1903 - October 20, 1987) in

[1] There is a one million dollar prize being awarded by Clay Mathematics Institute waiting for who solve this problem. *http://www.claymath.org/*

1941. His results concerning the scaling of the energy spectrum is one of the the most simple (but not less brilliant) and deepest in the field [40, 41, 42, 43].

Another very important physicist in the field of turbulence was Robert Kraichnan (Jan 15, 1928- Feb 26, 2008), who made major contribution to the area. In particular in two-dimensional turbulence and introducing the so called Kraichnan passive scalar model [2, 44, 45].

This chapter is organized as follows. First in section 2.1, a brief introduction to fully developed turbulence is given. In section 2.2 the truncated Euler equation and the absolute equilibrium are presented followed by a discussion of thermalization in section 2.3. Section 2.4 is devoted to introduce the basics of the eddy-damped quasi-normal Markovian theory and how its application is relevant to the truncated Euler relaxation. Then the hyper-viscous limit and the relation between bottlenecks and thermalization is discussed in section 2.5. In section 2.6 we point out the differences between partial differential equations and the corresponding truncated system. Finally sections 2.7 and 2.8 contain two publications. In the first one, a phenomenological two-fluid model which take in account the large-scale dissipative effects of truncated Euler flows is introduced. In the second work the role of helicity on the thermalization of truncated Euler flows is studied.

2.1 Introduction to fully developed turbulence.

The basic equations governing the dynamics of a barotropic viscous fluid of density ρ and velocity $\mathbf{u}$ are

$$\rho\partial_t\mathbf{u} + \rho(\mathbf{u}\cdot\nabla)\mathbf{u} = -\nabla p + \nu\rho\nabla^2\mathbf{u} \tag{2.1}$$

$$\partial_t\rho + \nabla\cdot(\rho\mathbf{u}) = 0, \tag{2.2}$$

$$f(p,\rho) = 0 \tag{2.3}$$

where p is the pressure, ν the kinematic viscosity and $f(p,\rho)$ the barotropic relation between density and pressure.

Equation (2.1) is known as the Navier-Stokes equation and (2.2) as the continuity equation.

For a compressible fluid an important dimensionless quantity is the Mach number defined as $M = u_L/c$ where u_L is a characteristic velocity and $c = \sqrt{\frac{\partial p}{\partial \rho}}$ is the velocity of sound.

In this chapter we will only consider small Mach number, where neglecting the propagation of sound waves the fluid can be considered as incompressible. In this limit, equations (2.1-2.2) reduce to

$$\partial_t\mathbf{u} + (\mathbf{u}\cdot\nabla)\mathbf{u} = -\frac{1}{\rho}\nabla p + \nu\nabla^2\mathbf{u} \tag{2.4}$$

$$\nabla\cdot\mathbf{u} = 0. \tag{2.5}$$

In the inviscid case ($\nu = 0$) the system (2.4-2.5) is known as the Euler equation.

An other very important dimensionless quantity is the Reynolds number defined as

$$R = \frac{Lu_L}{\nu}, \tag{2.6}$$

where L is the characteristic length of the system. This number estimates the relative importance of the inertial terms $(\mathbf{u} \cdot \nabla)\mathbf{u}$ with respect to viscous effects $\nu\Delta\mathbf{u}$. Indeed, the first term contains two velocities and one spatial derivative while the second term contains the viscosity, one velocity and two spatial derivatives. The order of magnitude of their ratio is thus (velocity $\times$ length)/viscosity.

In the low R limit, the nonlinear term in equation (2.4) can be neglected and it can often be treated analytically, this kind of flow are called *laminar*. On the contrary, for large Reynolds number the flow becomes *turbulent* and is extremely complex. Statistical tools are needed to obtain a quantitative understanding of the system.

The transition from laminar to turbulent flows it is characterized by the symmetries permitted by the system (Eqs. 2.4-2.5 and boundaries) that are successively broken as R increases [21]. However at very large Reynolds number, some of this symmetries are recovered in a statistical sense. Turbulence at very large Reynolds numbers with some of the symmetries recovered in a statistical sense is called *fully developed turbulence* [21].

Remark that the pressure in equation (2.4) is not a dynamic variable, indeed it is completely determined by the incompressibility condition (2.5). Taking the divergence of the equation (2.4) we observe that the pressure satisfies the Poisson equation

$$\nabla^2 p = -\partial_{ij}(u_i u_j) \tag{2.7}$$

where we have set the density to $\rho = 1$, ∂_{ij} denotes $\frac{\partial^2}{\partial_i \partial_j}$ and summation over repeated index is understood. Thus after eliminating the pressure from equation (2.4) the Navier-Stokes is rewritten as

$$\partial_t u_i + (\delta_{il} - \partial_{il}\nabla^{-2})\partial_j(u_j u_l) = \nu\nabla^2 u_i. \tag{2.8}$$

Remark that this is a non local equation due to the ∇^{-2} operator and the divergence free condition of the velocity field is automatically assured provided that initial condition satisfies $\nabla \cdot \mathbf{u} = 0$. The pressure can be also eliminated from equation (2.4) introducing the vorticity

$$\omega = \nabla \times \mathbf{u}. \tag{2.9}$$

Taking the curl of Eq. (2.4) and using the vectorial identity $\nabla|\mathbf{u}|^2 = 2\mathbf{u} \cdot \nabla\mathbf{u} + 2\mathbf{u} \times (\nabla \times \mathbf{u})$ leads to the vorticity equation

$$\partial_t \omega = \nabla \times (\mathbf{u} \times \omega) + \nu\nabla^{2\text{‘}}\omega. \tag{2.10}$$

Note that in (2.10) the non-local character is also present. Indeed, if we want to recover

$\mathbf{u}$ the same ∇^{-2} operator must be applied to the vorticity.

In the following we will assume periodical boundary conditions and for simplicity we will use the box $[0, 2\pi]^3$. This choice of boundary conditions is relevant to the study of homogeneous turbulence. Equation (2.10) can be easily implemented numerically using pseudo-spectral codes [14]. The Fourier transform will be denoted hereafter by the hat symbol $\widehat{\ }$.

2.1.1 Conservation laws

In any dynamical system, the conserved quantities or the balance equations play a fundamental role. The following global quantities,

$$E = \langle \frac{1}{2}|\mathbf{u}|^2 \rangle \qquad \Omega = \langle \frac{1}{2}|\omega|^2 \rangle \tag{2.11}$$

$$H = \langle \mathbf{u} \cdot \omega \rangle \qquad H_\omega = \langle \omega \cdot \nabla \times \omega \rangle, \tag{2.12}$$

where $\langle \cdot \rangle$ denotes here spatial average, are important in turbulence.

The quantities defined in (2.11-2.12) are the mean energy (per unit of mass) E, the mean enstrophy Ω, the mean helicity H and the mean vortical helicity H_ω.

It is straightforward to demonstrate that the quantities defined in (2.11-2.12) satisfy the following balance equation

$$\frac{dE}{dt} = -2\nu\Omega, \qquad \frac{dH}{dt} = 2\nu H_\omega. \tag{2.13}$$

Remark that in the inviscid case the energy and helicity (we will omit hereafter the word *mean*) are conserved quantities. The conservation of the helicity was discovered by Moreau [24] in 1961 and its dynamical importance was also pointed out by Moffat [25] in 1969. Since then several studies on the influence of helicity have been carried out, see for example [3, 46, 47].

In two-dimensions the helicity identically vanishes and there is an additional conservation law for the enstrophy

$$\frac{d\Omega}{dt} = -2\nu P, \tag{2.14}$$

where $P = \langle \frac{1}{2}|\nabla \times \omega|^2 \rangle$ is the *palinstrophy*. The phenomenology of two-dimensional turbulence will be further discussed in chapter 3.

One of the most basic quantity of turbulence is the energy dissipation rate

$$\epsilon = -\frac{dE}{dt}. \tag{2.15}$$

The local dissipation rate is defined as

$$\varepsilon_{\text{local}} = \frac{1}{2}\nu \sum_{ij} (\partial_i u_j + \partial_j u_i)^2. \tag{2.16}$$

Note that we have that $\varepsilon = \langle \varepsilon_{\rm local} \rangle = \langle \nu |\omega|^2 \rangle$. This relation can be simply derived by rewriting equation (2.7) as

$$\nabla^2 p = \Sigma - W \tag{2.17}$$

with $\Sigma = \frac{1}{4}\sum_{ij}(\partial_i u_j + \partial_j u_i)^2$ and $W = \frac{1}{4}\sum_{ij}(\partial_i u_j - \partial_j u_i)^2$. About this last equation there is an interesting analogy that was stressed in reference [48] quoted here:

It is therefore natural to establish an analogy to electrostatics, with the pressure corresponding to the potential resulting from negative and positive charges distributed according to the square vorticity and the energy dissipation, respectively. The vorticity concentrations thus act like sources of low pressure and their greatest relative concentration relatively to the energy dissipation concentrations acting as source of high-pressure will be the cause of spatial correlation between turbulent activity and low-pressure regions. This analogy motivated an experimental technic using small bubbles to visualize vortex filaments [49]. Visualization of vortex lines are displayed in figure 2.1.

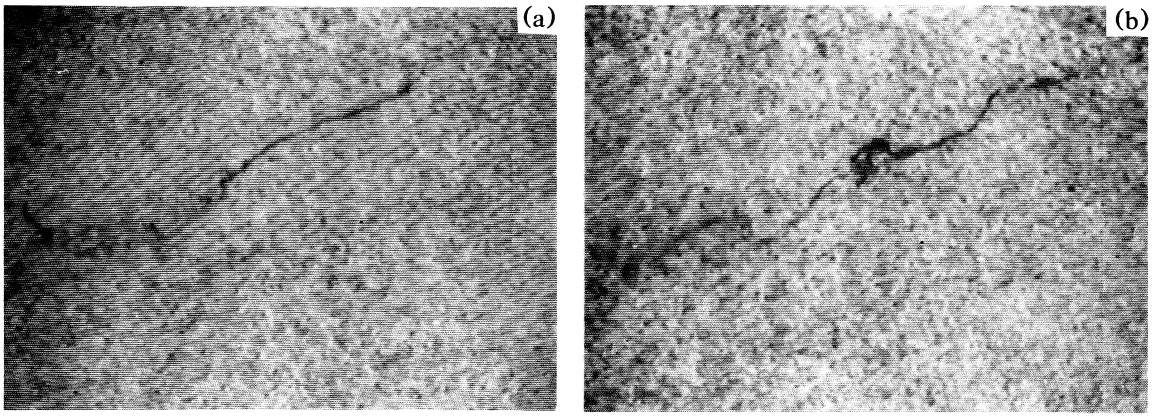

Fig. 2.1: Detail of two successive video images showing a side view of a vorticity filament observed in a turbulent flow at Reynolds number of 80000. Its length is of order of 5 cm while its diameter is of the order of 1 mm. a) THe filament at its formation. b) Its destabilization to form kinks. Taken from reference [49]

.

It is very useful to decompose the energy as the sum of the energy at each scale ℓ. This can be easily done using the Fourier transform of the velocity field and summing over wavenumbers of same modulus. In practice, the energy spectrum is defined by summing $|\hat{\mathbf{u}}(\mathbf{k}', t)|^2$ on spherical shells of width $\Delta k = 1$,

$$E(k,t) \;=\; \frac{1}{2} \sum_{k-\Delta k/2 < |\mathbf{k}'| < k+\Delta k/2} |\hat{\mathbf{u}}(\mathbf{k}', t)|^2 \,. \tag{2.18}$$

By construction we have $E = \sum_k E(k)$. The helicity spectrum is defined in the same way replacing $|\hat{\mathbf{u}}(\mathbf{k}', t)|^2$ by $\hat{\omega}(\mathbf{k}', t) \cdot \hat{\mathbf{u}}(-\mathbf{k}', t)$. Note the energy dissipation rate is

expressed in term of the energy spectrum as

$$\epsilon = 2\nu \int k^2 E(k)\, dk. \tag{2.19}$$

2.1.2 Richardson cascade and Kolmogorov phenomenology.

One of the most important concepts in turbulence is the idea of cascades. Suppose that the system originally at rest is forced at a large-scale ℓ_I, then the system will dissipate the energy following the balance equation (2.11). As at very early times the velocity field created has only variation at large-scales the energy dissipation rate will be very small. However, due to nonlinear terms, the energy will be carried to small-scales down to a scale where the dissipation will be strong enough to stop the cascade. This thus led to the physical image of the "Richardson cascade" [50]. The energy injected in the fluid at scale ℓ_I "cascades" down to smaller scales. This process stops when scales ℓ_d small enough for the energy to be dissipated into heat are reached. One can picture this cascade as a succession of eddies instabilities happening at scales $\ell_I = \ell_0 > r\ell_0 > r_0^2 > \dots \ell_d$ with $r < 1$, as illustrated in figure 2.3

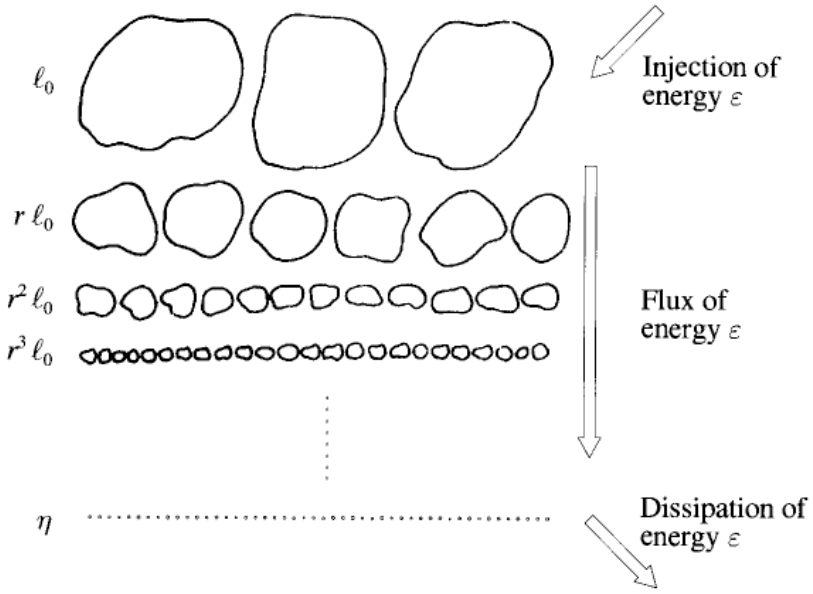

Fig. 2.2: Representation of the Richardson cascade. Figure taken from reference [21].

In 1941, Kolmogorov [40, 41, 42] found quantitative expressions for the intensity of fluid motions at scale ℓ and for the dissipation scale ℓ_d.

Let us first remark that the Navier-Stokes equation is invariant under Galilean transformations: if $u(x,t)$ is a Navier-Stokes solution, then $u(x - u_0 t, t) + u_0$ is also a

solution. A constant advection has thus no dynamical effect on the evolution of the flow. Accordingly, we define the intensity of the motions at scale ℓ to be the typical velocity variation δu_ℓ over distance ℓ.

The Richardson cascade leads us to a first hypothesis:

- $H_0 : \varepsilon$ is independent of ν.

The only combination of δu_I and ℓ_I with a correct dimension is $\delta u_I^3/\ell_I$. Thus

$$\varepsilon \sim \frac{\delta u_I^3}{\ell_I}. \tag{2.20}$$

The scaling law for $\delta u(\ell)$ will be obtained using the following two hypotheses:

- $H_I : \delta u(\ell)$ does not depend on ν (for $\ell_d < \ell < \ell_I$)
- $H_2 : \delta u(\ell)$ is a function of only ε and ℓ.

Dimensional analysis yields

$$\delta u(\ell) \sim (\varepsilon \ell)^{1/3}. \tag{2.21}$$

Using (2.20), (2.21) can be written

$$\delta u(\ell) \sim \delta u_I \left(\frac{\ell}{\ell_I}\right)^{1/3} \tag{2.22}$$

Let us remark that H_2 amounts to say that $\delta u(\ell)$ is a function of ℓ_I only through ε. Or, in other words, that there is no way by observing at scale ℓ to distinguish between two turbulence having the same ε but driven at two different injection scales.

We can compute the Reynolds number associated with motions at scale ℓ

$$R_\ell \sim \frac{\delta u(\ell)\ell}{\nu} = \frac{\varepsilon^{1/3}\ell^{4/3}}{\nu}.$$

Viscous dissipation will take place at scales ℓ_d such that $R_{\ell_d} \sim 1$. It follows that

$$\ell_d \sim \nu^{3/4}\varepsilon^{-1/4}. \tag{2.23}$$

Using (2.20), (2.23) can also be written

$$\ell_d \sim \ell_I R_I^{-3/4}. \tag{2.24}$$

The scaling 2.21 leads to an energy spectrum

$$E(k) = C_K \varepsilon^{2/3} k^{-5/3}. \tag{2.25}$$

The constant C_K is known as the Kolmogorov constant and was supposed to be universal. Its value has been found about 1.5 [51].

The energy dissipation scales can also be expressed substituting the Kolmogorov spectrum in the energy dissipation rate (2.19) and finding the wavenumber k_d where the dissipation is negligible. That corresponds to the equation

$$\varepsilon \sim 2\nu \int^{k_d} \varepsilon^{2/3} k^{1/3} dk, \tag{2.26}$$

which leads to

$$k_d \sim \varepsilon^{1/4} \nu^{-3/4} \sim \ell_d^{-1}. \tag{2.27}$$

These arguments are the most important contribution to the theory of turbulence and the Kolomogorov spectrum (2.28) has been obtained many times in experiments and numerical simulations [48, 52] (see also [21] chapter 5 or [53] chapter 6 for a longer discussion).

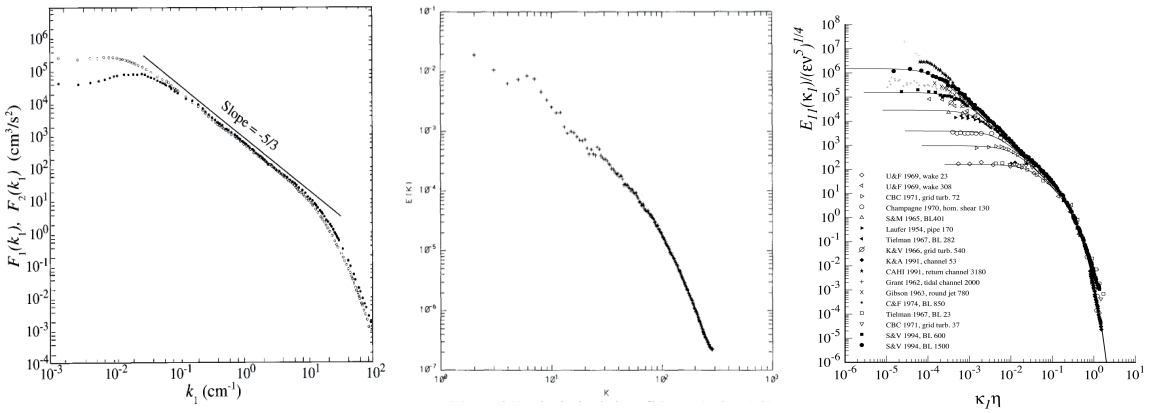

Fig. 2.3: Left: Energy spectrum from [48] where the Kolmogorov $-5/3$-scaling extends between $k = 6$ and $k = 60$. Center: Energy spectrum form [52]. Right: Measurements of one-dimensional longitudinal velocity spectra. Here η is the Kolomogorov dissipative scale. See reference [53] chapter 6 for details.

Finally it is important to remark that in the derivation of the Kolmogorov scaling, the universality assumption leads that in the inertial range the energy spectrum only depends on ε and k. In fact, if the Kolmogorov dissipation wave-number k_d (Eq. 2.27) is take in to account, simple dimension analysis modifies the spectrum as

$$E(k) = C_K \varepsilon^{2/3} k^{-5/3} F(\frac{k}{k_d}), \tag{2.28}$$

where F is a universal function converging to 1 in the large Reynolds number limit ($k/k_d \to 0$). This can leads to small modifications of the $-5/3$ Kolmogorov scaling law.

The universality of Kolmogorov phenomenology of turbulence was questioned by Landau [54]. His objection is based on the idea that C_K must depend on the detailed

geometry of the production of turbulence. Suppose that we have a system with N subsystems, each one with different values of the mean dissipation rate ε_i and Kolmogorov energy spectra $E_i(k)$ in the inertial zone. For the whole system we can define

$$\bar{E}(k) = \frac{1}{N}\sum_i E_i(k) \text{ and } \bar{\varepsilon} = \frac{1}{N}\sum_i \varepsilon_i. \tag{2.29}$$

Universality assumption implies that for the whole system we have $\bar{E}(k) = C_K \bar{\varepsilon}^{2/3} k^{-5/3}$. It follows from the definitions (2.29) that

$$\left(\frac{1}{N}\sum_i \varepsilon_i\right)^{2/3} = \frac{1}{N}\sum_i \varepsilon_i^{2/3}. \tag{2.30}$$

The previous relation does not hold unless the ε_i are all equals. The contradiction depends on the possibility of consider the different systems as being part of a whole system. If such whole system cannot be consider then there is no way to question the universality of the Kolmogorov constant. For a further discussion see section 4 of chapter 6 in reference [21].

2.1.3 Kolmogorov's four-fifths law

There is an important exact result on turbulence also due to Kolmogorov [42] known as the 4/5-law that will be given here for completeness of the exposition. Under the hypothesis of homogeneity and isotropy (also that ε remains finite in the high R numbers) Kolmogorov derived the following result [21]

In the limit of infinite Reynolds number, the third order (longitudinal) structure function of homogeneous isotropic turbulence evaluated for increments ℓ small compared to the integral scale, is given in terms of the mean energy dissipation per unit of mas ε by

$$\langle \big(\delta u_{\|}(\mathbf{r},\ell)\big)^3 \rangle = -\frac{4}{5}\varepsilon\ell, \tag{2.31}$$

where the longitudinal velocity increment is $\delta u_{\|}(\mathbf{r},\ell) = [\mathbf{u}(\mathbf{r}+\ell) - \mathbf{u}(\mathbf{r})| \cdot \frac{\ell}{\ell}$.

2.2 Truncated Euler equation

2.2.1 Basic definition

The truncated Euler equation was introduced for its statistical importance in references [1, 7]. It is obtained performing a spherical Galerkin truncation at wave-number $k_{\max}$

on the Euler equation

$$\partial_t \mathbf{u} + (\mathbf{u}\cdot\nabla)\mathbf{u} = -\frac{1}{\rho}\nabla p \tag{2.32}$$

$$\nabla\cdot\mathbf{u} = 0. \tag{2.33}$$

The Galerkin truncation consist in taking the Fourier transform of the Euler equation and keeping only a finite number of Fourier modes. This yields the following finite system of ordinary differential equations for the Fourier transform of the velocity $\hat{\mathbf{u}}(\mathbf{k})$ ($\mathbf{k}$ is a 3 D vector of relative integers satisfying $|\mathbf{k}| \leq k_{\max}$):

$$\partial_t \hat{u}_\alpha(\mathbf{k},t) = -\frac{i}{2}\mathcal{P}_{\alpha\beta\gamma}(\mathbf{k})\sum_{\mathbf{p}} \hat{u}_\beta(\mathbf{p},t)\hat{u}_\gamma(\mathbf{k}-\mathbf{p},t), \tag{2.34}$$

where $\mathcal{P}_{\alpha\beta\gamma} = k_\beta P_{\alpha\gamma} + k_\gamma P_{\alpha\beta}$ with $P_{\alpha\beta} = \delta_{\alpha\beta} - k_\alpha k_\beta/k^2$.

This time-reversible finite-dimensional dynamical system exactly conserves the energy E and helicity H.

2.2.2 Absolute equilibrium, a general discussion.

The truncated Euler equation is known to posses statistical stationary solutions called absolute equilibria [1, 3, 7, 4]. These equilibrium states correspond to Gaussian probabilities, that are solutions of the associated Liouville equation.

We will now review the Liouville equation and the absolute equilibrium that correspond to a general dynamical system defined by

$$\dot{\mathbf{X}}(t) = \mathbf{F}(\mathbf{X}) \tag{2.35}$$

where $\mathbf{X}$ is a n-dimensional vector and $\mathbf{F}$ is at least of class C^1. The Liouville equation describes the time evolution of the phase space distribution function $P(\mathbf{X})$, more precisely the temporal evolution of the probability $P(\mathbf{X})d^nX$ of finding the system in the phase space volume d^nX at $\mathbf{X}$. This equation express the conservation of the probability current in phase space, and it reads:

$$\frac{\partial P(\mathbf{X},t)}{\partial t} + \sum_i \frac{\partial}{\partial X_i}\left(F_i(\mathbf{X})P(\mathbf{X},t)\right) = 0. \tag{2.36}$$

We say that the system satisfies a generalized Liuoville theorem if

$$\nabla\cdot\mathbf{F}(\mathbf{X}) = 0. \tag{2.37}$$

This is of course the case of Hamiltonian systems, which are described by the vector of

conjugate variables $\mathbf{X} = (q_1, \ldots, q_n, p^1 \ldots, p^n)$ and the equation of motion

$$X_\mu(t) = \epsilon_{\mu\nu} \frac{\partial H}{\partial X_\nu} \tag{2.38}$$

where H is the Hamiltonian and $\epsilon_{\mu\nu}$ the symplectic tensor. Equation (2.37) is automatically satisfied noting that $\epsilon_{\mu\nu}$ is an antisymmetric tensor and H is supposed to be C^2.

For a system satisfying (2.37) the Liouville equations is expressed as

$$\frac{\partial P(\mathbf{X}, t)}{\partial t} + \mathbf{F}(\mathbf{X}) \cdot \nabla P(\mathbf{X}, t) = 0. \tag{2.39}$$

Suppose now that the system (2.35) admits a constant of movement K, therefore we have that

$$\frac{dK}{dt} = \frac{\partial K}{\partial X_i} \frac{\partial X_i}{\partial t} = \frac{\partial K}{\partial X_i} \cdot \mathbf{F}(\mathbf{X}) = \nabla K \cdot \mathbf{F}(\mathbf{X}) = 0. \tag{2.40}$$

It follows then from equations (2.39) and (2.40) that

$$P_{\text{st}}(\mathbf{X}) = \frac{1}{Z} e^{-\beta K}, \tag{2.41}$$

where Z is a normalization constant, is a stationary probability provided that $e^{-\beta K}$ is integrable over the whole phase space. The stationary probability (2.41) is known as the *absolute equilibrium*. In general if the system has m conserved quantities, βK must be replaced by a linear combination of the invariants and the system will have m *temperatures*.

Truncated Euler absolute equilibria

For simplicity will now only consider flows with a vanishing helicity. The case of helical flows will be covered in section 2.8. With vanishing helicity the only relevant invariant of the truncated Euler equation is the kinetic energy

$$E = \frac{1}{2} \sum_{\mathbf{k}} |\hat{\mathbf{u}}(\mathbf{k}, t)|^2. \tag{2.42}$$

Note that as the energy is a quadratic functional of the velocity the absolute equilibria are simple Gaussian fields. However there are some more subtle facts about on the statistical ensemble which merit some explanation [7].

To explicitly construct the ensemble we must note that due to the incompressibility condition, the velocity satisfies $\mathbf{k} \cdot \hat{\mathbf{u}}(\mathbf{k}) = 0$ and therefore not all of the three component of $\hat{\mathbf{u}}(\mathbf{k})$ are independent. Furthermore the relation $\hat{\mathbf{u}}(\mathbf{k})^* = \hat{\mathbf{u}}(-\mathbf{k})$ obeyed by the Fourier transform of physical space real field also impose supplementary constrains. To avoid these difficulties we will treat the real and imaginary parts of $\hat{\mathbf{u}}(\mathbf{k})$ separately by

introducing two new real field defined by $\hat{u}_\nu(\mathbf{k}) = \hat{a}_\nu(\mathbf{k}) + i\hat{b}_\nu(\mathbf{k})$. First note that as the fields $\hat{a}_\nu(\mathbf{k})$ and $\hat{b}_\nu(\mathbf{k})$ are reals $\hat{a}_\nu(-\mathbf{k}) = \hat{a}_\nu(\mathbf{k})$ and $\hat{b}_\nu(-\mathbf{k}) = -\hat{b}_\nu(\mathbf{k})$. Finally, it is possible to construct two orthonormal vector $\mathbf{n}_1(\mathbf{k})$ and $\mathbf{n}_2(\mathbf{k})$ spanning the plane perpendicular to $\mathbf{k}$. We introduce then four new variables $a_r(\mathbf{k}) = n_r(\mathbf{k}) \cdot \hat{\mathbf{a}}(\mathbf{k})$ and $b_r(\mathbf{k}) = n_r(\mathbf{k}) \cdot \hat{\mathbf{b}}(\mathbf{k})$ for $r = 1, 2$. Defining the set of wavevectors

$$\Lambda_{k_{\max}} = \{\mathbf{k}|\, k < k_{\max} \wedge (kx \geq 0 \vee (k_x = 0, k_y \geq 0) \vee (k_x = k_y = 0, k_z \geq 0)\} \tag{2.43}$$

we have by construction that $\{a_r(\mathbf{k}), b_r(\mathbf{k})|\mathbf{k} \in \Lambda_{k_{\max}}, r = 1, 2\}$ is a set of independent real variables.

It is straightforward to show that the energy can be rewritten as

$$E = \sum_{\mathbf{k}\in\Lambda_{k_{\max}}} \sum_{r=1}^{2} [a_r(\mathbf{k})^2 + b_r(\mathbf{k})^2] \tag{2.44}$$

The absolute equilibria is thus simply

$$P_{\text{st}}\left(a_r(\mathbf{k}), b_r(\mathbf{k})|\mathbf{k} \in \Lambda_{k_{\max}}, r = 1, 2\right) = \frac{1}{Z} e^{-\beta E}. \tag{2.45}$$

To reconstruct the momentum of the velocity field from the absolute equilibrium (2.45), one possibility is to directly compute the orthogonal vectors $\mathbf{n}_1(\mathbf{k})$, $\mathbf{n}_2(\mathbf{k})$ and make the calculations. A simpler way is by using vectorial arguments. Indeed, first note that

$$\langle \hat{u}_\nu(\mathbf{k})\hat{u}_\mu(-\mathbf{k})\rangle = \langle \hat{a}_\nu(\mathbf{k})\hat{a}_\mu(-\mathbf{k})\rangle + \langle \hat{b}_\nu(\mathbf{k})\hat{b}_\mu(-\mathbf{k})\rangle = 2\langle \hat{a}_\nu(\mathbf{k})\hat{a}_\mu(\mathbf{k})\rangle \tag{2.46}$$

where here $\langle\cdot\rangle$ denotes ensemble average. Observe then that $\langle \hat{a}_\nu(\mathbf{k})\hat{a}_\mu(\mathbf{k})\rangle$ is a symmetric tensor which vanish if one component is contracted with $\mathbf{k}$. It follows then that

$$\langle \hat{a}_\nu(\mathbf{k})\hat{a}_\mu(\mathbf{k})\rangle = P_{\mu\nu} A(k) \tag{2.47}$$

where $P_{\mu\nu} = \delta_{\mu\nu} - \frac{k_\mu k_\nu}{k^2}$ is the projector into divergence-free functions and $A(k)$ is a function to be determined. Contracting the index μ, ν we obtain

$$\langle \hat{a}_\mu(\mathbf{k})\hat{a}_\mu(\mathbf{k})\rangle = 2\langle a_1(\mathbf{k})^2\rangle = (d-1)A(k) \tag{2.48}$$

it follows that $A(k) = 2/(d-1)\beta$ where d is the dimension of the space. Finally the the second order momentum reads

$$\langle \hat{u}_\nu(\mathbf{k})\hat{u}_\mu(-\mathbf{k})\rangle = \frac{2}{(d-1)\beta} P_{\mu\nu} \tag{2.49}$$

Note that equation (2.49) leads to the absolute equilibrium energy spectra

$$E(k) = \frac{2S_{d-1}}{(d-1)\beta} k^{d-1} \tag{2.50}$$

where S_{d-1} is the surface of the unitary d-sphere ($S_2 = 4\pi$ and $S_1 = 2\pi$). Note that the relation $\langle |\hat{\mathbf{u}}(\mathbf{k})|^2 \rangle = \frac{2}{\beta}$ (deduced from 2.49) can be obtained directly by using a simple equipartition argument.

It will be important for the discussion in the rest of this thesis to remember that energy equipartition leads to a k^2-power law scaling in three-dimension and k^1 scaling in two-dimensions.

2.3 Cascades and thermalization

We present here some results on the thermalization under the truncated Euler dynamics first obtained in Cichowlas et al [5]. They studied the so called Taylor-Green vortex defined by the initial data

$$u_x^{TG} = \sin x \cos y \cos z \tag{2.51}$$
$$u_y^{TG} = -\cos x \sin y \cos z \tag{2.52}$$
$$u_z^{TG} = 0. \tag{2.53}$$

This vortex has several symmetries which when are take into account allow speed up of numerical computations by a factor 32 and corresponding gain in memory storage (see appendix B). They performed direct numerical simulation (DNS) with a standard pseudo-spectral code dealiased with the 2/3-rule [14]. In practice, this rule means that if a resolution of N^d collocation points is used, the truncation wave number is $k_{\max} = N/3$ (and not $N/2$). This lost in resolution is completely necessary in order to ensure that the truncated system is exactly conservative (see Appendix B for details). In the following when we refer to a numerical simulation with a resolution of N^d, $k_{\max} = N/3$ must to be understood.

What they found, after long time integrations using resolutions up to 1600^3, is that there is a clear spontaneous scale separation in the energy spectrum. At small scales the energy spectrum rise as k^2. These thermalized modes create a kind of *micro-world* providing an effective dissipation at large scales. A progressive thermalization was observed, the k^2-thermalized zone extend to large scales. The temporal evolution of energy spectrum taken from reference [5] is displayed in figure 2.4.

For a deeper understanding of this thermalization observe that from figure 2.4 it is natural to define the wave-number k_{th} where the thermalized k^2 power-law zone starts. The temporal evolution of this wavenumber explicitly indicates the degree of thermalization of the system. We can also define the thermalized energy which plays the role of the energy dissipated from the large scales. Using $k_{\text{th}}(t)$ this energy is expressed

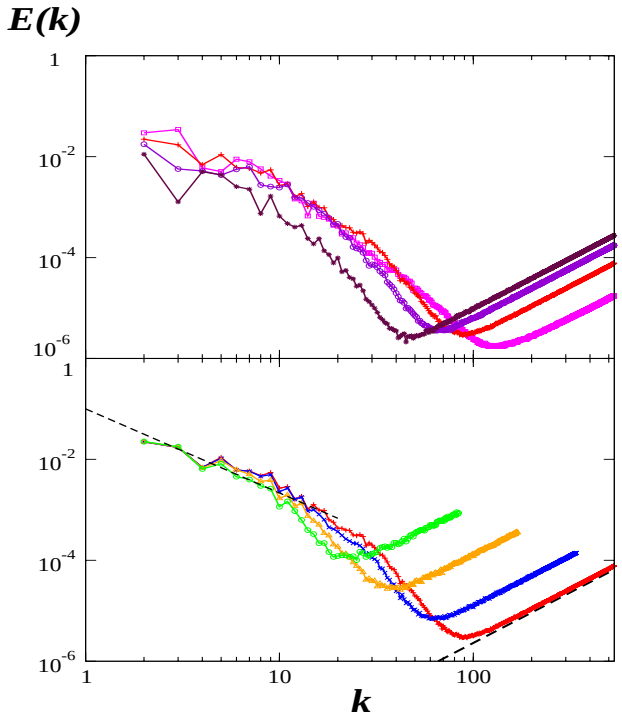

Fig. 2.4: Energy spectra, top: resolution 1600^3 at $t = (6.5, 8, 10, 14)$ ($\diamond$, $+$, $\circ$, $*$); bottom: resolutions 256^3 (circle $\circ$), 512^3 (triangle $\triangle$), 1024^3 (cross $\times$) and 1600^3 (cross $+$) at $t = 8$. The dashed lines indicate $k^{-5/3}$ and k^2 scalings. Figure taken from [5].

as

$$E_{\rm th}(t) = \sum_{k=k_{\rm th}(t)}^{k_{\rm max}} E(k,t). \tag{2.54}$$

The temporal evolution of $k_{\rm th}$ and $E_{\rm th}$ is displayed in figure 2.5. Note that $E_{\rm th}$ is an increasing function and that at large times it contains almost all the available energy $E = 0.125$.

Cichowlas et al [5] also gave an estimate of the characteristic time of effective dissipation τ_k of modes close to $k_{\rm th}$. The derivation was based on the existence of a fluctuation-dissipation theorem [8] that ensures that dissipation around equilibrium has the same characteristic time scales as the equilibrium time correlation function. They exactly determined the parabolic decorrelation time by

$$\tau_k^2 \partial_{tt} \left\langle u_\nu(\mathbf{k},t) u_\mu(\mathbf{k}',0)\right\rangle|_{t=0} = -\tau_k^2 \left\langle \partial_t u_\nu(\mathbf{k},t) \partial_{t'} u_\mu(\mathbf{k}',t)\right\rangle|_{t=t'=0} = \left\langle u_\nu(\mathbf{k},0) u_\mu(\mathbf{k}',0)\right\rangle, \tag{2.55}$$

where the time translation invariance has been used [20]. The decorrelation time is then found replacing the time derivative of the field with the right hand side of truncated Euler equation (2.34). The fourth order moment was then computed using the Wick

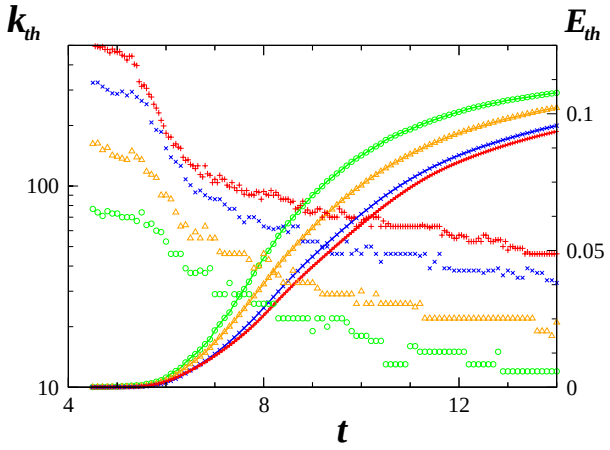

Fig. 2.5: Time evolution of the ratio $k_{\rm th}/k_{\rm d}$ at resolutions 256^3 (circle $\circ$), 512^3 (triangle $\triangle$), 1024^3 (cross $\times$) and 1600^3 (cross $+$) . Figure taken from [5].

theorem and the absolute equilibrium relation for the second order momentum (Eq. 2.49). The correlation time they found is

$$\tau_k = \frac{C}{k\sqrt{E_{\rm th}}} \tag{2.56}$$

with $C = 1.43382$. Using this time they proposed a spectral density of energy dissipation of the form $\varepsilon(k,t) = \frac{1}{\tau_k}E(k,t)$. On the other hand the total dissipated energy can be estimated by

$$\varepsilon_{\rm th}(t) = \frac{dE_{\rm th}}{dt}. \tag{2.57}$$

If the dissipation takes place in a range $\alpha k_{\rm d}$ around k_d, equating $\varepsilon(k_{\rm d})\alpha k_d = \epsilon_{\rm th}$ yields to

$$k_{\rm d} \sim \left(\frac{\varepsilon_{\rm th}}{E_{\rm th}^{3/2}}\right)^{1/4} k_{\rm max}^{3/4}. \tag{2.58}$$

It is expected that $k_{\rm d} \sim k_{\rm th}$. The temporal evolution of $\varepsilon_{\rm th}(t)$ and $k_{\rm th}/k_{\rm d}$ is displayed in figure 2.6. Note that the dissipation of energy behaves as in Navier-Stokes viscous flows (see for example [21] chapter 5) and presents a clear maximum near of $t_{\rm max} = 8$.

A Kolmogorov spectrum followed by an equipartition range was also observed in a spectral diffusion model describing the time evolution of the energy spectrum [55]. This model is a second order differential equation that admits an stationary solution compatible with the simultaneous $k^{-5/3}$-k^2 scalings.

To summarize the results of [5], they showed that the evolution of large-scale initial data relax toward the thermodynamic equilibrium under the truncated Euler equation. The thermalization takes place first a small scales, these modes act as fictitious mi-

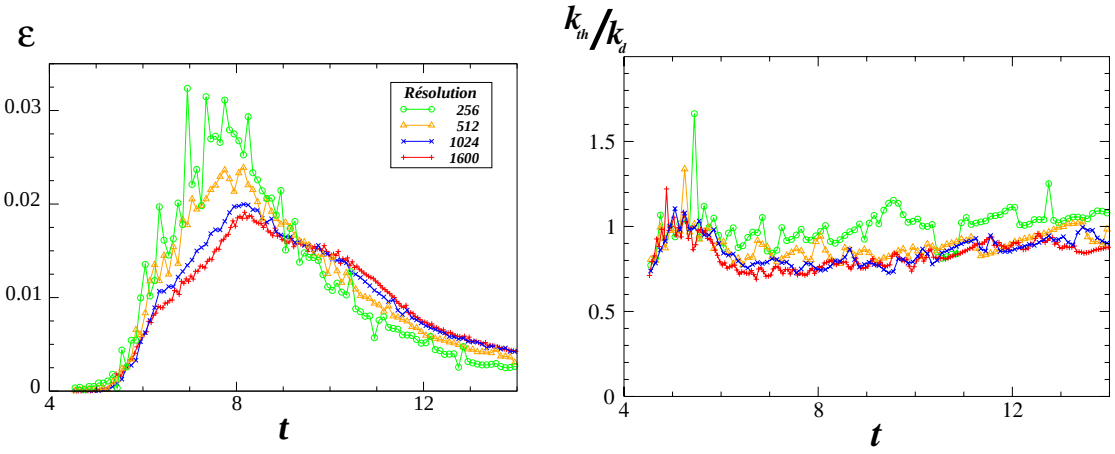

Fig. 2.6: Left: Temporal evolution of total dissipated energy form [20]. Right: Time evolution of the ratio $k_{\rm th}/k_{\rm d}$ at resolutions 256^3 (circle $\circ$), 512^3 (triangle $\triangle$), 1024^3 (cross $\times$) and 1600^3 (cross $+$) from [5].

croworld, or thermic bath, creating at large-scale effective viscosity. The large-scale dynamics thus behave as a viscous fluid and they are compatible with a K41 scaling.

2.4 Eddy-damped quasi-normal Markovian theory

Many statistical theories attempt to find relations between the cumulants in order to derive the statistics of the system. This is the case for example of the Kinetic theory which describes the macroscopic properties of gases. One paradoxical fact of such theories is that although the the departing equations are time reversible the final kinetic equations have lost this property. This irreversible dynamics is usually characterized by H-theorems and the corresponding molecular viscosities can be derived using Chapman-Enskog expansions.

A typical example is the BBGKY (Bogoliubov-Born-Green-Kirkwood-Yvon) hierarchy where the Lioville equation for N particles is transformed after some manipulations into a chain of equations. The first equation relates the one-particle density probability with the two-particle density probability, the second equation the three with the two and one density probability and so on. This quite complex system (as hard to solve as the original Liouville equation) can be simplified under an additional hypothesis, a *closure* relating the density probability functions. A simple case is the deduction of Boltzmann equation where the fundamental assumption is the hypothesis of *molecular chaos*: the velocities of colliding particles are uncorrelated, and independent of position [56]. Thus that the two-particles density probability is expressed as the product of the one-particle distribution.

This panorama is quite frequent in statistical mechanical. It also occurs when

finding equation for the moments or cumulants of a field following non-linear evolution equations, as Euler or Navier-Stokes. If the non-linearity is quadratic then typically the equation for the n-order cumulant involves the $(n+1)$-cumulant and also those of lower order. Thus at order n the system cannot be solved without a closure. This fundamental problem is perhaps one of the most difficult in turbulence theory.

2.4.1 Basic assumptions

In this section we will describe the main assumptions of one important closure in turbulence: the eddy-damped quasi-normal Markovian theory (EDQNM) [7]. Some results based on EDQNM will then be used in this thesis.

Quasi-Normal theory

The first (and reasonably) hypothesis is the isotropy of the flow. Under this assumption the second order cumulant is completely determined by the energy spectrum $E(k,t)$. By direct manipulation of equation (2.34) we obtain that the energy spectrum satisfies

$$\left[\frac{\partial}{\partial t} + 2\nu k^2\right] E(k,t) = T(k,t) \tag{2.59}$$

$$\left[\frac{\partial}{\partial t} + \nu(k^2+p^2+q^2)\right] T_{\alpha\beta\gamma}(\mathbf{k},\mathbf{p},t) = F_{\alpha\beta\gamma}(\mathbf{k},\mathbf{p},\mathbf{q},t) \tag{2.60}$$

where

$$T(k,t) = -4\pi k^2 k_\rho \, Im\left[\sum_{\mathbf{p}} T_{\sigma\rho\sigma}(\mathbf{k},\mathbf{p},t)\right] \tag{2.61}$$

$$\langle u_\alpha(\mathbf{k},t) u_\beta(\mathbf{p},t) u_\gamma(\mathbf{q},t)\rangle = T_{\alpha\beta\gamma}(\mathbf{k},\mathbf{p},t)\delta(\mathbf{k}+\mathbf{p}+\mathbf{q} \tag{2.62}$$

and $F_{\alpha\beta\gamma}(\mathbf{k},\mathbf{p},\mathbf{q},t)$ is a function of the fourth and second order cumulants.

The next assumption is to assume that the statistics of the Fourier modes are approximately Gaussian with zero mean so the fourth order cumulant can be neglected and therefore $F_{\alpha\beta\gamma}(\mathbf{k},\mathbf{p},\mathbf{q},t)$ is a function only of the second order moments (or $E(k)$). However is it not assumed that third order moment vanishes (as they would be for zero mean Gaussian variable). The application of the Gaussian hypothesis to the fourth but not the third order moment is called *quasi-Gaussian* or *quasi-normal* assumption [2].

The right hand side of equation (2.60) being function only of lower order momentum can be directly integrated:

$$T_{\alpha\beta\gamma}(\mathbf{k},\mathbf{p},t) = \int_0^t e^{-\nu(k^2+p^2+q^2)(t-s)} F_{\alpha\beta\gamma}(\mathbf{k},\mathbf{p},\mathbf{q},s)\, ds. \tag{2.63}$$

[2] This assumption can be justified at low Reynolds number.

Replacing (2.63) in equation (2.61) and then in (2.59) we obtain a closed equation for the energy spectrum. The resulting equation is

$$\left[\frac{\partial}{\partial t}+2\nu k^2\right]E(k,t)=\iint_{\triangle}(xy+z^3)\int_0^t\Theta^0_{kpq}(t-s)[k^2pE(p,s)E(q,s)-p^3E(q,s)E(k,s)]\,ds\frac{dp\,dq}{pq},\tag{2.64}$$

with $\Theta^0_{kpq}(\tau)=e^{-\nu(k^2+p^2+q^2)\tau}$ [3] and $\triangle$ is a strip in p,q space such that the three wavevectors $\mathbf{k}$, $\mathbf{p}$, $\mathbf{q}$ form a triangle. x, y, z, are the cosine of the angles opposite to $\mathbf{k}$, $\mathbf{p}$, $\mathbf{q}$. Figure 2.7 displays a scheme of such triangle and the integration region $\triangle$.

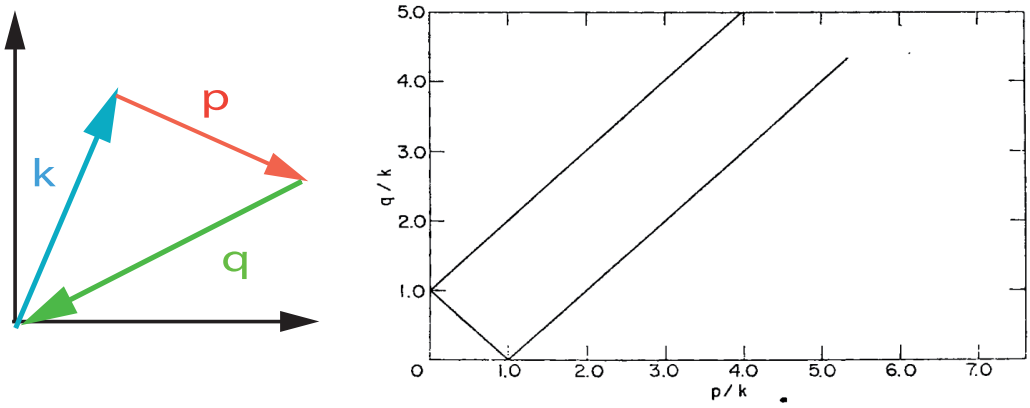

Fig. 2.7: Left: scheme of a triangle formed by the vectors $\mathbf{k}$, $\mathbf{p}$ and $\mathbf{q}$. Right: $\triangle$ strip. Taken from [7].

The main problem of this equation is that the positivity of energy spectrum is not preserved [4]. The problem is basically due to the long memory of the right hand side of equation (2.64). Nonlinear effects can cut off the interaction more efficiently than the viscosity.

Eddy-damped quasi-normal theory.

The solution to the above problem is to assume Markovianity. This done by dropping the temporal dependence on the past of $E(\cdot,s)$ in equation (2.64) and replacing the viscous time νk^2 by an eddy-damped term η_k which takes into account the nonlinear interaction. The resulting equation is

$$\left[\frac{\partial}{\partial t}+2\nu k^2\right]E(k,t)=\iint_{\triangle}\Theta_{kpq}(xy+z^3)[k^2pE(p,t)E(q,t)p^3E(q,t)E(k,t)]\frac{dp\,dq}{pq}\tag{2.65}$$

[3] Note that $\int_0^t\Theta^0_{kpq}(\tau)[\ldots]\,ds$ gives a characteristic time of order $\sim 1/\nu(k^2+p^2+q^2)$.

where the characteristic time Θ_{kpq} is defined by

$$\Theta_{kpq} = \frac{1 - \exp\left(-(\eta_k + \eta_p + \eta_q)t\right)}{\eta_k + \eta_p + \eta_q}. \tag{2.66}$$

In the Eddy-damped quasi-normal (EDQNM) theory the eddy damped η_k is defined as

$$\eta_k = \nu k^2 + \lambda \sqrt{\int_0^k s^2 E(s,t)\, ds}. \tag{2.67}$$

and $\lambda = 0.36$ is the classical value needed to recover the good value for the Kolmogorov constant C_K.

An important property of EDQNM that it is compatible with both Kolmogorov $k^{-5/3}$ law and absolute equilibria. This equation has been the object of many studies because it allows to obtain very large Reynolds number with less computational cost than in DNS [4].

2.4.2 Thermalization

The EDQNM theory has also been used to study the thermalization. Bos and Bertoglio [6] used the EDQNM equation in the inviscid case $\nu = 0$ and similar results to DNS of Cichowlas et al. [5] were obtained. Figure 2.8 displays the temporal evolution under EDQNM of the energy spectrum. The k^4-scaling at large scales correspond to their

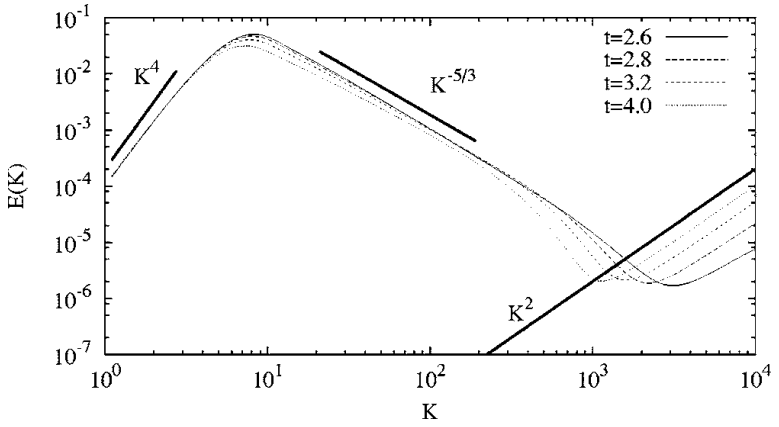

Fig. 2.8: a) Temporal evolution of energy spectrum of EDQNM with a resolution corresponding to 32768^3 of a DNS. Taken from [6].

choice of the initial condition. A large Kolmogorov spectrum range followed by an equipartition zone is observed. The thermalized zone progressively extend to large scales as in DNS of Cichowlas et al. [5].

The EDQNM theory also delivers an analytic expression of the eddy viscosity that was obtained by M. Lesieur and D. Schertzer [57]:

$$\nu_{\text{eddy}} = \frac{1}{15}\int_{k_i}^{k_{max}} \Theta_{kpp}\left[5E(p) + p\frac{\partial E(p)}{\partial p}\right] dp. \tag{2.68}$$

Bos and Bertoglio [6] used the concept of eddy-viscosity to explain the scaling of k_{th} during the thermalization. Using equation (2.68) in the thermalized range ($E(k) \sim E_{\text{th}}k^2/k_{\text{max}}^3$) we obtain that

$$\nu_{\text{eddy}} \sim \frac{\sqrt{E_{\text{th}}}}{k_{\text{max}}}. \tag{2.69}$$

Replacing this eddy-viscosity in the Kolomogorov dissipation scale k_d (Eq. (2.27)), the dissipation scale proposed by Cichowlas et al. in equation (2.58) is immediately recovered. Bos and Bertoglio [6] observed that the temporal evolution of k_d is also in good agreement with k_{th}.

The EDQNM is thus a good tool for understanding the thermalization process of truncated Euler dynamics

2.5 Hyper-viscous limit, bottlenecks and thermalization.

In 2008 Firsch et al. [9] considered the incompressible hyper-viscous Navier-Stokes equation

$$\partial_t \mathbf{u} + (\mathbf{u}\cdot\nabla)\mathbf{u} = -\nabla p - \frac{\nu}{k_G^{2\alpha-2}}\left(-\nabla^2\right)^{\alpha}\mathbf{u} \tag{2.70}$$

$$\nabla\cdot\mathbf{u} = 0. \tag{2.71}$$

and they investigated the hyper-viscous limit $\alpha \to \infty$. In equation (2.70) k_G^{-1} has the dimension of a length.

The hyper-viscous limit of equation (2.70) is closely related to truncated Euler equation. Intuitively, if we write the dissipative term in Fourier space and take the limit we find

$$\nu k_G^2\left(\frac{k}{k_G}\right)^{2\alpha} \xrightarrow[\alpha\to\infty]{} \begin{cases} 0 & \text{if } k < k_G \\ \infty & \text{if } k > k_G. \end{cases}$$

Therefore Fourier modes with wavenumbers smaller than k_G do not feel any dissipation. Those wavenumbers larger than k_G are immediately damped and remains zero just as in the truncated Euler equation. Of course, the preceding argument is intuitive and not a mathematical demonstration. The interaction of modes with k_G is a delicate point, however these interactions are suppressed in the limit $\alpha \to \infty$ in the present case, as argued in reference [9].

When equation (2.70) is forced at large scales it is expected that, for large times a steady state will be reached with a balance between the energy input and the hyper-

viscous dissipation. The behavior of this steady state in the hyper-viscous limit was studied in [9]. To perform DNS for large α is extremely expensive if the different spectral ranges need to be identified. The authors, using the idea that EDQNM reproduce well the dynamics of truncated Euler [6], performed several simulations for different values of α up to $\alpha = 729$ of the corresponding EDQNM equation. Numerical results taken from [9] are presented in figure 2.9. A remarkable fact is observed: a bottleneck takes

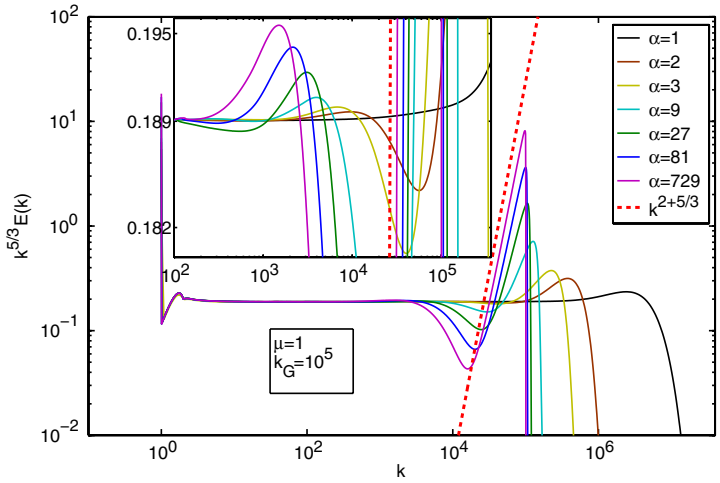

Fig. 2.9: Log-log plots of the compensated spectrum $k^{5/3}E(k)$ versus k from a numerical integration of the hyperviscous EDQNM Eq.(2.70) for different values of α; inset: enlarged spectra showing a secondary bottleneck. Taken from [21].

place in the energy spectra after the inertial range and before to the exponentially fall down at the dissipation scale. This bottleneck increases with α until it reaches a k^2 scaling at large wavenumber as in the truncated Euler equation. Of course, as this is a steady state no progressive thermalization will take place.

Bottlenecks in hydrodynamics turbulence due to an inefficient energy transfer before the dissipative zone has been discussed in [10, 11, 12, 13] (for more reference see reference [21,22] of Frisch et al.[9]). They also have been suggested in reference [15] to exist in superfluid turbulence before entering in the Kelvin waves cascades zone. Frisch et al.[9] thus reinterpreted bottlenecks as an incomplete thermalization.

Two systems where bottlenecks due to thermalized Fourier modes take place at an intermediate range (not as a direct effect of truncation) will be reported in this thesis. The first one is in the two-dimensional magnetohydrodynamics with a strong background magnetic field in chapter 3 and the second one in the long-time dynamics of truncated Gross-Pitaevskii equation studied in chapter 6

2.6 Partial differential equation or a set of ordinary differential equation with many degrees of freedom?

At this point we have developed the basic concepts to understand the relaxation toward the equilibrium of spectrally truncated Euler flows. However there are some crucial aspects in the truncated systems that are sometimes forgotten or even hidden in the scientific literature. The very existence of the UV cut-off $k_{\max}$ is often presented just as numerical artifact. The purpose of this section is to put in evidence, something that becomes clear once explained.

When a smooth field is represented by a truncated Fourier series, there is an implicit assumption supposed. It is that the energy spectrum of the field decays fast enough to ensure that the differences between the truncated Fourier series and the original field are exponentially small in $k_{\max}$ [4]. This is the reason when simulating the Navier-Stokes equation with a given resolution there is maximal Reynolds number permitted. The Kolmogorov dissipative wavenumber (2.27) must satisfy $k_d < k_{\max}$.

The exponential decay becomes very clear if the smooth function can be developed in Fourier series, by the Parseval theorem we have for a function $f \in C^\infty$ that

$$\frac{1}{V}\int |\partial_i^n f(\mathbf{x})|^2 d^D x = \sum_{\mathbf{k}} k_i^{2n} |\hat{f}_{\mathbf{k}}|^2 < \infty, \forall n \in \mathbb{N}. \tag{2.72}$$

It follows then that $\hat{f}_{\mathbf{k}}$ must decay faster than any power. This is of course not the case of absolute equilibria where the energy spectrum grows at large k.

The exponential decay motivates the study of singularities by the logarithmic decrement technics [58]. But in this technic there is a deeper conceptual point about the singularities, clearly explained by Frisch et al in reference [18], whose title says that the singularities are *Not out of the Blue*, meaning that singularities do not suddenly appears, we can see them coming from the complex plane to the real axis. Indeed, if we have a Fourier representation of the field

$$\mathbf{u}(\mathbf{x}, t) = \sum_{\mathbf{k}} e^{i\mathbf{k}\cdot\mathbf{k}} \hat{\mathbf{u}}_{\mathbf{k}}(t), \tag{2.73}$$

we can extend $\mathbf{u}(\mathbf{x}, t)$ to the complex plane replacing $\mathbf{x}$ by $\mathbf{z} = \mathbf{x} + i\mathbf{y}$ as long as the series converges. This automatically define the analyticity strip $\delta(t)$ such that if $|\mathbf{y}| < \delta(t)$ then the series converges. Therefore there is no singularity (in the real axis) if $\delta(t)$ remains positive. That is why mathematical and numerical studies on singularity try to bound $\delta(t)$ inferiorly (or show that it vanishes in a finite time) [16, 17, 18, 19, 20, 21].

It is thus of crucial importance to distinguish between two different regimes when numerical integration is performed. It is known [14] that with a given resolution there is a maximum time where the spectral convergence of truncation is ensured. This time corresponds to the moment when the energy arrives to the smallest scale resolved

[4] Difference meaning for instance the L^2-norm distance.

($\sim k_{\max}^{-1}$) [5]. Beyond this time, once the spectral convergence is lost, the original partial differential equation (PDE) is no anymore, strictly speaking, approximated by the truncated equation. Note that because of thermalization the field is described by an equilibrium probability distribution (Gaussian for truncated Euler) and therefore is not differentiable at any point.

A natural question then arises, why continue with the temporal integration beyond this limit? The answer is that because beyond this time, we are integrating the truncated equations, which are a well posed set of very large number of ordinary differential equation which can share a statistical behavior at small scales with a kind of dissipative large-scale dynamics closely related to the original PDE.

The existence of a thermalized zone is in general, a property of truncated systems and therefore strongly depends on $k_{\max}$. This is a quite general statements, however bottlenecks related to thermalization can be present in a intermediate range if a very inefficient energy transfer is present (see chapter 3 and 6).

To summarize this discussion, if a numerical integration of a PDE (in the strict meaning of the word) is carried, as soon as the energy spectrum starts to rise up at small scales, the integration must be stopped. Larger computers and resolutions are then needed to continue. On the other hand, if one allows the system to thermalize many interesting dynamical effects can be observed in the truncated system that is related to but not strictly the original PDE.

2.7 *Publication:* "Two-fluid model of the truncated Euler equations"

In this section we introduce the publication *"Two-fluid model of the truncated Euler equations"* published during this thesis [35]. In this article we study in detail the thermalization reported in [5, 20] and a quantitative description of the dissipation at large scales in the truncated Euler equation is given.

The article is structured as follows. First, after reviewing the basic definitions, a low-pass filter is introduced allowing the definition of a large-scale velocity $\mathbf{v}^<(\mathbf{x})$ and small-scale velocity $\mathbf{v}^>(\mathbf{x})$. The filter is centered at k_{th} thus $\mathbf{v}^>(\mathbf{x})$ corresponds to thermalized contribution of the velocity. The statistics of the fluctuation $\mathbf{v}^>(\mathbf{x})$ are then studied and shown to be quasi-normal.

Then, using the spectral filter a local heat is defined as

$$Q(\mathbf{r}) = \frac{1}{2}\left[(\mathbf{v}^>)^2\right]^<(\mathbf{r}). \tag{2.74}$$

This field contains the large-scales of the kinetic energy of the thermalized part of the

[5] The smallest energy containing scale correspond in fact to the logarithmic decrement $\delta(t)$, obtained by fitting with a least-square method the logarithm of the energy spectrum at large k with $\log\left[c(t)k^{-m(t)}e^{-2\delta(t)}\right]$. The factor 2 in the exponential is quite obvious from the definition of the analyticity strip.

flow and satisfies by construction $\langle Q(r)\rangle = E_{\rm th}$. It is observed that this field is not homogeneous and follows a diffusion process.

This results motivates the introduction a phenomenological two-fluid model of the truncated Euler equation, where one of the fluids describes the large scale velocity field and the other represents the thermalized high-wavenumber modes, described by a temperature field T:

$$\begin{aligned}
\partial_t v_i^< + v_j^< \partial_j v_i^< &= -\partial_i \tilde{p} + \partial_j \sigma'_{ij} && (2.75)\\
\partial_i v_i^< &= 0 && (2.76)\\
\partial_t T + v_j^< \partial_j T &= \mathcal{D}T + \frac{1}{2c}\left(\partial_j v_i^< + \partial_i v_j^<\right)\sigma'_{ij} && (2.77)
\end{aligned}$$

where

$$\begin{aligned}
\sigma'_{ij} &= \mathcal{F}^{-1}[\nu_{\rm eff}(k)(ik_i\hat{v}_j^< + ik_j\hat{v}_i^<)] && (2.78)\\
\mathcal{D}T &= \mathcal{F}^{-1}[-k^2 D_{\rm eff}(k)\mathcal{F}[T]] && (2.79)
\end{aligned}$$

and $\mathcal{F}[\cdot]$ denotes the Fourier transform and σ'_{ij} is a generalized form of the standard viscous strain tensor [54].

The effective viscosity $\nu_{\rm eff}$ and thermal diffusion $D_{\rm eff}(k)$ of the model are then determined using the EDQNM closure and Monte-Carlo numerical computations. These diffusivities are found to be time and wavenumber dependent.

Once this model is established, it is directly compared to the original data coming from the temporal evolution of truncated Euler equation and it was found to be in good agreement.

Available online at www.sciencedirect.com
ScienceDirect
Physica D 237 (2008) 2015–2019
PHYSICA D
www.elsevier.com/locate/physd

Two-fluid model of the truncated Euler equations

Giorgio Krstulovic*, Marc-Étienne Brachet

Laboratoire de Physique Statistique de l'Ecole Normale Supérieure, Associé au CNRS et aux Universités Paris VI et VII, 24 Rue Lhomond, 75231 Paris, France

Available online 17 November 2007

Abstract

A phenomenological two-fluid model of the (time-reversible) spectrally-truncated $3D$ Euler equation is proposed. The thermalized small scales are first shown to be quasi-normal. The effective viscosity and thermal diffusion are then determined, using EDQNM closure and Monte-Carlo numerical computations. Finally, the model is validated by comparing its dynamics with that of the original truncated Euler equation.

PACS: 47.27.eb; 47.27.em; 47.15.ki

Keywords: Truncated Euler equations; Absolute equilibrium; EDQNM

1. Introduction

It is well known that the (inviscid and conservative) truncated Euler equation admits absolute equilibrium solutions with Gaussian statistics, equipartition of kinetic energy among all Fourier modes and thus an energy spectrum $E(k) \sim k^2$ [1]. Recently, Cichowlas et al. [2,3] observed that the Euler equation, with a very large (several hundreds) spectral truncation wavenumber $k_{\max}$, has long-lasting transients which behave just as those of high Reynolds-number viscous flow; in particular they found an approximately $k^{-5/3}$ inertial range followed by a dissipative range. How is such a behaviour possible? It was found that the highest-k modes thermalize at first, displaying a k^2 spectrum. Progressively the thermalized region extends to lower and lower wavenumbers, eventually covering the whole range of available modes. At intermediate times, when the thermalized regime only extends over the highest wavenumbers, it acts as a thermostat that pumps out the energy of larger-scale modes. Note that similar $k^{-5/3}/k^2$ spectra have already been obtained within the Leith model of hydrodynamic turbulence which is a simple differential closure [4], and earlier similar mixed cascade/thermodynamic states (but with spectra different from $k^{-5/3}/k^2$) were discussed in the wave turbulence literature (e.g. [5]).

The purpose of the present work is to build a quantitative two-fluid model for the relaxation of the $3D$ Euler equation. In Section 2, after a brief recall of basic definitions, the statistics of the thermalized small scales are studied during relaxation. They are shown to be quasi-normal. Our new two-fluid model, involving both an effective viscosity and a thermal diffusion, is introduced in Section 3. The effective diffusion laws are then determined, using an EDQNM closure prediction and direct Monte-Carlo computations. The model is then validated by comparing its predictions with the behaviour of the original truncated Euler equation. Finally Section 4 is our conclusion.

2. Relaxation dynamics of truncated Euler equations

2.1. Basic definitions

The truncated Euler equation (1) are classically obtained [1] by performing a Galerkin truncation ($\hat{v}(k) = 0$ for $\sup_\alpha |k_\alpha| > k_{\max}$) on the Fourier transform $\mathbf{v}(\mathbf{x}, t) = \sum \hat{\mathbf{v}}(\mathbf{k}, t) e^{i\mathbf{k}\cdot\mathbf{x}}$ of a spatially periodic velocity field obeying the (unit density) three-dimensional incompressible Euler equations, $\partial_t \mathbf{v} + (\mathbf{v} \cdot \nabla)\mathbf{v} = -\nabla p, \nabla \cdot \mathbf{v} = 0$. This procedure yields the following finite system of ordinary differentials equations for the complex variables $\hat{\mathbf{v}}(\mathbf{k})$ ($\mathbf{k}$ is a 3 D vector of relative integers (k_1, k_2, k_3) satisfying $\sup_\alpha |k_\alpha| \leq k_{\max}$)

$$\partial_t \hat{v}_\alpha(\mathbf{k}, t) = -\frac{i}{2} \mathcal{P}_{\alpha\beta\gamma}(\mathbf{k}) \sum_{\mathbf{p}} \hat{v}_\beta(\mathbf{p}, t) \hat{v}_\gamma(\mathbf{k} - \mathbf{p}, t) \tag{1}$$

* Corresponding author.
E-mail address: krstulov@lps.ens.fr (G. Krstulovic).

0167-2789/$ - see front matter
doi:10.1016/j.physd.2007.11.008

where $\mathcal{P}_{\alpha\beta\gamma} = k_\beta P_{\alpha\gamma} + k_\gamma P_{\alpha\beta}$ with $P_{\alpha\beta} = \delta_{\alpha\beta} - k_\alpha k_\beta / k^2$ and the convolution in (1) is truncated to $\sup_\alpha |k_\alpha| \leq k_{\max}$, $\sup_\alpha |p_\alpha| \leq k_{\max}$ and $\sup_\alpha |k_\alpha - p_\alpha| \leq k_{\max}$.

This time-reversible system exactly conserves the kinetic energy $E = \sum_k E(k,t)$, where the energy spectrum $E(k,t)$ is defined by averaging $\hat{\mathbf{v}}(\mathbf{k}',t)$ on spherical shells of width $\Delta k = 1$,

$$E(k,t) = \frac{1}{2} \sum_{k-\Delta k/2<|\mathbf{k}'|<k+\Delta k/2} |\hat{\mathbf{v}}(\mathbf{k}',t)|^2. \tag{2}$$

2.2. Small scales statistics

Perhaps the most striking result of Cichowlas et al. [2] was the spontaneous generation of a (time dependent) minimum of the spectrum $E(k,t)$ at wavenumber $k_{\rm th}(t)$ where the scaling law $E(k,t) = c(t)k^2$ starts. Thus, the energy dissipated from large scales into the time dependent statistical equilibrium is given by

$$E_{\rm th}(t) = \sum_{k_{\rm th}(t)<k} E(k,t). \tag{3}$$

In this section we use the so-called Taylor–Green [6] initial condition to (1): the single-mode Fourier transform of $u^{\rm TG} = \sin x \cos y \cos z$, $v^{\rm TG} = -u^{\rm TG}(y,-x,z)$, $w^{\rm TG} = 0$.

In order to separate the dynamics of large-scale ($k < k_{\rm th}$) and the statistics of small-scales ($k > k_{\rm th}$) we define the low- and high-pass filtered fields

$$f^<(\mathbf{r}) = \sum_k F(\mathbf{k}) \hat{f}_\mathbf{k} e^{i\mathbf{k}\cdot\mathbf{r}} \tag{4}$$

$$f^>(\mathbf{r}) = 1 - f^<(\mathbf{r}) \tag{5}$$

where $f(\mathbf{r})$ is an arbitrary field and $\hat{f}_k$ its Fourier transform; we have chosen $F(\mathbf{k}) = \frac{1}{2}(1 + \tanh[\frac{|k|-k_{\rm th}}{\Delta k}])$, with $\Delta k = 1/2$.

This filter allows us to define the large-scale velocity field $\mathbf{v}^<$ and the spatially dependent thermalized energy (or heat) associated to quasi-equilibrium. Using the trace of the Reynold's tensor [7], $R_{ij} = \frac{1}{2}(v_i^> v_j^>)^<$, we define the local heat as

$$Q(\mathbf{r}) = \frac{1}{2}\left[(\mathbf{v}^>)^2\right]^<(\mathbf{r}). \tag{6}$$

By construction of the filters, (4) and (5) the heat spatial average is equal to the dissipated energy (3) $\langle Q(r)\rangle = E_{\rm th}$. Fig. 1a shows a $2D$ cut of the heat Q on the surface $z = \frac{\pi}{2}$, where a cold zone is seen to be present at the centre of the impermeable box ($x = [0,\pi]$, $y = [0,\pi]$, $z = [0,\pi]$). An isosurface of the hottest zones is displayed on Fig. 1b. It is apparent on both figures that $Q(\mathbf{r})$ is not spatially homogeneous.

2.3. Heat diffusion

The simplest quantities to study in order to quantify the evolution of Q, are the spatial average $Q(t) = \langle Q(\mathbf{r},t)\rangle$ and the root mean square variation $\Delta Q = \sqrt{\langle (Q^2 - \langle Q\rangle^2)\rangle}$. These quantities are shown in Fig. 2, where that the mean heat is seen

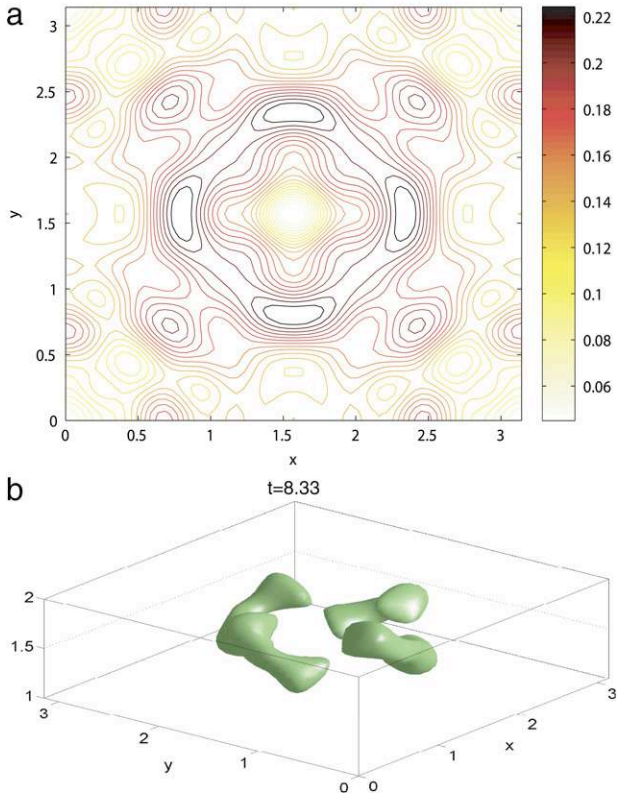

Fig. 1. Cut at $z = \frac{\pi}{2}$ of Q (a) and the isosurface $Q(r) = 0.8 Q_{\max} = 0.42$ (b).

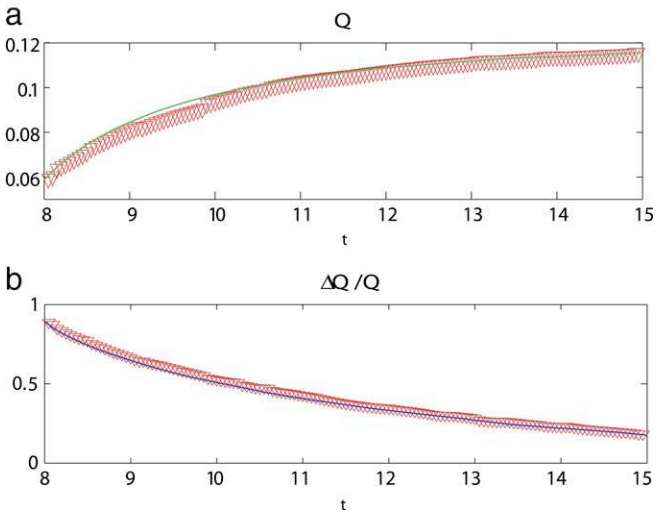

Fig. 2. Plots of $Q(t)$ (a) and $\Delta Q(t)/Q(t)$ (b); solid lines are the results of the two-fluid model (see Section 3).

to increases in time, due to the energy coming from the large eddies, as was shown precedently in [2]. The relative fluctuation $\Delta Q/Q$ is seen to decrease from 0.9 to 0.2.

The next natural question is related to the statistical distribution of the small eddies $v^>$: are they approximately Gaussian, like an absolute equilibrium? A histogram of $v_x^>$ is shown in Fig. 3. As the heat is not homogeneous, we also computed the histogram of the normalized field $\tilde{v}_x^> = v_x^>/\sqrt{Q}$ which seems to better obey Gaussian statistics as can be seen on

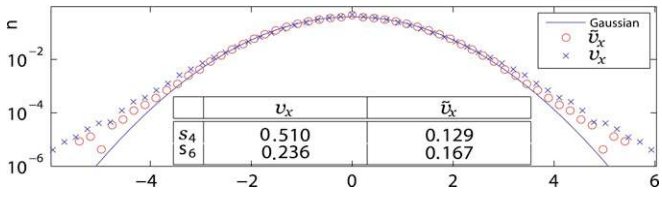

Fig. 3. Histogram of $v_x^>$ and $\tilde{v}_x^>$ and normalized cumulant s_4 and s_6 (odd cumulants vanish because of symmetries).

Fig. 3 and comparing the firsts normalized cumulant $s_n = \frac{c_n}{\sqrt{c_2^n}}$ (c_n is the cumulant of order n) in the table.

3. Two-fluid model

We now introduce our phenomenological two-fluid model of the truncated Euler equation. One of the fluids describes the large scale velocity field and the other represents the thermalized high-wavenumber modes described by a temperature field $T = Q/c$ (c is the specific heat, explicitly given by $c = 8k_{\max}^3$). This model is somewhat analogous to Landau's standard two-fluid model of liquid helium at finite temperature T where there is a natural cut-off wavenumber for thermal excitations: the classical-quantum crossover wavenumber $k_{\max}$ given by $\hbar k_{\max} c_S = k_B T$ (c_S is the sound velocity and k_B Boltzmann's constant). In Landau's model $k_{\max}$ is temperature dependent and the specific heat c is proportional to T^3. In constrast, $k_{\max}$ and the specific heat are constant in our model that reads:

$$\partial_t v_i^< + v_j^< \partial_j v_i^< = -\partial_i \tilde{p} + \partial_j \sigma'_{ij} \tag{7}$$

$$\partial_i v_i^< = 0 \tag{8}$$

$$\partial_t T + v_j^< \partial_j T = \mathcal{D}T + \frac{1}{2c}\left(\partial_j v_i^< + \partial_i v_j^<\right)\sigma'_{ij} \tag{9}$$

where

$$\sigma'_{ij} = \mathcal{F}^{-1}[\nu_{\text{eff}}(k)(ik_i \hat{v}_j^< + ik_j \hat{v}_i^<)] \tag{10}$$

$$\mathcal{D}T = \mathcal{F}^{-1}[-k^2 D_{\text{eff}}(k)\mathcal{F}[T]] \tag{11}$$

and $\mathcal{F}[\cdot]$ denotes the Fourier transform. σ'_{ij} is a generalized form of the standard viscous strain tensor [8]. The precise form of the anomalous diffusion terms ν_{eff} and D_{eff} will be determined below, in Sections 3.1 and 3.2.

The advection terms in Eq. (7) are readily obtained from the Reynolds equations for the filtered velocity by remarking that the diagonal part of the Reynolds stress can, because of incompressibility, be absorbed in the pressure. Eq. (10) represents a simple model of the traceless part of the Reynolds tensor [7]. In the same vein, the advection terms in Eq. (9) are readily obtained together with higher-order moments (see equation (1) of Reference [9]). The dissipation and source terms in (9) are thus simple models of the higher-order moments. It is easy to show that in the present model $\langle \frac{1}{2}\mathbf{v}^{<2} + cT\rangle$ is conserved, corresponding to the energy conservation in the truncated Euler equation.

As the fluctuations $\Delta Q/Q$ are small (see above) we will furthermore assume that ν_{eff} and D_{eff} only depend on $\langle Q\rangle = E_{\text{th}}$. Thus the evolution of the filtered velocity $\mathbf{v}^<$ is independent of the fluctuations ΔQ. As $[E_{\text{th}}] = L^2T^{-2}$, simple dimensional analysis yields the following form for the function ν_{eff} and D_{eff}:

$$\begin{aligned}\nu_{\text{eff}} &= \frac{\sqrt{E_{\text{th}}}}{k_{\max}} f\left(\frac{k}{k_{\max}}, \frac{k_0}{k_{\max}}\right);\\ D_{\text{eff}} &= \frac{\sqrt{E_{\text{th}}}}{k_{\max}} \Psi\left(\frac{k}{k_{\max}}, \frac{k_0}{k_{\max}}\right)\end{aligned} \tag{12}$$

where $k_0 = 2\pi/L_p$ the smallest nonzero wavenumber (L_p is the periodicity length, 2π in the present simulations).

3.1. EDQNM determination of viscosity

An analytical determination of function ν_{eff} is possible using the eddy-damped quasi-Markovian theory (EDQNM) [10]. It is known that this model well reproduces the dynamics of truncated Euler Equation, including the $k^{-5/3}$ and k^2 scalings and the relaxation to equilibrium [11].

The EDQNM closure furnishes an integro-differential equation for the spectrum $E(k,t)$:

$$\frac{\partial E(k,t)}{\partial t} = T_{NL}(k,t) \tag{13}$$

where the nonlinear transfer T_{NL} is modeled as

$$\begin{aligned}T_{NL}(k,t) = \int\int_{\triangle} \Theta_{kpq}(xy+z^3)[k^2 pE(p,t)E(q,t)\\ - p^3 E(q,t)E(k,t)]\frac{\mathrm{d}p\,\mathrm{d}q}{pq}.\end{aligned} \tag{14}$$

In (14) $\triangle$ is a strip in p, q space such that the three wavevectors $\mathbf{k}$, $\mathbf{p}$, $\mathbf{q}$ form a triangle. x, y, z, are the cosine of the angles opposite to $\mathbf{k}$, $\mathbf{p}$, $\mathbf{q}$. Θ_{kpq} is a characteristic time defined as

$$\Theta_{kpq} = \frac{1-\exp(-(\eta_k+\eta_p+\eta_q)t)}{\eta_k+\eta_p+\eta_q} \tag{15}$$

and the eddy damped η is defined as

$$\eta_k = \lambda\sqrt{\int_0^k s^2 E(s,t)\mathrm{d}s}. \tag{16}$$

Classically $\lambda = 0.36$ and the truncation is imposed omitting all interactions involving waves numbers larger than $k_{\max}$ in (14).

A simple and important stationary solution of (13) is the absolute equilibrium with equipartition of the kinetic energy and corresponding spectrum $E(k) \sim k^2$.

To compute the EDQNM effective viscosity ν_{eff} we consider an absolute equilibrium with a small perturbation added in the mode of wavenumber k_{pert} and study the relaxation to equilibrium. The corresponding ansatz is $E(p,t) = \frac{3E_{\text{th}}}{k_{\max}^3}p^2 + \gamma(t)\delta(p-k_{\text{pert}})$ and we suppose $E_{\text{th}} \gg \gamma$, so that the total energy is almost constant and equal to E_{th}.

Using the long time limit of (15) and expanding the EDQNM transfer (14) to first order in γ yields for the delta containing part, after a lengthy but straightforward computation:

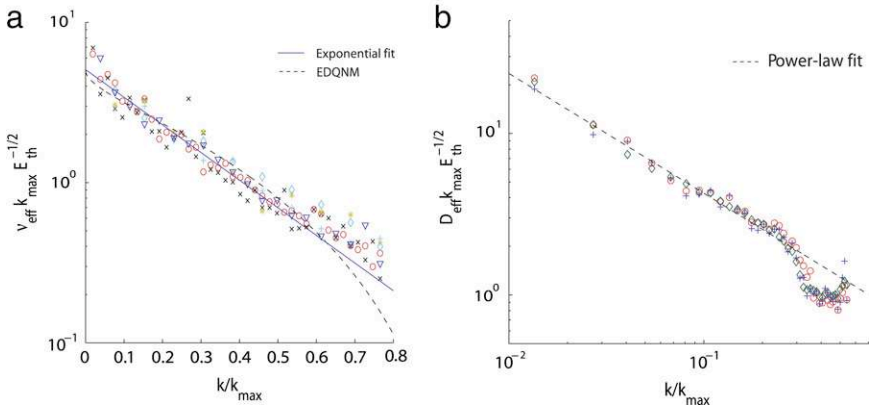

Fig. 4. Effective viscosity $\nu_{\rm eff}$ (a) and thermal diffusivity $D_{\rm eff}$ (b) determined by Monte Carlo computations performed at different values of $E_{\rm th}$ and $k_{\rm max}$ (see text).

$$T_{NL}(k,t) = -\gamma(t)\delta(k-k_{\rm pert})k^2\frac{\sqrt{E_{\rm th}}}{k_{\rm max}}\frac{\sqrt{30}}{\lambda}I\left(\frac{k}{k_{\rm max}}\right) \tag{17}$$

where I is given by the explicit integral

$$I(x) = \sqrt{x} \times \int_1^{\frac{2-x}{x}}\int_{-1}^{1}\frac{(p^2-1)(1-q^2)(q^2+p^2(1+2q^2))}{(p^2-q^2)(2^{\frac{5}{2}}+((p-q)^{\frac{5}{2}}+(p+q)^{\frac{5}{2}}))}\mathrm{d}q\,\mathrm{d}p.$$

Using (13) and (17) and the basic definition of the two-fluid model (7)–(11), we obtain

$$\nu_{\rm eff}(k) = \frac{\sqrt{E_{\rm th}}}{k_{\rm max}}\frac{\sqrt{30}}{2\lambda}I\left(\frac{k}{k_{\rm max}}\right). \tag{18}$$

The function $f(x=\frac{k}{k_{\rm max}},0)$ in (12) is thus given by

$$f(x,0) = \frac{\sqrt{30}}{2\lambda}I(x). \tag{19}$$

In the limit $x \to 0$, it is simple to show that f has a finite value $f(0,0) = \frac{7}{\sqrt{15}\lambda}$. Thus the EDQNM prediction in the small $k/k_{\rm max}$ limit is

$$\nu_{\rm eff} = \frac{\sqrt{E_{\rm th}}}{k_{\rm max}}\frac{7}{\sqrt{15}\lambda}, \tag{20}$$

with $\frac{7}{\sqrt{15}\lambda} = 5.021$ for the classic value of $\lambda = 0.36$. This asymptotic value can also be obtained from the EDQNM eddy viscosity expression calculated by Lesieur and Schertzer [12] using an energy spectrum $E(k) \sim k^2$.

3.2. Monte-Carlo determination of viscosity and thermal diffusion

In order to numerically determine the effective viscosity $\nu_{\rm eff}(k)$ of the two-fluid model, we use a general-periodic code to study the relaxation of an absolute equilibrium perturbed by adding a stationary solution of the Euler equation. We thus consider the initial condition

$$u = \cos kx \sin ky + u_{\rm eq} \tag{21}$$

$$v = -\sin kx \cos ky + v_{\rm eq} \tag{22}$$

$$w = w_{\rm eq} \tag{23}$$

where the (solenoidal and Gaussian) absolute equilibrium velocity field satisfies $\langle u_{\rm eq}^2 + v_{\rm eq}^2 + w_{\rm eq}^2\rangle = 2E_{\rm th}$.

The resulting amplitude of the rotation in (21)–(23) is found, after a short transient, to decay exponentially in time. The function $\nu_{\rm eff}(k)$ is then obtained by finding the halving time τ_k, for which $\hat{v}_\alpha(\mathbf{k}, t_0+\tau_k) = \hat{v}_\alpha(\mathbf{k},t_0)/2$, with t_0 chosen larger than the short transient time. The effective dissipation thus reads

$$\nu_{\rm eff}(k) = \log 2/(k^2\tau_k). \tag{24}$$

The values of $\nu_{\rm eff}(k)k_{\rm max}/\sqrt{E_{\rm th}}$ are shown in Fig. 4a for different values of $E_{\rm th}, k, k_{\rm max}$. A very good agreement with the EDQNM prediction is observed. Note that there is not dependence in the dimensionless parameter $k_0/k_{\rm max}$ (see Eq. (12)).

An exponential fit of all data in Fig. 4a gives

$$\nu_{\rm eff} = 5.0723\frac{\sqrt{E_{\rm th}}}{k_{\rm max}}\mathrm{e}^{-3.97k/k_{\rm max}}. \tag{25}$$

Note that the limit $k/k_{\rm max} \to 0$ is consistent with the EDQNM prediction (20).

Another simple numerical experiment can be used to characterize the thermal diffusion: the relaxation of a spatially-modulated *pseudo*-equilibrium defined by

$$\left\langle u^2+v^2+w^2\right\rangle = 2E_{\rm th} + 2\epsilon\cos(kx) \tag{26}$$

with $\epsilon < E_{\rm th}$.

An x-dependent temperature can be recovered by averaging $u^2+v^2+w^2$ over y and z. Numerical integration of the truncated Euler equation with the initial condition (26) produces an amplitude ϵ that decays exponentially, as in the case studied for the determination of effective viscosity. The thermal diffusivity $D_{\rm eff}$ is determined in the same way as in Eq. (24) and the corresponding data are shown in Fig. 4b. A power-law fit gives

$$D_{\rm eff} = 0.7723\frac{\sqrt{E_{\rm th}}}{k_{\rm max}}(k/k_{\rm max})^{-0.74}. \tag{27}$$

The negative exponent in (27) is characteristic of hypodiffusive processes.

We can define an effective Prandtl number as the ratio $P_{\rm eff}(k) = \nu_{\rm eff}(k)/D_{\rm eff}(k)$. The Prandtl number is plotted in

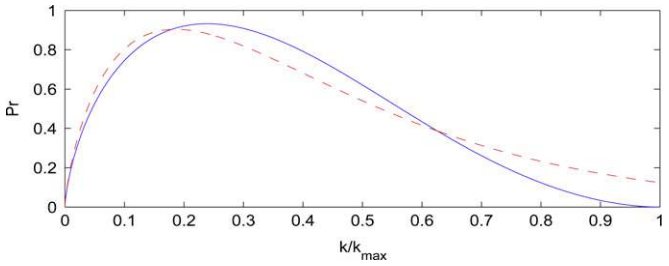

Fig. 5. Effective Prandtl number $P_{\text{eff}} = \nu_{\text{eff}}/D_{\text{eff}}$. (For interpretation of the references to colour in this figure legend, the reader is referred to the web version of this article.)

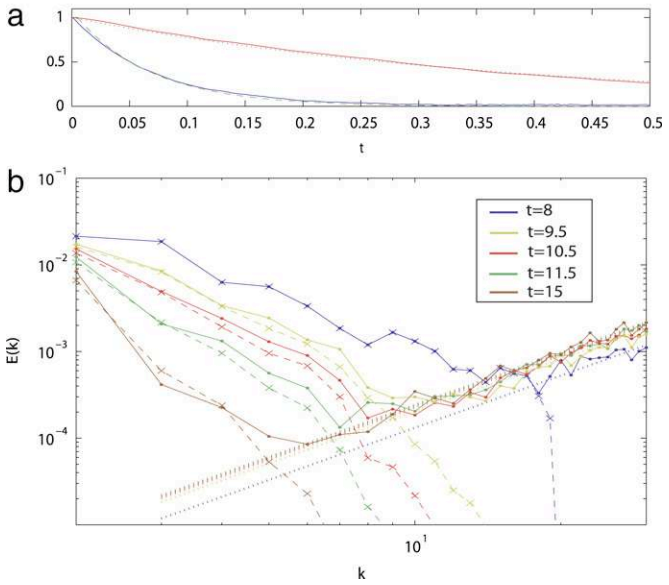

Fig. 6. (a) Time decay of rotation (21) and (22) (upper curve) and temperature modulation (26) (bottom curve). Solid line: truncated Euler equations and dashed line: two-fluid model. (b) Time-evolution of energy spectra, truncated Euler equation: solid lines and two-fluid model: dashed lines. (For interpretation of the references to colour in this figure legend, the reader is referred to the web version of this article.)

Fig. 5, where the solid blue line is obtained using the EDQNM prediction (20) and the fit (27) and the dashed red line is obtained using the fits (25) and (27). Note that the Prandtl vanishes in the the small $k/k_{\max}$ limit and verifies $P_{\text{eff}} < 1$ for all wavenumbers.

3.3. Validation of the model

In this section, numerical integration of the the two-fluid model equations (7)–(11) are performed using a pseudo-spectral code. Time marching is done using second-order leapfrog finite difference scheme and even and odd time-steps are periodically recoupled by fourth-order Runge–Kutta. The effective viscosity and diffusivity are updated at each time step by resetting $E_{\text{th}} = \langle Q \rangle$. The obtained data is compared with that directly produced from the truncated Euler equation.

The time-evolutions resulting from initial data (21) and (22) (in red) and (26) (in blue), both normalized to one and with the same value of E_{th} is displayed on Fig. 6a. Good agreement with the two-fluid model is obtained in both cases and the faster relaxation of the temperature modulation is related to the smallness of $P_{\text{eff}} < 1$.

We now compare, the evolution of non-trivial spectra of the truncated Euler equation (1) and the two-fluid model. The truncated Euler equation is integrated using the Taylor–Green initial data. At $t \sim 8$, when a clear scales separation is present, the large-scale fields $\mathbf{v}^<$ (see Eq. (4)) and the heat Q (Eq. (6)) are computed and used as initial data for the two-fluid model (7)–(11). The subsequent evolution of the two-fluid model is then compared with that of the truncated Euler equation.

Both spectra, plotted in Fig. 6b, are in good agreement. The straights lines represents the thermalized zone $E(k, t) = c(t)k^2$ in the spectrum of the truncated Euler equation, where $c(t)$ is determined by the condition $\langle Q(t) \rangle = \sum_{k>k_{\text{th}}} c(t)k^2$.

The value of $Q(t)$ and $\Delta Q/Q$ are plotted in Fig. 2 (solids lines); the evolution of the fluctuation of the temperature are well reproduced too by the two-fluid model.

4. Conclusion

The thermalized small scales were found to follow a quasi-normal distribution. The effective viscosity was determined, using both EDQNM and Monte Carlo. (Hypo)diffusion of heat was obtained and the effective Prandtl number found to vanish at small $k/k_{\max}$. The two-fluid model was found to be in good quantitative agreement with the original truncated Euler equations.

Acknowledgments

We acknowledge useful discussions with A. Pouquet and the support of ECOS, CONICYT and IDRIS.

References

[1] S. Orszag, Statistical theory of turbulence, in: R. Balian, J.L. Peube (Eds.), Les Houches 1973: Fluid Dynamics, Gordon and Breach, New York, 1977.
[2] C. Cichowlas, P. Bonaïti, M. Brachet, Effective dissipation and turbulence in spectrally truncated euler flows, Phys. Rev. Lett. 95 (26) (2005).
[3] C. Cichowlas, Equation d'Euler tronquée: de la dynamique des singularités complexes à la relaxation turbulente, Université Pierre et Marie Curie - Paris VI, 2005.
[4] C. Connaughton, S. Nazarenko, Warm cascades and anomalous scaling in a diffusion model of turbulence, Phys. Rev. Lett. 92 (4) (2004) 044501.
[5] S. Dyachenko, A. Newell, A. Pushkarev, V.E. Zakharov, Optical turbulence: Weak turbulence, condensates and collapsing filaments in the nonlinear Schrödinger equation, Physica D 57 (1992) 96–160.
[6] G.I. Taylor, A.E. Green, Mechanism of the production of small eddies from large ones, Proc. R. Soc. Lond. A 158 (1937) 499–521.
[7] B. Mohammadi, O. Pironneau, Analysis of the $k - \epsilon$ Turbulence Model, John Wiley & Sons, Masson, 1994.
[8] L. Landau, E. Lifchitz, Mécanique des Fluides, MIR, 1971.
[9] B.E. Launder, G.J. Reece, W. Rodi, Progress in the development of a Reynolds-stress turbulence closure, J. Fluid Mech. 68 (1975) 537–566.
[10] S. Orzag, Analytical theories of turbulence, J. Fluid Mech. 41 (363) (1970).
[11] W.J.T. Bos, J.-P. Bertoglio, Dynamics of spectrally truncated inviscid turbulence, Phys. Fluids 18 (2006) 071701.
[12] M. Lesieur, D. Schertzer, Amortissement auto-similaire d'une turbulence à grand nombre de Reynolds, J. Mec. 17 (1978) 609.

2.8 *Publication:* "Cascades, thermalization, and eddy viscosity in helical Galerkin truncated Euler flows"

We present here the publication *Cascades, thermalization, and eddy viscosity in helical Galerkin truncated Euler flows* made in collaboration with Pablo Mininni and Annick Pouquet [36]. In this work the dynamics of the truncated Euler equations with helical initial conditions is studied. The thermalization studied by Cichowlas et al [5] is thus generalized. With helical flows the thermalization takes place trough a mixed energy and helicity direct cascade.

The Kraichnan absolute equilibrium [3] with non vanishing helicity H is observed at large wavenumber. These absolute equilibrium differs with the one studied in section 2.2.2 by the existence of two temperatures. The probability distribution is

$$P_{\rm st}(\mathbf{u}(\mathbf{k})) = \frac{1}{Z} e^{-\alpha E - \beta H}, \tag{2.80}$$

and the energy and helicity spectra (equation (4) of the article) can be derived from it. Strong helicity effects are found using initial data concentrated at high wavenumbers.

We then compare the truncated Euler run with a Navier-Stokes run and some similarities are found. Using the argument that bottlenecks can be explained by an incomplete thermalization (section 2.5 or Ref. [9]) the excess of relative helicity found at small scales in the viscous run (previously reported in [59]) is related to the thermalization of the truncated helical Euler flow.

The differences that are observed in the behavior of truncated Euler and Navier-Stokes spectra are qualitatively understood using the eddy viscosity (see Sec. 2.4, Eq.2.69)

$$\nu_{\rm eddy} \sim \frac{\sqrt{E_{\rm th}}}{k_{\rm max}} \tag{2.81}$$

that, because of its explicit dependence on $E_{\rm th}$, varies considerably during the thermalization when compared to the constant viscosity of Navier-Stokes run.

Finally, using the scale and time dependent eddy-viscosity computed in the publication *"Two-fluid model of the truncated Euler equations"* [35] the large-scales of the truncated Euler flow are shown to quantitatively follow an effective Navier-Stokes dynamics based on a variable time dependent eddy viscosity.

Cascades, thermalization, and eddy viscosity in helical Galerkin truncated Euler flows

G. Krstulovic,[1] P. D. Mininni,[2,3] M. E. Brachet,[1,3] and A. Pouquet[3]

[1]*Laboratoire de Physique Statistique de l'Ecole Normale Supérieure, associé au CNRS et aux Universités Paris VI et VII, 24 Rue Lhomond, 75231 Paris, France*

[2]*Departamento de Física, Facultad de Ciencias Exactas y Naturales, Universidad de Buenos Aires, Ciudad Universitaria, 1428 Buenos Aires, Argentina*

[3]*NCAR, P.O. Box 3000, Boulder, Colorado 80307-3000, USA*

(Received 4 June 2008; revised manuscript received 23 February 2009; published 6 May 2009)

The dynamics of the truncated Euler equations with helical initial conditions are studied. Transient energy and helicity cascades leading to Kraichnan helical absolute equilibrium at small scales, including a linear scaling of the relative helicity spectrum are obtained. Strong helicity effects are found using initial data concentrated at high wave numbers. Using low-wave-number initial conditions, the results of Cichowlas *et al.* [Phys. Rev. Lett. **95**, 264502 (2005)] are extended to helical flows. Similarities between the turbulent transient evolution of the ideal (time-reversible) system and viscous helical flows are found. Using an argument in the manner of Frisch *et al.* [Phys. Rev. Lett. **101**, 144501 (2008)], the excess of relative helicity found at small scales in the viscous run is related to the thermalization of the ideal flow. The observed differences in the behavior of truncated Euler and (constant viscosity) Navier-Stokes are qualitatively understood using the concept of eddy viscosity. The large scales of truncated Euler equations are then shown to follow quantitatively an effective Navier-Stokes dynamics based on a variable (scale dependent) eddy viscosity.

DOI: 10.1103/PhysRevE.79.056304 PACS number(s): 47.27.Gs, 05.20.Jj

I. INTRODUCTION

The role played by helicity in turbulent flows is not completely understood. Helicity is relevant in many atmospheric processes, such as rotating convective (supercell) thunderstorms, the predictability of which may be enhanced because of its presence [1]. However helicity, which is a conserved quantity in the three-dimensional (3D) Euler equation, plays no role in the original theory of turbulence of Kolmogorov. Later studies of absolute equilibrium ensembles for truncated helical Euler flows by Kraichnan [2] gave support to a scenario where in helical turbulent flows both the energy and the helicity cascade toward small scales [3], a phenomena recently verified in numerical simulations [4–6]. The thermalization dynamics of nonhelical spectrally truncated Euler flows were studied in [7]. Long-lasting transients due to the effect of thermalized small-scales were shown to behave similarly to the dissipative Navier-Stokes (NS) equation. Note that analogous dissipative mechanisms involving small-scale thermalization were proposed in the contexts of lattice gases and superfluidity. The thermalizing quantities are respectively discrete Boolean entities [8] in lattice gases [9] and sound waves in superfluid turbulence [10]. Also note that the Galerkin truncated nonhelical Euler dynamics was recently found to emerge as the asymptotic limit of high-order hyperviscous hydrodynamics and that bottlenecks observed in viscous turbulence may be interpreted as an incomplete thermalization [11].

In this paper we study truncated helical Euler flows and consider the transient turbulent behavior as well as the late time equilibrium of the system. Here is a short summary of our main results. The relaxation toward a Kraichnan helical absolute equilibrium [2] is observed for the first time. Transient mixed energy and helicity cascades are found to take place, while more and more modes gather into the Kraichnan time-dependent statistical equilibrium. The results obtained in [7] for nonhelical flows are extended to the helical case. Strong helicity effects are also found using initial data concentrated at high wave numbers. The concept of eddy viscosity, as previously developed in [7,12], is used to qualitatively explain differences observed between the truncated Euler and high-Reynolds number (fixed viscosity) Navier-Stokes. Finally, the truncated Euler large scale modes are shown to quantitatively follow an effective Navier-Stokes dynamics based on a (time and wave-number dependents) eddy viscosity that does not depend explicitly on the helicity content in the flow.

II. METHODS

Performing spherical Galerkin truncation at wave-number $k_{\max}$ on the incompressible ($\nabla\cdot\mathbf{u}=0$) and spatially periodic Euler equation $\partial_t\mathbf{u}+(\mathbf{u}\cdot\nabla)\mathbf{u}=-\nabla p$ yields the following finite system of ordinary differential equations for the Fourier transform of the velocity $\hat{\mathbf{u}}(\mathbf{k})$ ($\mathbf{k}$ is a 3D vector of relative integers satisfying $|\mathbf{k}|\leq k_{\max}$):

$$\partial_t\hat{u}_\alpha(\mathbf{k},t)=-\frac{i}{2}\mathcal{P}_{\alpha\beta\gamma}(\mathbf{k})\sum_{\mathbf{p}}\hat{u}_\beta(\mathbf{p},t)\hat{u}_\gamma(\mathbf{k}-\mathbf{p},t), \qquad (1)$$

where $\mathcal{P}_{\alpha\beta\gamma}=k_\beta P_{\alpha\gamma}+k_\gamma P_{\alpha\beta}$ with $P_{\alpha\beta}=\delta_{\alpha\beta}-k_\alpha k_\beta/k^2$.

This time-reversible system exactly conserves the energy $E=\Sigma_k E(k,t)$ and helicity $H=\Sigma_k H(k,t)$, where the energy and helicity spectra $E(k,t)$ and $H(k,t)$ are defined by averaging, respectively $\frac{1}{2}|\hat{\mathbf{u}}(\mathbf{k}',t)|^2$, and $\hat{\mathbf{u}}(\mathbf{k}',t)\cdot\hat{\omega}(-\mathbf{k}',t)$ ($\omega=\nabla\times\mathbf{u}$ is the vorticity) on spherical shells of width $\Delta k=1$. It is trivial to show from the definition of vorticity that $|H(k,t)|\leq 2kE(k,t)$.

We will use as initial condition $\mathbf{u}_0$ the sum of the two Arnold, Beltrami, and Childress (ABC) flows in the modes $k=3$ and $k=4$,

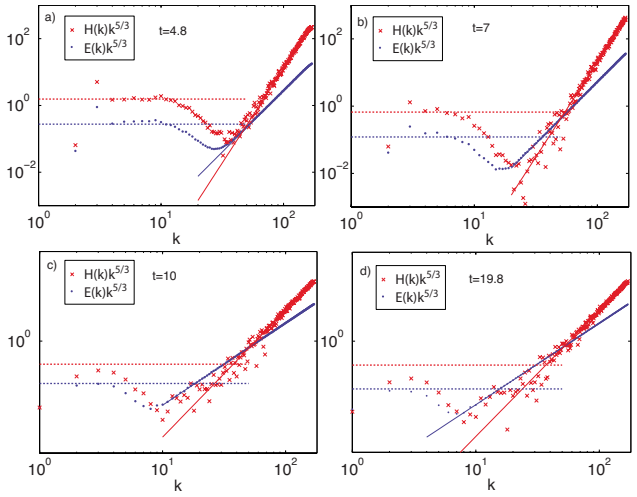

FIG. 1. (Color online) Compensated energy (•••) and helicity spectra (×××) with the predictions [Eq. (4)] in solid lines and Eq. (6) in dotted lines. (a) $t=4.8$. (b) $t=7$. (c) $t=10$. (d) $t=19.8$.

$$\mathbf{u}_0(x,y,z) = \mathbf{u}^{(3)}_{\mathrm{ABC}}(x,y,z) + \mathbf{u}^{(4)}_{\mathrm{ABC}}(x,y,z), \tag{2}$$

where the basic ABC flow is a maximal helicity stationary solution of Euler equations in which the vorticity is parallel to the velocity, explicitly given by

$$\begin{aligned}\mathbf{u}^{(k)}_{\mathrm{ABC}}(x,y,z) = \frac{u_0}{k^2}\{&[B\cos(ky) + C\sin(kz)]\hat{x}\\ &+ [C\cos(kz) + A\sin(kx)]\hat{y}\\ &+ [A\cos(kx) + B\sin(ky)]\hat{z}\}.\end{aligned} \tag{3}$$

The parameters will be set to $A=0.9$, $B=1$, $C=1.1$, and $u_0 = (A^2+B^2+C^2)^{-1/2}(1/3^4+1/4^4)^{-1/2}$. With this choice of normalization the initial energy is $E=0.5$ and helicity $H=3\times4\times(3^3+4^3)/(3^4+4^4)=3.24$.

Numerical solutions of Eq. (1) are efficiently produced using a pseudospectral general-periodic code [13] with 512^3 Fourier modes that is dealiased using the 2/3 rule [14] by spherical Galerkin truncation at $k_{\max}=170$. The equations are evolved in time using a second-order Runge-Kutta method, and the code is fully parallelized with the message passing interface (MPI) library. The numerical method used is nondispersive and conserves energy and helicity with high accuracy.

III. SIMULATIONS

Figure 1 shows the time evolution of the energy and helicity spectra that evolve from Eq. (2) compensated by $k^{5/3}$. The plots clearly display a progressive thermalization similar to that obtained in Cichowlas *et al.* [7] but with the nonzero helicity cascading to the right.

The truncated Euler equation dynamics is expected to reach at large times an absolute equilibrium that is a statistically stationary Gaussian exact solution of the associated Liouville equation [15,16]. When the flow has a nonvanishing helicity, the absolute equilibria of the kinetic energy and helicity predicted by Kraichnan [2] are

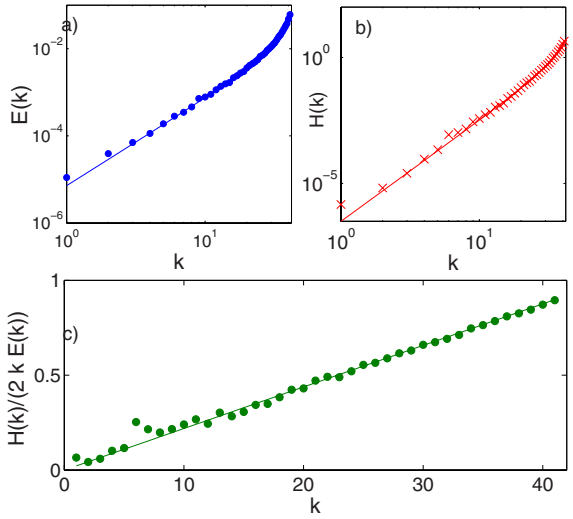

FIG. 2. (Color online) Thermalized energy at $t=21$ for a run with (a) $k_{\max}=42$, (b) helicity, and (c) relative helicity spectra with the predictions [Eq. (4)] (solid lines) corresponding to initial condition (2) but with wave numbers [3,4] changed to [28, 30].

$$E(k) = \frac{k^2}{\alpha}\frac{4\pi}{1-\beta^2k^2/\alpha^2}, \quad H(k) = \frac{k^4\beta}{\alpha^2}\frac{8\pi}{1-\beta^2k^2/\alpha^2}, \tag{4}$$

where $\alpha>0$ and $\beta k_{\max}<\alpha$ to ensure integrability. The values of α and β are uniquely determined by the total amount of energy and helicity (verifying $|H|\le 2k_{\max}E$) contained in the wave-number range $[1,k_{\max}]$ [2].

The final values of α and β (when total thermalization is obtained) corresponding to the initial energy and helicity are $\alpha=4.12\times10^7$ and $\beta=7695$. Therefore the dimensionless number β^2k^2/α^2 is at most of the order 10^{-4} and Eq. (4) thus lead to almost pure power laws for the energy and helicity spectra, as is manifested in Fig. 1(d). Figure 1 thus shows a time evolving helical quasiequilibrium. The Kraichnan prediction [Eq. (4)] for the high-k part of the spectra are shown (in solid lines) in Fig. 1. The plot shows an excellent agreement with the prediction.

To obtain stronger helicity effects requires a different type of initial data. Modifying in the initial condition [Eq. (2)] the wave numbers [3,4] to [28,30] and running with $k_{\max}=42$ yields $\beta^2k_{\max}^2/\alpha^2=0.846$. The final energy, helicity, and relative helicity spectra are displayed in Fig. 2, where strong helicity effects are apparent. The results are again consistent with the prediction given by Eq. (4). However note that these strong effects were obtained using initial data with $k_0 \sim k_{\max}$ that precludes the cascading of the initial energy and helicity to much higher wave numbers.

IV. THERMALIZED ENERGY AND HELICITY

In order to study the thermalization dynamics of the main run presented in Fig. 1 in the spirit of Cichowlas *et al.* [7], we define $k_{\mathrm{th}}(t)$ as the wave number where the thermalized power-law zone starts. We define the thermalized energy and helicity as

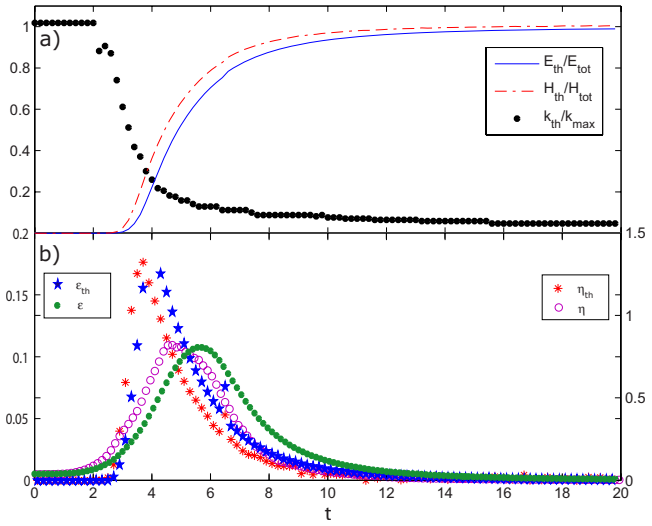

FIG. 3. (Color online) (a) Temporal evolution of $E_{\rm th}$ (–), $H_{\rm th}$ (·–·), and $k_{\rm th}(t)$ (···) normalized by their respective initial values. $E_{\rm tot}=0.5$, $H_{\rm tot}=3.24$, and $k_{\rm max}=170$. (b) Left vertical axis: temporal evolution of $\epsilon_{\rm th}=\frac{dE_{\rm th}}{dt}$ (★★★) and Navier-Stokes energy dissipation $\epsilon=2\nu_0\Sigma_{k=1}^{k_{\rm max}}k^2E(k)$ (•••). Right vertical axis: $\eta_{\rm th}=\frac{dH_{\rm th}}{dt}$ (∗∗∗) and NS helicity dissipation $\eta=\nu_0\Sigma_{k=1}^{k_{\rm max}}k^2H(k)$ (∘∘∘).

$$E_{\rm th}(t)=\sum_{k_{\rm th}(t)}^{k_{\rm max}}E(k,t),\quad H_{\rm th}(t)=\sum_{k_{\rm th}(t)}^{k_{\rm max}}H(k,t),\tag{5}$$

where $E(k,t)$ and $H(t,k)$ are the energy and helicity spectra.

The temporal evolutions of $E_{\rm th}$,$H_{\rm th}$, and $k_{\rm th}(t)$ are shown in Fig. 3. The values of $\alpha(t)$ and $\beta(t)$ during thermalization can then be obtained from $E_{\rm th}(t)$, $H_{\rm th}(t)$, and $k_{\rm th}(t)$ by inverting the system of Eqs. (5) using $\frac{\beta^2}{\alpha^2}k_{\rm max}^2\ll 1$.

Figures 1 and 3 clearly display a progressive thermalization similar to that obtained in Cichowlas *et al.* [7] but with the nonzero helicity cascading to the right. The low-k part of the compensated spectrum in Fig. 1 presents a flat zone that amounts to $k^{-5/3}$ scaling for both the energy and helicity spectra. This $k^{-5/3}$ behavior was predicted by Brissaud *et al.* [3] in viscous fluids when there are simultaneous energy and helicity cascades. The energy and helicity fluxes, ϵ and η, respectively, determine the prefactor in the inertial range of the spectra:

$$E(k)\sim\epsilon^{2/3}k^{-5/3},\quad H(k)\sim\eta\epsilon^{-1/3}k^{-5/3}.\tag{6}$$

Helical flows have been also studied in high-Reynolds number numerical simulations of the NS equation. Simultaneous energy and helicity cascades leading to the scaling [Eq. (6)] have been confirmed when the system is forced at large scales [4–6].

The energy and helicity fluxes, ϵ and η, at intermediate scales in our truncated Euler simulation can be estimated using the time derivative of the thermalized energy and helicity: $\epsilon_{\rm th}=\frac{dE_{\rm th}}{dt}$ and $\eta_{\rm th}=\frac{dH_{\rm th}}{dt}$, whose temporal evolutions are shown in Fig. 3. The predictions [Eq. (6)] for the low-k part of the spectra are shown (in dotted lines) in Fig. 1. The plot shows a good agreement with the data. Note that Fig. 1(a) corresponds to $t=4.8$ that is just after the time when both the maximum energy and helicity fluxes (to be interpreted below as "dissipation" rates of the nonthermalized components of the energy and the helicity) are achieved, see Fig. 3. In this way $E_{\rm th}$ and $H_{\rm th}$ determine the thermalized part of the spectra, while their time derivative determines an inertial range.

V. DISSIPATION AND TRUNCATED EULER

We now compare the dynamics of the truncated Euler equation with that of the unforced high-Reynolds number NS equation [i.e., Eq. (1) with $-\nu_0k^2\hat{u}_\alpha(\mathbf{k},t)$ added in the right-hand side] using initial condition (2). The viscosity is set to $\nu_0=5\times10^{-4}$, the smallest value compatible with accurate computations using $k_{\rm max}=170$. A behavior qualitatively similar to that of the truncated Euler equation is obtained [see Fig. 3(b)]. However, the maxima of the energy and helicity fluxes (or dissipation rates) occur later and with smaller values.

We referred above to dissipation in the context of the ideal (time-reversible) flow. A proper definition of dissipation in the truncated Euler flow is now in order. Thermalized modes in truncated Euler are known to provide an eddy viscosity $\nu_{\rm eddy}$ to the modes with wave numbers below the transition wave number [7]. It was shown in [12] that Monte Carlo determinations of $\nu_{\rm eddy}$ are given with good accuracy by the Eddy damped quasinormal Markovian (EDQNM) two-point closure, previously known to reproduce well direct numerical simulation results [17]. For helical flows, the EDQNM theory provides coupled equations for the energy and helicity spectra [18], in which using Eq. (4) in an analogous way to [12] we find a very small correction of $\nu_{\rm eddy}$ that depends on the total amount of helicity and is of order $\Delta\nu_{\rm eddy}/\nu_{\rm eddy}\sim\beta k_{\rm max}/\alpha\sim10^{-2}$. Thus the presence of helicity does not affect significantly the dissipation at large scales and can be safely neglected in the eddy viscosity expressions. Similar results are found in a large-eddy simulation approach to Navier-Stokes dynamics: the adjunction of helical contributions to eddy viscosity was not producing significant changes in the results [19] (note however that such is not the case in the presence of rotation [20]).

The eddy viscosity has a strong dependence in k and can also be obtained, in the limit $k/k_{\rm max}\to0$, from the EDQNM eddy viscosity of Lesieur and Schertzer [21] using here an energy spectrum $E(k)\sim k^2$. The result reads as

$$\nu_{\rm eddy}=\frac{\sqrt{E_{\rm th}}}{k_{\rm max}}\frac{7}{\sqrt{15\lambda}},\tag{7}$$

with $\lambda=0.36$ (the one parameter of the EDQNM approach, chosen as to recover a Kolmogorov constant as measured in the laboratory). The eddy viscosity $\nu_{\rm eddy}$ is thus an increasing function of time, see $E_{\rm th}(t)$ in Fig. 3.

The time evolution of truncated Euler and Navier-Stokes spectra are compared in Fig. 4. At early times the value of $E_{\rm th}$ is very small and therefore the NS viscosity ν_0 is larger than $\nu_{\rm eddy}$, as manifested by the NS dissipative zone in Fig. 4(a). As $E_{\rm th}(t)$ increases, both viscosities become equal ($t=2.7$). Later, at $t=3.8$, the Navier-Stokes spectrum crosses

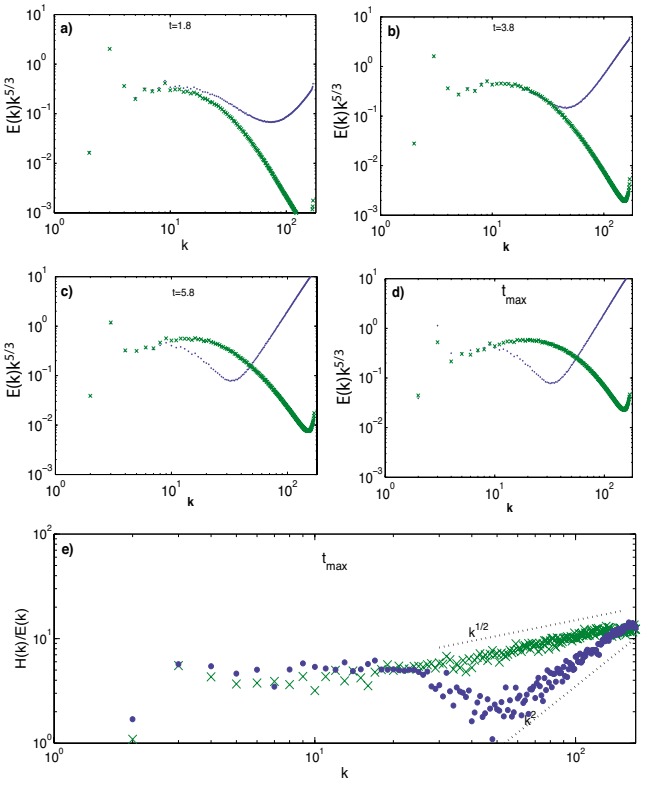

FIG. 4. (Color online) Compensated energy spectra $k^{5/3}E(k)$ of truncated Euler ($\cdots$) and Navier-Stokes ($\times\times\times$). (a) $t=1.8$, (b) $t=3.8$, (c) $t=5.8$. (d) Maximum energy-dissipation time ($t=4.4$ for truncated Euler and $t=5.6$ for NS). (e) Compensated relative helicity spectra $H(k)/E(k)$ of truncated Euler ($\cdots$) and Navier-Stokes ($\times\times\times$) at maximum energy-dissipation time. The dashed black lines show $k^{1/2}$ and k^2 power laws.

the truncated Euler one [Fig. 4(b)]. The eddy viscosity ν_{eddy} is then much larger than ν_0 and the truncated Euler dissipative zone lies below the NS one, see Fig. 4(c). This behavior is also conspicuous when the spectra are compared at maximum energy-dissipation time ($t=4.4$ for truncated Euler and $t=5.6$ for NS), see Fig. 4(d). The corresponding relative helicity spectra $H(k)/[2kE(k)]$, compensated by $2k$, is displayed in Fig. 4(d). A flat compensated spectrum in Fig. 4(d) is apparent throughout the inertial range (up to $k\sim 25$) for both the NS and the truncated Euler runs. This amounts to a scaling of k^{-1} for the relative helicity, corresponding to the previously discussed approximate $k^{-5/3}$ law for both the energy and helicity spectra. As Kraichnan predicted, in the thermalized range of the truncated Euler run the compensated spectrum of relative helicity goes as k^2. At small scales the NS compensated spectrum of relative helicity grows, possibly as $k^{1/2}$ or steeper, indicating, as previously noted (see Fig. 16 of Ref. [6]), that the spectrum of helicity at small scales is dropping slower than the spectrum of energy.

The decay of relative helicity in the inertial range can be interpreted as a recovery of mirror symmetry in the small scales. However, in the thermalized range of the truncated Euler run, the smallest scales have maximum helicity. These two results taken together, along with the arguments of Frisch *et al.* [11] relating bottlenecks to incomplete thermalization, strongly suggest that the excess of relative helicity observed at small scales in viscous runs [the $k^{1/2}$ law of Fig. 4(d)] is related to the phenomenon of thermalization in the ideal runs.

The different time scales of behavior of the truncated Euler and Navier-Stokes runs apparent in Figs. 3 and 4 were qualitatively explained above in terms of the time dependence of ν_{eddy}. We now proceed to check more quantitatively the validity of an effective dissipation description of thermalization in truncated Euler. To wit, we introduce an effective Navier-Stokes equation for which the dissipation is produced by an effective viscosity that depends on time and wave number.

We will use the effective viscosity obtained in [12] which is consistent with both direct Monte Carlo calculations and EDQNM closure and is explicitly given by

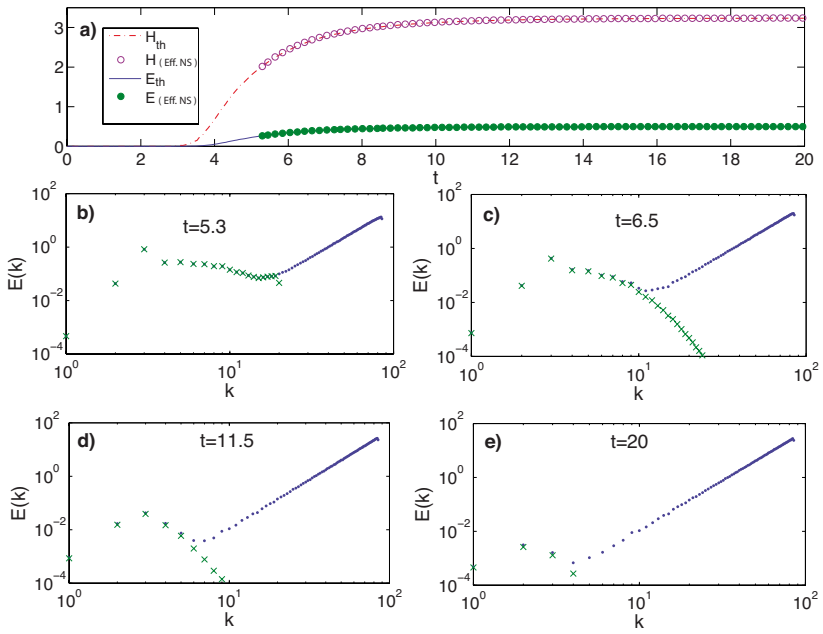

FIG. 5. (Color online) Effective NS run with $k_{\max}=85$. (a) Temporal evolution of E_{th} (–), H_{th} (·–·) from truncated Euler, energy (•••), and helicity (◦◦◦) from effective NS. [(b)–(e)] Temporal evolution of compensated energy spectra of truncated Euler ($\cdots$) and effective Navier-Stokes ($\times\times\times$).

$$\nu_{\text{eff}}(k) = \nu_{\text{eddy}} e^{-3.97k/k_{\max}},$$

with ν_{eddy} given in Eq. (7).

We thus integrate Eq. (1) with the viscous term $-\nu_{\text{eff}}(k)k^2\hat{u}_\alpha(\mathbf{k},t)$ added to the right-hand side. The parameter E_{th} that fixes the eddy viscosity in Eq. (7) is evolved using the effective NS dissipation by

$$\frac{dE_{\text{th}}}{dt} = \sum_{k=1}^{k_{\max}} 2\nu_{\text{eff}}(k)k^2E(k). \tag{8}$$

This ensures consistency between the effective NS dissipated energy and the truncated Euler thermalized energy that drives ν_{eddy}.

To initialize the effective NS equation we integrate the truncated Euler Eq. (1) with initial condition (2) until the k^2-thermalized zone is clearly present ($t=4.77$). The value of E_{th} is then computed using Eq. (5). The low-passed velocity $\mathbf{u}^<$, defined by

$$\mathbf{u}^<(\mathbf{r}) = \sum \frac{1}{2}\{1 + \tanh[2(|\mathbf{k}| - k_{\text{th}})]\}\hat{\mathbf{u}}_\mathbf{k} e^{i\mathbf{k}\cdot\mathbf{r}},$$

is used as initial data for the effective Navier-Stokes dynamics.

Results of a truncated Euler and effective NS with $k_{\max}=85$ are shown in Fig. 5. In Fig. 5(a) the energy and helicity dissipated in effective NS [$E_{\text{tot}}-E(t)$ and $H_{\text{tot}}-H(t)$, respectively] are compared to E_{th} and H_{th} showing a good agreement. Next, the temporal evolution of both energy spectra from the initial time $t=5.3$ [Fig. 5(b)] to $t=20$ [Fig. 5(e)] is confronted, demonstrating that the low-k dynamics of truncated Euler is well reproduce by the effective Navier-Stokes equations.

VI. CONCLUSION

In summary, we observed the relaxation of the truncated Euler dynamics toward a Kraichnan helical absolute equilibrium. Strong helicity effects were found using initial data concentrated at high wave numbers. Using low-wavenumber initial conditions, transient mixed energy, and helicity cascades were found to take place. Eddy viscosity was found to qualitatively explain the different behaviors of truncated Euler and (constant viscosity) Navier-Stokes. The excess of relative helicity at small scales in the viscous run was related to the thermalization in the ideal runs, using an argument in the manner of Frisch *et al.* [11]. The large scale of the Galerkin truncated Euler were shown to quantitatively follow an effective Navier-Stokes dynamics based on a variable helicity-independent eddy viscosity. As a result, with its built-in eddy viscosity, the Galerkin truncated Euler equations appears as a minimal model of turbulence.

ACKNOWLEDGMENTS

We acknowledge discussions with U. Frisch and J. Z. Zhu. P.D.M. acknowledges support from the Carrera del Investigador Científico of CONICET. The computations were carried out at NCAR and IDRIS (CNRS). NCAR was sponsored by NSF. G.K. acknowledges the support of CONICYT.

[1] D. K. Lilly, J. Atmos. Sci. **43**, 126 (1986).
[2] R. H. Kraichnan, J. Fluid Mech. **59**, 745 (1973).
[3] A. Brissaud, U. Frisch, J. Leorat, M. Lesieur, and A. Mazure, Phys. Fluids **16**, 1366 (1973).
[4] V. Borue and S. A. Orszag, Phys. Rev. E **55**, 7005 (1997).
[5] Q. N. Chen, S. Y. Chen, and G. L. Eyink, Phys. Fluids **15**, 361 (2003).
[6] P. D. Mininni, A. Alexakis, and A. Pouquet, Phys. Rev. E **74**, 016303 (2006).
[7] C. Cichowlas, P. Bonaïti, F. Debbasch, and M. E. Brachet, Phys. Rev. Lett. **95**, 264502 (2005).
[8] U. Frisch, B. Hasslacher and Y. Pomeau, Phys. Rev. Lett. **56**, 1505 (1986).
[9] S. Succi, P. Santangelo and R. Benzi, Phys. Rev. Lett. **60**, 2738 (1988).
[10] C. Nore, M. Abid, and M. E. Brachet, Phys. Rev. Lett. **78**, 3896 (1997).
[11] U. Frisch, S. Kurien, R. Pandit, W. Pauls, S. S. Ray, A. Wirth, and J. Z. Zhu, Phys. Rev. Lett. **101**, 144501 (2008).
[12] G. Krstulovic and M. E. Brachet, Physica D **237**, 2015 (2008).
[13] D. O. Gómez, P. D. Mininni, and P. Dmitruk, Phys. Scr. **T116**, 123 (2005); Adv. Space Res. **35**, 889 (2005).
[14] D. Gottlieb and S. A. Orszag, *Numerical Analysis of Spectral Methods: Theory and Applications* (SIAM, Philadelphia, 1977).
[15] S. A. Orszag, J. Fluid Mech. **41**, 363 (1970).
[16] The Liouville equation requires a statistical ensemble of initial data however, by ergodicity, the small scales of *a single* initial condition do statistically equilibrate.
[17] W. J. T. Bos and J.-P. Bertoglio, Phys. Fluids **18**, 071701 (2006).
[18] J. C. André and M. Lesieur, J. Fluid Mech. **81**, 187 (1977).
[19] J. Baerenzung, H. Politano, Y. Ponty, and A. Pouquet, Phys. Rev. E **77**, 046303 (2008).
[20] P. D. Mininni and A. Pouquet, Phys. Rev. E **79**, 026304 (2009); J. Baerenzung, P. D. Mininni, and A. Pouquet (unpublished).
[21] M. Lesieur and D. Schertzer, J. Mec. **17**, 609 (1978).

3. CASCADES AND THERMALIZATION IN TWO-DIMENSIONAL MAGNETOHYDRODYNAMICS

In this chapter we study the thermalization of flows described by the two-dimensional Euler and magnetohydrodynamics (MHD) equations. It is shown that there are some similarities with the three dimensional case, however the relaxation dynamics is richer because of the existence of additional conserved quantities and different cascades. Finally the thermalization of truncated MHD flows with and without a constant magnetic field in the background. When a strong magnetic field is applied, there is a slowdown in the transfer of energy toward small scales and a partial thermalization take place first in an intermediate range. An article in collaboration with Annick Pouquet is in preparation.

3.1 Introduction: Two-dimensional magnetohydrodynamics turbulence

Typically turbulent flows are intrinsically three dimensional and vortical structures are not confined to a plane. However in certain cases there exist a clear scale separation between variations of the fields in one direction and the two others. In these situations one dimension can be safely neglected. This kind of flow idealize geophysical situations as in the Earth atmosphere (with no magnetic field) where flows can be considered as thin layers [60]. Two-dimensional magnetohydrodynamics (MHD) flows can be also relevant to describe solar winds or plasmas [61, 62].

Two-dimensional turbulence has played an important role in the understanding of the underlying physics of turbulence. It has been extensively studied in the last decades of the 20^{th} century. In particular following the work of Kraichnan in the late 60's [2], in which the existence of an inertial range where the kinetic energy is carried from small to large scales was predicted. Two-dimensional turbulence and MHD were also largely studied using numeric simulations because of the relatively easiness to reach large Reynolds numbers and reasonably credible scaling laws [63, 64, 65, 66, 67, 68].

The experimental set-up to achieve two-dimensional turbulence is very difficult, and to obtain a genuine two dimensional system is a hard task. However this experimental area has been very active and well developed studying, in particular, the inverse cascade with soap film and stratified shallow layers of fluids [69, 70, 71, 72]. Large vortical structures keeping their coherence for long periods of time were reported. Figure 3.1

shows one of these structures in an experiment with thin soap film carried out by Couder [69].

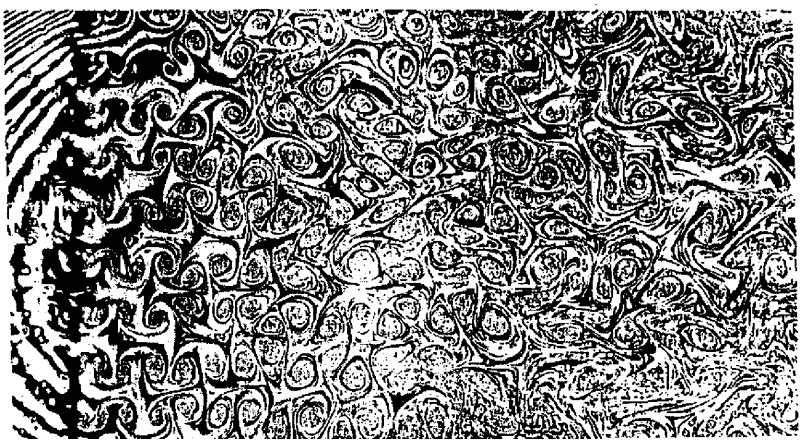

Fig. 3.1: Grid generated turbulence obtained by towing an array of cylinders through a still horizontal soap film. Figure taken from reference [72].

This chapter is organized as follows, first a brief introduction to the basic equations governing the dynamics of incompressible MHD flows is given. The second section is devoted to the study of thermalization of non conducting flows described by the truncated Euler equations. Finally, the third section the thermalization of MHD truncated flows is studied.

3.1.1 Basic equations

When we consider conducting fluids such as plasmas or liquid metals, the flow includes an electromagnetic field which generates currents in the fluid, creating forces and changing the flow itself. The basic hydrodynamics equations of motion for the fluid will then be coupled with the Maxwell equations. The evolution of an incompressible conducting flow of constant density ρ is given by the set of equations

$$\rho\partial_t\mathbf{u} + \rho(\mathbf{u}\cdot\nabla)\mathbf{u} = -\nabla p + \mathbf{j}\times\mathbf{b} + \nu\rho\nabla^2\mathbf{u} \tag{3.1}$$

$$\mathbf{j} = \frac{1}{\mu_0}\nabla\times\mathbf{b} \tag{3.2}$$

$$\partial_t\mathbf{b} = -\nabla\times\mathbf{E} \tag{3.3}$$

$$\frac{1}{\sigma}\mathbf{j} = \mathbf{E} + \mathbf{u}\times\mathbf{b} \tag{3.4}$$

$$\nabla\cdot\mathbf{u} = 0 \qquad \nabla\cdot\mathbf{b} = 0 \tag{3.5}$$

where $\mathbf{b}$ is the magnetic field, $\mathbf{E}$ the electric field, $\mathbf{j}$ the current, μ the magnetic permeability in a vacuum and σ the electrical conductivity.

Defining the magnetic diffusivity $\eta = 1/\sigma\mu_0$, expressing $\mathbf{E}$ as a function of $\mathbf{b}$ and $\mathbf{u}$ and using equations (3.2) and (3.4) we obtain the induction equations

$$\partial_t \mathbf{u} + (\mathbf{u}\cdot\nabla)\mathbf{u} = -\frac{1}{\rho}\nabla p - \frac{1}{\rho\mu_0}\,\mathbf{b}\times(\nabla\times\mathbf{b}) + \nu\nabla^2\mathbf{u} \tag{3.6}$$

$$\partial_t \mathbf{b} = \nabla\times(\mathbf{u}\times\mathbf{b}) + \eta\nabla^2\mathbf{b} \tag{3.7}$$

$$\nabla\cdot\mathbf{u} = 0 \quad , \quad \nabla\cdot\mathbf{b} = 0. \tag{3.8}$$

In the following the magnetic field will be normalized by $\sqrt{\mu_0\rho}$, hence $\mathbf{u}$ and $\mathbf{b}$ have the same dimensions[1]. We will set $\rho = 1$ and consider the fields defined on the domain $[0, 2\pi]^2$ with periodic boundary conditions.

There are three important dimensionless numbers associated with the dynamics of magnetohydrodynamics flows [2]. They are the kinetic Reynolds number Re_{kin}, the magnetic Reynolds number Re_{mag} and the magnetic Prandtl number P_r defined by

$$Re_{\text{kin}} = \frac{u_L L}{\nu} \qquad Re_{\text{mag}} = \frac{u_L L}{\eta} \qquad P_r = \frac{Re_{\text{mag}}}{Re_{\text{kin}}} = \frac{\nu}{\eta} \tag{3.9}$$

where u_L and L are a characteristic velocity and length respectively. The first two number express the ratio of inertial forces to viscous or magnetic diffusion while the magnetic Prandtl number express the ratio of the diffusivities. The existence of an inertial range is expected at large Reynolds numbers and the magnetic Prandtl number varies within a very wide range for different physical system. It is of the order 10^{-5} in the interior of planet and the VKS[3] experiment, 10^{-2} at the convection zone of the sun and 10^{28} in galaxy clusters.

In two-dimensions, due to incompressibility, equations (3.6-3.8) can be written in a much simpler way by introducing a pseudoscalar potential $\psi(x, y, t)$ called the stream function and the magnetic potential $a(x, y, t)$. Using these scalar potential the velocity and magnetic field are expressed as

$$u_x(x, y) = \partial_y\psi(x, y) \qquad u_y(x, y) = -\partial_x\psi(x, y), \tag{3.10}$$

$$b_x(x, y) = \partial_y a(x, y) \qquad b_y(x, y) = -\partial_x a(x, y), \tag{3.11}$$

Replacing the potentials into equations (3.6-3.8), after a little bit of algebra, the induc-

[1] In fact, $\mathbf{b}$ is expressed in terms of Alvén velocity. See subsection 3.1.2 for an Alfvén waves description.

[2] There is another dimensionless number given by the quotient of magnetic and kinetic energy $\langle|\mathbf{b}|^2\rangle/\langle|\mathbf{u}|^2\rangle$. This number will be of order one in the present chapter.

[3] Von-Karman Sodium

tion equations can be rewritten as

$$\frac{\partial \psi}{\partial t} = \frac{1}{\nabla^2}\{\psi, \nabla^2\psi\} - \frac{1}{\nabla^2}\{a, \nabla^2 a\} + \nu\nabla^2\psi \tag{3.12}$$

$$\frac{\partial a}{\partial t} = \{\psi, a\} + \eta\nabla^2 a. \tag{3.13}$$

where $\{f, g\} = \partial_x f \partial_y g - \partial_x g \partial_y f$.

Note that by definition the vorticity and current satisfy

$$\omega(x, y) = \partial_y u_x(x, y) - \partial_x u_y(x, y) = -\nabla^2\psi(x, y) \tag{3.14}$$

$$j(x, y) = \partial_y b_x(x, y) - \partial_x b_y(x, y) = -\nabla^2 a(x, y) \tag{3.15}$$

and similarly the kinetic and magnetic energy read $\frac{1}{2}(u_x(x, y)^2 + u_y(x, y)^2) = \frac{1}{2}|\nabla\psi(x, y)|^2$ and $\frac{1}{2}(b_x(x, y)^2 + b_y(x, y)^2) = \frac{1}{2}|\nabla a(x, y)|^2$.

It is also important to remark that regrouping some terms in equation (3.13) and reintroducing the velocity the magnetic potential satisfies

$$\frac{\partial a}{\partial t} + \mathbf{u} \cdot \nabla a = \eta\nabla^2 a, \tag{3.16}$$

and therefore a it is advected as a passive scalar by the fluid. However note that this does not imply a similar behavior for the magnetic field $\mathbf{b}$.

3.1.2 Alfvén waves

The MHD equations (3.6-3.8) are for incompressible fields, however when a strong magnetic field is imposed to the system magnetic waves propagates in a plane perpendicular to its wave-vector. These perturbations of the magnetic fields are known as Alfvén waves and when considering small amplitudes the MHD equations can be treated perturbatively [73].

Suppose then that a strong constant magnetic field b_0 aligned with x-axe is introduce, replacing $\mathbf{b} \to b_0\hat{x} + \mathbf{b}$ into equations (3.6-3.8) we obtain for the potentials the following evolution equations

$$\frac{\partial \psi}{\partial t} = \frac{1}{\nabla^2}\{\psi, \nabla^2\psi\} - \frac{1}{\nabla^2}\{a, \nabla^2 a\} + b_0\frac{\partial a}{\partial x} + \nu\nabla^2\psi \tag{3.17}$$

$$\frac{\partial a}{\partial t} = \{\psi, a\} + b_0\frac{\partial \psi}{\partial x} + \eta\nabla^2 a. \tag{3.18}$$

For small amplitudes of magnetic and velocity fields equations (3.17-3.18) satisfy the

linear equations

$$\frac{\partial \psi}{\partial t} = b_0 \frac{\partial a}{\partial x} + \nu \nabla^2 \psi \tag{3.19}$$

$$\frac{\partial a}{\partial t} = b_0 \frac{\partial \psi}{\partial x} + \eta \nabla^2 a. \tag{3.20}$$

For the ideal case these equations lead to the Alfvén waves

$$\psi(\mathbf{x}, t) = e^{i(\omega(k)t - \mathbf{k}\cdot\mathbf{x})} \tag{3.21}$$

$$a(\mathbf{x}, t) = -e^{i(\omega(k)t - \mathbf{k}\cdot\mathbf{x})} \tag{3.22}$$

with the dispersion relation $\omega(k) = b_0 k_x = \mathbf{b_0} \cdot \mathbf{k}$ (usually written as $\omega = b_0 k_\parallel$). Note that these waves are exact solutions of the fully non-linear system (3.17-3.18) .

The presence of Alfvén waves modifies the energy spectra, collision between wave packets leads to turbulent cascades. This will be further discussed in section 3.3.2.

The phenomenology of magnetohydrodynamics and hydrodynamics (for non conducting fluid) are very different in the sense that cascades are not the same, scaling laws differ and the inviscid invariants of Euler equation ($\nu = 0$, $\eta = 0$, $b \equiv 0$) are not recovered form the MHD invariants when $b \to 0$. For this reason, each case will be discussed in different sections of the present chapter.

3.2 Two-dimensional turbulence and thermalization

For a non conducting fluid, the induction equations (3.6-3.8) reduce to the Navier-Stokes equation

$$\partial_t \mathbf{u} + (\mathbf{u} \cdot \nabla)\mathbf{u} = \nabla p + \nu \nabla^2 \mathbf{u} \tag{3.23}$$

$$\nabla \cdot \mathbf{u} = 0 \tag{3.24}$$

which, expressed in terms of the stream function, reads

$$\frac{\partial \psi}{\partial t} = \frac{1}{\nabla^2}\{\psi, \nabla^2 \psi\} + \nu \nabla^2 \psi. \tag{3.25}$$

When the viscosity in equation (3.23) or (3.25) is zero we recover the two-dimensional Euler equation.

The conserved quantities of the Euler equation can be easily obtained by using the identity valid for any periodic function f, g, h of class C^1

$$\int f\{g, h\} dx\, dy = \int h\{f, g\} dx\, dy. \tag{3.26}$$

It is straightforward to demonstrate the energy balance

$$\frac{dE_{\rm kin}}{dt} = -2\nu\Omega \tag{3.27}$$

where $E_{\rm kin} = \frac{1}{2}\int |\mathbf{u}|^2\, d^2x$ is the kinetic energy and $\Omega = \frac{1}{2}\int \omega^2\, d^2x$ is the enstrophy. We also have the followings balance relations for the *casimirs*

$$\frac{d\mathcal{C}_n}{dt} = \frac{d}{dt}\int \frac{1}{n}\omega^n(x,y)dx\,dy = \nu\int \omega^{n-1}\nabla^2\omega dx\,dy. \tag{3.28}$$

One of the main differences between two and three dimensional inviscid incompressible hydrodynamics is the appearance of an infinity of new conserved quantities in $2d$. In addition to the energy (helicity vanishes in $2d$) the enstrophy ($n = 2$ in Eq.3.28) plays a fundamental role as another conserved quantity in $2d$ turbulence.

3.2.1 Cascades

Perhaps one of the most striking theoretical results on two-dimensional turbulence, first pointed out in the late 60's by Kraichnan [2], is the possibility of an inverse cascade of energy and a direct enstrophy cascade.

Denoting by ε the net rate of energy transfer and following Kolmogorov [40] assumptions of that the energy spectrum $E(k)$ depends only on ε and k leads to the following energy spectra for the inertial zone

$$E(k) = C_K \varepsilon^{\frac{2}{3}} k^{-5/3}, \tag{3.29}$$

where C_K is a dimensionless constant. Alternatively, assuming that $E(k)$ depends only on the net rate of enstrophy transfer and wave-number k, the corresponding energy spectrum reads

$$E(k) = C_{Kr}\eta^{\frac{2}{3}} k^{-3} \tag{3.30}$$

with C_{Kr} another dimensionless constant. The scaling law (3.30) has actually a logarithmic correction steaming from the highly non-local interactions.

Studying the transfer of energy and enstrophy Kraichnan showed that the $-5/3$ range leads to $\varepsilon < 0$ and the -3 range leads to $\eta > 0$, illustrating the direction of enstrophy and energy cascade.

3.2.2 Two-dimensional truncated Euler equation

The truncated two-dimensional equation is defined here as in previous chapter by performing a spherical Galerkin truncation at wave-number $k_{\rm max}$ on the incompressible and spatially periodic two-dimensional Euler equation. Writing equation (3.25) in Fourier

space the truncated two-dimensional Euler equation reads

$$\frac{\partial \psi_{\mathbf{k}}}{\partial t} = \frac{1}{k^2} \sum_{\mathbf{p},\mathbf{q}} (\mathbf{p} \times \mathbf{q}) q^2 \psi_{\mathbf{p}} \psi_{\mathbf{q}} \delta_{\mathbf{k},\mathbf{p}+\mathbf{q}} \tag{3.31}$$

with $\mathbf{p} \times \mathbf{q} = p_x q_y - p_y q_x$, $\delta_{\mathbf{k},\mathbf{p}}$ the Kronecker delta and where the Fourier modes $\psi_{\mathbf{k}}$ vanish if $|\mathbf{k}| \geq k_{\max}$.

This time-reversible ($t \to -t$, $\psi_{\mathbf{k}} \to -\psi_{\mathbf{k}}$) truncated dynamics also conserves the kinetic energy E and the enstrophy Ω. However, because of truncation the conservation of the other *Casimirs* is lost.

As usual the energy and enstrophy spectra are defined by summing $|\hat{\mathbf{u}}(\mathbf{k}', t)|^2$ and $|\hat{\omega}(\mathbf{k}', t)|^2$ on spherical shells of width $\Delta k = 1$,

$$E(k,t) = \frac{1}{2} \sum_{k-\Delta k/2 < |\mathbf{k}'| < k+\Delta k/2} |\hat{\mathbf{u}}(\mathbf{k}', t)|^2 \tag{3.32}$$

$$\Omega(k,t) = \frac{1}{2} \sum_{k-\Delta k/2 < |\mathbf{k}'| < k+\Delta k/2} |\hat{\omega}(\mathbf{k}', t)|^2 , \tag{3.33}$$

with $\hat{\mathbf{u}}(\mathbf{k}, \mathbf{t})$ and $\hat{\omega}(\mathbf{k}, \mathbf{t})$ the Fourier transforms of the velocity and vorticity fields.

3.2.3 Absolute equilibrium

As in three dimension the $2d$ truncated Euler equation admits statistical stationary solutions known as absolute equilibria. These equilibrium states are an equipartition distribution for the constant of motion [74]

$$\beta\Omega + \alpha E = \sum_{\mathbf{k}} (\beta k^2 + \alpha) |\mathbf{u}(\mathbf{k})|^2. \tag{3.34}$$

This equipartition distribution leads for the energy and enstrophy spectra to the following formulae

$$E(k) = \frac{2\pi k}{\alpha + \beta k^2} \tag{3.35}$$

$$\Omega(k) = \frac{2\pi k^2}{\alpha + \beta k^2}, \tag{3.36}$$

where the factor $2\pi k$ in the numerator comes from the contribution of all wave-numbers of magnitude k.

The *temperatures* α and β are determined by the total energy E_{kin} and enstrophy Ω_{tot} and different values of this quantities lead to very different scaling laws.

3.2.4 Numerical simulations of two-dimensional truncated Euler equation

Thermalization by direct cascade of enstrophy

In this section we numerically study the thermalization of large-scale initial data under the evolution of the truncated Euler equation. The initial condition chosen for this section is

$$\psi(x,y) = \frac{1}{k_a}\sin k_a x \sin k_a y + \frac{2}{k_b}\cos k_b x, \tag{3.37}$$

with the parameters set to $k_a = 1$ and $k_b = 2$.

Numerical solutions of equation (3.31) are efficiently produced using a pseudo-spectral general-periodic code with 1024^2 collocation points that is dealiased using the 2/3 rule [14] by spherical Galerkin truncation at $\mathbf{k}_{\max} = 341$. The equations are evolved in time using a fourth order Runge-Kutta method. The numerical method used is non-dispersive and conserves energy and enstrophy with high accuracy. In the following when we refer to a numerical simulation with a resolution of N^2, $k_{\max} = N/3$ must to be understood (see appendix B for details).

The temporal evolution of the enstrophy spectra is displayed in Figure 3.2. Observe that, as in $3d$, a clear scale separations also appears. The plots clearly display a progressive thermalization with the enstrophy cascading to the right.

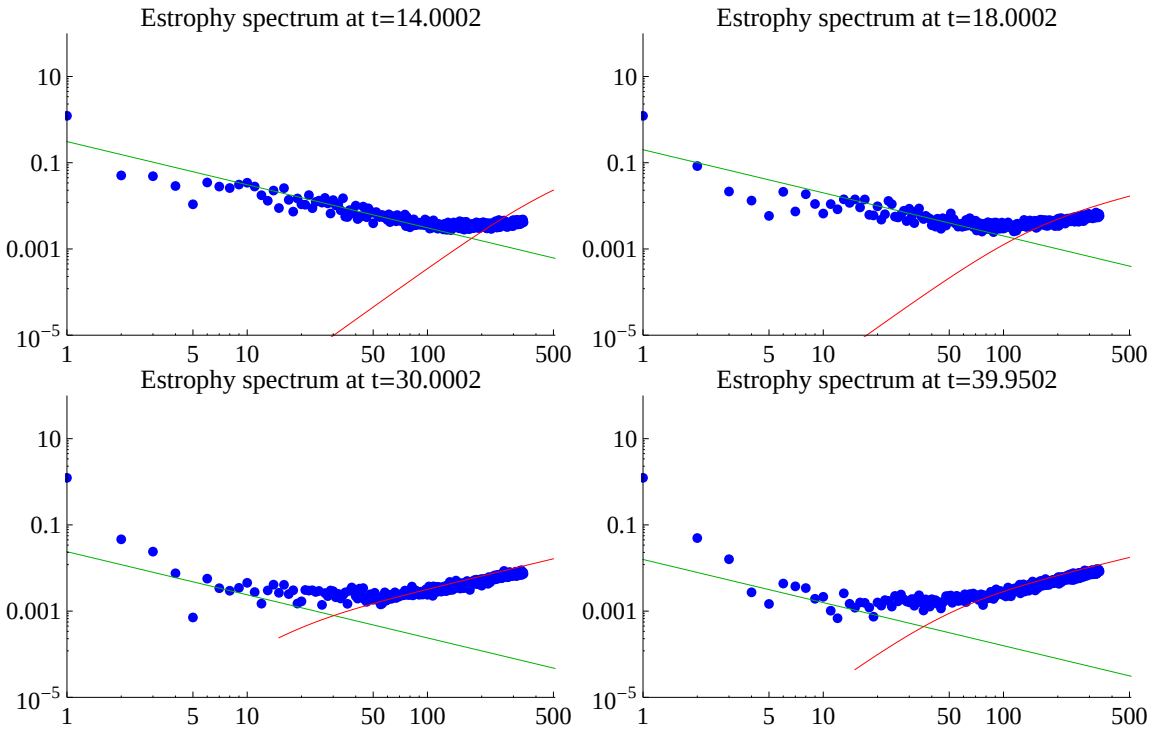

Fig. 3.2: Temporal evolution of enstrophy espectra.

In order to study the thermalization dynamics we define $k_{\rm th}(t)$ as the wave-number where the thermalized power-law zone starts and the thermalized energy and enstrophy as

$$E_{\rm th}(t) = \sum_{k_{\rm th}(t)}^{k_{\rm max}} E(k,t)\,, \qquad \Omega_{\rm th}(t) = \sum_{k_{\rm th}(t)}^{k_{\rm max}} \Omega(k,t). \tag{3.38}$$

The temporal evolution of these two quantities together with $k_{\rm th}$ is displayed on figure 3.3. Note that the thermalized enstrophy increase from zero at early times to an amount

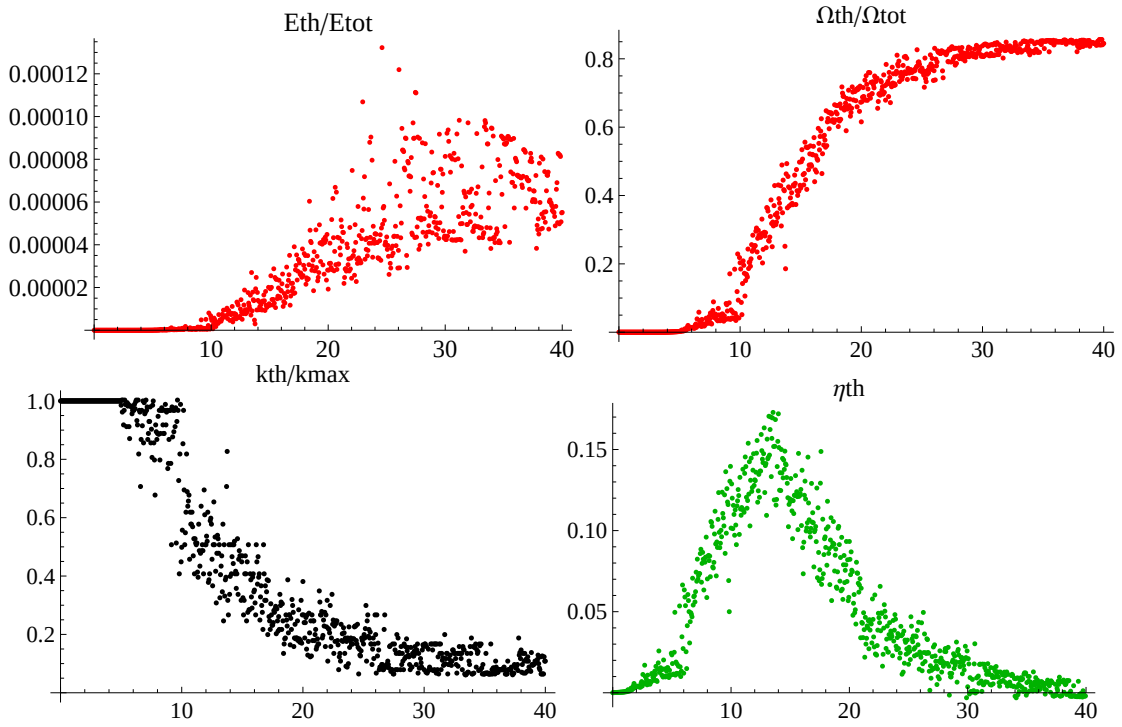

Fig. 3.3: Temporal evolution of $E_{\rm th}/E_{\rm tot}$, $\Omega_{\rm th}\Omega_{\rm tot}$, $k_{\rm th}/k_{\rm max}$ and $\eta_{\rm th} = \frac{d\Omega_{\rm th}}{dt}$

of the order of the total enstrophy available in the system. Using the values of $\Omega_{\rm th}$ and $E_{\rm th}$ we can compute the values of α and β in equation (3.35) and (3.36). The Kraichan absolute equilibria are displayed as solid lines at the small scales of figure 3.2. Observe that they curve down at the left of the thermalized zone. They correspond to the k^3-scaling of the high enstrophy containing absolute equilibria.

At large-scale an enstrophy cascade is taking place and we expect from equation (3.2) a k^{-1}-scaling law. The enstrophy dissipation rate $\eta_{\rm th}$ can be estimated defining it as the time derivative of $\Omega_{\rm th}$. The respective spectra are also displayed as solid lines at large scales on figure 3.2. Observe that in the inertial zone both, scaling law and prefactor, are in good agreement with $\Omega(k) \sim \eta_{\rm th}^{2/3} k^{-1}$.

Note that the relaxation dynamics of two-dimension is *mutatis mutandis* similar to that of in $3d$: a direct cascade of enstrophy (energy in $3d$) followed by an equilibration

of enstrophy (energy in $3d$) at small scale. However a big difference can be observed in the respective spectra before entering in the thermalized zone: there is no dissipative zone in two-dimensions.

This difference can be clarified by simple scaling arguments. In three dimensions, the effective (or eddy) viscosity generated by the thermalized scales was suggested to scale as [6]

$$\nu_{\rm eddy}^{3d} \sim \frac{\sqrt{E_{\rm th}}}{k_{\rm max}}. \tag{3.39}$$

Using this expression for the viscosity the Kolomogorv dissipation scale $k_{\rm d}$ reads

$$k_{\rm d} \sim \left(\frac{\varepsilon}{{\nu_{\rm eddy}^{2d}}^3}\right)^{1/4} \sim \left(\frac{\varepsilon}{E_{\rm th}^{3/2}}\right)^{1/4} k_{\rm max}^{3/4}. \tag{3.40}$$

For the runs studied in $3d$ having a direct cascade of energy [5, 36] the wavenumber scale $\varepsilon/E_{\rm th}^{3/2}$ is of order $(u_I^3/\ell_I)/u_I^3) = k_I$ and does not depend on $k_{\rm max}$. Therefore the Kolmogorov dissipation scale is smaller that $k_{\rm max}$ allowing the existence of a dissipative zone. In two dimensions the situation is different, if there exists an effective viscosity it will be generated by the Fourier modes in the enstrophy thermalized zone. By dimension analysis the effective viscosity would be

$$\nu_{\rm eddy}^{2d} \sim \frac{\sqrt{\Omega_{\rm th}}}{k_{\rm max}^2}. \tag{3.41}$$

In the same way, replacing $\nu_{\rm eddy}^{2d}$ in the Kolomogorv dissipation scale for an enstrophy cascade we obtain

$$k_{\rm d} \sim \left(\frac{\eta^{1/3}}{\nu_{\rm eddy}^{2d}}\right)^{1/2} \sim \left(\frac{\eta^{1/3}}{\Omega_{\rm th}^{1/2}}\right)^{1/2} k_{\rm max}. \tag{3.42}$$

The number $\eta^{1/3}/\Omega_{\rm th}^{1/2}$ is of order for one large-scale initial data and therefore $k_{\rm d} \sim k_{\rm max}$ explaining the absence of a dissipative zone in two-dimensional runs.

More sophisticated arguments for the absence of dissipative zone during the thermalization in two-dimensions can be given by the calculations of the eddy viscosity with EDQNM theory. The EQDNM eddy viscosity felt by the flow at the wave-number k product of the thermalized modes between $k_{\rm th}$ and $k_{\rm max}$ is given by the formula [74]

$$\nu_{\rm eddy}(k|k_{\rm th}) = \frac{\pi}{4}\int_{k_{\rm th}}^{k_{\rm max}} \Theta_{qqk}\frac{d}{dq}[q^2U(q)]dq, \tag{3.43}$$

with $U(q)$ the excitation per mode ($E(k) = \pi k U(k)$) and Θ_{kpq} a characteristic time. The thermalized zone is characterized by an equipartition of enstrophy, it follows then that $q^2U(q) \sim \beta^{-1}$. We obtain thus a vanishing eddy viscosity in (3.43) and consequently no dissipation zone could be observed..

Intermediate-scale initial data

The relaxation toward equilibrium of large-scale initial data by a direct cascade of enstrophy and existence of an inverse energy cascade naturally suggest the study of thermalization of small-scale initial data looking how the energy is carried to large scales.

For numerical study, we chose the initial condition (3.37) with $k_a = k_b = 110$ and resolution of 1024^2. The temporal evolution of the energy spectrum is observed in figure 3.4. The blue straight lines correspond to scalings k^3 and k^{-3} while the red curve correspond to the absolute equilibrium obtained with the total energy $E_{\text{tot}} = 5/4$ and the total enstrophy $\Omega_{\text{tot}} = 18150$ of this run. Observed that, near of $t = 1$ (Fig. 3.4.a),

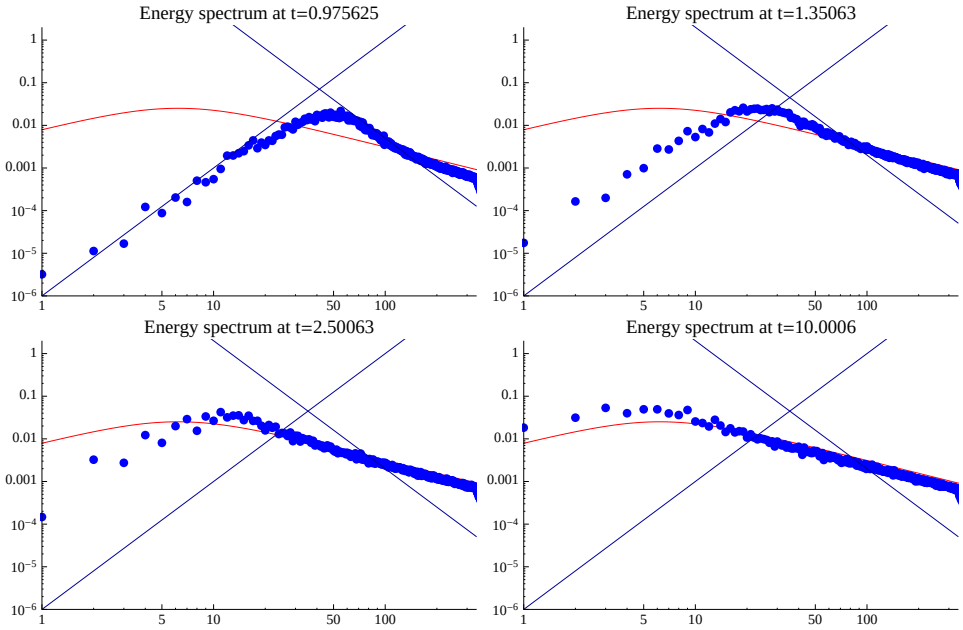

Fig. 3.4: Temporal evolution of energy espectra.

at small scales an enstrophy cascade is taking place and a compatible k^{-3} spectrum followed of an enstrophy equilibration k^{-1} spectrum appears. At large scales the level of the energy spectrum rises following a k^3 scaling low. This correspond to effect of the nonlinear interaction of two large wavenumbers beating a low wavenumber. This forcing correspond to the so called eddy-noise [75]. It is apparent on figure 3.5, where the energy flux is displayed at early times, that no inverse energy cascade is established. Remark that there is a non constant negative flux for large scales and positive flux for highest wave-numbers.

The discrepancies at small wave-numbers in figure 3.4 .d between the absolute equilibrium are probably due theoretical formulae (3.35-3.36) suppose a continuos distribution of wave-number on the sphere at this is not valid for the first modes.

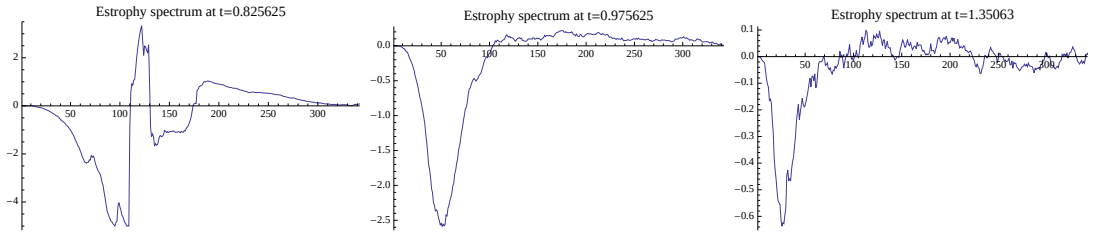

Fig. 3.5: Temporal evolution of energy flux.

Having shown two ways to reach the equilibrium we conclude the study of the thermalization under the dynamics of the two-dimensional truncated Euler equation. The next section is devoted to the study of the whole $2d$ MHD truncated equations.

3.3 Two-dimensional magnetohydrodynamics and thermalization

3.3.1 Two-dimensional MHD equations

We consider now the full set of equations (3.12-3.13) describing the magnetohydrodynamic. In the ideal case ($\nu = 0$, $\eta = 0$) these equations conserve the energy

$$E = \frac{1}{2}\int d^2x \, [|\mathbf{u}|^2 + |\mathbf{b}|^2] \tag{3.44}$$

$$\tag{3.45}$$

and also have an infinite numbers of conserved quantities of the form

$$\mathcal{C} = \int d^2x \, [f(a) + \nabla^2\psi g(a)] \tag{3.46}$$

where f and g are arbitrary functions.

Among these infinity conserved quantities of equation 3.46 two remarkable quantities are obtained for $f(a) = a^2, g(a) = 0$ and for $f(a) = 0, g(a) = a$. The last one is called cross helicity and it is usually written as

$$H_c = \int d^2x \, \mathbf{b} \cdot \mathbf{u}. \tag{3.47}$$

The conserved square magnetic potential will be denoted A.

It is possible to demonstrate that in the ideal case the presence of a constant magnetic field $\mathbf{b_0}$ implies that equations (3.17-3.18) only conserve the total energy and the cross helicity.

As Kraichnan remarked [74], the conserved quantities of MHD equations do not go over into the conserved quantities of hydrodynamics equations except for the total energy. We can expect then a very different behavior, even if the magnetic field is very weak.

3.3.2 MHD turbulent cascades

Here we will summarize the different cascades present in two-dimensional MHD. An inverse cascade of magnetic potential is associated with the conservation of the mean square magnetic potential[63]. Defining $A(k)$ as the magnetic potential spectrum the corresponding Kolmogorov spectrum is

$$A(k) = C_A \varepsilon_A^{2/3} k^{-7/3} \tag{3.48}$$

where ε_A is the rate of square magnetic potential transfer.

The same arguments applied to the energy lead to a $-5/3$ law for both magnetic and kinetic energy spectrum

$$E_{\text{kin}}(k) \approx E_{\text{mag}}(k) \sim C_K \varepsilon^{2/3} k^{-5/3}. \tag{3.49}$$

However Iroshnikov [76] and Kraichnan [77] argued that this similarity scaling is invalid. The presence of Alfven waves introduce an other time scale, that must be take into account. Under the hypothesis of isotropy the Iroshnikov-Kraichnan spectrum reads

$$E_{\text{kin}}(k) \approx E_{\text{mag}}(k) = C_{IK} (\varepsilon b_{\text{rms}})^{1/2} k^{-3/2}. \tag{3.50}$$

where b_{rms} is root mean square magnetic field.

When a strong magnetic field $\mathbf{b_0}$ is applied the assumption of isotropy is not further valid. However, if the velocity and magnetic fluctuation are small compared with $|\mathbf{b_0}|$ the system can be treated analytically with the wave-turbulce approach. This theory gives an anisotropic energy spectrum

$$E(k) \sim k_\perp^{-2}. \tag{3.51}$$

where $k_\perp$ is the component of $\mathbf{k}$ perpendicular to $\mathbf{b_0}$.

Other authors [78] propose that even with a strong magnetic field, the anisotropic Kolmogorov spectrum $E(k) \sim k_\perp^{-5/3}$ can be recovered. This will be possible because due to dynamical effects the eddy turnover time and the Alfvén wave time becomes equal at each scales.

The correct scaling for MHD flow is far from being established, numerical simulations can help to clarify the problem, however the difference between spectra (3.49) and (3.51) are so subtle that to give a clear response requires a delicate study and very high resolution simulations.

3.3.3 Truncated MHD equations

The truncated MHD equations for the pair of Fourier modes $\psi_{\mathbf{k}}$ and $a_{\mathbf{k}}$ are defined in a similar way to the truncated Euler equation

$$\frac{\partial \psi_{\mathbf{k}}}{\partial t} = \frac{1}{k^2}\sum_{\mathbf{p},\mathbf{q}}(\mathbf{p}\times\mathbf{q})q^2\psi_{\mathbf{p}}\psi_{\mathbf{q}}\delta_{\mathbf{k},\mathbf{p}+\mathbf{q}} - \frac{1}{k^2}\sum_{\mathbf{p},\mathbf{q}}(\mathbf{p}\times\mathbf{q})q^2 a_{\mathbf{p}}a_{\mathbf{q}}\delta_{\mathbf{k},\mathbf{p}+\mathbf{q}} \tag{3.52}$$

$$\frac{\partial \psi_{\mathbf{k}}}{\partial t} = -\sum_{\mathbf{p},\mathbf{q}}(\mathbf{p}\times\mathbf{q})\psi_{\mathbf{p}}a_{\mathbf{q}}\delta_{\mathbf{k},\mathbf{p}+\mathbf{q}}, \tag{3.53}$$

with $\mathbf{p}\times\mathbf{q} = p_x q_y - p_y q_x$, $\delta_{\mathbf{k},\mathbf{p}}$ the Kronecker delta and Fourier modes satisfying $\psi_{\mathbf{k}} = 0, a_{\mathbf{k}} = 0$ if $|\mathbf{k}| \geq k_{\max}$.

This truncated system only conserved the quadratic invariants

$$E = \frac{1}{2}\sum_{\mathbf{k}}|\mathbf{u}_{\mathbf{k}}|^2 + |\mathbf{b}_{\mathbf{k}}|^2 = \frac{1}{2}\sum_{\mathbf{k}}k^2(|\psi_{\mathbf{k}}|^2 + |a_{\mathbf{k}}|^2) \tag{3.54}$$

$$H_c = \sum_{\mathbf{k}}\mathbf{u}_{\mathbf{k}}\cdot\mathbf{b}_{-\mathbf{k}} = \sum_{\mathbf{k}}k^2\psi_{\mathbf{k}}a_{-\mathbf{k}} \tag{3.55}$$

$$A = \frac{1}{2}\sum_{\mathbf{k}}|a_{\mathbf{k}}|^2 \tag{3.56}$$

The respective spectra can be defined in analogue way that in the previous section.

3.3.4 Absolute equilibrium of MHD flows

The absolute equilibrium are the equipartition distribution of the invariant [79, 74]

$$\alpha E + \beta A + \gamma H_c = \frac{1}{2}\sum_{\mathbf{k}}(\alpha k^2|\psi_{\mathbf{k}}|^2 + 2\gamma k^2\psi_{\mathbf{k}}a_{-\mathbf{k}} + (\alpha k^2+\beta)|a_{\mathbf{k}}|^2) \tag{3.57}$$

which leads the following equilibrium spectra

$$E_u(k) = \frac{2\pi k}{2}\frac{k^2\alpha+\beta}{k^2(\alpha^2-\gamma^2)+\alpha\beta} \tag{3.58}$$

$$E_b(k) = \frac{2\pi k}{2}\frac{k^2\alpha}{k^2(\alpha-\gamma)(\alpha+\gamma)+\alpha\beta} \tag{3.59}$$

$$H_c(k) = -2\pi k\frac{k^2|\gamma|}{k^2(\alpha-\gamma)(\alpha+\gamma)+\alpha\beta} \tag{3.60}$$

Note that for small values of β and γ we have equipartition of energy $E_v(k) = E_b(k) \sim 2\pi k/\alpha$.

3.3.5 Numerical simulations of two dimensional truncated MHD equations

Thermalization by direct cascade of energy

To study the thermalization by direct cascade of energy we use as initial conditions the so called Orszag-Tang (OT) [64] vortex defined by the potentials

$$\psi(x,y) = 2(\cos x + \cos y) \tag{3.61}$$
$$a(x,y) = 2\cos x + \cos 2y. \tag{3.62}$$

The short time dynamics is identical to that one studied in [65] at resolution of 512^2 Fourier modes (until $t = 1$). We integrate the truncated MHD equation until $t = 20$ using a resolution of 1024^2. The temporal evolution of the kinetic and magnetic energy is displayed on figure 3.6.

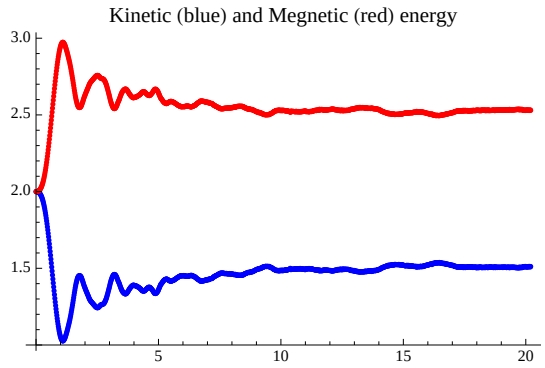

Fig. 3.6: Temporal evolution of $E_{\rm Kin}$ and $E_{\rm mag}$. 1024^2 Fourier modes.

The temporal evolution of kinetic and magnetic energy spectra (compensated by $k^{3/2}$) are shown in figure 3.7. Observe on figure 3.6 that for large time the energies converge to different values. However looking at the energy spectra in figure 3.7 we observe that the difference comes from the large scales.

As in the case of large-scale initial data thermalization under truncated Euler equation evolution, a clear scale separation appears in the energy spectra. It is possible then to define the thermalization wave-number $k_{\rm th}$ and the thermalized total energy (3.38). The temporal evolution of $E_{\rm th}$ is displayed in figure 3.8.a. In a similar way it is also possible to define the thermalized kinetic and magnetic energy but they are indistinguishable as it is apparent from the energy spectra on figure 3.7.

We can estimate then the energy dissipation rate as $\varepsilon_{\rm th} = \frac{dE_{\rm th}}{dt}$. To compare the inertial zone with the spectra of equations (3.49) and (3.51) we first plot the temporal evolution $(\varepsilon_{\rm th}/\max[\varepsilon_{\rm th}])^{3/2}$ and $(b_{\rm rms}\varepsilon/\max[b_{\rm rms}\varepsilon])^{1/2}$ in figure 3.8.b. The scaling laws of equation (3.49) (solid green line) and (3.51) (solid blue line) are displayed in figure 3.7 at large scales. The numerical constant of spectra (3.49) and (3.51) have been set to

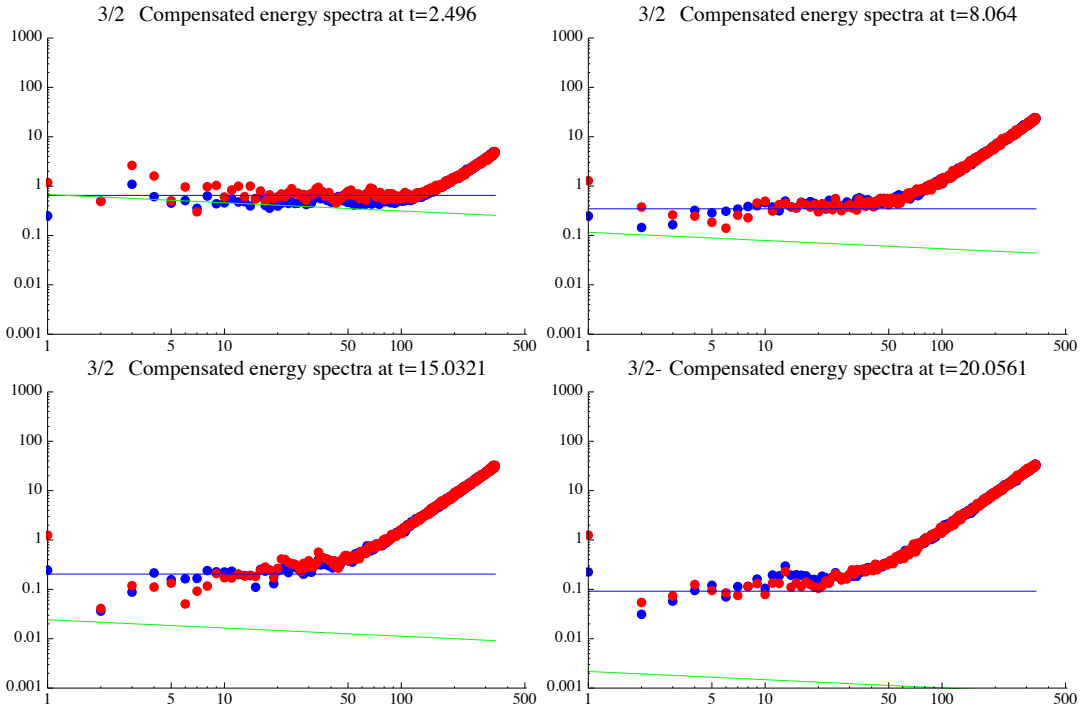

Fig. 3.7: 3/2-compensated kinetic (blue) and magnetic (red) espectra.

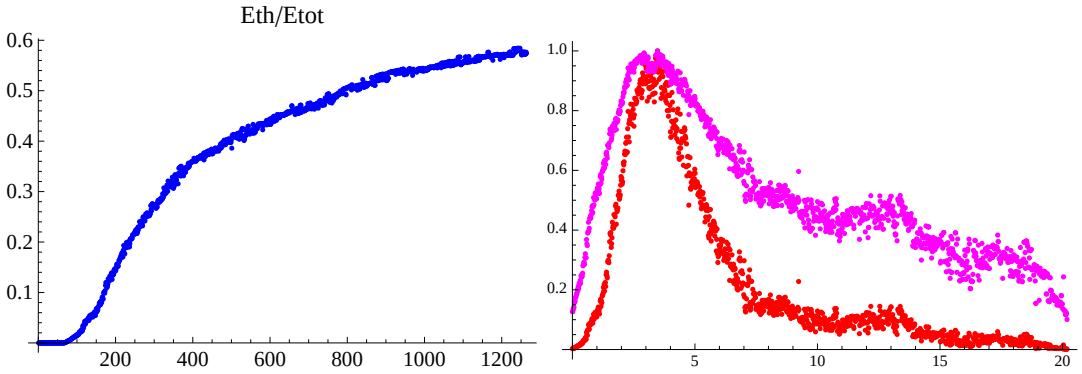

Fig. 3.8: Temporal evolution of a) $E_{\rm th}/E_{\rm tot}$ and c) $\varepsilon/\varepsilon_{\rm max}^{3/2}$ and $(b_{\rm rms}\varepsilon/\max[b_{\rm rms}\varepsilon])^{1/2}$. Resolution of 1024^2.

$C_K = 4$ and $C_{IK} = 0.5$ in order to fit large-scale part of the spectrum at the maximum time of dissipation (Fig. 3.7.a). Remark that the large-scale zone is more in favor of an Iroshnikov-Kraichnan spectrum than a Kolmogorov spectrum.

Remark that in figure 3.7 that as in the truncated Euler equation flows, there is no dissipative zone. This can also be understood by using the EDQNM eddy viscosity. For MHD flow the eddy viscosity acting on velocity field is the sum of the eddy viscosity

ν^{uu}_{eddy} coming from velocity field contribution and ν^{ub}_{eddy} coming from the magnetic field. In the same way, the eddy viscosity acting on the magnetic field is the sum of ν^{bu}_{eddy} and ν^{bb}_{eddy} with obvious notations. Explicitly these eddy viscosities read [63]

$$\nu^{uu}_{\text{eddy}}(k|k_{\text{th}}) = \frac{\pi}{4}\int_{k_{\text{th}}}^{k_{\max}} \Theta_{qqk}\frac{d}{dq}[qE_u(q)]dq \qquad \nu^{ub}_{\text{eddy}}(k|k_{\text{th}}) = \frac{\pi}{4}\int_{k_{\text{th}}}^{k_{\max}} \Theta_{qqk}[3E_b(q) - q\frac{dE_b}{dq}(q)]dq$$
$$\nu^{Bv}_{\text{eddy}}(k|k_{\text{th}}) = \pi\int_{k_{\text{th}}}^{k_{\max}} \Theta_{qqk}E_u(q)dq \qquad \nu^{bb}_{\text{eddy}}(k|k_{\text{th}}) = -\pi\int_{k_{\text{th}}}^{k_{\max}} \Theta_{qqk}E_b(q)dq \tag{3.63}$$

Note that as in the thermalized zone $E_u(q) \approx E_b(q)$ the the eddy viscosity acting on the magnetic field vanish, nevertheless the velocity field feels a non zero eddy viscosity at large scale. By dimensional analysis this eddy viscosity will depend on E_{th} and $k$max as in formula (3.39). Following the same arguments as in the previous section we find the corresponding dissipative scale for the Iroshnikov-Kraichnan spectrum[4]

$$k_d = \left(\frac{\varepsilon}{b_0\nu^2_{\text{eddy}}}\right)^{1/3} \sim \left(\frac{\varepsilon}{b_0 E_{\text{th}}}\right)^{1/3} k^{2/3}_{\max}. \tag{3.64}$$

The EDNQM eddy viscosity thus predicts the existence of dissipative zone that is however not apparent on fig.3.7. This discrepancy may be due to the lack of resolution. In $3D$ truncated Euler the dissipative becomes apparent at resolutions above 256^3 (see refs [35, 5]). We thus expect to observe a dissipative zone in $2D$ truncated MHD in resolutions at or above 4096^2.

The thermalization by a direct cascade of energy presented here, is not a property that is particular to the Orszag-Tang vortex, the same kind of computations were performed with random large-scale initial data with different correlations and similar results were obtained.

Thermalization of small-scale initial data

To study how the equilibrium is reached when the kinetic and magnetic energy is initially located at small scales we perform numerical integration of truncated MHD equations (3.52) and (3.53) using the initial condition

$$\psi(x,y) = \frac{1}{k_a}\sin k_a x \sin k_a y + \frac{2}{k_b}\cos k_b x \tag{3.65}$$
$$a(x,y) = \frac{2}{q_a}\cos q_a x + \frac{1}{q_b}\cos q_b y, \tag{3.66}$$

with $k_a = 160\,, k_b = 321\,, q_a = 319$ and $q_b = 320$. Simulation is performed using a resolution of 1024^2.

[4] k_d is estimated using IK spectrum E_{IK} in the inertial range: $\varepsilon \sim \nu_{eddy}\int^{k_d} E_{\text{IK}}(q)q^2dq$.

The temporal evolution of magnetic potential spectrum is displayed in figure 3.9. Solid lines show $k^{-7/3}$ and k^1 scaling laws. Observe that there is a very fast dynamics,

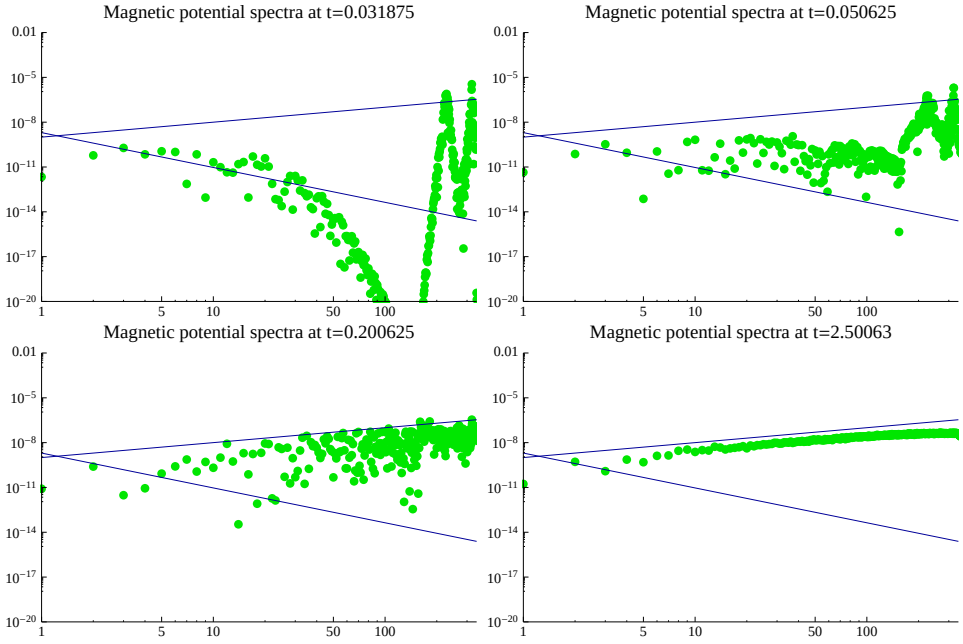

Fig. 3.9: Temporal evolution of magnetic potential spectrum. Solid lines show $k^{-7/3}$ and k^1 scaling laws.

where early large-scale magnetic potential flow is generated, followed by an equipartition of square magnetic potential.

Figure 3.10 shows the temporal evolution of kinetic (blue) and magnetic spectra (red). The solid lines are k^1 and k^3-scaling. Just after the large-scale energy is generated a progressive thermalization form large to small scale is produced. The final state correspond to a equipartition of magnetic potential leading to the k^3-scaling law and a kinetic energy equipartition (k^1-scaling). This absolute equilibrium correspond to formulae (3.58-3.59) with $\gamma \approx 0$ and $\alpha k_{\max}^2/\beta \sim 1$.

3.3.6 Alfvén waves, thermalization and FPUT

It is known that some linear system do not reach equilibrium as was indicated in one of the first numerical simulation carried by Fermi, Pasta, Ulam and Tsingou in the early 50's [80]. They studied a chain of pendulums with a weakly cubic coupling term. They showed that this system does not go to equilibrium and that recurrences appear for the Fourier modes. This can be explained because in the continuum limit the chain satisfies the Korteweg-de Vries equation which is know to posses solitons.

In this section we investigate how the presence of a constant magnetic field modifies the thermalization. Introducing a strong magnetic field the system becomes a quasi one-

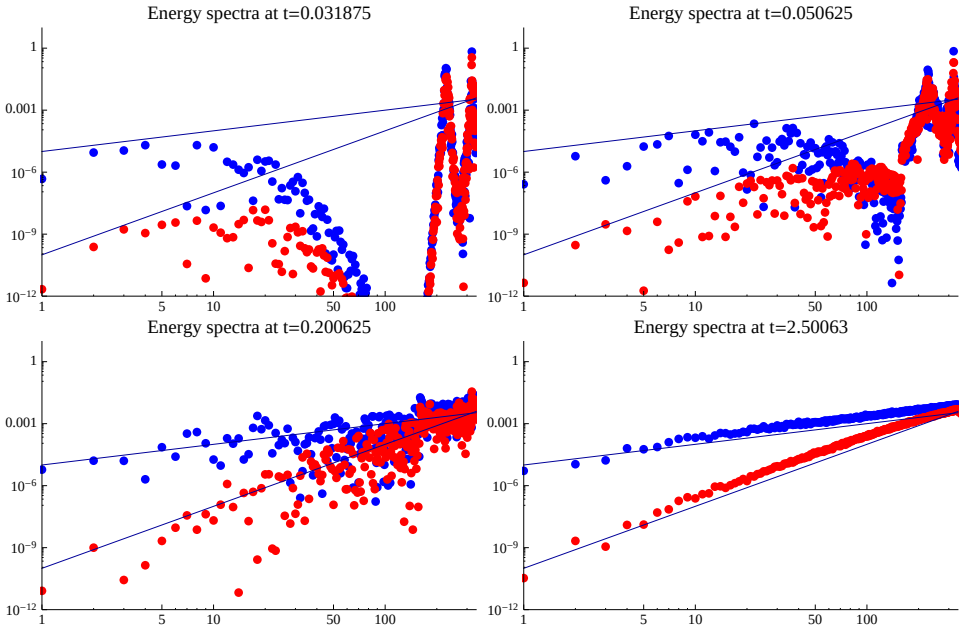

Fig. 3.10: Kinetic (blue) and magnetic (red) espectra. The solid lines are k^1 and k^3-scaling.

dimensional nonlinear wave system and the FPUT problem could thus play a relevant role in the relaxation toward the equilibrium.

We consider the truncated MHD equations in presence of a constant magnetic field $\mathbf{b_0} = b_0\hat{x}$

$$\frac{\partial \psi_{\mathbf{k}}}{\partial t} = \frac{1}{k^2}\sum_{\mathbf{p},\mathbf{q}}(\mathbf{p}\times\mathbf{q})q^2\psi_{\mathbf{p}}\psi_{\mathbf{q}}\delta_{\mathbf{k},\mathbf{p}+\mathbf{q}} - \frac{1}{k^2}\sum_{\mathbf{p},\mathbf{q}}(\mathbf{p}\times\mathbf{q})q^2 a_{\mathbf{p}}a_{\mathbf{q}}\delta_{\mathbf{k},\mathbf{p}+\mathbf{q}} + ib_0k_x a_{\mathbf{k}} \tag{3.67}$$

$$\frac{\partial a_{\mathbf{k}}}{\partial t} = -\sum_{\mathbf{p},\mathbf{q}}(\mathbf{p}\times\mathbf{q})\psi_{\mathbf{p}}a_{\mathbf{q}}\delta_{\mathbf{k},\mathbf{p}+\mathbf{q}} + ib_0k_x\psi_{\mathbf{k}}, \tag{3.68}$$

with $\mathbf{p}\times\mathbf{q} = p_xq_y - p_yq_x$, $\delta_{\mathbf{k},\mathbf{p}}$ the Kronecker delta and the Fourier modes satisfying $\psi_{\mathbf{k}} = 0, a_{\mathbf{k}} = 0$ if $|\mathbf{k}| \geq k_{\max}$.

The problem of how the presence of Alfvén waves can inhibit or slowdown the convergence to equilibrium was (indirectly) studied in reference [65]. The authors were interested in the study of the regularity of $2D$ MHD equation using the logarithmic decrement technic [58] (see chapter 2, section 2.6 for a brief discussion). If the fields are regular then the energy spectra must decay at least exponentially at large wave-number k. Based on this assumption the logarithmic decrement $\delta(t)$ is defined by the large k asymptotic of energy spectra

$$E_u(k) \approx E_b(k) \sim e^{-2\delta(t)k}. \tag{3.69}$$

Therefore we have that the fields remain regular until time t^* if and only if $\delta(t) > 0$ for all $t < t^*$. The authors conclude that up to resolution of 512^2 there is not numerical evidence of finite time singularities. Furthermore, when a constant magnetic field was applied the $\delta(t)$-increment seemed to be bounded away from zero. They attributed this to the presence of Alfvén waves which can slowdown nonlinear interaction by propagating the Elssaesser fields $\mathbf{u} + \mathbf{b}$ and $\mathbf{u} - \mathbf{b}$ in opposite directions parallel to the imposed magnetic field. If the increment $\delta(t)$ is really bounded then no thermalization can be achieved because, an energy equipartition spectrum is incompatible with the exponential decay given by equation (3.70).

A more accurate observation of the increment $\delta(t)$ reveals that in contrast with the case of absent magnetic field, where a temporal exponential decay of $\delta(t)$ is observed, the constant magnetic field effectively slowdowns the decreasing of $\delta(t)$. However it is not possible to conclude that it remains inferiorly bounded for all times. It is important to remark at this point that when $\delta(t)$ is obtained from numerical data there is a natural inferior bound beyond which the increment becomes senseless. More precisely $\delta(t)$ can be considered as the smallest effective excited scale in the flow and it can not be smaller than $2\pi/k_{\max}$.

We performed longer time integration of equations (3.67) and (3.68) for different values of the magnetic field b_0 using a resolution of 512^2. The logarithm increment is obtained as in reference [65] by fitting the long wave-number range with the spectrum

$$E_{\text{tot}}(k) = c(t)k^{-m(t)}e^{-2\delta(t)k}, \tag{3.70}$$

and the minimum admissible value is determined by the relation $\delta(t)2k_{\max} = 1$.

The temporal evolution of $\delta(t)$ for different values of magnetic field is displayed in figure 3.11 in *log-lin* plot. The orange line corresponds to the minimum admissible value of $\delta(t)$ for a run of resolution 512^2. Figure 3.11 reproduces results obtained in [65] until $t = 1.75$ where the authors stop the numerical integration (indicated by the vertical line). Note that, effectively, the presence of a magnetic field slowdowns the nonlinear interaction and $\delta(t)$ remains above the minimum admissible value for a longer time, but it finally cross the line near $t = 3$. From the study of the $\delta(t)$ increment we can deduce that the system can reach the equilibrium even in presence of a strong magnetic field, but that the convergence is indeed slowdown.

To show numerically the relaxation to equilibrium, we performed long-time integrations of the OT vortex and used a weak ($b_0 = 0.5$) and strong ($b_0 = 4$ and $b_0 = 8$) magnetic fields. The temporal evolution of these runs is displayed on figure 3.12. The two solid lines respectively correspond to $k^{-3/2}$ and k^1 scalings. Remark that at $t = 1.2$ in both runs the large scales are almost equal however the down of the transfer of energy is evident at large wave-numbers. Posteriorly, an apparent bottleneck appears at an intermediate range for the runs with a stronger magnetic field. Finally the three runs start to thermalize at small scales.

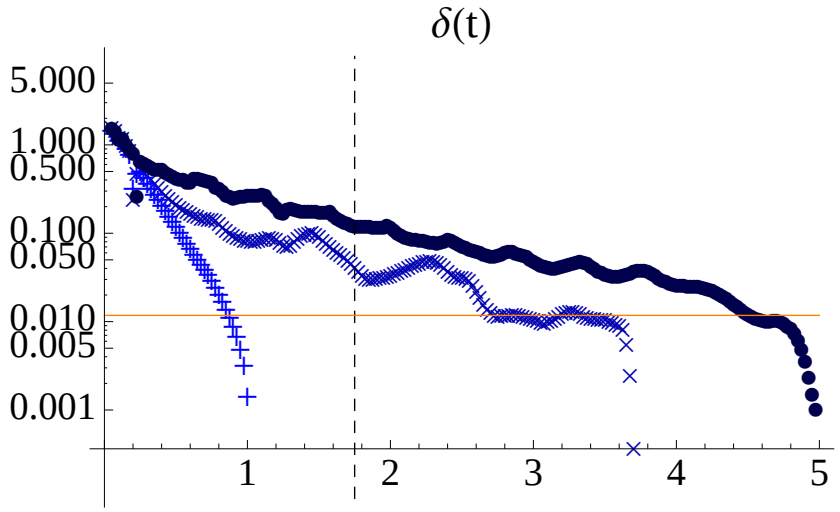

Fig. 3.11: Temporal evolution of logarithm increment $\delta(t)$ with $b_0 = 0.5$ (+), $b_0 = 4$ (×) and $b_0 = 8$ (•). Resolution of 512^2.

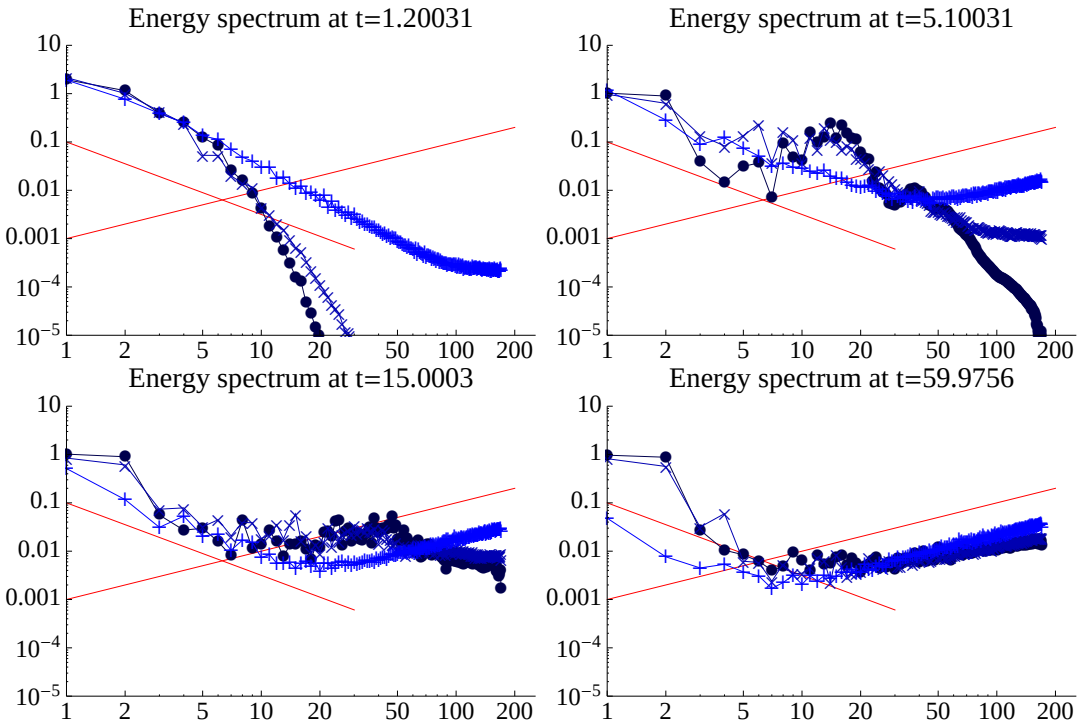

Fig. 3.12: Temporal evolution of energy spectrum with $b_0 = 0.5$ (+), $b_0 = 4$ (×) and $b_0 = 8$ (•). Solid lines correspond to $k^{-3/2}$ and k^1 scalings. Resolution of 512^2 collocation points.

3.4 Conclusions

In this chapter we have shown that the truncated Euler equation relax toward the equilibrium in an analogous way to the three dimensional case. The main difference is presence of a direct cascade of enstrophy. This quantity plays the role of the energy in $3d$, thermalizing in equipartition at large wave-number and yielding a k^{-1} law in the inertial zone. A remarkable difference with the $3d$ situation is the absence of a dissipative zone that is probably due to a vanishing $2d$ eddy viscosity.

The MHD flows were shown to thermalize under the truncated induction equation evolution. Similar to the $3d$ case of non magnetic flows, the direct cascade of energy leads to equipartition at large wave-number. An Iroshnikov-Kraichnan $k^{-3/2}$-spectrum is observed in the inertial zone of the $2d$ case. When a strong magnetic field is applied the Alfvén waves slowdown the nonlinear interactions and a big bottleneck appears in an intermediate zone before the equipartition range extends to the smallest scales.

It would be interesting, in a future work, to reproduce in higher resolutions the simulations involving a strong magnetic field in order to try to determinate the different scalings.

4. GENERATION AND CHARACTERIZATION OF ABSOLUTE EQUILIBRIUM OF COMPRESSIBLE FLOWS.

This chapter is devoted to the characterization of absolute equilibrium of compressible flows. As the energy is not quadratic the absolute equilibria are not simple Gaussian fields. A general stochastic algorithm that produce realizations of absolute equilibrium of Hamiltonian system is presented. This algorithm is then applied to irrotational compressible flows.

In this chapter we summarize the results of the publication *Generation and characterization of absolute equilibrium of compressible flows* [37] made in collaboration with Carlos Cartes and Enrique Tirapegui.

4.1 Introduction: Compressible Flows

We consider here the compressible Euler equation

$$\rho\partial_t\mathbf{u} + \rho(\mathbf{u}\cdot\nabla)\mathbf{u} = -\nabla p \tag{4.1}$$

$$\partial_t\rho + \nabla\cdot(\rho\mathbf{u}) = 0. \tag{4.2}$$

For isentropic fluids the pressure is related to the enthalpy w by [54]

$$\nabla w = \frac{\nabla p}{\rho}.$$

In what follows we will assume that the fluid is barotropic dynamics. The pressure field is thus a function of ρ. We also suppose that the density field is close to 1 throughout the fluid and therefore the dependence in ρ of w can be written as

$$w(\rho) = c^2(\rho - 1)$$

where c is the speed of sound.

Equations (4.1-4.2) conserve the energy H, the density Q and the momentum $\mathbf{P}$

defined by

$$H = \int d^d x [\frac{1}{2}\rho(\mathbf{x},t)|\mathbf{u}(\mathbf{x},t)|^2 + \varepsilon(\rho)]. \tag{4.3}$$

$$Q = \int d^d x \rho(\mathbf{x},t) \tag{4.4}$$

$$\mathbf{P} = \int d^d x \rho(x,t)\mathbf{u}(\mathbf{x},t) \tag{4.5}$$

with $\varepsilon(\rho) = \frac{c^2}{2}(\rho-1)^2$ is the internal energy. Note that as the energy is not quadratic the absolute equilibrium are not Gaussian and cannot be easily obtained. This point motivates the introduction of a stochastic algorithm to obtain the stationary probability. For small fluctuations (or low temperature) the absolute equilibrium was studied by Kraichnan [81]. This algorithm will be generalized and used to study the truncated Gross-Pitaevskii equation in chapter 6.

4.2 Algorithm to generate absolute equilibrium

Let $H(p_\mu, q^\mu)$ be a hamiltonian with corresponding canonical equations

$$\dot{q}^\mu = \frac{\partial H}{\partial p_\mu} \qquad \dot{p}_\mu = -\frac{\partial H}{\partial q^\mu}. \tag{4.6}$$

The stochastic algorithm is defined by the Langevin equation

$$\dot{q}^\mu = \frac{\partial H}{\partial p_\mu} \tag{4.7}$$

$$\dot{p}_\mu = -\frac{\partial H}{\partial q^\mu} - \nu\frac{\partial H}{\partial p^\mu} + \sqrt{2\eta\nu}\xi_\mu(t) \tag{4.8}$$

$$\langle \xi_\mu(t)\xi_\nu(t')\rangle = \delta_{\mu\nu}\delta(t-t'). \tag{4.9}$$

and it is shown in the article that the stationary probability is

$$P_{\mathrm{st}}(p_\mu, q^\mu) = \frac{1}{Z}e^{-\frac{1}{\eta}H(p_\mu,q^\mu)}. \tag{4.10}$$

This algorithm when is applied to a simple case of an anharmonic oscillator with the Hamiltonian $H(p,q) = \frac{p^2}{2m} + \frac{mw^2q^2}{2} + \frac{\alpha q^4}{4}$ gives a very natural dissipation proportional to $\dot{q}$.

Another algorithm is introduced based in a gradient stochastic relaxation which

shares the same stationary probability:

$$\dot{q}^{\mu} = -\nu\frac{\partial H}{\partial q^{\mu}} + \sqrt{2\eta\nu}\xi^{1}_{\mu}(t) \tag{4.11}$$

$$\dot{p}_{\mu} = -\nu\frac{\partial H}{\partial p^{\mu}} + \sqrt{2\eta\nu}\xi^{2}_{\mu}(t) \tag{4.12}$$

$$\langle \xi^{s}_{\mu}(t)\xi^{s'}_{\nu}(t')\rangle = \delta_{\mu\nu}\delta_{ss'}\delta(t-t'). \tag{4.13}$$

Note that this algorithm is independent of the Hamiltionian structure. Both algorithm are discussed and compared in the article.

4.3 *Publication:* "Generation and characterization of absolute equilibrium of compressible flows"

In the first part of the article a short review on thermalization of truncated Euler is given. Then the relaxation to equilibrium of irrotational compressible spectrally truncated Euler flows is studied.

The stochastic algorithm is first applied to the incompressible Euler equation written in terms of the Weber-Clebsch potentials $\tilde{\lambda}^i, \tilde{\mu}^i$ [82]. The statistics of the velocity field written with the Clebsch potential are found to be Gaussian validating the algorithm.

Then, the algorithm is applied to irrotational compressible fluids. The absolute equilibrium is characterized and the distribution is shown to be non-Gaussian.

Finally, we apply the algorithm with a large-scale modulated temperature a quasi-equilibrium is obtained. Then in the relaxation under the dynamics of truncated irrotational compressible equation, an oscillating behavior is observed suggesting the presence of second sound waves.

International Journal of Bifurcation and Chaos, Vol. 19, No. 10 (2009) 3445–3459

GENERATION AND CHARACTERIZATION OF ABSOLUTE EQUILIBRIUM OF COMPRESSIBLE FLOWS

GIORGIO KRSTULOVIC, CARLOS CARTES and MARC BRACHET
Laboratoire de Physique Statistique de l'Ecole Normale Supérieure, associé au CNRS et aux Universités Paris VI et VII, 24 Rue Lhomond, 75231 Paris, France

ENRIQUE TIRAPEGUI
Departamento de Física, Facultad de Ciencias Físicas y Matemáticas de la Universidad de Chile, Blanco Encalada 2008, Santiago, Chile

Received June 1, 2008; Revised December 13, 2008

A short review is given of recent papers on the relaxation to (incompressible) absolute equilibrium. A new algorithm to construct absolute equilibrium of spectrally truncated compressible flows is described. The algorithm uses stochastic processes based on the Clebsch representation of the velocity field to generate density and velocity fields that follow by construction the absolute equilibrium stationary probability. The new method is shown to reproduce the well-known Gaussian results in the incompressible limit. The irrotational compressible absolute equilibrium case is characterized and the distribution is shown to be non-Gaussian. The high-temperature compressible spectra are found not to obey k^2 scaling. Finally, oscillating behavior in constant-pressure variable-temperature relaxation is obtained, suggesting the presence of second sound.

Keywords: Truncated Euler equation; Clebsch potentials; compressible fluids; relaxation.

1. Introduction

It is well-known [Lee, 1952; Kraichnan, 1973; Orszag, 1977] that the (inviscid and conservative) incompressible Euler equation (Galerkin) truncated by keeping only a finite number of spatial Fourier harmonics admits absolute equilibrium solutions with Gaussian statistics, equipartition of kinetic energy among all Fourier modes and thus an energy spectrum $E(k) \sim k^2$.

A recent series of papers [Cichowlas *et al.*, 2005; Bos & Bertoglio, 2006; Krstulovic & Brachet, 2008; Krstulovic *et al.*, 2009; Frisch *et al.*, 2008], focusing on the dynamics of convergence toward absolute equilibrium, revived the interest in these matters by producing new and unexpected results. It was found in particular that in this time-reversible system (long-lasting) transients are obtained that mimic (irreversible) viscous flows.

The purpose of this paper is to extend these recent results to compressible flows. The absolute equilibrium is Gaussian in the case of incompressible flows, because the conserved quantities (energy and helicity) are quadratic. In the case of compressible flows the conserved quantities are not quadratic and the corresponding stationary probability is thus non-Gaussian. It is therefore a nontrivial problem to generate such a compressible absolute equilibrium flow.

The main result of this paper is a new algorithm to generate compressible absolute equilibrium.

We use the Hamiltonian Clebsch representation of the velocity field to generate density and velocity fields that follow by construction the absolute equilibrium stationary probability.

The paper is organized as follows: in Sec. 2 we give a short review of the recent series of papers on the dynamics of convergence toward absolute equilibrium in the incompressible case. In this section, we also review several early papers related to the compressible dynamics. Although these papers do not explicitly refer to absolute equilibrium, they implicitly do so by introducing wave turbulence theory with ultraviolet cutoff. An explicit example of relaxation toward equilibrium in the compressible case is then given in Sec. 3. Our new algorithm is detailed in Sec. 4. In Sec. 5, numerical simulations are presented, first the algorithm is verified in the incompressible case and then the compressible absolute equilibria are studied. Preliminary results relating to the presence of second sound in constant pressure variable temperature relaxation are given in Sec. 6. Finally Sec. 7 is our conclusion.

2. A Short Review on Truncated Euler

This section contains a short review of the recent papers on the dynamics of convergence toward absolute equilibrium in the incompressible case. We will also review several early papers related to the compressible dynamics. These papers do not explicitly refer to absolute equilibrium, however, they implicitly do so by introducing wave turbulence theory with an explicit ultraviolet cutoff that is mandatory to make the theory finite.

2.1. *Basic definitions*

The truncated incompressible Euler equation is a finite system of ordinary differential equations for the complex variables $\hat{\mathbf{u}}(\mathbf{k})$ ($\mathbf{k}$ is a 3D vector of relative integers (k_1, k_2, k_3) satisfying $\sup_\alpha |k_\alpha| \leq k_{\max}$)

$$\partial_t \hat{u}_\alpha(\mathbf{k}, t) = -\frac{i}{2} \mathcal{P}_{\alpha\beta\gamma}(\mathbf{k}) \sum_{\mathbf{p}} \hat{u}_\beta(\mathbf{p}, t) \hat{u}_\gamma(\mathbf{k} - \mathbf{p}, t) \tag{1}$$

where $\mathcal{P}_{\alpha\beta\gamma} = k_\beta P_{\alpha\gamma} + k_\gamma P_{\alpha\beta}$ with $P_{\alpha\beta} = \delta_{\alpha\beta} - k_\alpha k_\beta / k^2$ and the convolution in (1) is truncated to $\sup_\alpha |k_\alpha| \leq k_{\max}$, $\sup_\alpha |p_\alpha| \leq k_{\max}$ and $\sup_\alpha |k_\alpha - p_\alpha| \leq k_{\max}$.

This system is classically obtained [Orszag, 1977] from the (unit density) three-dimensional incompressible Euler equation

$$\partial_t \mathbf{u} + (\mathbf{u} \cdot \nabla)\mathbf{u} = -\nabla p \tag{2}$$

$$\nabla \cdot \mathbf{u} = 0 \tag{3}$$

by performing a Galerkin truncation ($\hat{\mathbf{u}}(\mathbf{k}) = 0$ for $\sup_\alpha |k_\alpha| > k_{\max}$) on the Fourier transform $\mathbf{u}(\mathbf{x}, t) = \sum \hat{\mathbf{u}}(\mathbf{k}, t) e^{i\mathbf{k}\cdot\mathbf{x}}$ of the spatially periodic velocity field $\mathbf{u}$.

This time-reversible system exactly conserves the energy $E = \sum_k E(k, t)$ and helicity $H = \sum_k H(k, t)$, where the energy and helicity spectra $E(k, t)$ and $H(k, t)$ are defined by

$$E(k, t) = \frac{1}{2} \sum_{k - \Delta k/2 < |\mathbf{k}'| < k + \Delta k/2} |\hat{\mathbf{v}}(\mathbf{k}', t)|^2 \tag{4}$$

$$H(k, t) = \sum_{k - \Delta k/2 < |\mathbf{k}'| < k + \Delta k/2} \hat{\mathbf{u}}(\mathbf{k}', t) \cdot \hat{\omega}(-\mathbf{k}', t) \tag{5}$$

with spherical shells of width $\Delta k = 1$.

2.2. *Incompressible flows*

Cichowlas *et al.* [2005], Cichowlas [2005] observed that the incompressible Euler equation, (Galerkin) truncated as in (1) using a large spectral truncation wavenumber $k_{\max}$, displays long-lasting transients behaving just like high-Reynolds number viscous flow. In particular, they found an approximately $k^{-5/3}$ inertial range followed by a dissipative range. Such a behavior is possible because the highest-k modes thermalize at first, through a mechanism discovered by Lee [1952], leading to a k^2 spectrum. Progressively the thermalized region extends to lower and lower wavenumbers, eventually covering the whole range of available modes. At intermediate times, when the thermalized regime only extends over the highest wavenumbers, it acts as a thermostat that pumps out the energy of larger-scale modes. The energy spectrum for different values of $k_{\max}$ and its temporal evolution taken from [Cichowlas, 2005] are shown in Fig. 1. In this context, the spectrally truncated Euler equations appeared as a minimal model of turbulence.

Bos and Bertoglio [2006] studied the evolution of the turbulent energy spectrum for the inviscid spectrally truncated Euler equations using Eddy-Damped Quasi-Normal Markovian (EDQNM) closure calculations. They observed that the EDQNM

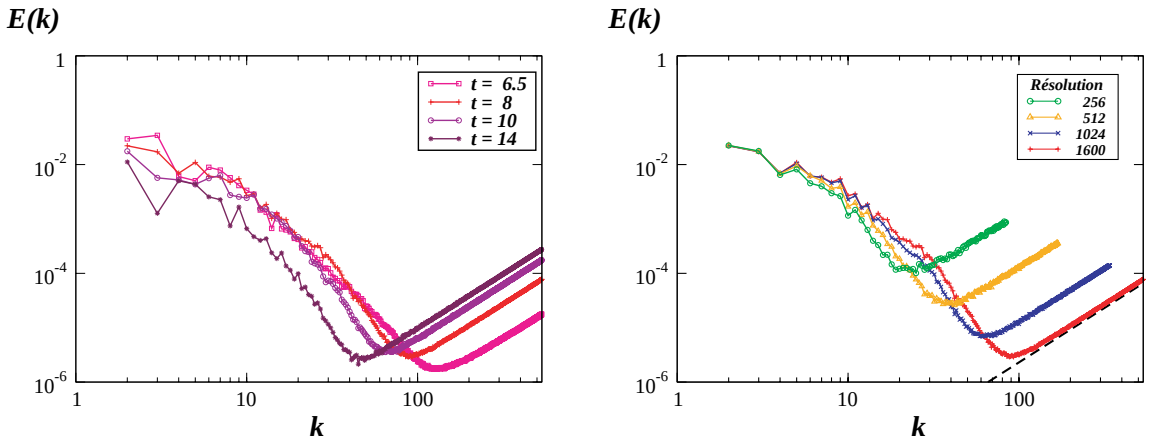

Fig. 1. Energy spectra, left: resolution 1600^3 at $t = (6.5, 8, 10, 14)$ ($\diamond$, $+$, $\circ$, $*$); right: resolutions 256^3 (circle $\circ$), 512^3 (triangle $\triangle$), 1024^3 (cross $\times$) and 1600^3 (cross $+$) at $t = 8$. The dashed lines indicate k^2 scaling. Figure taken from [Cichowlas, 2005].

closure reproduced the behavior found in the direct numerical simulations of reference [Cichowlas *et al.*, 2005]. They showed that the dissipation range was created by nonlinear interactions with the modes in equipartition. They defined a nonlocal effective eddy viscosity, based on the most energetic modes in the equipartition zone and the cutoff wave number.

Krstulovic and Brachet [2008] proposed a phenomenological two-fluid model of the (time-reversible) spectrally-truncated 3D Euler equation. They showed that the thermalized small scales follow a quasi-normal distribution. They determined the effective viscosity and thermal diffusion, using EDQNM closure and Monte-Carlo numerical computations, yielding compatible values. (Hypo)diffusion of heat was obtained using Monte Carlo and the corresponding effective Prandtl number was found to vanish in the small $k/k_{\max}$ limit. Overall, the phenomenological two-fluid model was found to be in good quantitative agreement with the original truncated Euler equations.

Krstulovic *et al.* [2008] studied for the first time the relaxation toward a Kraichnan [1973] helical absolute equilibrium. They found transient mixed energy and helicity cascades and used the concept of eddy viscosity, as previously developed in [Cichowlas *et al.*, 2005] and [Krstulovic & Brachet, 2008], to qualitatively explain the differences observed between truncated Euler and high-Reynolds number (fixed viscosity) Navier–Stokes. They finally showed that the truncated Euler large scale modes quantitatively follow an effective Navier–Stokes dynamics based on a (time and wavenumber dependent) eddy viscosity that did not depend explicitly on the helicity content in the flow.

Frisch *et al.* [2008] showed that the use of a high power α of the Laplacian in the dissipative term of hydrodynamical equations leads asymptotically to truncated inviscid *conservative* dynamics with a finite range of spatial Fourier modes. They found that, just as in reference [Cichowlas *et al.*, 2005], the modes at large wavenumbers thermalize, whereas modes at small wavenumbers obey ordinary viscous dynamics. They interpreted the energy bottleneck observed for finite α as incomplete thermalization.

2.3. *Compressible flows*

Putterman and Roberts [1982, 1983] investigated the solution to nonlocal dispersive classical hydrodynamics at the fourth order of nonlinearity. An extra degree of freedom appeared as a result of the additive conservation of wave number in the interaction of beams of sound waves, representing a broken symmetry. Imposing an ultraviolet cutoff to obtain finite results, they found that the resulting nonlinear high-order equations of motion for the background plus a distribution of sound waves were identical to the Landau two-fluid hydrodynamics used to describe superfluid Helium.

Larraza and Putterman [1986] showed that if a nonlinear medium is pumped with energy, in the form of mechanical waves, sufficiently far from equilibrium the wave turbulence can support a transition from diffusive to propagative energy transport that bears deep similarities to second sound in Helium.

Connaughton *et al.* [2005] studied the formation of a large-scale coherent structure (a condensate) in classical wave equations by considering the defocusing nonlinear Schrodinger equation as a representative model. They formulated a thermodynamic description of the classical condensation process by using a wave turbulence theory with ultraviolet cutoff. They found a subcritical condensation process in 3D, and no transition in 2D. Numerical simulations of the NLS equation with stochastic initial conditions were found to be in quantitative agreement with the equilibrium distribution of the kinetic equation derived from the NLS equation.

3. Relaxation in Compressible Spectrally Truncated Euler Flows

In this section, we study the relaxation to equilibrium of irrotational compressible spectrally truncated Euler flows. The dynamics is described by a density field ρ and the velocity $\mathbf{u}$ that is represented by the velocity potential ϕ. The dynamics is given by the continuity and Bernoulli equations:

$$\frac{\partial \rho}{\partial t} = -\nabla \cdot (\rho \nabla \phi) \tag{6}$$

$$\frac{\partial \phi}{\partial t} = -\frac{1}{2}\mathbf{u}^2 - \frac{\partial \varepsilon}{\partial \rho}(\rho) \tag{7}$$

$$\mathbf{u} = \nabla \phi \tag{8}$$

$$\varepsilon(\rho) = \frac{1}{2c^2}(\rho - 1)^2 \tag{9}$$

where $\varepsilon(\rho)$ is the internal energy of the fluid and c the speed of sound, when $\rho = 1$.

This time-reversible system ($t \to -t, \phi \to -\phi$) conserves the total mass, the momentum and the total energy:

$$Q = \int d^d x \rho(x,t) \tag{10}$$

$$\mathbf{P} = \int d^d x \rho(x,t) \nabla \phi(x,t) \tag{11}$$

$$H = \int d^d x \left[\frac{1}{2} \rho(x,t) \nabla \phi(x,t)^2 + \varepsilon(\rho) \right]. \tag{12}$$

As done in the incompressible case in [Cichowlas *et al.*, 2005; Krstulovic *et al.*, 2009] we now study the Galerkin truncated version of Eqs. (6)–(8) for the Fourier transforms $\hat{\rho}(\mathbf{k},t) \equiv \hat{\rho}_{\mathbf{k}}(t)$ and $\hat{\phi}(\mathbf{k},t) \equiv \hat{\phi}_{\mathbf{k}}(t)$ of the dynamical variables. This spectrally truncated system reads

$$\frac{\partial \hat{\rho}_{\mathbf{k}}}{\partial t}(t) = \sum_{\mathbf{p}} \hat{\rho}_{\mathbf{k}-\mathbf{p}}(t) \hat{\phi}_{\mathbf{p}}(t) \mathbf{k} \cdot \mathbf{p} \tag{13}$$

$$\frac{\partial \hat{\rho}_{\mathbf{k}}}{\partial t}(t) = \frac{1}{2} \sum_{\mathbf{p}} \hat{\phi}_{\mathbf{k}-\mathbf{p}}(t) \hat{\phi}_{\mathbf{p}}(t) (\mathbf{k} - \mathbf{p}) \cdot \mathbf{p} + \frac{1}{c^2} \widehat{(1-\rho)}_{\mathbf{k}}(t) \tag{14}$$

where the convolution in Eqs. (13) and (14) are truncated to $\sup_\alpha |k_\alpha| \le k_{\max}$, $\sup_\alpha |p_\alpha| \le k_{\max}$ and $\sup_\alpha |k_\alpha - p_\alpha| \le k_{\max}$. This system also exactly conserves Q, P and H.

Let us now define, as in the incompressible case (4), the internal, kinetic and total energy spectra by,

$$E_{\text{kin}}(k,t) = \frac{1}{2} \sum_{k - \frac{\Delta k}{2} < |\mathbf{k}'| < k + \frac{\Delta k}{2}} \widehat{\rho \mathbf{u}}_{-\mathbf{k}'}(t) \cdot \widehat{\mathbf{u}}_{\mathbf{k}'}(t) \tag{15}$$

$$E_{\text{int}}(k,t) = \frac{c^2}{2} \sum_{k - \frac{\Delta k}{2} < |\mathbf{k}'| < k + \frac{\Delta k}{2}} |\widehat{(\rho - 1)}_{\mathbf{k}'}|^2(t) \tag{16}$$

$$E(k,t) = E_{\text{kin}}(k,t) + E_{\text{int}}(k,t) \tag{17}$$

By construction we have $H = \sum_k E(k,t)$. Note that the systems (13) and (14) (as well as (6)–(8)) possesses a Hamiltonian structure. Equations (13) and (14) can thus be rewritten using the Hamiltonian

$$H = \sum_{\mathbf{k}} \frac{1}{2} \widehat{\rho \mathbf{u}}_{\mathbf{k}} \widehat{\mathbf{u}}^*_{\mathbf{k}} + \frac{1}{2c^2} |\widehat{(\rho - 1)}_{\mathbf{k}}|^2 \tag{18}$$

as the canonical equations

$$\frac{\partial \hat{\rho}_{\mathbf{k}}}{\partial t}(t) = \frac{\partial H}{\partial \hat{\phi}^*_{\mathbf{k}}}, \quad \frac{\partial \hat{\phi}^*_{\mathbf{k}}}{\partial t}(t) = -\frac{\partial H}{\partial \hat{\rho}_{\mathbf{k}}}, \tag{19}$$

where $\hat{\rho}_{\mathbf{k}}, \hat{\phi}^*_{\mathbf{k}}$ are thus conjugate variables.

As in incompressible truncated Euler, this system admits a stationary statistical solution with a probability distribution function given by $P\{\hat{\rho}_{\mathbf{k}}, \hat{\phi}_{\mathbf{k}}\} \sim e^{-\beta H}$. As H is not quadratic, the p.d.f. will not be Gaussian and no equipartition can be expected in the energy spectrum (17) because of the correlation between $\hat{\rho}_{\mathbf{k}}$ and $\hat{\phi}_{\mathbf{k}}$ for different wavenumbers. However, rewriting $\hat{\rho}_{\mathbf{k}} = 1 + \hat{\rho}'_{\mathbf{k}}$, the Hamiltonian can be written as $H = H_{\mathbf{G}} + H_{\mathbf{NG}}$

with

$$H_{\mathbf{G}} = \sum_{\mathbf{k}} \frac{1}{2}k^2|\hat{\phi}_{\mathbf{k}}|^2 + \frac{1}{2c^2}|\hat{\rho}'_{\mathbf{k}}|^2 \tag{20}$$

$$H_{\mathbf{NG}} = \sum_{\mathbf{k}} \frac{1}{2}\widehat{\rho' \mathbf{u}_{\mathbf{k}}}\hat{\mathbf{u}}^*_{\mathbf{k}}. \tag{21}$$

Note that for large values of β, $H_{\mathbf{NG}}$ can be safely neglected and statistics becomes Gaussian and equipartition, yielding in this limit $E(k) \sim k^2$ (in three dimensions).

It is well known that a conservative nonlinear systems with a high number of freedom degrees may, in general, not relax to an equilibrium state and time periodic localized structures can appear, as in the classical Fermi–Pasta–Ulam–Tsingou problem [Fermi *et al.*, 1955]. In order to study the relaxation to the equilibrium of truncated irrotational compressible flows and avoid long transient we will use an initial condition, close to the equilibrium state, given by a Gaussian field perturbed by a large-scale modulation of the velocity potential. This initial condition reads

$$\rho_0(x,y,z) = 1 + \rho'_{\mathrm{G}}(x,y,z) \tag{22}$$

$$\phi(x,y,z) = \frac{1}{8\sqrt{3}}(\sin 4x + \sin 4y + \sin 4z) + \phi_{\mathrm{G}}(x,y,z) \tag{23}$$

where $\hat{\rho}'_{\mathbf{Gk}}, \hat{\phi}_{\mathbf{Gk}}$ are distributed with a probability proportional to $e^{-\beta H_{\mathrm{G}}}$.

Numerical solutions of Eqs. (13) and (14) are efficiently produced using a standard pseudo-spectral general-periodic code with 128^3 Fourier modes that is dealiased using the 2/3 rule [Gottlieb & Orszag, 1977] by a Galerkin truncation at $k_{\max} = 42$. The numerical method used is nondispersive and conserves mass, momentum and energy with high accuracy. The value of β is chosen large enough to ensure that there are no points with negative ρ. The total initial energy (18) of this run is $H = 2.136$.

Figure 2 shows the temporal evolution of the energy spectrum. Note that the system effectively relaxes but at the final time $t = 43.69$ in Fig. 2(d),

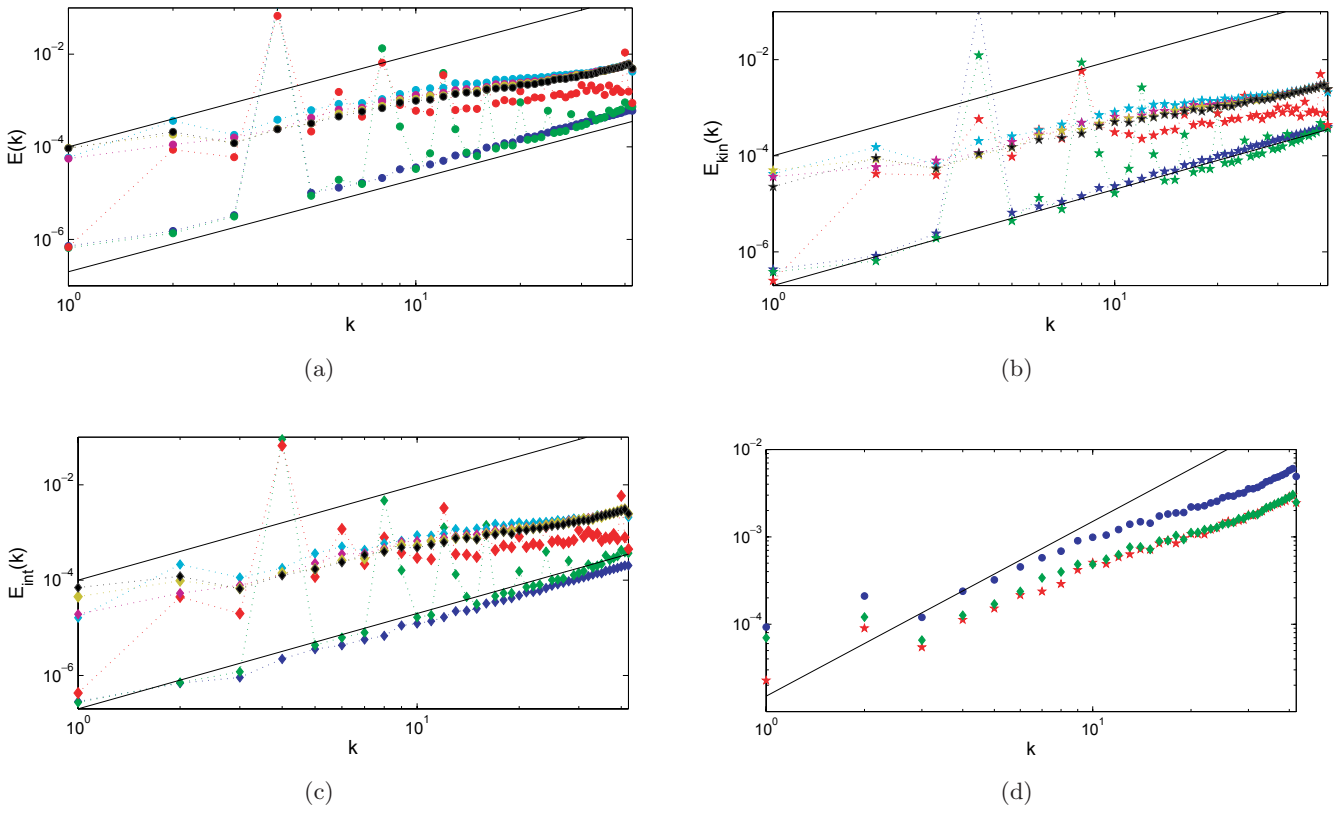

Fig. 2. Temporal evolution of compressible energy spectra (15)–(17). $t = 0$, 0.94, 6.19, 18.69, 31.19, 37.44, 43.69. Solid line represents a k^2 spectrum. (a) Total energy spectrum. (b) Kinetic energy spectrum. (c) Internal energy spectrum. (d) Total kinetic and internal energy spectra for $t = 43.69$.

there is no clear k^2 law in the spectrum. This fact can be understood by noting that the k^2 law is a consequence of equipartition of energy which, in turn, requires that the total energy can be written as a sum of independent contributions from each mode, as in the incompressible case (4). In the compressible case, equipartition will not be obtained because of the non-Gaussian term (21).

An algorithm to generate such a general non-Gaussian absolute equilibria thus appears of practical interest for many applications such as the determination of eddy-viscosities or a two-fluid description. We now turn to this general problem.

4. New Algorithm to Generate Absolute Equilibrium

4.1. *Stochastic processes and stationary probability of Hamiltonian systems*

We want to construct a stochastic process with a probability distribution that converges to the stationary probability given by the Boltzmann weight. This can be done in a canonical way for any Hamiltonian system. Let $H(p_\mu, q^\mu)$ be a Hamiltonian with the corresponding canonicals equations

$$\dot{q}^\mu = \frac{\partial H}{\partial p_\mu}, \quad \dot{p}_\mu = -\frac{\partial H}{\partial q^\mu} \tag{24}$$

In what follows, we suppose the existence of a stable equilibrium point.

Let us first modify the equations by adding a dissipative term to the equation for $\dot{p}_\mu$

$$\dot{q}^\mu = \frac{\partial H}{\partial p_\mu} \tag{25}$$

$$\dot{p}_\mu = -\frac{\partial H}{\partial q^\mu} - \nu \frac{\partial H}{\partial p^\mu} \tag{26}$$

with $\nu > 0$. The dissipation introduced here is the most natural in a physical sense, as we will show later in the basic example of an oscillator. The dynamic has an evident Lyapunov functional given by the Hamiltonian H:

$$\frac{dH}{dt} = \frac{\partial H}{\partial q^\mu}\dot{q}^\mu + \frac{\partial H}{\partial p_\mu}\dot{p}_\mu = -\nu \frac{\partial H}{\partial p^\mu}\frac{\partial H}{\partial p_\mu} \leq 0, \tag{27}$$

therefore the system will converge to the stable equilibrium point.

Finally, let us introduce a white Gaussian forcing term. The Langevin equation, which completely defines the stochastic process, reads

$$\dot{q}^\mu = \frac{\partial H}{\partial p_\mu} \tag{28}$$

$$\dot{p}_\mu = -\frac{\partial H}{\partial q^\mu} - \nu \frac{\partial H}{\partial p^\mu} + \sqrt{2\eta\nu}\xi_\mu(t) \tag{29}$$

$$\langle \xi_\mu(t)\xi_\nu(t')\rangle = \delta_{\mu\nu}\delta(t-t'). \tag{30}$$

Note that when η and ν are small, the system (28)–(30) is a perturbation of the original Hamiltonian dynamics. In what follows, this system will be called the *damped Hamiltonian* method.

The Fokker–Planck equation for the evolution of the transition probability $P(p_\mu, q^\mu)$ of this process is [Langouche *et al.*, 1982; van Kampen, 2001]

$$\frac{\partial}{\partial t}P = -\frac{\partial}{\partial q^\mu}\left[\frac{\partial H}{\partial p_\mu}P\right] + \frac{\partial}{\partial p_\mu}\left[\frac{\partial H}{\partial q^\mu}P + \nu\frac{\partial H}{\partial p^\mu}P + \eta\nu\frac{\partial P}{\partial p^\mu}\right] \tag{31}$$

$$= \{H, P\} + \nu\frac{\partial}{\partial p_\mu}\left[\frac{\partial H}{\partial p^\mu}P + \eta\frac{\partial P}{\partial p^\mu}\right] \tag{32}$$

where $\{f, g\} = (\partial f/\partial q_\mu)(\partial g/\partial p^\mu) - (\partial f/\partial p_\mu)(\partial g/\partial q^\mu)$ is the Poisson bracket. As H is a conserved quantity of the original Eqs. (24), any function of a conserved quantity will vanish in the Poisson bracket and hence a stationary probability reads

$$P_{\mathrm{st}}(p_\mu, q^\mu) = \frac{1}{Z}e^{-\frac{1}{\eta}H(p_\mu, q^\mu)}. \tag{33}$$

Let us now remark that there exists another simple stochastic process which shares the same stationary probability. Its dynamics is given by gradient equations:

$$\dot{q}^\mu = -\nu\frac{\partial H}{\partial q^\mu} + \sqrt{2\eta\nu}\xi^1_\mu(t) \tag{34}$$

$$\dot{p}_\mu = -\nu\frac{\partial H}{\partial p^\mu} + \sqrt{2\eta\nu}\xi^2_\mu(t) \tag{35}$$

$$\langle \xi^s_\mu(t)\xi^{s'}_\nu(t')\rangle = \delta_{\mu\nu}\delta_{ss'}\delta(t-t') \tag{36}$$

however, we believe that the process (28)–(30) is of more physical and theoretical interest.

In the case of a Hamiltonian depending on fields, the generalization of Eqs. (28)–(30) are trivial replacing partial derivatives by functional derivatives and the $\delta_{\mu\nu}$ Kronecker delta in Eq. (30) by a Dirac delta. It is important to remark that absolute equilibria will formally lead, in this case, to

infinity energy solutions, therefore a UV cut-off must be understood leading to truncated equations in Fourier space.

4.1.1. *A simple example: Anharmonic oscillator*

Let us first consider the example of an anharmonic oscillator, the Hamiltonian for this system is $H(p,q) = (p^2/2m) + (mw^2q^2/2) + (\alpha q^4/4)$. The Langevin equation (28)–(30) reads

$$\dot{q} = \frac{1}{m}p \tag{37}$$

$$\dot{p} = -m\omega^2 q - \alpha q^3 - \frac{\nu}{m}p + \sqrt{2\eta\nu}\xi(t) \tag{38}$$

$$\langle \xi(t)\xi(t')\rangle = \delta(t-t'). \tag{39}$$

These equations can be rewritten as

$$m\ddot{q} = -m\omega^2 q - \alpha q^3 - \nu\dot{q} + \xi(t) \tag{40}$$

$$\langle \xi(t)\xi(t')\rangle = \delta(t-t') \tag{41}$$

and they are just the equations of a classical forced-damped anharmonic oscillator. In this sense, the dissipation introduced in (26) is very natural and with a simple physical interpretation.

4.2. *Hamiltonian formulation for general compressible fluids*

We have shown in Sec. 3 that irrotational compressible flows admit a Hamiltonian formulation. This can be easily extended to general compressible fluids. The equations that describe the dynamics of general inviscid fluids are the Euler and continuity equation for the velocity field $\mathbf{u}$

$$\partial_t \rho = -\nabla\cdot(\rho\mathbf{u}) \tag{42}$$

$$D_t\mathbf{u} = -\nabla w, \tag{43}$$

where D_t is the convective derivative defined as

$$D_t = \partial_t + \mathbf{u}\cdot\nabla,$$

ρ is the density and w is the enthalpy for unit of mass. For isoentropic fluids the enthalpy is related to the pressure field p by

$$\nabla w = \frac{\nabla p}{\rho}.$$

For the purposes of this work we assume a barotropic dynamics, hence the pressure field has functional dependence only in ρ. We also suppose that the density field is approximately uniform throughout the fluid and therefore the dependence in ρ of w can be written as

$$w(\rho) = c^2(\rho - 1)$$

where c is the speed of sound for a unit density fluid.

It is well known that it is possible to find a variational principle for Eqs. (42) and (43) with the help of the *Weber–Clebsch Transformation* [Mobbs, 1982]

$$\mathbf{u} = \sum_{i=1}^{3}\lambda^i\nabla\mu^i + \nabla\phi\,, \tag{44}$$

here, we write the velocity field as a function of the scalar fields $\lambda^i(x,t)$, $\mu^i(x,t)$ and $\phi(x,t)$.

In order to show explicitly the Hamiltonian structure of Eqs. (42) and (43) we redefine

$$\tilde{\lambda}^i = \rho\lambda^i \tag{45}$$

and with this representation of $\mathbf{u}$ we define the Lagrangian

$$L = \int dx^3dt\left(\rho\partial_t\phi + \sum_{i=1}^{3}\tilde{\lambda}^i\partial_t\mu^i + \mathcal{H}\right),$$

where $\mathcal{H}$ is the Hamiltonian density

$$\mathcal{H} = \rho\frac{\mathbf{u}^2}{2} + \varepsilon(\rho)$$

and $\varepsilon(\rho)$ is the internal energy (9) which is related to w [Landau & Lifchitz, 1971] by the relation

$$\rho\frac{\partial\varepsilon}{\partial\rho} = \varepsilon + p = \rho w. \tag{46}$$

With this choice of variables, $\tilde{\lambda}^i, \tilde{\mu}^i$ and $\hat{\rho}_{\mathbf{k}}, \hat{\phi}_{\mathbf{k}}$ are now conjugate variables. The corresponding canonical equations are then

$$\partial_t\rho = \frac{\delta\mathcal{H}}{\delta\phi} = -\nabla\cdot(\rho\mathbf{u}) \tag{47}$$

$$\partial_t\phi = -\frac{\delta\mathcal{H}}{\delta\rho} = -\mathbf{u}\cdot\nabla\phi + \frac{\mathbf{u}^2}{2} - \frac{\partial\varepsilon}{\partial\rho} \tag{48}$$

$$\partial_t\tilde{\lambda}^i = \frac{\delta\mathcal{H}}{\delta\mu^i} = -\nabla\cdot(\mathbf{u}\tilde{\lambda}^i) \tag{49}$$

$$\partial_t\mu^i = -\frac{\delta\mathcal{H}}{\delta\tilde{\lambda}^i} = -\mathbf{u}\cdot\nabla\mu^i. \tag{50}$$

Let us remark that Eq. (47) is the continuity equation (42) and that Eq. (48) is the Bernoulli equation, with an extra advective term.

In order to recover the Euler equation (43) from Eqs. (47)–(50) note that reintroducing the definition (45) of $\tilde{\lambda}^i$ in Eq. (49) and using Eq. (47) we obtain $\partial_t \lambda^i = -\mathbf{u}\cdot\nabla\lambda^i$. Computing then $D_t\mathbf{u}$ using the definition (44), the identity $[\nabla, D_t] \equiv (\nabla\mathbf{u})\cdot\nabla$ and thermodynamic relation (46), Eq. (42) is obtained after some simple algebra.

The general system (47)–(50) admits two simple limits. First, when ρ is constant, the flow is incompressible and the dynamics reduces to equations of motion for λ^i and μ^i. In this case, there is no need to independently solve for ϕ, because this field is determined by the incompressibility condition $\nabla\cdot\mathbf{u} = 0$. A second simple case is when the flow is compressible and irrotational. As the velocity is a purely potential flow, the Clebsch variables λ^i, μ^i vanish and the dynamics reduces to equations of motion for the fields ρ and ϕ only, as in Sec. 3.

4.3. *Langevin equation converging to absolute equilibrium*

Our new algorithms are obtained by inserting within the Langevin equations (28)–(30) the Hamiltonian corresponding to the two particular cases of the preceding subsection.

4.3.1. *Incompressible flows*

When ρ is constant, the Hamiltonian (46) reduces to

$$\mathcal{H} = \int d^3x\, \frac{1}{2}(\lambda^i\nabla\mu^i - \nabla\phi)^2 \tag{51}$$

with the corresponding Langevin equation:

$$\frac{\partial\lambda^i}{\partial t} = -\mathbf{u}\cdot\nabla\lambda^i \tag{52}$$

$$\frac{\partial\mu^i}{\partial t} = -\mathbf{u}\cdot\nabla\mu^i + \nu\,\mathbf{u}\cdot\nabla\lambda^i + \sqrt{2\eta\nu}\,\xi^i(x,t) \tag{53}$$

$$\nabla\cdot\mathbf{u} = 0 \tag{54}$$

$$\langle\xi^i(x,t)\xi^j(x',t')\rangle = \delta_{ij}\delta^3(x-x')\delta(t-t') \tag{55}$$

Note that the stationary probability is in some way similar to that of $\lambda-\phi^4$ theory in the Clebsch variables. Although the velocity $\mathbf{v}$ must have an equipartition k^2 spectrum (in 3D), the statistical properties of the Clebsch pairs are not at all trivial.

4.3.2. *Irrotational flows*

In the compressible irrotational case where only the fields ρ and ϕ are not zero, we recover the Hamiltonian (12) and the corresponding Langevin equation reads:

$$\frac{\partial\rho}{\partial t} = -\nabla\cdot(\rho\nabla\phi) \tag{56}$$

$$\frac{\partial\phi}{\partial t} = -\frac{1}{2}(\nabla\phi)^2 - \frac{\partial\epsilon}{\partial\rho}(\rho) + \nu\nabla\cdot(\rho\nabla\phi) + \sqrt{2\eta\nu}\,\xi(x,t) \tag{57}$$

$$\langle\xi(x,t)\xi(x',t')\rangle = \delta^3(x-x')\delta(t-t'). \tag{58}$$

Note that when ρ is a small fluctuation around a homogeneous value ρ_0 given by the minimum of $\varepsilon(\rho)$, the dissipation looks like a diffusion term and taking the gradient in Eq. (57), we obtain a Navier–Stokes like equation.

Another important property of this Langevin Eqs. (56)–(58) is that the mean value of ρ (average over space and realization of the process) is conserved as in the original Hamiltonian dynamics (6) and (7). This property is not preserved in the gradient dynamics (35) and (36). In this case, it follows directly from Eq. (35), and the Hamiltonian (12), that the dynamics of $\langle\rho\rangle$ is given by

$$\frac{\partial}{\partial t}\langle\rho\rangle = -\frac{1}{2}\langle\nabla\phi^2\rangle - \left\langle\frac{\partial\epsilon}{\partial\rho}\right\rangle$$

and hence, using the internal energy (9) the stationary value of $\langle\rho\rangle$ is

$$\langle\rho\rangle_{\mathrm{st}} = 1 - \frac{1}{2c^2}\langle\nabla\phi^2\rangle_{\mathrm{st}}. \tag{59}$$

Remark that this usual equation of state (9) can lead to high values of η [see Eq. (33)] to negative values of ρ. This non-physical situation can be avoided by changing the equation of state to one physically more compatible with the dynamics of high amplitude waves, considering for instance, terms of order $O((\rho-1)^4)$ in (9).

5. Numerical Validation

5.1. *Incompressible rotational flows*

We now proceed to validate our new algorithm in the well-known test case of incompressible fluids. Although the Hamiltonian (51) is not quadratic, the velocity $\mathbf{u}$ must be Gaussian and therefore the energy spectrum of the velocity must follow a k^2 law.

In the case of absolute equilibria of incompressible fluids, there are only two independent components of velocity due to the divergence free condition (54). It can be shown [Orszag, 1970; Cichowlas, 2005] that the second order moment of a Fourier mode is

$$\langle \hat{u}_\mu(\mathbf{k},t)\hat{u}_\nu(-\mathbf{k},t)\rangle = \eta\left(\delta_{\mu\nu} - \frac{k_\mu k_\nu}{k^2}\right) = \eta P_{\mu\nu}(\mathbf{k}), \tag{60}$$

and therefore the kinetic energy $\mathcal{H}$ is obtained from Eq. (60)

$$\mathcal{H} = \sum_{|k_\alpha|\le k_{\max}} \frac{1}{2}\langle \hat{u}_\alpha(\mathbf{k},t)\hat{u}_\alpha(-\mathbf{k},t)\rangle = \frac{\eta}{2}\sum_{|k_\alpha|\le k_{\max}} P_{\alpha\alpha}(\mathbf{k}). \tag{61}$$

As $P_{\alpha\alpha} = 2$ then $\mathcal{H} = \eta\mathcal{N}$ where $\mathcal{N}$ is the number of degrees of freedom.

We perform the numerical integration of (52)–(55) using a standard pseudo-spectral method with a Galerkin truncation at the mode $k_{\max}$ with the 2/3 rule.

In Fig. 3 we plot temporal evolution of the total energy of the velocity field for the gradient and damped Hamiltonian method. We set $\nu = 1$ for all present simulations. We can see a faster convergence to the stationary value of the energy in the gradient method.

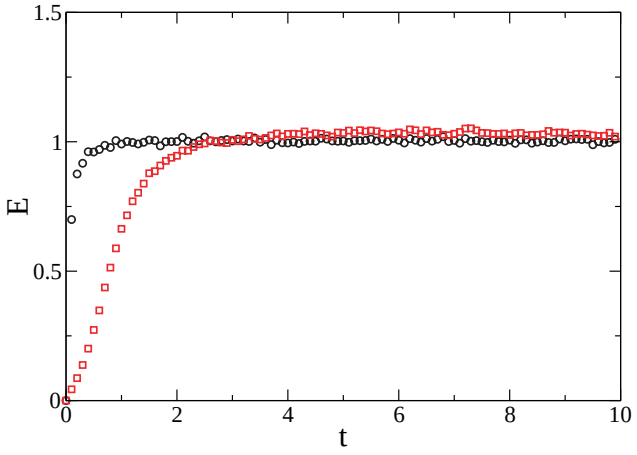

Fig. 3. Temporal evolution of the total energy (51) of the velocity field for the gradient and damped Hamiltonian method (∘ and □) for simulations made with a resolution of 48^3 and $\nu = 1$.

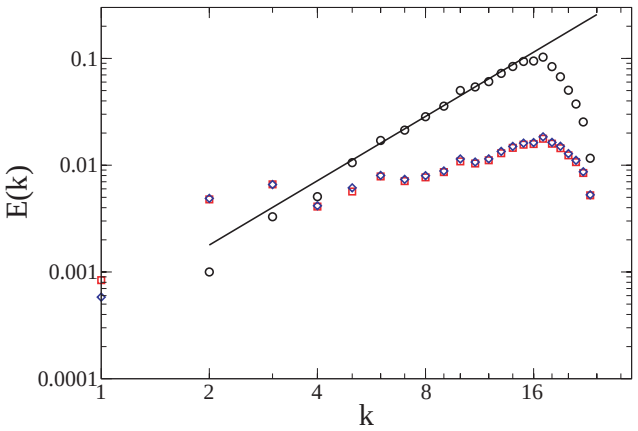

Fig. 4. Energy spectrum for the velocity, λ and μ fields (∘, □ and ⋄) of the gradient case for a simulation with a resolution 48^3. The continuous line represents an ideal k^2 spectrum.

As usual, we define the energy spectrum of λ and μ by averaging on spherical shells

$$E_\lambda(k,t) = \frac{1}{2}\sum_{k-\Delta k/2<|\mathbf{k}'|<k+\Delta k/2} |\hat{\lambda}_{\mathbf{k}'}|^2(t) \tag{62}$$

$$E_\mu(k,t) = \frac{1}{2}\sum_{k-\Delta k/2<|\mathbf{k}'|<k+\Delta k/2} |\hat{\mu}_{\mathbf{k}'}|^2(t), \tag{63}$$

and the averaged spectra over a set of a hundred realizations of the process is shown in Fig. 4. We can see a good agreement of the velocity spectrum with the equipartition scaling $\sim k^2$. We remark that scaling of λ and μ fields appears to obey scaling laws that seem different from k^2.

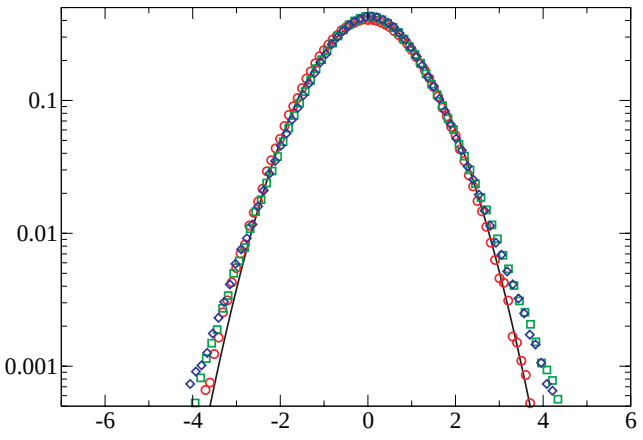

Fig. 5. Histogram for the x component of the velocity, λ and μ fields (∘, □ and ⋄) for the damped Hamiltonian case from a simulation made with a resolution of 48^3. The continuous line represents an ideal Gaussian distribution for the velocity.

Finally, a normalized histogram of λ, μ and one component of $\mathbf{u}$ are plotted in Fig. 5. It is manifest in the figure that the statistics of the velocity field are approximatively Gaussian (compare the tails with those of the λ and μ fields). We, therefore, conclude that our new algorithm is validated in the sense that it reproduces the Gaussian statistics in the incompressible limit.

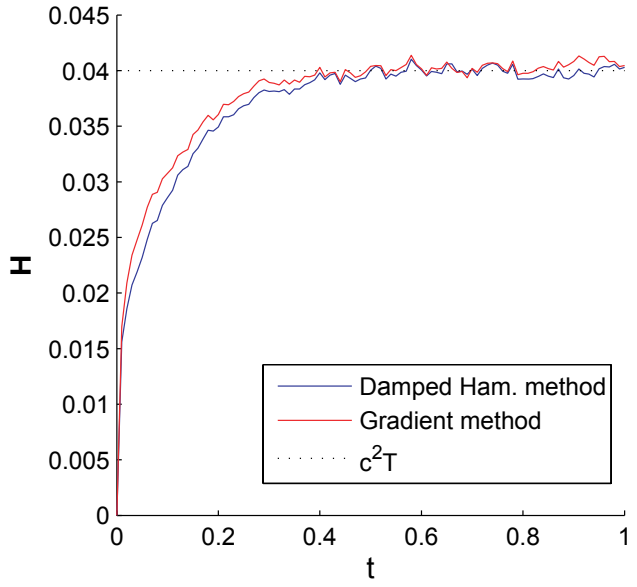

(a)

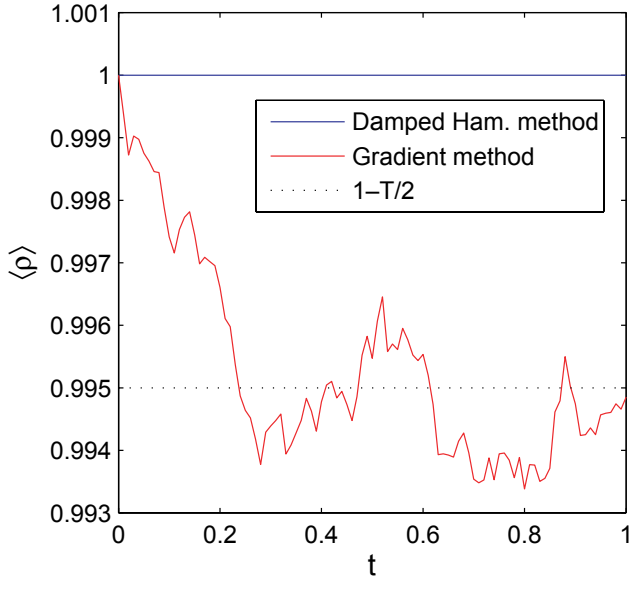

(b)

Fig. 6. (a) Convergence of compressible energy (12). (b) Plot of $\langle\rho\rangle$. Straight line: Gaussian value, $T = 0.01$.

5.2. *Compressible irrotational flows*

In order to validate our new algorithm in the compressible case (see Sec. 4.3.2) we will check that it generates data that is a statistical stationary solution of the original equation of motion and that it reproduces the spectrum obtained by direct relaxation in Sec. 3.

At low values of η, the distribution of ρ, ϕ is almost Gaussian and the predicted value of relevant quantities using the Hamiltonian (12) and the stationary probability density (33) read

$$\langle(\rho-1)^2\rangle = \frac{\mathcal{N}\eta}{c^2}, \quad \langle(\nabla\phi)^2\rangle = \mathcal{N}\eta, \quad \langle H\rangle = \mathcal{N}\eta$$

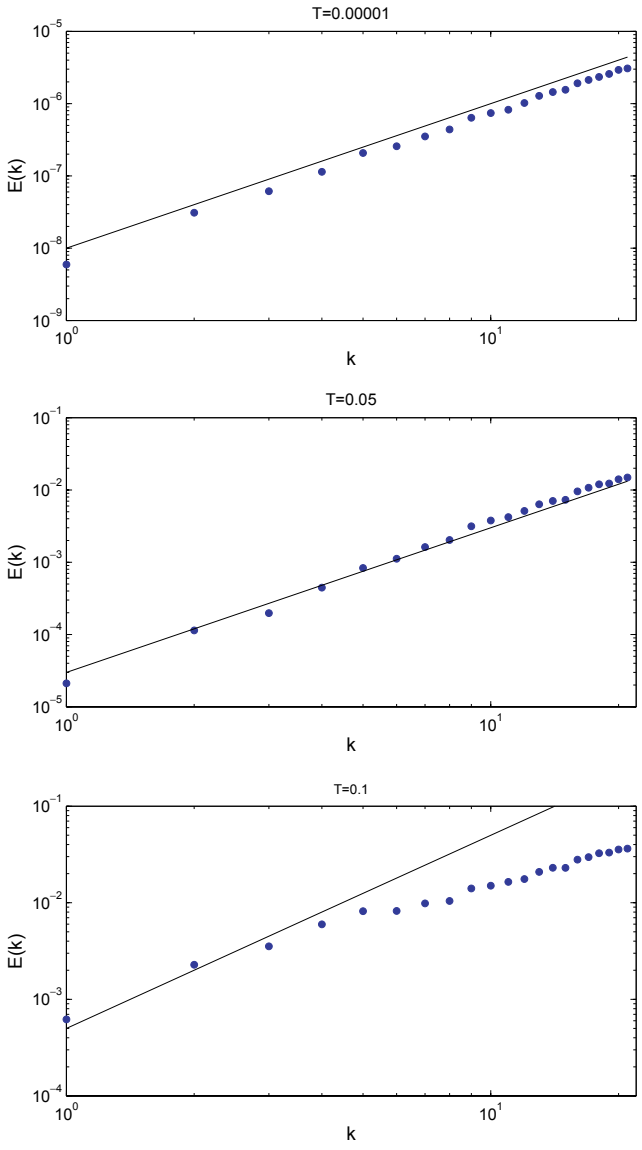

Fig. 7. Total compressible energy spectra for $T = 0.0001$, 0.05, 0.1.

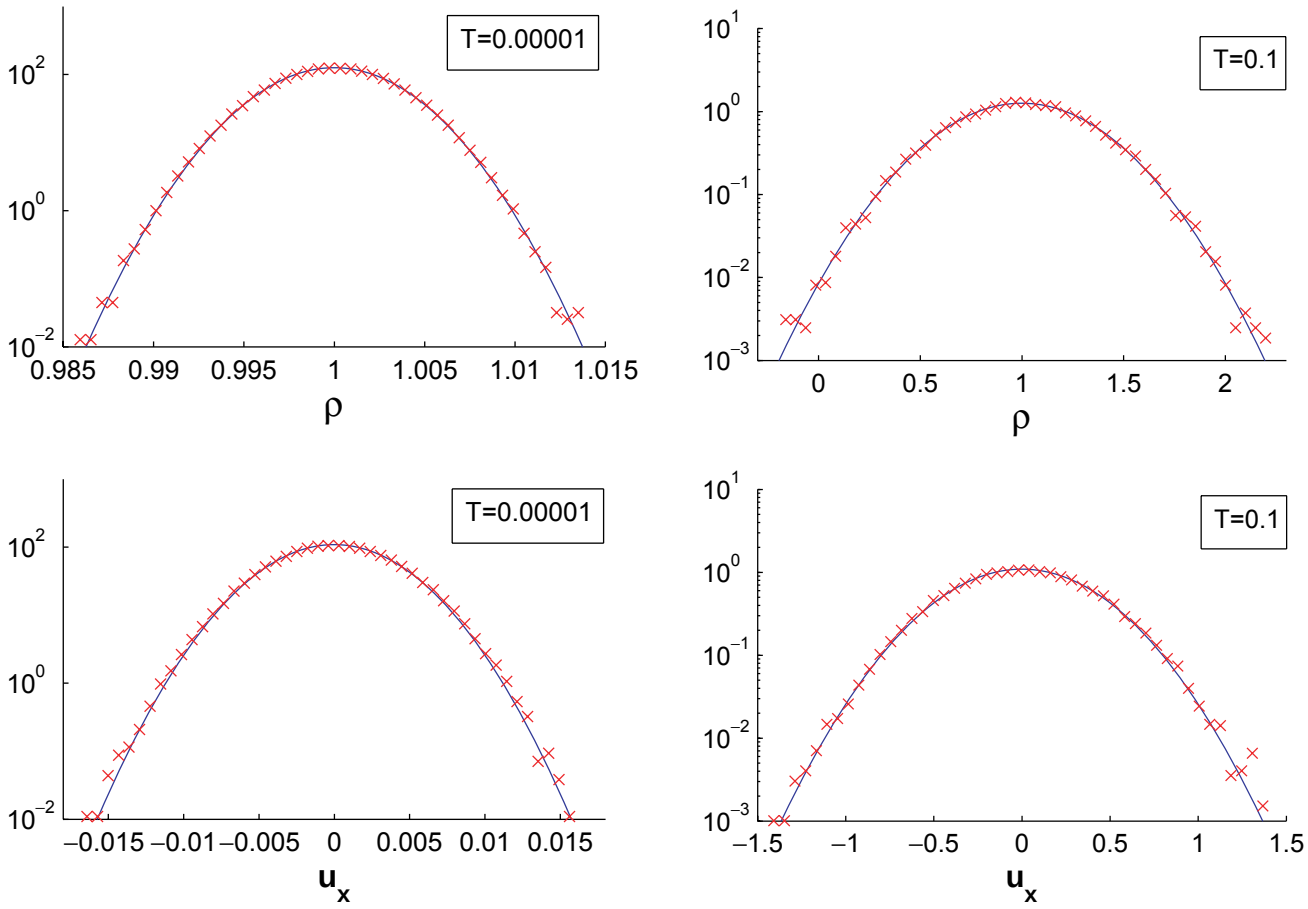

Fig. 8. Histograms of ρ and u_x obtained from Eqs. (56)–(58).

where $\mathcal{N}$ is the number of degrees of freedom. We redefine

$$\frac{1}{\eta} \equiv \beta = \frac{\mathcal{N}}{c^2 T}.$$

In what follows, we vary T in the numerics from $T = 0.00001$ to $T = 0.1$ using 64^3 Fourier modes and we set $c = 2$ and $\nu = 1$, using the usual equation of state (9). We start from the homogenous and minimum energy solution $\rho(x, t = 0) = 1, \phi(x, t = 0) = 0$ and the integration of Eqs. (56)–(58) is performed until convergence is achieved.

Figure 6 shows the convergence of the energy using both methods (56)–(58) and (35)–(36) at $T = 0.01$. We checked that the final data is a statistical stationary solution of the continuity and Bernouilli equations (6)–(8) (data not shown). Note that the convergence of the gradient method is not much faster than that of the damped Hamiltonian method. In this gradient case, the spatial average of the density fluctuates around the stationary value given by Eq. (59) $\langle\rho\rangle_{\text{st}} = 1 - (1/2)T$.

Figure 7 displays the energy spectra (17) computed on the time-converged solution of Eqs. (56)–(58), at different values of the temperature. Note that at high temperature the k^2 law is not manifest in the spectrum. This spectrum should be compared with those of Fig. 2(d) that were obtained by the relaxation of the original dynamics. The similarity of the spectra confirms that equipartition is not obtained in the compressible case because of the non-Gaussian term (21).

In Fig. 8, we show an histogram of $u_x = \partial_x \phi$ and ρ together with the Gaussian predictions, we see that they seem to remain Gaussian even for the highest values of $T = 0.1$. There are some low probability events with $\rho < 0$ and higher values of T will lead to more negatives values of ρ.

Note, however, that the total distribution is non-Gaussian. Indeed, if it remained Gaussian at higher values of T, the correlation between $\nabla\phi^2$ and $\rho - 1$ will vanish and this it is not observed in Fig. 9 where the histograms of $z = (\rho - 1)\nabla\phi^2$

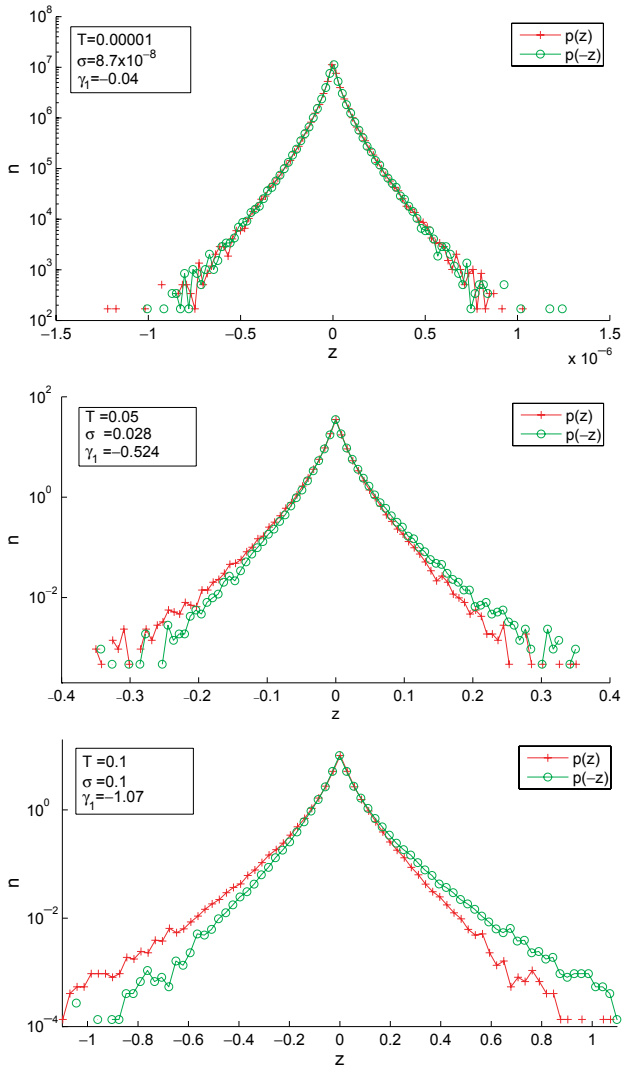

Fig. 9. Histograms of $z = (\rho - 1)\nabla\phi^2$ and $-z$ for $T = 0.0001, 0.05, 0.1$. In the insert the standard deviation σ and skewness γ_1.

and $-z$ are shown. Note that for the lowest temperature Fig. 9(a), the standard deviation is extremely small, the pdf is symmetric and all points are heavily concentrated around $z = 0$, the correlation between $\nabla\phi^2$ and $\rho - 1$ is thus completely negligible. However, for higher temperatures Figs. 9(b) and 9(c), the pdf becomes asymmetrical and the skewness $\gamma_1 = \mu_3/\sigma^3$, where μ_3 is the third moment about the mean and σ is the standard deviation, are of order one.

6. Relaxation of Initial Data with Temperature Oscillation

Let us now consider a practical application of our algorithm. We want to study how truncated irrotational compressible flows relax to the equilibrium. A big difference with the incompressible case studied in [Cichowlas *et al.*, 2005; Krstulovic & Brachet, 2008] is that waves can appear as the principal mechanism of homogenization as in the Landau two-fluid model for superfluids [Landau & Lifchitz, 1971] where the temperature waves propagate at a *second sound* speed slower than pressure waves. Indeed, Larraza and Putterman [1986] argued that, in a nonlinear medium pumped with energy sufficiently far from equilibrium the wave turbulence can support a transition from diffusive to propagative energy transport that bears deep similarities to second sound in Helium.

In this section we give preliminary results that seem to suggest that such a behavior is present. However, these results need to be confirmed and further studies will be presented in a future publication.

In order to check for the presence of this mechanism, we need to reduce the emission of (first) sound that would trivially generate propagative dynamics. To wit, we prepare an initial condition with constant pressure. In compressible flows, the pressure appears in the δ_{ij} contribution of the momentum flux density tensor

$$\Pi_{ij} = \rho u_i u_j + \delta_{ij} p \tag{64}$$

where for the internal energy (9), the pressure simply reads $p = (c^2/2)\rho^2$.

Consider now fluctuating fields replacing $\rho \to \rho + \rho'$ and $u_i \to u_i + u'_i$, where the quantities with primes are of zero mean and with the obvious correspondence $\widehat{u}_{j\mathbf{k}} = ik_j\hat{\phi}_{\mathbf{k}}$ and $\widehat{u}_{j\mathbf{k}} = ik_j\hat{\phi}'_{\mathbf{k}}$. The mean value of Π_{ij} over the different realization then reads

$$\langle\Pi_{ij}\rangle = \rho u_i u_j + \langle\rho u'_i\rangle u_j + \langle\rho u'_j\rangle u_i + \rho\langle u'_i u'_j\rangle + \langle\rho' u'_i u'_j\rangle + \delta_{ij}\frac{c^2}{2}(\rho^2 + \langle\rho'^2\rangle). \tag{65}$$

If we assume isotropy we obtain

$$\langle u'_i u'_j\rangle = \frac{\delta_{ij}}{d}\langle\mathbf{u}'^2\rangle \quad \langle\rho' u'_i u'_j\rangle = \frac{\delta_{ij}}{d}\langle\rho'\mathbf{u}'^2\rangle,$$

where d is the dimension of the space. The δ_{ij} contribution part of $\langle\Pi_{ij}\rangle$ is then

$$\tilde{p} = \frac{c^2}{2}\rho^2 + \frac{c^2}{2}\langle\rho'^2\rangle + \frac{\rho}{d}\langle\mathbf{u}'^2\rangle + \frac{1}{d}\langle\rho'\mathbf{u}'^2\rangle. \tag{66}$$

Consider that the small fluctuations of the fields are approximatively given by the stationary Gaussian pdf $P\{\hat{\rho}_{\mathbf{k}}, \hat{\phi}_{\mathbf{k}}\} \sim e^{-\beta\tilde{H}}$ where $\beta = \mathcal{N}/(c^2 T)$ and

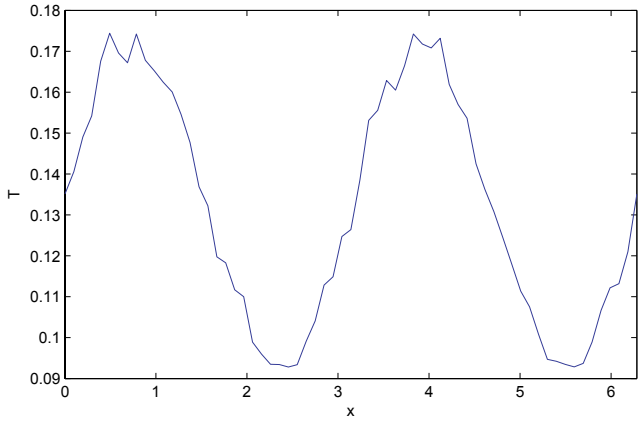

(a1)

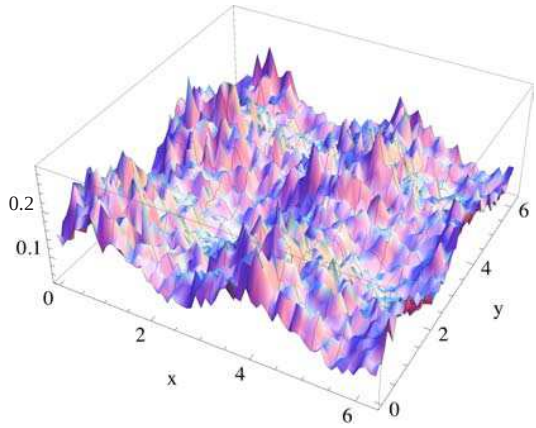

(b1)

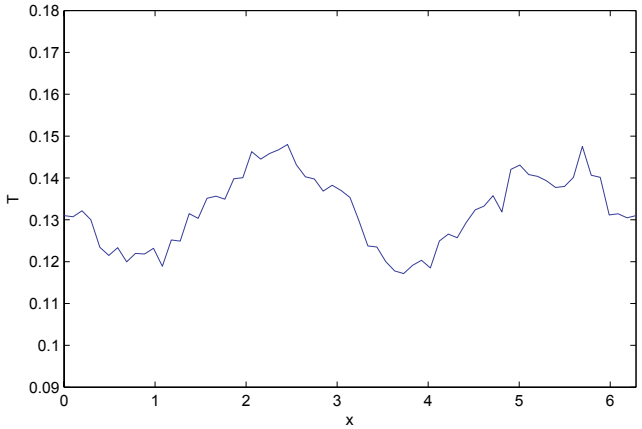

(a2)

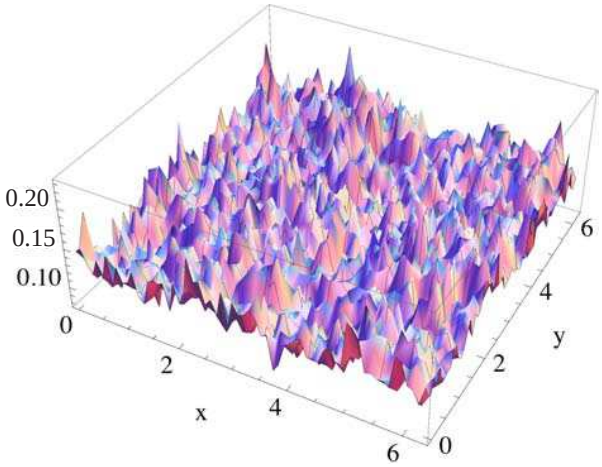

(b2)

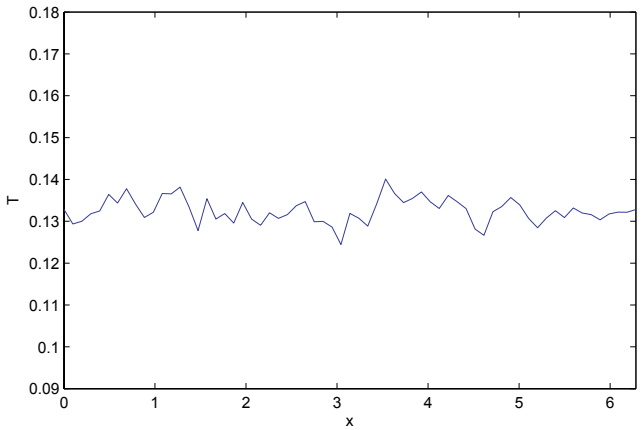

(a3)

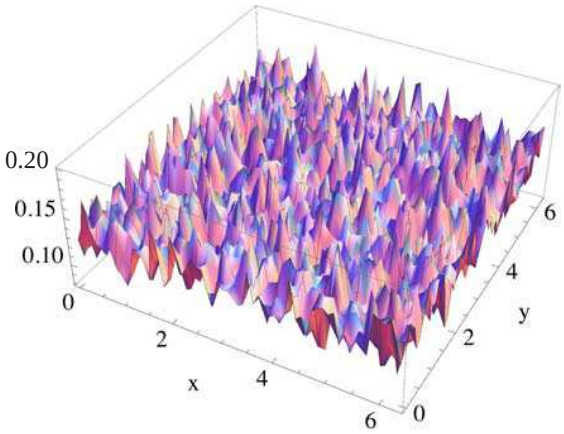

(b3)

Fig. 10. Temporal evolution of the spatially averaged temperatures over z, y [(a1)–(a3)] and z [(b1)–(b3)] corresponding to initial data (72) at $t = 0$, 1.4, 2.8.

$\tilde{H} = H_{\rm G} - \mu Q$ is defined in Eqs. (10), (11) and (20). After a straightforward calculation, it is possible to show that

$$\langle \rho \rangle = 1 + \frac{\mu}{c^2} \tag{67}$$

$$\langle \mathbf{u}'^2 \rangle = \frac{c^2}{1+\mu/c^2} \langle \rho'^2 \rangle = \frac{c^2}{1+\mu/c^2} T \tag{68}$$

$$\langle H \rangle = \frac{c^2}{2} \frac{2+\mu/c^2}{1+\mu/c^2} T. \tag{69}$$

Then $\tilde{p}$ reads at leading order

$$\tilde{p} = \frac{c^2}{2} \left(1 + \frac{\mu}{c^2}\right)^2 + \frac{d+2}{2d} c^2 T. \tag{70}$$

Thus setting

$$\frac{\mu}{c^2} = -1 + \sqrt{1 - T(d+2)/d} \tag{71}$$

yields a constant pressure $\tilde{p} = c^2/2$.

Consider now T and $\mu(T)$ given by Eq. (71) that are slow space variable functions where T has a sinus modulation

$$T(x,y,z) = T_0(1 + \epsilon(\sin(2x) + \sin(2y) + \sin(2z))). \tag{72}$$

We set in the present numeric simulation $T_0 = 0.03$ and $\epsilon = 0.3$. The temporal evolution of the spatially averaged temperatures over z, y and z is shown in Fig. 10. Note that there is a fast decay of the amplitude of the modulation as predicted in [Larraza & Putterman, 1986] for compressible flows. Remark that at $t = 1.4$ the phase of the wave changed in a factor π, that gives a rough estimate of the oscillation frequency $\omega_T = \pi/1.4 = 2.244$. This value is smaller than the frequency of first sound $\omega = ck = 4$.

The presence of an oscillating behavior in this constant pressure variable temperature relaxation strongly suggests the existence of second sound. However, this interesting behavior needs to be confirmed and studied in more detail. In the future, we will investigate the relaxation of full, first and second sound perturbations.

7. Conclusion

Our new method to generate absolute equilibrium of spectrally truncated compressible flows has been shown to reproduce the well-known Gaussian results in the incompressible limit. The irrotational compressible absolute equilibrium case was characterized and the distribution was shown to be non-Gaussian. The spectrum were found not to obey a k^2 scaling, just as those obtained directly by relaxation of the original dynamics. Finally, oscillating behavior in constant pressure variable temperature relaxation was obtained, suggesting the presence of second sound.

Acknowledgments

We acknowledge support from an ECOS/CONICYT action and one of the authors (ET) is grateful to the Project ACT 15 of CONICYT, Chile. The computations were carried out at IDRIS (CNRS).

References

Bos, W. J. T. & Bertoglio, J.-P. [2006] "Dynamics of spectrally truncated inviscid turbulence," *Phys. Fluids* **18**, 071701.

Cichowlas, C. [2005] *Equation d'Euler tronquée: de la dynamique des singularités complexes à la relaxation turbulente*, Université Pierre et Marie Curie — Paris VI.

Cichowlas, C., Bonaïti, P., Debbasch, F. & Brachet, M. E. [2005] "Effective dissipation and turbulence in spectrally truncated Euler flows," *Phys. Rev. Lett.* **95**, 26.

Connaughton, C., Josserand, C., Picozzi, A., Pomeau, Y. & Rica, S. [2005] "Condensation of classical nonlinear waves," *Phys. Rev. Lett.* **95**, 26.

Fermi, E., Pasta, J. & Ulam, S. [1955] *Studies of Nonlinear Problems. I*, Los Alamos Report LA 1940.

Frisch, U., Kurien, S., Pandit, R., Pauls, W., Ray, S. S., Wirth, A. & Zhu, J.-Z. [2008] "Hyperviscosity, Galerkin truncation and bottlenecks in turbulence," *Phys. Rev. Lett.* **101**, 144501.

Gottlieb, D. & Orszag, S. A. [1977] *Numerical Analysis of Spectral Methods* (SIAM, Philadelphia).

Kraichnan, R. H. [1973] "Helical turbulence and absolute equilibrium," *J. Fluid Mech.* **59**, 745–752.

Krstulovic, G. & Brachet, M. E. [2008] "Two-fluid model of the truncated Euler equations," *Physica D* **237**, 2015–2019.

Krstulovic, G., Mininni, P. D., Brachet, M. E. & Pouquet, A. [2009] "Cascades, thermalization and eddy viscosity in helical Galerkin truncated Euler flows," *Phys. Rev. E* **79**, 056304.

Landau, L. & Lifchitz, E. [1971] *Mécanique des Fluides* (MIR).

Langouche, F., Roekaerts, D. & Tirapegui, E. [1982] *Functional Integration and Semiclassical Expansions* (D. Reidel Pub. Co. Hingham).

Larraza, A. & Putterman, S. J. [1986] "Second sound in wave turbulence: A clue to the cause of anomalous plasma diffusivity," *Phys. Rev. Lett.* **57**, 22.

Lee, T. D. [1952] "On some statistical properties of hydrodynamical and magneto-hydrodynamical fields," *Quart. J. Appl. Math.* **10**, 69.

Mobbs, S. D. [1982] "Variational principles for perfect and dissipative fluid flows," *Proc. R. Soc. Lond. A* **381**, 457–468.

Orszag, S. A. [1970] "Analytical theories of turbulence," *J. Fluid Mech.* **41**, 363.

Orszag, S. A. [1977] *Statistical Theory of Turbulence*, Les Houches 1973: Fluid Dynamics, eds. Balian, R. & Peube, J. L. (Gordon and Breach, NY).

Putterlman, S. J. & Roberts, P. H. [1982] "Non-linear hydrodynamics and a one fluid theory of superfluid HE-4," *Phys. Lett. A* **89**, 444–447.

Putterman, S. J. & Roberts, P. H. [1983] "Classical non-linear waves in dispersive nonlocal media, and the theory of superfluidity," *Physica A* **117**, 369–397.

van Kampen, N. G. [2001] *Stochastic Processes in Physics and Chemistry* (North-Holland).

Part II

SUPERFLUIDS

5. THERMODYNAMICS OF CLASSICAL TRUNCATED AND QUANTUM SYSTEM

In this chapter we review some basic formulae of statistical mechanics. First we recall the classic and quantum statistics. Then the Raleigh-Jeans and Planck distribution are explicitly given. The ultra-violet catastrophe is then discussed. Next, we show the condensation process of classical non-interacting gases that is analogous to that one of Bose-Einstein condensation. Finally, low-temperature calculations for a weakly-interacting Bose gases are given in the quantum case. .

5.1 Basic formulae of statistical mechanics

5.1.1 Classical statistics

In the following we will consider the Hamiltonian of $\mathcal{N}$ independent harmonic oscillators of frequency ω_k

$$H(p_k, q_k) = \sum_{k=1}^{\mathcal{N}} \frac{p_k^2}{2m} + \frac{1}{2} m\omega_k^2 q_k^2, . \tag{5.1}$$

The partition function in the canonical ensemble, is a multiple integral over the phase space and its formula it is given by the semi-classical expression [56, 83]

$$\mathcal{Z}(T, V, \mathcal{N}) = \int \frac{dq^{\mathcal{N}} d^{\mathcal{N}} p}{(2\pi\hbar)^{\mathcal{N}}} e^{-\beta H(p_k, q_k)}, \tag{5.2}$$

where $\beta^{-1} = k_B T$ with k_B the Boltzman constant.

In analogy to quantum mechanics, instead of using the conjugate variables p_k, q_k, we will use the complex variables (that correspond to the creation and destruction operators in quantum mechanics)

$$a_k^\dagger = \sqrt{\frac{m\omega_k}{2\hbar}} q_k + \frac{i}{\sqrt{2m\hbar\omega_k}} p_k \tag{5.3}$$

$$a_k = \sqrt{\frac{m\omega_k}{2\hbar}} q_k - \frac{i}{\sqrt{2m\hbar\omega_k}} p_k. \tag{5.4}$$

After this transformation the Hamiltonian H in eq.(5.1) is expressed as

$$H(a_k, a_k^\dagger) = \sum_{k=1}^{\mathcal{N}} \epsilon_k a_k^\dagger a_k, \tag{5.5}$$

where $\epsilon_k = \hbar\omega_k$. The canonical partition function (5.2) is rewritten as

$$\mathcal{Z}(T, V, \mathcal{N}) = \int \prod_{k=1}^{\mathcal{N}} \frac{da_k^\dagger da_k}{(2\pi)^{\mathcal{N}}} e^{-\beta \sum_{k=1}^{\mathcal{N}} \epsilon_k a_k^\dagger a_k} = \prod_{k=1}^{\mathcal{N}} \int_{n_k=0}^{\infty} dn_k e^{-\beta\epsilon_k n_k} \tag{5.6}$$

where we have written the complex element of area in polar coordinate ($da_k^\dagger da_k = 2|a_k|d|a_k|d\theta$) and then make the change of variable to the *occupation number* variable $n_k = |a_k|^2$. The canonical partition function thus reads

$$\mathcal{Z}^{\mathrm{CL}}(T, V, \mathcal{N}) = \prod_{k=1}^{\mathcal{N}} \frac{1}{\beta\epsilon_k} \tag{5.7}$$

Observe that as consequence of classical statistics and the quadratic Hamiltonian the equipartition the energy [1] of each oscillator is $k_B T$. This property is know as the theorem of the energy equipartition. It trivially follows that

$$\overline{n_k}^{\mathrm{CL}} = \frac{1}{\beta\epsilon_k} \tag{5.8}$$

$$\overline{H} = \sum_{k=1}^{\mathcal{N}} k_B T = \mathcal{N} k_B T \tag{5.9}$$

As usual, the canonical potential is defined as [84, 56, 83],

$$F = -\beta^{-1} \log \mathcal{Z}, \tag{5.10}$$

from it directly follows all thermodynamic quantities. For example the entropy S is

$$S = -\left.\frac{\partial F}{\partial T}\right|_{V,\mathcal{N}} = k_B \sum_{k=1}^{\mathcal{N}} \left[1 + \log \beta\epsilon_k\right]. \tag{5.11}$$

Remember that for a classical system, the entropy is not completely defined. It depends on the phase space normalization constant. This problem is fixed with quantum mechanics which fixes this value to $2\pi\hbar$ (see eq.(5.2)).

[1] In the canonical ensemble the energy is $\overline{E} = -\partial_\beta \log \mathcal{Z}^{\mathrm{CL}}$

5.1.2 Quantum statistics

We now review the Bose-Einstein statistics. Consider a quantum system of indistinguishable particles. A state of the system will be characterized by the occupation numbers $\{n_k, k \in \mathbb{N}\}$. The energy H and the total number of particles N of the system are thus

$$H = \sum_{k=1}^{\infty} \epsilon_k n_k \tag{5.12}$$

$$N = \sum_{k=0}^{\infty} n_k. \tag{5.13}$$

For bosons the quantum canonical partition function is given by [56, 83]

$$\mathcal{Z}(T, V, N) = {\sum_{\{n_k\}}}' \exp\{-\beta \sum_{k=1}^{\infty} \epsilon_k n_k\} \tag{5.14}$$

where the sum is performed over all the occupation numbers $\{n_k\}$ such that $N = \sum_k n_k$. This last restriction is quite complicated to handle. To overcome this problem, the grand canonical ensemble is often used. In this ensemble the system can interchange particles with an external *reservoir*. The quantum grand canonical partition function is defined [56, 83] as

$$\mathcal{Z}(T, V, \mu) = \sum_{\{n_k\}} \exp\{-\beta \sum_{k=1}^{\infty} (\epsilon_k - \mu) n_k\}, \tag{5.15}$$

where μ is the chemical potential and without restrictions on $\{n_k\}$. This function can be simplified because it is a geometrical series:

$$\mathcal{Z}^{\mathrm{Q}}(T, V, \mu) = \prod_{k=1}^{\infty} \frac{1}{1 - e^{-\beta(\epsilon_k - \mu)}}. \tag{5.16}$$

We also have that the occupation number of particles in the state k is

$$\overline{n_k}^{\mathrm{Q}} = \frac{1}{e^{\beta(\epsilon_k - \mu)} - 1} \tag{5.17}$$

Recall that equipartition is recovered from (5.17) in the limit $\beta\epsilon_k \ll 1$, or equivalently $\hbar\omega_k \ll k_B T$.

5.2 Rayleigh-Jeans and Planck distribution

We discuss now the ultra-violet (UV) catastrophe present in classical system and manifest in the black body radiation problem. The Rayleigh-Jeans and Planck distribution

for the black body radiation are obtained from eqs. (5.8) and (5.17) by replacing the dispersions relation relation $\epsilon(\mathbf{p}) = c|\mathbf{p}|$. In three dimension the the spectral density of states $\rho(\mathbf{p})$ on the shell $|\mathbf{p}| = p$ is given by

$$\rho(\mathbf{p}) = s_{\mathrm{p}} \frac{p^2 V}{2\pi^2 \hbar^3}, \tag{5.18}$$

where the polarization factor is $s_{\mathrm{p}} = 2$ for photons.

The Rayleigh-Jeans and Planck energy distributions per unit of volume are simply $u^{\mathrm{RJ}}(p) = \epsilon(\mathbf{p}) n_{\mathbf{p}}^{\mathrm{CL}} \rho(\mathbf{p})/V$ and $u^{\mathrm{P}}(p) = \epsilon(\mathbf{p}) n_{\mathbf{p}}^{\mathrm{Q}} \rho(\mathbf{p})/V$. Expressing the momentum in term of the frequency $\omega = cp/\hbar$ we obtain

$$u^{\mathrm{RJ}}(\omega) d\omega = \frac{\omega^2}{c^3 \pi^2} k_B T d\omega \tag{5.19}$$

$$u^{\mathrm{P}}(\omega) d\omega = \frac{\omega^2}{c^3 \pi^2} \frac{\hbar \omega}{e^{\frac{\hbar \omega}{k_B T}} - 1} \tag{5.20}$$

Observe that both distributions coincide for low frequencies satisfying (or high temperature) $\hbar\omega \ll k_B T$. The Planck distribution has a exponential cut-off at the frequency $\omega_{\max} = k_B T/\hbar$.

The total energy is given by the integral over all the frequencies. That leads to an infinite energy for the Rayleigh-Jeans distribution. This unphysical situation, known as UV catastrophe, is naturally solved by the quantum mechanics description taken into account in the Planck distribution. Using the UV cut-off in the Rayleigh-Jeans distribution the energies are

$$E^{\mathrm{RJ}} = V \frac{\omega_{\max}^3}{3c^3 \pi^2} k_B T \tag{5.21}$$

$$E^{\mathrm{P}} = V \frac{\pi^2}{15} \frac{1}{\hbar^3 c^3} k_B^4 T^4 \tag{5.22}$$

We have explicitly introduced the cut-off $\omega_{\max}$ because it naturally appears in the thermodynamics of truncated system as those studied in chapter 2-4 (truncated Euler and MHD equations) and in the truncated Gross-Pitaevskii equation that will be studied next in chapter 6. Observe that the temperature dependence of the classical Rayleigh-Jeans energy and the quantum Planck energy are very different. The specific heat does not vanishes at low temperatures in the classical system and it is proportional to the number of degree of freedom (or frequencies allowed) $\mathcal{N} = V \frac{\omega_{\max}^3}{3c^3\pi^2}$ of the system. We will see in chapter 6 that the degree of freedom of a truncated system must be taken into account in order to correctly define the thermodynamics and it plays the role of particle with an associated "chemical potential".

5.3 Condensation of non-interacting gases with classical statistics

It is well know that at low temperatures quantum statistics for bosons (5.16) lead to situation where a large fraction of the boson occupies the fundamental state. This process is called the Bose-Einstein condensate [54]. The fraction of condensate particles N_0/N is given by

$$\frac{N_0}{N} = 1 - \left(\frac{T}{T_\mathrm{c}}\right)^{3/2} \tag{5.23}$$

where $T_\mathrm{c} = \frac{2\pi\hbar^2}{k_B m}\left[\frac{N}{V}\frac{1}{2.612}\right]^{2/3}$ is the condensation temperature.

The Bose-Einstein it is not an exclusive property of quantum statistics. It has been shown [30] that an analogous process takes place in a classical system with a truncation wavenumber.

Consider a 3-dimensional classical system where the energy are the number of particles are given by (5.12-5.13), with the dispersion relation $\epsilon(p) = \frac{p^2}{2m}$ and to avoid the UV divergences the momentum satisfies $|\mathbf{p}| \leq p_\mathrm{max}$. The grand partition function of the system trivially generalized from the canonical partition function eq.5.6 introducing the chemical potential as

$$\mathcal{Z}(T,V,\mu) = \prod_{|\mathbf{p}|\leq P_\mathrm{max}} \int_{n_\mathbf{p}=0}^{\infty} dn_\mathbf{p} e^{-\beta(\epsilon_\mathbf{p}-\mu)n_\mathbf{p}} = \prod_{|\mathbf{p}|\leq P_\mathrm{max}} \frac{1}{\beta(\epsilon_\mathbf{p}-\mu)} \tag{5.24}$$

Assuming a continuos repartition of momentum and using the spectral density $\rho(p)$ (5.18) with $s_\mathrm{p} = 1$, the grand canonical potential reads

$$\begin{aligned}\Omega(T,V,\mu) &= \beta^{-1}\int_0^{P_\mathrm{max}} dp \frac{p^2 V}{2\pi^2\hbar^3}\log\left[\beta(\epsilon_\mathbf{p}-\mu)\right] \qquad (5.25)\\ &= -\frac{P_\mathrm{max}^3 V}{6\pi^2\hbar^3\beta}\left[\frac{2}{3} + \frac{2(-2m\mu)^{3/2}\tan^{-1}\left(\frac{P_\mathrm{max}}{\sqrt{-2m\mu}}\right)}{{P_\mathrm{max}}^3} + \frac{4m\mu}{{P_\mathrm{max}}^2} - \log\left\{\beta\left(\frac{{P_\mathrm{max}}^2}{2m}-\mu\right)\right\}\right].\end{aligned}$$

From the standard thermodynamic relation [84, 56, 83],

$$\overline{N} = -\frac{\partial\Omega}{\partial\mu} \quad \text{and} \quad \overline{H} = \Omega - \beta\frac{\partial\Omega}{\partial\beta} + \mu\overline{N}, \tag{5.26}$$

we obtain

$$\overline{N} = \frac{P_{\max}^3 V}{6\pi^2\hbar^3\beta}\left[\frac{6m\sqrt{-2m\mu}\tan^{-1}\left(\frac{P_{\max}}{\sqrt{-2m\mu}}\right)}{{P_{\max}}^3} - \frac{6m}{{P_{\max}}^2}\right] \tag{5.27}$$

$$\overline{H} = \frac{P_{\max}^3 V}{6\pi^2\hbar^3\beta}\left[1 + \frac{6m\mu\sqrt{-2m\mu}\tan^{-1}\left(\frac{P_{\max}}{\sqrt{-2m\mu}}\right)}{{P_{\max}}^3} - \frac{6m\mu}{{P_{\max}}^2}\right] \tag{5.28}$$

It was shown in reference [30] that this system exhibits a condensation transition at finite temperature. That means that the chemical potential vanishes and the eq.(5.27) cannot be solved for a fixed N and $T < T_c$. Contours of $\overline{N}$ with $\hbar = 1$, $m = 1$, $V = 1$ and $P_{\max} = \sqrt{2}$ are displayed in Fig.5.1

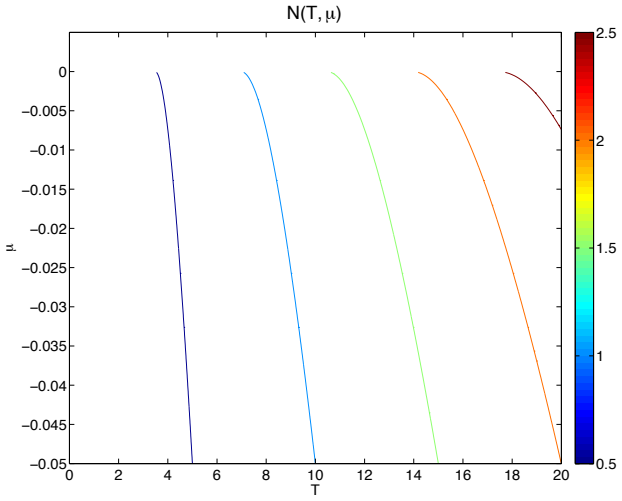

Fig. 5.1: Contours of $\overline{N}$. $\hbar = 1$, $m = 1$, $V = 1$, $P_{\max} = \sqrt{2}$. We observe a vanishing μ at $T = \pi^2/\sqrt{2}$ for $\overline{N} = 1$

The transition temperature is obtained replacing $\mu = 0$ in eq.(5.27) and it is given by

$$T_c = \frac{N\pi^2\hbar^3}{mP_{\max}V}. \tag{5.29}$$

Analogously to Bose-Einstein condensation, for temperature lower than T_c the integral over the momentum (5.26) does not capture the contribution due to condensate. Introducing the condensate population N_0 we find that the exited population satisfies

$$\frac{N_0}{N} = 1 - \frac{mP_{\max}V}{N\pi^2\beta\hbar^3}. \tag{5.30}$$

The number of condensed particles thus vanishes linearly at $T = T_c$.

In references [29, 30, 31] the condensation of non-linear waves described by the Fourier truncated Gross-Pitaevskii equation (TGPE) was reported. They performed microcanonical simulations by long-time integration of TGPE. Using a modified wave turbulence theory with ultraviolet cutoff, Connaughton et al. [30] argued that the transition to condensation should be subcritical. However, the authors later argued that, as weak turbulence theory is expected to breakdown nearby the transition to condensation, the subcritical nature of the transition predicted by the theory was not physical [31]. In the next chapter 6 (and the article [38] therein) we study this transition in the grand canonical ensemble. We then (numerically) show that the condensation transition of TGPE corresponds the second order transition described by the $\lambda - \phi^4$ theory with two components.

5.4 Low-temperature thermodynamics for weakly interacting Bose gases with quantum statistics

We now turn to the explicit computation of the low-temperature thermodynamics of weakly interacting Bose gas. In the approximation of small momenta the Hamiltonian of a system of bosons interacting in pairs is [85]

$$\hat{H} = \sum_{\mathbf{p}} \frac{p^2}{2m} a^\dagger_{\mathbf{p}} a_{\mathbf{p}} + \frac{g^2}{2V} \sum_{\mathbf{p_1},\mathbf{p_2}} a^\dagger_{\mathbf{p_1}} a^\dagger_{\mathbf{p_2}} a_{\mathbf{p_1}} a_{\mathbf{p_2}}. \tag{5.31}$$

where $g = \frac{4\pi a \hbar^2}{m}$, with a the s-wave scattering length.

In a Bose gas at low temperature most of the particle are in the condensate mode $\mathbf{p} = \mathbf{0}$. It is thus reasonable to treat the number operator $a^\dagger_{\mathbf{0}} a_{\mathbf{0}}$ as a number. Expanding the Hamiltonian (5.31) and explicitly introducing the number a_0 we obtain

$$\hat{H} = \frac{g}{2V} |A_{\mathbf{0}}|^4 + \sum_{\mathbf{p}} \frac{p^2}{2m} a^\dagger_{\mathbf{p}} a_{\mathbf{p}} + \frac{g}{2V} \sum_{\mathbf{p}\neq\mathbf{0}} a^{*2}_{\mathbf{0}} a_{\mathbf{p}} a_{-\mathbf{p}} + a^2_{\mathbf{0}} a^\dagger_{\mathbf{p}} a^\dagger_{-\mathbf{p}} + \dots. \tag{5.32}$$

where be have kept only the quadratic terms in the operators $a^\dagger_{\mathbf{p}}$. This the so-called Bogoliubov approximation [85, 86].

We now want to compute the statistics with the Hamiltonian (5.32). Remark that the total number operator

$$\hat{N} = |a_0|^2 + \sum_{\mathbf{p}\neq\mathbf{0}} a^\dagger_{\mathbf{p}} a_{\mathbf{p}} \tag{5.33}$$

does not commute with H due to non-diagonal terms and therefore the canonical statistics cannot be applied directly (see section 2.2 of reference [86] and references therein). To go around this problem we use the grand canonical ensemble. Furthermore, we will

use a more general ensemble also including the momentum operator

$$\hat{\mathbf{P}} = \sum_{\mathbf{p}} \mathbf{p} a^{\dagger}_{\mathbf{p}} a_{\mathbf{p}}, \tag{5.34}$$

that allows the system to exchange momentum with the *reservoir*.

We thus need the eigenvalues of the operator

$$\hat{F} = \hat{H} - \mu \hat{N} - \mathbf{W} \cdot \hat{\mathbf{P}}. \tag{5.35}$$

The operator $\hat{F}$ can diagonalized using the Bogoliubov transformation

$$a_{\mathbf{p}} = u_p b_{\mathbf{p}} + v_p b^{\dagger}_{-\mathbf{p}}. \tag{5.36}$$

where u_p and v_p are determined by imposing the diagonalization and $b_{\mathbf{p}}$ are called phonons annihilation operators. Next in chapter 6 (article [38]) the calculations corresponding to the classical version of the problem are explicitly performed.

After the transformation eq.(5.35) becomes

$$\hat{F} = \frac{g}{2V}|a_{\mathbf{0}}|^4 - \mu |a_{\mathbf{0}}|^4 + \sum_{\mathbf{p}\neq+\mathbf{0}} (\epsilon(p;\mu) - \mathbf{W}\cdot\mathbf{p}) b^{\dagger}_{\mathbf{p}} b_{\mathbf{p}} \tag{5.37}$$

where

$$\epsilon(p;\mu) = \sqrt{\frac{p^2}{2m}\left(\frac{p^2}{2m} + 2\mu\right)}. \tag{5.38}$$

Using classical statistics for a_0 and Bose-Einstein statistics for the phonons the grand canonical partition function is (keeping only non-vanishing terms in the thermodynamic limit [2])

$$\mathcal{Z} = e^{\frac{\beta V \mu^2}{2g}} \prod_{\mathbf{p}\neq\mathbf{0}}^{\infty} \frac{1}{1 - e^{-\beta(\epsilon(p;\mu) - \mathbf{W}\cdot\mathbf{p})}}. \tag{5.39}$$

Setting $W = (0,0,w)$ the grand canonical potential splits as

$$\Omega = \Omega_0 + \Omega_{\mathrm{ph}} \tag{5.40}$$

with

$$\Omega_0 = -\frac{V\mu^2}{2g} \tag{5.41}$$

$$\Omega_{\mathrm{ph}} = -\beta^{-1} \int_0^{\infty}\int_{-1}^{1} dp dz \frac{p^2 V}{4\pi^2\hbar^3} \log\left[\frac{1}{1 - e^{-\beta\left(\sqrt{\frac{p^2}{2m}\left(\frac{p^2}{2m}+2\mu\right)} - wpz\right)}}\right] \tag{5.42}$$

[2] The thermodynamic is taken over the grand canonical potential $\Omega = -\beta^{-1}\log\mathcal{Z}$ as $V\left(\lim_{V\to\infty}\frac{\Omega}{V}\right)$.

The integral in (5.42) cannot be done explicitly. However, it can be developed in powers of β^{-1} and w. To obtain a such development an integration by parts is first carried over the logarithmic term. Then the change of variable $\epsilon(p;\mu) = \varepsilon$ is used. Finally, the integral is expanded in Talyor series and the integration is made over the energies. The first orders of Ω obtained by this procedure explicitly read

$$\Omega = -\frac{V\mu^2}{2g} - \frac{\pi^2 m^{3/2} V}{90\beta^4\mu^{3/2}\hbar^3} - \frac{\pi^2 m^{5/2} V w^2}{45\beta^4\mu^{5/2}\hbar^3} + \frac{\pi^4 m^{3/2} V}{126\beta^6\mu^{7/2}\hbar^3} + \frac{\pi^4 m^{5/2} V w^2}{18\beta^6\mu^{9/2}\hbar^3}\ldots \tag{5.43}$$

All the thermodynamic quantities follow from this expression. For example the specific heat and the momentum[3] are given by

$$C = \frac{2\pi^2 m^{3/2} V}{15\mu^{3/2}\hbar^3} + \frac{4\pi^2 m^{5/2} V w^2}{15\mu^{5/2}\hbar^3} + \ldots \tag{5.44}$$

$$\overline{P} = \frac{2\pi^2 m^{5/2} V w}{45\beta^4\mu^{5/2}\hbar^3} - \frac{\pi^4 m^{5/2} V w}{9\beta^6\mu^{9/2}\hbar^3} + \ldots \tag{5.45}$$

This expression correspond to those obtained in the low-temperature limit by using the dispersion relation $\epsilon(\mathbf{p}) = (\mu/m)^{1/2} p$ [85].

5.5 Conclusions

In this chapter we have reviewed some basic formulae of statistical mechanics, including the partition function for classic and quantum statistics. Using this formulae, the black body radiation distribution was studied. The UV catastrophe, that is present in all the system studied in this thesis, was discussed.

We have also shown that transition analogous to the Bose-Einstein condensation also takes place with classical statistics. The idea that classical statistics can reproduce some aspects of quantum system is well known. It was argued by Davis et al. [29] that at finite temperature classical field statistics can be used to describe a Bose-Einstein condensate (BEC). The main point is that in the limit where the exited states are highly occupied ($N_p \gg 1$) the classical fluctuation of the field can overwhelm the quantum fluctuations. In this context, the truncated Gross-Pitaevskii equation (TGPE) has been proposed as a model BEC at finite temperature. We expect then that the approach of TGPE should work at the lambda transition temperature. Some properties and results on this equation will be presented in the next chapter.

Finally, the explicit calculation of the low-temperature Bose-Einstein grand canonical potential has been given. The potential was obtained using the Bogoliubov dispersion relation and performing series expansions.

[3] The momentum is computed as $\overline{P} = -\frac{\partial\Omega}{\partial w}$.

6. TRUNCATED GROSS-PITAEVSKII EQUATION. THERMALIZATION, MUTUAL FRICTION AND COUNTERFLOW EFFECTS

In this chapter we review the mathematical description of superfluid by the Gross-Pitaevski equation (GPE) and its basic properties. This will allow us to discus our publication presented at the end of this chapter that deals on on thermalization, mutual friction and counterflow effects in TGPE. First, the GPE is introduced and the conservation laws are explicitly given. Next, the acoustic propagation is reviewed and the energy decomposition in terms of hydrodynamical variables is introduced. Then, the applicability of Kolmogorov phenomenology of turbulence to superfluids is discussed. Finally, the last section contains the publication (to be submitted). Some supplementary material (mainly 3D density visualizations) is given at the end of the chapter

6.1 Introduction

The phenomenology of superfluid is usually modeled by the Landau two-fluid model [54]. This model supposes that there are two interpenetrating fluids present in the system, the one corresponding to a perfect and potential fluid is know as the *superfluid* and the other one corresponds to a viscous fluid due to thermal excitations is called *normal* fluid. It is important to remark that such description considering two different fluids is a mathematical construction, there is no way to physically separate the two fluids. Nevertheless, there are many physical aspect that the Landau two-fluid model allows to understand.

At finite temperature, when thermal excitations are present, these two fluids interact producing the effect of mutual friction and counterflows. On the contrary, at very low temperature, the thermal excitations are so weak that the normal fluid can be neglected. Is in such approximation that the Gross-Pitaevskii equation appears as model of superfluidity [87, 88]. This equation is a partial differential equation (PDE) for a complex function ψ that reads

$$i\hbar\frac{\partial\psi}{\partial t} = -\frac{\hbar^2}{2m}\nabla^2\psi + g|\psi|^2\psi, \tag{6.1}$$

where $|\psi|^2$ is the number of particle per unit volume, m is the mass of the condensed

particles and $g = \frac{4\pi a\hbar^2}{m}$ with a the s-wave scattering length. This equation is also known as (defocusing) non-linear Schrödinger equation. When $g < 0$ it is known as focusing NLSE.

Equation (6.1) comes from a variational principle with the action

$$\mathcal{A} = \int dt\, d^3x \left[\frac{i\hbar}{2}\left(\bar{\psi}\frac{\partial\psi}{\partial t} - \psi\frac{\partial\bar{\psi}}{\partial t}\right)\right] - \int dt H \tag{6.2}$$

where

$$H = \int d^3x \left(\frac{\hbar^2}{2m}|\nabla\psi|^2 + \frac{g}{2}|\psi|^4\right) \tag{6.3}$$

is the Hamiltonian.

Observe that a global change of phase of the wavefunction ψ implies a change of the density at equilibrium. Equation (6.1) is sometimes written with an extra $\mu\psi$ term. This term has no dynamical effect and can be arbitrarily added.

There exists a one-to-one correspondence between fluid dynamics and GPE. It is given by the Madelung transformation defined by

$$\psi(\mathbf{x}, t) = \sqrt{\frac{\rho(\mathbf{x}, t)}{m}}\exp\left[i\frac{m}{\hbar}\phi(\mathbf{x}, t)\right], \tag{6.4}$$

where $\rho(\mathbf{x}, t)$ is the density and $\phi(\mathbf{x}, t)$ is the potential velocity such that $\mathbf{v} = \nabla\phi$. The Madelung transformation (6.4) is singular on the zeros of ψ. As two conditions are required (the real and imaginary part of ψ must vanish) these singularities generally take place on points in two-dimension and on curves in three-dimensions. The Onsager-Feynman quantum of velocity circulation around vortex lines $\psi = 0$ is given by h/m.

Equation (6.1) expressed in terms of the hydrodynamical variables reads

$$\frac{\partial\rho}{\partial t} + \nabla\cdot\rho\mathbf{v} = 0 \tag{6.5}$$

$$\frac{\partial\phi}{\partial t} + \frac{1}{2}(\nabla\phi)^2 + \frac{g}{m^2}\rho - \frac{\hbar^2}{2m^2}\frac{\nabla^2\sqrt{\rho}}{\sqrt{\rho}} = 0 \tag{6.6}$$

Equation (6.5) is the continuity equation and eq.(6.6) is the known as the Bernoulli equation plus a term called quantum pressure. These are the equations governing the dynamics of isentropic, compressible and irrotational fluids.

6.1.1 Conserved quantities and Galilean invariance

Equation (6.1) is invariant under phase rotation, time and space translation. Using Noether theorem [89] it is straightforward to show that the conservation laws are

$$\partial_t(\psi\bar{\psi}) + \partial_k\left\{i\frac{\hbar}{2m}(\psi\partial_k\bar{\psi} - \bar{\psi}\partial_k\psi)\right\} = 0 \tag{6.7}$$

$$\partial_t\left(\frac{i\hbar}{2}(\psi\partial_j\bar{\psi} - \bar{\psi}\partial_j\psi)\right) + \partial_k\Pi_{kj} = 0 \tag{6.8}$$

$$\partial_t\left(\frac{\hbar^2}{2m}\partial_k\psi\partial_k\bar{\psi} + \frac{1}{2}g|\psi|^4\right) + \partial_k Q_k = 0 \tag{6.9}$$

where the momentum and energy flux respectively are

$$\Pi_{kj} = \frac{\hbar^2}{2m}(\partial_k\bar{\psi}\partial_j\psi + \partial_k\psi\partial_j\bar{\psi}) + (\frac{g}{2}|\psi|^4 - \frac{\hbar^2}{4m}\partial_{ll}|\psi|^2)\delta^k_j \tag{6.10}$$

$$Q_k = \frac{i\hbar^3}{4m^2}\left(\partial_k\psi\partial_{jj}\bar{\psi} - \partial_k\bar{\psi}\partial_{jj}\psi\right) + g|\psi|^2\left(\frac{i\hbar}{2m}(\psi\partial_k\bar{\psi} - \bar{\psi}\partial_k\psi)\right). \tag{6.11}$$

It follows directly from (6.7-6.9) that the Hamiltonian H, the total number of particles N and the momentum $\mathbf{P}$ defined by

$$H = \int_V d^3x\left(\frac{\hbar^2}{2m}|\nabla\psi|^2 + \frac{g}{2}|\psi|^4\right) \tag{6.12}$$

$$N = \int_V |\psi|^2\, d^3x \tag{6.13}$$

$$\mathbf{P} = \int_V \frac{i\hbar}{2}\left(\psi\nabla\bar{\psi} - \bar{\psi}\nabla\psi\right)\, d^3x. \tag{6.14}$$

are conserved by the GPE dynamics.

Finally remark that GPE (6.1) is invariant under the Galilean transformation

$$\psi'(\mathbf{x},t) = \psi(\mathbf{x} - \mathbf{v}_\mathrm{s}t, t)\exp\left\{\frac{im}{\hbar}\left[\mathbf{v}_\mathrm{s}\cdot\mathbf{x} - \frac{1}{2}v_\mathrm{s}^2 t\right]\right\}. \tag{6.15}$$

Under this transformation eqs.(6.10-6.14) transform as

$$H' = \frac{1}{2}mNv_\mathrm{s}^2 + \mathbf{P}\cdot\mathbf{v}_\mathrm{s} + H \tag{6.16}$$

$$N' = N \tag{6.17}$$

$$\mathbf{P}' = mN\mathbf{v}_\mathrm{s} + \mathbf{P}. \tag{6.18}$$

$$\Pi'_{kj} = mNv_{\mathrm{s}k}v_{\mathrm{s}j} + v_{\mathrm{s}k}P_j + v_{\mathrm{s}j}P_k + \Pi_{kj} \tag{6.19}$$

$$\mathbf{Q}' = (\frac{1}{2}mNv_\mathrm{s}^2 + \mathbf{P}\cdot\mathbf{v}_\mathrm{s} + H)\mathbf{v}_\mathrm{s} + \frac{1}{2}v_\mathrm{s}^2\mathbf{P} + \mathbf{\Pi}\cdot\mathbf{v}_\mathrm{s} + \mathbf{Q} \tag{6.20}$$

6.1.2 Sound propagation

The simplest stable solution of eq.(6.1) correspond to a wave function of homogeneous density $|\psi|^2 = |A_0|^2$. The linearization of eq.(6.1) around the solution $\psi = A_0 e^{-i\mu t}$ (with $\mu = g|A_0|^2/\hbar$) leads to the Bogoliubov dispersion relation

$$\omega(k) = \sqrt{\frac{g|A_0|^2}{m}k^2 + \frac{\hbar^2}{4m^2}k^4}. \tag{6.21}$$

The sound velocity thus given by $c = \sqrt{g|A_0|^2/m}$ and dispersive effects take place for length scales smaller than the coherence length defined as

$$\xi = \sqrt{\hbar^2/2m|A_\mathbf{0}|^2 g}. \tag{6.22}$$

ξ is also the length scale of the vortex core [27, 90].

6.1.3 Energy decomposition

Using the Madelung transformation (6.4) the energy can be decomposed into different terms of different nature. Following Nore et al. [27] we define the total energy per unit of volume $e_{\rm tot}$ as

$$e_{\rm tot} = \frac{1}{V}[H - \mu N] - \frac{\mu^2}{2g}. \tag{6.23}$$

This energy reexpressed in terms of the hydrodynamical variables reads

$$e_{\rm tot} = \frac{1}{V}\int d^3x \left[\frac{1}{2}(\sqrt{\rho}\mathbf{v})^2 + \frac{g}{2m}\left(\rho - \frac{\mu}{gm}\right)^2 + \frac{\hbar^2}{2m^2}\left(\nabla\sqrt{\rho}\right)^2\right] \tag{6.24}$$

We recognize three terms, the total kinetic energy $E_{\rm kin}$, the internal energy $E_{\rm int}$ and the quantum energy $e_{\rm q}$ defined by

$$e_{\rm kin} = \frac{1}{V}\int d^3x \frac{1}{2}(\sqrt{\rho}\mathbf{v})^2 \tag{6.25}$$

$$e_{\rm int} = \frac{1}{V}\int d^3x \frac{g}{2m^2}\left(\rho - \frac{\mu m}{g}\right)^2 \tag{6.26}$$

$$e_{\rm q} = \frac{1}{V}\int d^3x \frac{\hbar^2}{2m^2}\left(\nabla\sqrt{\rho}\right)^2. \tag{6.27}$$

With this decomposition we have $e_{tot} = e_{\rm kin} + e_{\rm int} + e_{\rm q}$.

To separate the energy coming from sound waves, the total kinetic energy can be further decomposed into compressible $e^{\rm c}_{\rm kin}$ and incompressible $e^{\rm i}_{\rm kin}$ by computing the kinetic term as $\sqrt{\rho}\mathbf{v} = (\sqrt{\rho}\mathbf{v})^{\rm c} + (\sqrt{\rho}\mathbf{v})^{\rm i}$ where $\nabla\cdot(\sqrt{\rho}\mathbf{v})^{\rm i} = 0$. This decomposition is obtained applying the projector $P_{\mu\nu} = \partial_\mu\partial_\nu - \frac{\delta_{\mu\nu}}{\nabla^2}$. The incompressible kinetic energy

contains the contribution of vortices to the kinetic energy.

As the quantities in integrals (6.25-6.27) are quadratic, the respective spectra $e^{\rm c}_{\rm kin}(k)$, $e^{\rm i}_{\rm kin}(k)$, $e_{\rm int}(k)$ and $e_{\rm q}$ can be easily defined by Parseval theorem summing over the angles. For instance the kinetic energy spectrum is defined as

$$e_{\rm kin}(k) = \int |\widehat{\sqrt{\rho}\mathbf{v}}(\mathbf{k})|^2 k^2 d\Omega_k, \tag{6.28}$$

where $d\Omega_k$ is the surface measure of the sphere [1].

6.1.4 Kolmogorov spectrum and Kelvin waves cascade

There is two main length scales in superfluid. The first one corresponds to the mean inter-vortex distance ℓ and the second one to the vortex core size ξ. At length scales much larger than ℓ is expected that the dynamics will be blind to the quantum nature of the vortex tangle. The phenomenology in this range of scale can be described by classical fluid dynamics. For a complex vortex tangle, we expect a turbulent behavior that can be thus described by Kolmogorov phenomenology (see chapter 2). This point has been largely investigated numerically and experimentally [26, 27, 91, 92, 28].

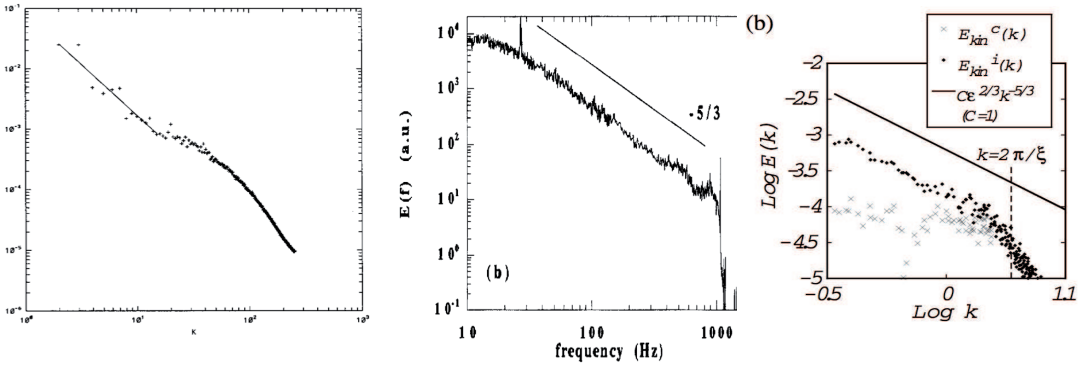

Fig. 6.1: Left) Incompressible kinetic energy spectrum from [27].Solid line shows least-square fit over $2 < k < 16$ $E^{\rm i}_{\rm kin} = 0.08k^{-1.7}$. Center) Pressure fluctuation at $T = 1.4K$ from [91] . c) Compressible and Incompressible kinetic energy spectrum from [93]

For scales smaller of the inter-vortex distance ℓ a different mechanism is expected. At these scales, vortex reconnection is important. Once the vortex reconnect, cusps are produced and Kelvin waves propagate along the vortex filament producing sound emission. This mechanism carries the energy from the scale to ℓ to smaller scales. It is expected to observe in this range a Kelvin wave cascade. There are many theoretical approaches to compute the exponent of the energy spectrum of the Kelvin waves cascade [94, 95, 96, 97]. Finally, as the energy transfer by Kelvin waves is less efficient than

[1] Remark that by definition $e_{\rm kin} = \int_k e_{\rm kin}(k)$

a direct (Kolmogorov) cascade a scenario with both, Kolmogorov and Kelvin waves cascades, joined by a k^2 power-law partial thermalized zone was suggested by [15].

6.2 Finite-temperature models of Bose-Einstein condensation

As discussed at the beginning of this chapter the GPE (6.1) is a valid description of weakly-interacting Bose-Einstein condensates (BEC) in the limit $T \to 0$ and neglects effects due to thermal fluctuations. There are several models that have been proposed to take into account the effect of the thermal cloud of uncondensed particles [90, 98]. In this section we will give a rough overview of how these different models arise. Most of the discussion is based on the review [90].

The starting point is the second quantization Hamiltonian expressed in the occupation number representation. It is written in terms of the Bose field operators $\hat{\Psi}(\mathbf{r},t)$ and $\hat{\Psi}^\dagger(\mathbf{r},t)$, that respectively represent the annihilation and creation of a particle in the point $\mathbf{r}$ at time t. The Hamiltonian reads

$$\hat{H} = \int d\mathbf{r}\hat{\Psi}^\dagger(\mathbf{r},t)\hat{h}_0\hat{\Psi}(\mathbf{r},t) + \frac{g}{2}\int d\mathbf{r}\hat{\Psi}^\dagger(\mathbf{r},t)\hat{\Psi}^\dagger(\mathbf{r},t)\hat{\Psi}(\mathbf{r},t)\hat{\Psi}(\mathbf{r},t) \tag{6.29}$$

where

$$\hat{h}_0 = -\frac{\hbar^2}{2m}\nabla^2 + V_{\text{ext}}(\mathbf{r},t). \tag{6.30}$$

is the operator describing a free particle in an external pseudo-potential $V_{\text{ext}}(\mathbf{r},t)$. In the second term of eq.(6.29) we have used the interaction potential $V(\mathbf{r}-\mathbf{r}') = g\delta(\mathbf{r}-\mathbf{r}')$ (with g defined just below eq.(6.1)). This approximation is valid for dilute gases ($na^3 \ll 1$ with n the particle density) at low temperature.

The temporal evolution of the Bose field is given by

$$i\hbar\frac{\partial\hat{\Psi}(\mathbf{r},t)}{\partial t} = [\hat{\Psi}(\mathbf{r},t),\hat{H}] = \hat{h}_0\hat{\Psi}(\mathbf{r},t) + g\hat{\Psi}^\dagger(\mathbf{r},t)\hat{\Psi}(\mathbf{r},t)\hat{\Psi}(\mathbf{r},t). \tag{6.31}$$

Assuming that there is a macroscopically occupied state (the condensate), it is natural to reexpress the Bose field in two part; $\hat{\Psi}(\mathbf{r},t) = \hat{\phi}(\mathbf{r},t) + \hat{\delta}(\mathbf{r},t)$ corresponding respectively to a field operator for the condensate part $\hat{\phi}(\mathbf{r},t)$ and the non-condensate part $\hat{\delta}(\mathbf{r},t)$.

In the limit of a large number of condensate atoms $N_0 \gg 1$ the operator $\hat{\phi}(\mathbf{r},t)$ can be replaced by a classical field often called the condensate wavefunction. This replacement is known as the Bogoliubov approximation. With this the Bose field becomes

$$\hat{\Psi}(\mathbf{r},t) = \phi(\mathbf{r},t) + \hat{\delta}(\mathbf{r},t). \tag{6.32}$$

This approximation breaks the global phase symmetry leading a to a non-conservation of the number of particles (intuitively $N_0 \pm 1 \approx N_0$ for $N_0 \gg 1$). It is thus natural to compute the statistics of this system in the grand canonical ensemble, however statistics

can also be computed in the canonical ensemble after the introduction of new operators (see [90, 86] for details).

The total density of particles $n(\mathbf{r},t)$ is thus written as

$$\begin{aligned} n(\mathbf{r},t) &= n_{\mathrm{c}}(\mathbf{r},t)+\tilde{n}(\mathbf{r},t) && (6.33)\\ n_{\mathrm{c}}(\mathbf{r},t) &= |\phi(\mathbf{r},\mathbf{t})|^2 && (6.34)\\ \tilde{n}(\mathbf{r},t) &= \langle\hat{\delta}^\dagger(\mathbf{r},\mathbf{t})\hat{\delta}(\mathbf{r},\mathbf{t})\rangle, && (6.35)\end{aligned}$$

where $n_{\mathrm{c}}(\mathbf{r},t)$ and $\tilde{n}(\mathbf{r},t)$ respectively are the condensate and the non-condensate density. As the thermal fluctuations typically overwhelm the quantum fluctuations the operator $\hat{\delta}$ is identified with the operator for the thermal cloud.

Replacing eq.(6.32) in (6.29) the Hamiltonian splits as

$$\begin{aligned} \hat{H} &= H_0+\hat{H}_1+\hat{H}_2+\hat{H}_3+\hat{H}_4 && (6.36)\\ H_0 &= \int d\mathbf{r}\left[\phi^*\hat{h}_0\phi+\frac{g}{2}|\phi|^4\right] && (6.37)\\ \hat{H}_1 &= \int d\mathbf{r}\left[\hat{\delta}^\dagger(\hat{h}_0+g|\phi|^2)\phi+h.c\right] && (6.38)\\ \hat{H}_2 &= \int d\mathbf{r}\left[\hat{\delta}^\dagger(\hat{h}_0+2g|\phi|^2)\hat{\delta}+\frac{g}{2}((\phi^*)^2\hat{\delta}\hat{\delta}+h.c.)\right] && (6.39)\\ \hat{H}_3 &= g\int d\mathbf{r}\left[\phi\hat{\delta}^\dagger\hat{\delta}^\dagger\hat{\delta}+h.c\right] && (6.40)\\ \hat{H}_4 &= \frac{g}{2}\int d\mathbf{r}\hat{\delta}^\dagger\hat{\delta}^\dagger\hat{\delta}\hat{\delta} && (6.41)\end{aligned}$$

where $h.c$ stands for Hermetian conjugate.

Most of the finite-temperature models of BEC are obtained by approximating the different contributions of the Hamiltonians in eq.(6.36). The most drastic approximation is to assume that all the particles are in the condensate (valid at $T\approx 0$) and consequently $\delta=\delta^\dagger=0$. This approximation directly leads to the GPE (6.1).

Mean-field models including finite temperature effects are based on closures analogous to those ones discussed in section 2.4; high-order powers of thermal operators are expressed in terms of lower-order powers as

$$\begin{aligned} \hat{\delta}^\dagger\hat{\delta}^\dagger\hat{\delta}\hat{\delta} &\simeq 4\langle\hat{\delta}^\dagger\hat{\delta}\rangle\hat{\delta}^\dagger\hat{\delta}+\langle\hat{\delta}^\dagger\hat{\delta}^\dagger\rangle\hat{\delta}\hat{\delta}+\langle\hat{\delta}\hat{\delta}\rangle\hat{\delta}^\dagger\hat{\delta}^\dagger-(2\langle\hat{\delta}^\dagger\hat{\delta}\rangle\langle\hat{\delta}^\dagger\hat{\delta}\rangle+\langle\hat{\delta}\hat{\delta}\rangle\langle\hat{\delta}^\dagger\hat{\delta}^\dagger\rangle) && (6.42)\\ \hat{\delta}^\dagger\hat{\delta}\hat{\delta} &\simeq 2\langle\hat{\delta}^\dagger\hat{\delta}\rangle\hat{\delta}+\hat{\delta}^\dagger\langle\hat{\delta}\hat{\delta}\rangle && (6.43)\\ \hat{\delta}^\dagger\hat{\delta}^\dagger\hat{\delta} &\simeq 2\hat{\delta}^\dagger\langle\hat{\delta}^\dagger\hat{\delta}\rangle+\langle\hat{\delta}^\dagger\hat{\delta}^\dagger\rangle\hat{\delta}. && (6.44)\end{aligned}$$

Observe that, by definition $\langle\delta^\dagger\rangle=\langle\delta\rangle=0$. In this approximation we thus have $\langle\hat{\delta}^\dagger\hat{\delta}\hat{\delta}\rangle=0$.

Inserting the preceding equations in eq.(6.36) leads to a quadratic Hamiltonian in the thermal operators. Considering different terms leads to the approximations: *Hartree-Fock, Hartree-Fock-Bogoliubov* and *Hartree-Fock-Bogoliubov-Popov*. These ap-

proximations do not describe dynamical effects because they discard particle-exchanges between thermal and condensate and between pairs of thermal atoms. These model and their respective approximations are described in detail in reference [90]. In general, they lead to a statistical description of the thermal cloud, computed with the reduced mean-field Hamiltonian and a time-independent modified GPE for the condensate that includes the mean values of thermal operators powers. This set of equations can be, in principle, self-consistently solved.

Dynamical effect can be directly obtained by replacing the Bogoliubov approximation (6.32) in the evolution equation (6.31) and then performing averages:

$$i\hbar\frac{\partial\phi}{\partial t} = [\hat{h}_0 + g|\phi|^2]\phi + 2g\langle\hat{\delta}^\dagger\hat{\delta}\rangle\phi + g\langle\hat{\delta}\hat{\delta}\rangle\phi^* + g\langle\hat{\delta}^\dagger\hat{\delta}\hat{\delta}\rangle \tag{6.45}$$

$$i\hbar\frac{\partial\tilde{n}}{\partial t} = \langle[\hat{\delta}^\dagger\hat{\delta}, \hat{H}]\rangle \tag{6.46}$$

These equations are an unclosed hierarchy because they involve powers of the thermal operators. This difficulty can be handled with an adequate closure, or an appropriate mean-field. The term $\langle\hat{\delta}^\dagger\hat{\delta}\hat{\delta}\rangle$ in eq.(6.45), that is neglected in the static approximation, plays a relevant role in the particle exchange of condensate and thermal atoms. A theory that takes into account this term is (among others) the Zaremba-Nikuni-Griffin (ZNG) framework, that yields a modified-dissipative GPE for the condensate coupled with a Boltzman equation for the thermal cloud. For completeness we write down the ZNG equations below. A derivation can also be found in the review [90].

Let us first introduce the distribution function $f(\mathbf{p}, \mathbf{r}, t)$ that, for an atom of momentum $\mathbf{p}$ at location $\mathbf{r}$ and time t, is defined as the expectation value

$$f(\mathbf{p}, \mathbf{r}, t) = \langle\hat{f}(\mathbf{p}, \mathbf{r}, t)\rangle \tag{6.47}$$

where $\hat{f}(\mathbf{p}, \mathbf{r}, t)$ is the Wigner operator

$$\hat{f}(\mathbf{p}, \mathbf{r}, t) = \int d\mathbf{r}' e^{i\mathbf{p}\cdot\mathbf{r}'/\hbar}\hat{\delta}^\dagger\left(\mathbf{r} + \frac{\mathbf{r}'}{2}, t_0\right)\hat{\delta}\left(\mathbf{r} - \frac{\mathbf{r}'}{2}, t_0\right) . \tag{6.48}$$

With this, the non-condensate density becomes

$$\tilde{n}(\mathbf{r}, t) = \int \frac{d\mathbf{p}}{(2\pi\hbar)^3} f(\mathbf{p}, \mathbf{r}, t) . \tag{6.49}$$

The ZNG equations are

$$
\begin{aligned}
i\hbar\frac{\partial\phi}{\partial t}(\mathbf{r},t) &= \left[\hat{h}_0 + g\left(|\phi(\mathbf{r},t)|^2 + 2\tilde{n}(\mathbf{r},t)\right) - iR(\mathbf{r},t)\right]\phi(\mathbf{r},r) && (6.50)\\
\frac{\partial f}{\partial t} &+ \frac{\mathbf{p}}{m}\cdot\nabla_{\mathbf{r}} f - (\nabla_{\mathbf{r}} U)\cdot(\nabla_{\mathbf{p}} f) = C_{12}[f] + C_{22}[f] && (6.51)\\
U(\mathbf{r},t) &= V_{\text{ext}}(\mathbf{r},t) + 2g\left[|\phi(\mathbf{r},t)|^2 + \tilde{n}(\mathbf{r},t)\right] && (6.52)\\
R(\mathbf{r},t) &= \frac{\hbar}{|\phi(\mathbf{r},r)|^2}\int\frac{d\mathbf{p}}{(2\pi\hbar)^3}C_{12}[f(\mathbf{p},\mathbf{r},t)]\ . && (6.53)
\end{aligned}
$$

The collision term C_{12} involves the transfer of an atom from the thermal cloud into the condensate and its inverse process, while the term C_{22} involves the collision between thermal atoms. These equations conserve the total number of particles. The expressions of C_{12} and C_{22} are quite complex and depend on the energy of excitations and on the values of $\tilde{n}$ and $\phi(\mathbf{r},t)$. Explicit formulae are given in reference [90].

The ZNG equations were recently numerically simulated in reference [99]. The authors studied the vortex dynamics in a harmonically trapped condensate. Putting an off-centered vortex the showed that it decays by spiraling out toward the edge of the condensate. They found that the decay agrees with the Hall-Vinen phenomenological mutual friction model for superfluid vortices [94]. This model consists in a dynamic equation for the vortex line velocity v_L

$$\mathbf{v}_{\text{L}} = \mathbf{v}_{\text{sl}} + \alpha\mathbf{s}'\times(\mathbf{v}_{\text{n}} - \mathbf{v}_{\text{sl}}) - \alpha'\mathbf{s}'\times[\mathbf{s}'\times(\mathbf{v}_{\text{n}} - \mathbf{v}_{\text{sl}})], \tag{6.54}$$

where s' is the tangent of the vortex line, $\mathbf{v}_{\text{sl}}$ is the is the local superfluid velocity that is the sum of the ambient superfluid velocity v_{s} and the self-induced vortex velocity u_{i} and v_{n} is the normal velocity. The constants α, α' depend on the temperature and are proportional to the normal density ρ_n.

There exists other approaches that are not based on mean-field theory, such as the stochastic GPE and the truncated TGPE (also known as Projected Gross-Pitaevskii equation, that is discussed in detail in publication below). There is not consensus at the moment on which is the best model.

In this thesis we use the approach of the truncated GPE that allows to naturally consider thermal fluctuations, a physical phenomenon that is not taken into account by mean-field theories. We will show in the publication included in the next section that the TGPE appears as a minimal model of superfluidity at finite temperature, where counterflows and mutual friction effects are naturally present.

6.3 Publication: "Energy cascade with small-scales thermalization, counter flow metastability and anomalous velocity of vortex rings in Fourier-truncated Gross-Pitaevskii equation"

In this section we introduce the results presented in the work *"Energy cascade with small-scales thermalization, counter flow metastability and anomalous velocity of vortex rings in Fourier-truncated Gross-Pitaevskii equation"* (to be submitted to *Physical Review B*). From the results detailed in the article presented below, two letters will be written and submitted to *Physical Review Letters*. The first letter will be devoted to the anomalous translational speed of vortex rings caused by thermally exited Kelvin waves. The second letter will address the new mechanism of thermalization by direct energy cascade.

We also add at the end of this section some supplementary figures that were not included in the article.

Energy cascade with small-scales thermalization, counterflow metastability and anomalous velocity of vortex rings in Fourier-truncated Gross-Pitaevskii equation

Giorgio Krstulovic and Marc Brachet
Laboratoire de Physique Statistique de l'Ecole Normale Supérieure, associé au CNRS et aux Universités Paris VI et VII, 24 Rue Lhomond, 75231 Paris, France
(Dated: March 16, 2010)

The statistical equilibria of the (conservative) dynamics of the Gross-Pitaevskii Equation (GPE) with a finite range of spatial Fourier modes are characterized using a new algorithm, based on a stochastically forced Ginzburg-Landau equation (SGLE), that directly generates grand canonical distributions. The SGLE–generated distributions are validated against finite-temperature GPE–thermalized states and exact (low-temperature) results obtained by steepest descent on the (grand canonical) partition function. A standard finite-temperature second-order λ-transition is exhibited.

A new mechanism of GPE thermalization through a direct cascade of energy is found using initial conditions with mass and energy distributed at large scales. A long transient with partial thermalization at small-scales is observed before the system reaches equilibrium. Vortices are shown to disappear as a prelude to final thermalization and their annihilation is related to the contraction of vortex rings due to mutual friction. Increasing the amount of dispersion at truncation wavenumber is shown to slowdown thermalization and vortex annihilation. A bottleneck that produces spontaneous effective self truncation with partial thermalization is characterized in the limit of large dispersive effects.

Metastable counter-flow states, with non-zero values of momentum, are generated using the SGLE algorithm. Spontaneous nucleation of vortex ring is observed and the corresponding Arrhenius law is characterized. Dynamical counter-flow effects on vortex evolution are investigated using two exact solutions of the GPE: traveling vortex rings and a motionless crystal-like pattern of vortex lines. Longitudinal effects are produced and measured on the crystal pattern. A dilatation of vortex rings is obtained for counter flows larger than their longitudinal velocity. The vortex ring longitudinal velocity has a dependence on temperature that is an order of magnitude above that of the perfect crystal, an effect that is related to the presence of finite-amplitude Kelvin waves. This anomalous vortex ring velocity is quantitatively reproduced by assuming equipartition of energy of the Kelvin waves. Orders of magnitude are given for the predicted effects in weakly interacting Bose-Einstein condensates and superfluid ^{4}He.

PACS numbers: 03.75.Kk, 05.30.Jp, 47.37.+q, 67.25.dk

Contents

I. INTRODUCTION

Finite temperature superfluids are typically described as a mixture of two interpenetrating fluids[1]. At low temperatures the normal fluid can be neglected and Landau's two-fluids model reduces to the Euler equation for an ideal fluid that is irrotational except on (singular) vortex lines around which the circulation of the velocity is quantized. At finite temperature, when both normal fluid and superfluid vortices are present (e.g. in the counterflow produced by a heat current) their interaction, called "mutual friction", must also be accounted for[2].

In the low-temperature regime the Gross-Pitaevskii equation (GPE) (also called the Nonlinear Schrődinger Equation) is an alternative description of superfluids and Bose-Einstein Condensates (BEC)[3]. The GPE is a partial differential equation (PDE) for a complex wave field that is related to the superflow's density and velocity by Madelung's transformation[4]. The (non singular) nodal lines of the complex wave field correspond to the quantum vortices that appear naturally in this model with the correct amount of velocity circulation. Just as the incompressible Euler equation, the GPE dynamics is known to produce[5–8] an energy cascade that leads to a Kolmogorov regime with an energy spectrum scaling as $E(k) \sim k^{-5/3}$. This Kolmogorov regime was also experimentally observed in low temperature helium[9,10]. In this experimental context, note that so much progress has been made that it is now possible to visualize superfluid vortices both in the low-temperature regime and in the presence of counter flow by following the trajectories of solid hydrogen tracers in helium[11,12].

It has been suggested that the GPE should also be able to describe the classical equilibrium aspects of a finite-temperature homogeneous system of ultracold gases, provided that that a projection (or truncation) on a finite number of Fourier modes is performed[3,13]. Such classical truncated systems have a long history in the context of fluid mechanics. Indeed, if the (conservative) Euler equation is spectrally truncated, by keeping only a finite number of spatial Fourier harmonics, it is well known that it admits absolute equilibrium solutions with Gaussian statistics and equipartition of kinetic energy among all Fourier modes[14–17].

Recently, a series of papers focused on the dynamics of convergence of the truncated Euler equation toward the absolute equilibrium. It was found that (long-lasting) transient are obtained that are able to mimic (irreversible) viscous effects because of the presence of a "gas" of partially-thermalized high-wavenumber Fourier modes that generates (pseudo) dissipative effects[18–23].

The main goal of the present paper is to obtain and study finite temperature dissipative and counter flow effects by extending to the Fourier-truncated GPE the dynamical results that were obtained in the framework of the truncated Euler equation. We now give a short review of what is already known about the truncated GPE dynamics.

The Fourier truncated Gross-Pitaevskii equation was first introduced in the context of Bose condensation by Davis et al.[13] as a description of the classical modes of a finite-temperature partially-condensed homogeneous Bose gas. They considered random initial data defined in Fourier space by modes with constant modulus and random phases up to some maximum wavenumber (determined by the energy). They found that, the numerical evolution of the truncated Gross-Pitaevskii equation reached (microcanonical) equilibrium and that a condensation transition of the equilibrium was obtained when the initial energy was varied.

The same condensation transition was later studied by Connaughton et al.[24] and interpreted as a condensation of classical nonlinear waves. Using a modified wave turbulence theory with ultraviolet cutoff, they argued that the transition to condensation should be subcritical. They found their theory in quantitative agreement with numerical integration of the GPE, using the same stochastic initial conditions than those of reference[13]. However, the authors later argued that, as weak turbulence theory is expected to breakdown nearby the transition to condensation, the subcritical nature of the transition predicted by their theory was not physical[25].

Berloff and Svistunov[26], starting from periodic initial conditions similar to those of Davis et al.[13], used a finite-difference scheme (exactly conserving energy and particle number) to characterized the dynamical scenario of the relaxation toward equilibrium. Using the same finite-difference scheme, Berloff and Youd[27] then studied the dissipative dynamics of superfluid vortices at nonzero temperatures and observed a contraction of the vortex rings that followed a universal decay law.

Our main results are the followings. The classical absolute equilibrium of ideal fluids when generalized to GPE superfluids describes a standard[28,29] second-order phase transition. Long transient with energy cascade and partial small-scales thermalization are present in the relaxation dynamics. Dynamical counter-flow effects on vortex evolution are naturally present in the system and the vortex ring have anomalous velocities caused by thermally excited Kelvin waves.

The paper is organized as follows: Section II is devoted to the basic theoretical background that is needed to account for the dynamics and thermalization of the Fourier truncated GPE.

In Sec. III, the thermodynamic equilibrium is explored. The microcanonical and grand canonical distributions are numerically shown to be equivalent. Exact analytical expressions for the low-temperature thermody-

namic functions are obtained. A standard second-order λ phase transition is exhibited at finite-temperature using the SGLE-generated grand canonical states.

In Sec. IV, the direct energy cascade is considered as a new mechanism for GPE thermalization. Using initial data with mass and energy distributed at large scales, a long transient with partial thermalization at small-scales is characterized. Vortex annihilation is observed to take place and is related to mutual friction effects. A bottleneck producing spontaneous self truncation with partial thermalization and a time-evolving effective truncation wavenumber is characterized in the limit of large dispersive effects at the maximum wavenumber of the simulation.

In Sec. V, the new SGLE algorithm is used to generate counter-flow states, with non-zero values of momentum, that are shown to be metastable under SGLE evolution. The spontaneous nucleation of vortex ring and the corresponding Arrhenius law are characterized. Dynamical counter-flow effects are investigated using vortex rings and straight vortex lines arranged in crystal-like patterns. An anomalous translational velocity of vortex ring is exhibited and is quantitatively related to the effect of thermally excited finite-amplitude Kelvin waves. Orders of magnitude are estimated for the corresponding effects in weakly interacting Bose-Einstein condensates and superfluid ^{4}He.

Section VI is our conclusion. The numerical methods and low-temperature thermodynamic functions are described in an appendix.

II. THEORETICAL BACKGROUND

This section deals with basic facts needed to understand the dynamics and thermalization of the Fourier truncated GPE. We first recall in section II A 1 the (untruncated) GPE dynamics, its associated conserved quantities and the corresponding spectra; this material can be skipped by the reader already familiar with the GPE model of superflow[4,6]. The Fourier truncated GPE, its thermodynamical limit and the different statistical ensembles are then defined.

The thermodynamics of the truncated system is introduced in section II B using the microcanonical distribution. The canonical and grand canonical distributions are also used as they allow to directly label the equilibrium states by temperature and particle numbers.

A stochastically forced Ginzburg-Landau equation (SGLE) is considered in section II C and shown to define a new algorithm that directly generates the grand canonical distributions.

A. Galerkin truncated Gross-Pitaevskii equation

1. Conservation laws and Galilean invariance of the GPE

Superfluids and Bose-Einstein condensates[3,30] can be described at low temperature by the Gross-Pitaevskii equation (GPE) that is a partial differential equation (PDE) for the complex field ψ that reads

$$i\hbar\frac{\partial\psi}{\partial t} = -\frac{\hbar^2}{2m}\nabla^2\psi + g|\psi|^2\psi, \tag{1}$$

where $|\psi|^2$ is the number of particles per unit volume, m is the mass of the condensed particles and $g = \frac{4\pi\tilde{a}\hbar^2}{m}$, with $\tilde{a}$ the s-wave scattering length. This equation conserves the Hamiltonian H, the total number of particles N and the momentum $\mathbf{P}$ defined in volume V by

$$H = \int_V d^3x \left(\frac{\hbar^2}{2m}|\nabla\psi|^2 + \frac{g}{2}|\psi|^4\right) \tag{2}$$

$$N = \int_V |\psi|^2\, d^3x \tag{3}$$

$$\mathbf{P} = \int_V \frac{i\hbar}{2}\left(\psi\nabla\overline{\psi} - \overline{\psi}\nabla\psi\right)\, d^3x. \tag{4}$$

It will be useful for the next sections to explicitly write the conservation law of the momentum $\partial_t\frac{i\hbar}{2}(\psi\partial_j\overline{\psi} - \overline{\psi}\partial_j\psi) + \partial_k\Pi_{kj} = 0$, where the momentum flux tensor Π_{kj} is defined as[6]

$$\Pi_{kj} = \frac{\hbar^2}{2m}(\partial_k\overline{\psi}\partial_j\psi + \partial_k\psi\partial_j\overline{\psi}) + \delta_{kj}(\frac{g}{2}|\psi|^4 - \frac{\hbar^2}{4m}\nabla^2|\psi|^2). \tag{5}$$

It is well known that the GPE (1) can be mapped into hydrodynamics equations of motion for a compressible irrotational fluids using the Madelung transformation defined by

$$\psi(\mathbf{x},t) = \sqrt{\frac{\rho(\mathbf{x},t)}{m}}\exp\left[i\frac{m}{\hbar}\phi(\mathbf{x},t)\right], \tag{6}$$

where $\rho(\mathbf{x},t)$ is the fluid density and $\phi(\mathbf{x},t)$ is the velocity potential such that $\mathbf{v} = \nabla\phi$. The Madelung transformation (6) is singular on the zeros of ψ. As two conditions are required (both real and imaginary part of ψ must vanish) these singularities generally take place on points in two-dimension and on curves in three-dimensions. The Onsager-Feynman quantum of velocity circulation around vortex lines $\psi = 0$ is given by h/m.

When eq.(1) is linearized around a constant $\psi = A_0$, the sound velocity is given by $c = \sqrt{g|A_0|^2/m}$ with dispersive effects taking place for length scales smaller than the coherence length defined by

$$\xi = \sqrt{\hbar^2/2m|A_{\mathbf{0}}|^2 g}. \tag{7}$$

ξ is also the length scale of the vortex core[3,6].

Following reference[5] we define the total energy per unit volume $e_{\rm tot} = (H - \mu N)/V - \mu^2/2g$ where μ is the chemical potential (see section II B). Using the hydrodynamical variables, $e_{\rm tot}$ can we written as the sum of three parts: the kinetic energy e_{kin}, the internal energy e_{int} and the quantum energy e_q defined by

$$e_{\rm kin} = \frac{1}{V}\int d^3x \frac{1}{2}(\sqrt{\rho}\mathbf{v})^2 \quad (8)$$

$$e_{\rm int} = \frac{1}{V}\int d^3x \frac{g}{2m^2}\left(\rho - \frac{\mu m}{g}\right)^2 \quad (9)$$

$$e_{\rm q} = \frac{1}{V}\int d^3x \frac{\hbar^2}{2m^2}\left(\nabla\sqrt{\rho}\right)^2. \quad (10)$$

Using Parseval's theorem, one can define corresponding energy spectra: e.g. the kinetic energy spectrum $e_{\rm kin}(k)$ is defined as the sum over the angles of $\left|\frac{1}{(2\pi)^3}\int d^3r e^{ir_jk_j}\sqrt{\rho}v_j\right|^2$. e_{kin} can be further decomposed into compressible $e^{\rm c}_{\rm kin}$ and incompressible $E^{\rm i}_{\rm kin}$, using $\sqrt{\rho}\mathbf{v} = (\sqrt{\rho}\mathbf{v})^{\rm c} + (\sqrt{\rho}\mathbf{v})^{\rm i}$ with $\nabla\cdot(\sqrt{\rho}\mathbf{v})^{\rm i} = 0$ (see[6] for details).

Finally note that the GPE (1) is invariant under the Galilean transformation

$$\psi'(\mathbf{x},t) = \psi(\mathbf{x}-\mathbf{v}_{\rm s}t,t)\exp\left\{\frac{im}{\hbar}\left[\mathbf{v}_{\rm s}\cdot\mathbf{x} - \frac{1}{2}v_{\rm s}^2 t\right]\right\}. \quad (11)$$

Under this transformation eqs.(2-4) transform as

$$H' = \frac{1}{2}mNv_{\rm s}^2 + \mathbf{P}\cdot\mathbf{v}_{\rm s} + H \quad (12)$$

$$N' = N \quad (13)$$

$$\mathbf{P}' = mN\mathbf{v}_{\rm s} + \mathbf{P}. \quad (14)$$

2. *Definition of the Fourier truncated GPE*

For a periodical $3d$ system of volume V the Fourier truncated GPE is defined by performing a Galerkin truncation that consists in keeping only the Fourier modes with wavenumbers smaller than a UV cut-off $k_{\rm max}$.

Expressing ψ in terms of the Fourier modes $A_{\mathbf{k}}$ as

$$\psi(\mathbf{x},t) = \sum_k A_{\mathbf{k}}(t)e^{i\mathbf{k}\cdot\mathbf{x}}, \text{ with } \quad \frac{\mathbf{k}}{k_{\rm min}} \in \mathbb{Z}^3, \quad (15)$$

and where $k_{\rm min} = 2\pi/V^{1/3}$ is the smallest wavenumber. The Galerkin (Fourier) truncated Gross-Pitaevskii equation (TGPE) is defined as

$$-i\hbar\frac{\partial A_{\mathbf{k}}}{\partial t} = -\frac{\hbar^2k^2}{2m}A_{\mathbf{k}} - \sum_{\mathbf{k_1},\mathbf{k_2}} A_{\mathbf{k_1}}A^*_{\mathbf{k_2}+\mathbf{k_1}}A_{\mathbf{k}+\mathbf{k_2}}, \quad (16)$$

where the Fourier modes satisfy $A_{\mathbf{k}} = 0$ if $k \geq k_{\rm max}$ and the sum is performed over all wavenumbers satisfying $|\mathbf{k_1}|, |\mathbf{k_2}|, |\mathbf{k_2}+\mathbf{k_1}|, |\mathbf{k}+\mathbf{k_2}| < k_{\rm max}$. This time-reversible finite system of ordinary differential equations with a large number of degree of freedom $\mathcal{N} \sim (k_{\rm max}/k_{\rm min})^3$ also conserves the energy, number of particles and momentum.

The direct numerical evolution of the convolution in eq.(16) would be very expensive in computational time $O(N^6)$, where N is the resolution. This difficulty is avoided by using pseudo-spectral methods[31] and the non-linear term is calculated in physical space, using FFTs that reduce the CPU time to $O(N^3\log N)$. Introducing the Galerkin projector $\mathcal{P}$ that reads in Fourier space$\mathcal{P}_{\rm G}[A_{\mathbf{k}}] = \theta(k_{\rm max}-k)A_{\mathbf{k}}$ with $\theta(\cdot)$ the Heavside function, the TGPE (16) can be written as

$$i\hbar\frac{\partial\psi}{\partial t} = \mathcal{P}_{\rm G}[-\frac{\hbar^2}{2m}\nabla^2\psi + g\mathcal{P}_{\rm G}[|\psi|^2]\psi]. \quad (17)$$

Equation (17) exactly conserves energy and mass and, if it is correctly de-aliased using the 2/3-rule[31] (dealiasing at $k_{\rm max} = \frac{2}{3}\frac{N}{2}$), it also conserves momentum (see Appendix A for a explicit demonstration). The Galerkin truncation also preserves the Hamiltonian structure with the truncated Hamiltonian $H = \int d^3x\left(\frac{\hbar^2}{2m}|\nabla\psi|^2 + \frac{g}{2}[\mathcal{P}_{\rm G}|\psi|^2]^2\right)$.

Note that perhaps a more standard definition of dealiasing in eq.(17) could have been $\mathcal{P}_{\rm G}[|\psi|^2\psi]$ using 1/2-rule (dealiasing at $k_{\rm max} = \frac{1}{2}\frac{N}{2}$) rather than $\mathcal{P}_{\rm G}[\mathcal{P}_{\rm G}[|\psi|^2]\psi]$ with the 2/3-rule. Using the former definition there is no restriction $|\mathbf{k_2}| < k_{\rm max}$ on the convolution in eq.(16). Both methods are equivalent in the partial differential equation (PDE) limit (exponential decay of energy spectrum for $k \ll k_{\rm max}$) and admit the same invariants. However the scheme of eq.(17) is preferable because $k_{\rm max}$ is larger at the same resolution. If dealiasing is not preformed in equation (17) the errors in the conservation of momentum can rise up to 50% in a few units of time (see Appendix A). In a finite difference scheme the conservation of momentum should also be checked carefully as it is bound to produce spurious effects.

Another effect caused by periodic boundary condition is that the velocity $\mathbf{v}_{\rm s}$ in the Galilean transformation (11) is quantized by the relation

$$\mathbf{v}_{\rm s} = \frac{\hbar}{m}\frac{2\pi}{V^{1/3}}\mathbf{n_s}, \quad (18)$$

where $\mathbf{n_s} \in \mathbb{Z}^3$ and $\mathbf{v}_{\rm s}$ becomes continuous only in the limit $\hbar/(mV^{1/3}) \to 0$. The Galilean invariance is slightly broken by the TGPE (16) because of modes close to the truncation wavenumber $k_{\rm max}$. However it is recovered in the PDE limit where high wavenumber modes are converging exponentially and also in the thermodynamic limit: $\frac{k_{\rm max}}{k_{\rm min}} \to \infty$ defined below because the offending terms represent only a surface effect in Fourier space.

3. *Thermodynamical limit and statistical ensembles*

Let us first note that the energy H, the number of particles N and the momentum $\mathbf{P}$ in eqs. (2-4) are all proportional to the total number of modes $\mathcal{N} \sim k_{\rm max}^3 V$

and therefore are all extensive quantities. Also note that by definition of the coherence length (7), the number $\xi k_{\max}$ determines the amount of dispersion at truncation wavenumber in the system.

The thermodynamic limit $V \to \infty$ of the truncated Gross-Pitaevskii system is thus defined as the limit

$$\mathcal{N} \to \infty \ , \quad \xi k_{\max} = \text{constant}, \tag{19}$$

in order to obtain equivalent systems. In this limit the relevant thermodynamic variables are the intensive quantities H/V, N/V and $\mathbf{P}/V$. In practice, to perform numerical computations we will fix the volume to $V = (2\pi)^3$ and we will vary $k_{\max}$ (see paragraphs before section III).

Let us define, as usual the microcanonical ensemble[32] by the probability dw of finding the system in states with given values of energy H_{in}, number of particles N_{in} (the subscript "in" stands for initial data) and momentum $\mathbf{P}_{\text{in}}$ given by:

$$dw = \text{cte}\, e^S \delta(H - H_{\text{in}})\delta(N - N_{\text{in}})\delta^3(\mathbf{P} - \mathbf{P}_{\text{in}}) dH dN d^3P, \tag{20}$$

where $S = \log \Gamma$ is the entropy with Γ the number of accessible micro-states.

Microcanonical statistical states can be obtained numerically by time-integrating the TGPE until the system reaches thermodynamic equilibrium[13,24]. These thermalized states are formally determined by the control values H_{in}, N_{in} and $\mathbf{P}_{\text{in}}$ that are set in the initial condition. It has been shown in references[13,24] by varying the values of H_{in} that TGPE present a phase transition analogous to the one of Bose-Einstein condensation, where the 0-wave-number $A_{\mathbf{0}}$ vanish for finite values of H_{in}. Note that an explicit expression of dw or S cannot be easily obtained in the microcanonical ensemble and therefore the temperature is not easily accessible.

A simple way to explicitly control the temperature is to use the canonical or grand canonical formulation. The grand canonical distribution probability is given by a Boltzman weight

$$\mathbb{P}_{\text{st}} = \frac{1}{\mathcal{Z}} e^{-\beta F} \tag{21}$$

$$F = H - \mu N - \mathbf{W}\cdot\mathbf{P}, \tag{22}$$

where $\mathcal{Z}$ is the grand partition function, β is the inverse temperature and μ is the chemical potential. In what follows we will refer to $\mathbf{W}$ as the counterflow velocity.

Note that when $\mathbf{W} = 0$, $F = H - \mu N$ and the statistic weight of distribution (21) corresponds to the $\lambda - \phi^4$ theory studied in second order phase transitions[28,29]. This point will be further discussed in subsection III C.

Finally remark that the states with $\mathbf{W} \neq 0$ are obtained, in the thermodynamic limit, by a Galilean transformation of the basic $\mathbf{W} = 0$ state (see below eq. (64)). However, for finite size systems, because of the quantification of the Galilean transformation (eqs.(11) and (18)) new metastable states with counterflow appear. These metastable states and their interactions with vortices will be studied in detail below in section V A.

In the grand canonical ensemble (21-22) the mean energy $\overline{H}$, number of particles $\overline{N}$ and momentum $\overline{\mathbf{P}}$ are easily obtained by defining the grand canonical potential

$$\Omega = -\beta^{-1} \log \mathcal{Z} \tag{23}$$

and using the relations

$$\overline{N} = -\frac{\partial \Omega}{\partial \mu}, \quad \overline{\mathbf{P}} = -\frac{\partial \Omega}{\partial \mathbf{P}}, \quad \overline{H} = \frac{\partial \Omega}{\partial \beta} + \mu \overline{N} + \mathbf{W}\cdot\mathbf{P}. \tag{24}$$

Note that the microcanonical states (20) are characterized by the values H_{in}, N_{in} and $\mathbf{P}_{\text{in}}$. On the other hand, the grand canonical states are controlled by the conjugate variables: β, μ and $\mathbf{W}$. The different statistical ensembles are expected to be equivalent in the thermodynamics limit (19) and therefore

$$H_{\text{in}} = \bar{H}\,, \quad N_{\text{in}} = \overline{N}\,, \quad \mathbf{P}_{\text{in}} = \overline{\mathbf{P}}, \tag{25}$$

in this limit. The equivalence of ensembles will be numerically tested below in subsection III A.

In the grand canonical ensemble, the pressure p is usually defined from the grand canonical potential (23) by the relation[32] $\Omega = -pV$. This definition presents two problems in the TGPE system. First, due to classical statistics Ω has a logarithmic divergence at $\beta = \infty$. Second, this definition does not coincide with the standard relation in fluid dynamics involving the diagonal part of the momentum flux tensor Π_{ij} (see eq.(5)). Both these problems can be solved by considering the total number of modes as a new thermodynamics variable, as we will see in the next section.

B. Thermodynamics of truncated system

When a Galerkin truncation is performed on a system a new variable $k_{\max}$ explicitly appears. One thus find that the thermodynamic potentials depend on the total number of modes. Denoting $\lambda_{\mathcal{N}}$ the conjugate variable to the total number of modes $\mathcal{N}$ the standard thermodynamic relation for the energy easily generalizes as

$$dE = -pdV + TdS + \mu dN + \lambda_{\mathcal{N}} d\mathcal{N} + \mathbf{W}\cdot d\mathbf{P} \tag{26}$$

with S the entropy and where we have included the total momentum dependence $d\mathbf{P}$ as in Landau two-fluid model[1]. $E = \overline{H}$ is the macroscopic energy and the bar over H stands for some ensemble average. We will omit the bar over the others microscopic quantities. Note that the Fourier modes formally play the role of "particles" and $\lambda_{\mathcal{N}}$ is formally the "chemical potential" associated to those "particles".

The thermodynamic potentials can be easily generalized to take in to account the new variables. It is useful to define the Gibbs potential G, grand canonical Ω and a generalized grand canonical potential Ω' (with a Legendre transformation on $\mathcal{N}$) as

$$G = E - TS + pV - \mathbf{W}\cdot\mathbf{P} \tag{27}$$

$$\Omega = E - TS - \mu N - \mathbf{W}\cdot\mathbf{P} \tag{28}$$

$$\Omega' = E - TS - \mu N - \lambda_{\mathcal{N}}\mathcal{N} - \mathbf{W}\cdot\mathbf{P} \tag{29}$$

from where their respective variations follows:

$$dG = Vdp - SdT + \mu dN + \lambda_{\mathcal{N}} d\mathcal{N} - \mathbf{P}\cdot\mathbf{dW} \quad (30)$$
$$d\Omega = -pdV - SdT - Nd\mu + \lambda_{\mathcal{N}} d\mathcal{N} - \mathbf{P}\cdot\mathbf{dW} \quad (31)$$
$$d\Omega' = -pdV - SdT - Nd\mu - \mathcal{N} d\lambda_{\mathcal{N}} - \mathbf{P}\cdot\mathbf{dW} \quad (32)$$

Based on standard arguments of extensive variables[32] and noting that $\lambda_{\mathcal{N}}$ and $\mathbf{W}$ are intensive variables we find the standard formula of the Gibbs potential with two types of particles

$$G = \mu N + \lambda_{\mathcal{N}} \mathcal{N}. \quad (33)$$

Using eqs.(27) and (33) in eqs.(28) and (29) we find

$$\Omega = -pV + \lambda_{\mathcal{N}}\mathcal{N}, \qquad \Omega' = -pV \quad (34)$$

The relations (26-34) determine all the thermodynamic variables and potentials. For instance note that the pressure p can be obtained from eq.(31), eq.(32) or eq.(34) by

$$p = -\left.\frac{\partial\Omega}{\partial V}\right|_{T,\mu,\mathcal{N},\mathbf{W}} = -\frac{\Omega - \lambda_{\mathcal{N}}\mathcal{N}}{V} = -\frac{\Omega'}{V} \quad (35)$$

where $\lambda_{\mathcal{N}} = \left.\frac{\partial\Omega}{\partial\mathcal{N}}\right|_{V,T,\mu,\mathbf{W}}$.

We proceed now to show that thermodynamic definition (35) of the pressure coincides with the standard relation in fluid dynamics. In order to make explicit the dependence of the energy H on the volume V let us define the dimensionless space variables $\tilde{x} = x/V^{\frac{1}{3}}$ and $\tilde{\psi} = V^{1/2}\psi$. Expressed in term of these variables the Hamiltonian (2) reads $H = \int d^3\tilde{x}\left(\frac{\hbar^2}{2m}\frac{1}{V^{\frac{2}{3}}}|\tilde{\nabla}\tilde{\psi}|^2 + \frac{1}{V}\frac{g}{2}|\tilde{\psi}|^4\right)$. Taking the derivative with respect to V and reintroducing x and ψ yields

$$\frac{\partial H}{\partial V} = -\frac{1}{V}\int d^3x\left(\frac{\hbar^2}{2m}\frac{2}{3}|\nabla\psi|^2 + \frac{g}{2}|\psi|^4\right). \quad (36)$$

This expression corresponds to the spatial average of the the diagonal part of Π_{ik}. As by definition $E = \overline{H}$ and the derivative has been implicitly done at constant total number of modes and momentum we find, using the thermodynamic relation (26) and eq.(36), that the pressure satisfies

$$p = -\left.\frac{\partial E}{\partial V}\right|_{S,N,\mathcal{N},\mathbf{P}} = -\left.\frac{\overline{\partial H}}{\partial V}\right|_{N,\mathcal{N},\mathbf{P}}, \quad (37)$$

where the second equality holds for adiabatic compressions[32].

Finally remark that replacing Ω in eq.(28) we obtain the thermodynamic relation

$$E + pV - \mu N - \mathbf{W}\cdot\mathbf{P} = TS + \lambda_{\mathcal{N}}\mathcal{N}. \quad (38)$$

Note that, in a classical system, the entropy is defined up to an additive constant related to the normalization of the phase-space. However the quantity $TS + \lambda_{\mathcal{N}}\mathcal{N}$ is completely determined because each term in the left hand side of eq.(38) is well defined. By the same arguments $d\left(\mathcal{N}\lambda_{\mathcal{N}}/T\right)$ is also a completely determined quantity. If the variable $\mathcal{N}$ had not been taken into account, the corresponding pressure would be $-\Omega/V$ and therefore wrongly defined and depending on the normalization constant. The grand canonical potential Ω will be explicitly obtained at low-temperature in subsection III B where the above considerations can be explicitly checked.

C. Generation of grand canonical distribution using a stochastic Ginzburg-Landau equation

Grand canonical equilibrium states given by the statistics (21-22) cannot be easily obtained because the Hamiltonian H in eq.(2) is not quadratic and therefore the statistical distribution is not Gaussian. Nevertheless it is possible to construct a stochastic process that converges to a stationary solution with equilibrium distribution (21-22). This process is defined by a Langevin equation consisting of a stochastic Ginbzurg-Landau equation (SGLE) that reads

$$\hbar\frac{\partial A_{\mathbf{k}}}{\partial t} = -\frac{1}{V}\frac{\partial F}{\partial A^*_{\mathbf{k}}} + \sqrt{\frac{2\hbar}{V\beta}}\,\hat{\zeta}(\mathbf{k},t) \quad (39)$$
$$\langle\zeta(\mathbf{x},t)\zeta^*(\mathbf{x}',t')\rangle = \delta(t-t')\delta(\mathbf{x}-\mathbf{x}'), \quad (40)$$

where F is defined in eq.(22) and $\hat{\zeta}(\mathbf{k},t)$ is the ($k_{\max}$-truncated) Fourier transform of the gaussian white-noise $\zeta(\mathbf{x},t)$ defined by eq.(40). The Langevin equation (39-40) explicitly reads in physical space

$$\hbar\frac{\partial\psi}{\partial t} = \mathcal{P}_{\mathrm{G}}[\frac{\hbar^2}{2m}\nabla^2\psi + \mu\psi - g\mathcal{P}_{\mathrm{G}}[|\psi|^2]\psi - i\hbar\mathbf{W}\cdot\nabla\psi] + \sqrt{\frac{2\hbar}{V\beta}}\mathcal{P}_{\mathrm{G}}[\zeta(\mathbf{x},t)]. \quad (41)$$

In the $T\to 0$ limit eq.(41) reduce to the advective real Ginzurg-Landau equation (up to a redefinition of μ) that was introduced in reference[6]. This equation has the same stationary solutions of than the TGPE (17) in a system of reference moving with velocity $\mathbf{W}$. When also included in the TGPE the term $\mu\psi$ in eq.(41) has, because of particle number conservation, the only effect of adding a global time-dependent phase factor to the solution.

The probability distribution $\mathbb{P}\left[\{A_{\mathbf{k}}, A^*_{\mathbf{k}}\}_{\mathbf{k}<\mathbf{k}_{\max}}\right]$ of the stochastic process defined by eqs.(39-40) can be shown to obey the following Fokker-Planck equation[33,34]

$$\frac{\partial\mathbb{P}}{\partial t} = \sum_{\mathbf{k}<\mathbf{k}_{\max}}\frac{\partial}{\partial A_{\mathbf{k}}}\left[\frac{1}{V\hbar}\frac{\partial F}{\partial A^*_{\mathbf{k}}}\mathbb{P} + \frac{1}{V\hbar\beta}\frac{\partial\mathbb{P}}{\partial A^*_{\mathbf{k}}}\right] + c.c\,. \quad (42)$$

It is straightforward to demonstrate that the probability distribution (21) is a stationary solution of eq.(42), provided that βF is a positive defined function of $\{A_{\mathbf{k}}, A^*_{\mathbf{k}}\}_{\mathbf{k}<\mathbf{k}_{\max}}$.

In order to directly control the value of the number of particles or the pressure, the SGLE must we supplied with one of two *ad-hoc* equation for the chemical potential. These equation simply read

$$\frac{\mathrm{d}\mu}{\mathrm{dt}} = -\nu_N(N-N^*)/V \quad (43)$$

$$\frac{\mathrm{d}\mu}{\mathrm{dt}} = -\nu_p(p-p^*) \quad (44)$$

where the pressure p is computed as $p = -\frac{\partial H}{\partial V}$ (see eq.(36)). Equation (43) controls the number of particles and fixes its mean value to the control value N^*. Similarly eq.(44) controls the pressure and fixes its value at p^*. Equations (43-44) are not compatible and they must not be used simultaneously. Depending on the type of the temperature scans, the SGLE must be used together with either eq.(43), eq.(44) or solely with a fixed value of μ.

In the rest of this paper we will perform several numerical simulations of the TGPE (16) and SGLE (41). For numerics, the parameters in SGLE (omitting the Galerkin projector $\mathcal{P}$) will be rewritten as

$$\frac{\partial\psi}{\partial t} = \alpha\nabla^2\psi + \Omega_0'\psi - \beta_0|\psi|^2\psi - i\mathbf{W}\cdot\nabla\psi + \sqrt{\frac{k_BT}{\alpha}}\zeta,$$

with similar changes for TGPE.

In terms of α, Ω_0' and β_0 the physical relevant parameters are the coherence length ξ and the velocity of sound c defined in section II A 1 (eq.(7) and text before). They can be are expressed as

$$\xi = \sqrt{\alpha/\Omega_0'}, \qquad c = \sqrt{2\alpha\beta_0\rho^*} \quad (45)$$

with $\rho^* = \Omega_0'/\beta_0$. The value of the density at $T = 0$ set to $\rho^* = 1$ in all the simulations presented below. In order to keep the value of intensive variables constant in the thermodynamic limit (19), with V constant and $k_{\max} \to \infty$ the inverse temperature is expressed as $\beta = 1/k_{\mathcal{N}}T$ where $k_{\mathcal{N}} = V/\mathcal{N}$. With these definitions the temperature T has units of energy per volume and $4\pi\alpha$ is the quantum of circulation.

With ξ fixed, the value of ξ/c only determine a time-scale. The velocity of sound is set to $c = 2$ and the different runs presented below are obtained by varying only the coherence length ξ, the temperature T, the counter-flow velocity $\mathbf{W}$ and the UV cut-off wavenumber $k_{\max}$. The number $\xi k_{\max}$ is kept constant when the resolution is changed, except in section IV B where dispersive effects are studied. Finally in all numerical results the energy and momentum are presented per unit of volume $V = (2\pi)^3$ and the control values of number of particles and pressure in eqs.(43-44) are set to $mN^*/V = \rho^* = 1$ and $p^* = c^2{\rho^*}^2/2 = 2$. Numerical integration are performed by using periodic pseudo-spectral codes and the time-stepping schemes are Runge-Kutta of order 4 for TGPE and implicit Euler for SGLE.

III. CHARACTERIZATION OF THERMODYNAMIC EQUILIBRIUM

In this section, the thermodynamic equilibrium is explored and characterized. The microcanonical and grand canonical distributions are first shown to be numerically equivalent in a range of temperatures by comparing the statistics of GPE and SGLE generated states in section III A. The steepest descent method is then applied to the grand partition function in section III B to obtain exact analytical expressions for the low-temperature thermodynamic functions. The basic numerical tools are validated by reproducing these low-temperature results. In section III C a standard second-order λ phase transition is exhibited at finite-temperature using the SGLE-generated grand canonical states and the deviations to low-temperature equipartition are characterized.

A. Comparison of microcanonical and grand canonical states

We now numerically compare the statistics of the grand canonical states produced by the new algorithm SGLE to the statistics of the microcanonical states obtained by long-time integrations of TGPE. The coherence length is set to $\xi = \sqrt{2}/10$ and 32^3 collocation points are used ($k_{\max} = 10$). The initial condition for the TGPE runs are chosen with random phases in a similar way than in references[13,24]. We obtain low, medium and high values of the energy with constant density $\rho = mN/V = 1$ (see table I).

TABLE I: Parameters of TGPE initial condition and time steps.

H	T	TGPE time steps	SGLE time steps
0.09	0.09	40000	9600
0.5	0.5	20000	9600
1.96	1.8	20000	9600
4.68	4	20000	5000

To compare with the SGLE generated statistics a scan in temperature at constant density $\rho = 1$ is performed in order to obtain the temperature corresponding to the energies of the TGPE runs. Using the thermalized final states obtained from TGPE and converged final states of SGLE histograms of the of the density $\rho(x)$ in physical space are confronted in Fig.1. They are found to be in excellent agreement.

Note that when the energy (or temperature) increases more weight becomes apparent on the histograms near $\rho = 0$, indicating the presence of vortices. The Gaussian character of the histogram in Fig. 1 a motivates the low-temperature calculation of the next section.

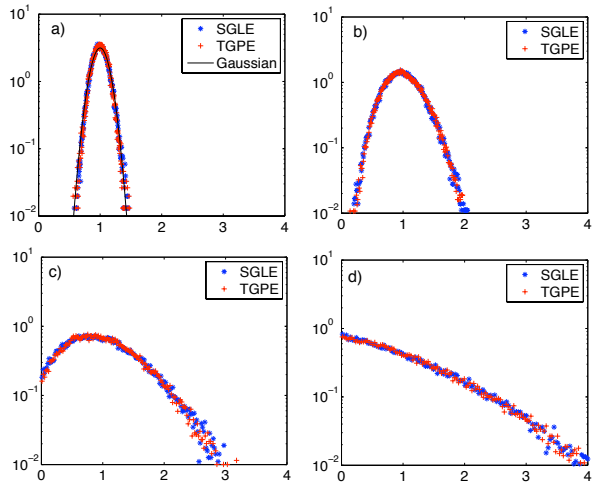

FIG. 1: Comparison of density histograms obtained by SGLE and TGPE dynamics ($\xi = 2/10\sqrt{2}$ and resolution 32^3) with energy equal to a) $H = 0.09$, b) $H = 0.51$, c) $H = 1.96$ and d) $H = 4.68$ (see table I). The solid line in a) is a Gaussian of standard deviation $\delta\bar{\rho}^2 = 0.016$ (see below eq.(59)) computed with the low-temperature calculations of section III B.

The SGLE converges much faster than the TGPE as apparent in table I. Because of the accurate conservative temporal scheme needed for the integration of the TGPE, the SGLE yields a large economy of the CPU time needed to reach equilibrium. On the local machines where these computations were performed the SGLE was typically more than 10 times faster than TGPE. Finally note that, even at this relatively low 32^3 resolution, the thermodynamic limit as been reached in the sense that the micro and grand canonical distribution coincides.

B. Low-temperature calculation

The gaussian histogram of Fig.1.a strongly suggest that some quadratic approximation should be able to obtain exact analytical expressions for the thermodynamic functions at low temperature. In this section we use a such an approximation to compute the grand partition function $\mathcal{Z}$ and the grand canonical potential[57] $\Omega = -\beta^{-1}\log\mathcal{Z}$ defined in (28).

The first step is to express the energy F of eq.(22) in terms of the Fourier amplitudes $A_{\mathbf{k}}$. This leads to a non quadratic function $F[A_{\mathbf{k}}, A^*_{\mathbf{k}}]$ explicitly given in appendix B (eqs.B1-B3). The grand partition function is a product integral over all the Fourier amplitudes

$$\mathcal{Z}(\beta,\mu,\mathbf{W}) = V^{\mathcal{N}}\int\frac{dA_{\mathbf{0}}dA^*_{\mathbf{0}}}{2\pi}\prod_{\mathbf{k}<\mathbf{k}_{\max}}\frac{dA_{\mathbf{k}}dA^*{}_{\mathbf{k}}}{2\pi}e^{-\beta F[A_{\mathbf{k}},A^*_{\mathbf{k}}]}. \tag{46}$$

The integrals in (46) cannot be done explicitly, however it is possible to give a low-temperature approximation using the method of *steepest descent*[28,35]. In addition to F an *external field* $-\mu_0|A_{\mathbf{0}}|^2V$ will be added in order to explicitly obtain the mean value of condensate Fourier mode $|A_{\mathbf{0}}|^2$ by direct differentiation. The physical partition function is obtained by setting $\mu_0 = 0$. The integrals are dominated by the saddle-point determined by $\frac{\partial F}{\partial A^*_{\mathbf{k}}} - \mu_0 A_{\mathbf{0}} V\delta_{\mathbf{k},\mathbf{0}} = 0$ that gives the solution (see eqs.(B4) and (B5))

$$g|A_{\mathbf{0}}|^2\big|_{\rm sp} = \mu + \mu_0 \qquad A_{\mathbf{k}} = 0 \text{ for } \mathbf{k} \neq \mathbf{0}, \tag{47}$$

where the subscript "sp" stands for saddle-point. Note that in general $|A_{\mathbf{0}}|^2 \neq |A_{\mathbf{0}}|^2\big|_{\rm sp}$ and the mean value is equal to the saddle-point one only at $T = 0$. Other solutions that can be obtained when $\mathbf{W} \neq 0$ will be discussed in detail in section V.

In the saddle-point $A_{\mathbf{k}} = 0$ for $\mathbf{k} \neq \mathbf{0}$, we thus need to keep only quadratic terms in $A_{\mathbf{k}}$ to obtain the low-temperature approximation. Denoting $\mathbf{p} = \hbar\mathbf{k}$, at leading order F can be rewritten as $F = F_0 + F_1 + F_2$ with

$$F_0 = V(\frac{g}{2}|A_{\mathbf{0}}|^4 - \mu|A_{\mathbf{0}}|^2) \tag{48}$$

$$F_1 = V\sum_{\mathbf{p}\neq\mathbf{0}}(\frac{p^2}{2m} - \mu + 2g|A_{\mathbf{0}}|^2 - \mathbf{W}\cdot\mathbf{p})|A_{\mathbf{p}}|^2 \tag{49}$$

$$F_2 = V\frac{g}{2}\sum_{\mathbf{p}\neq\mathbf{0}} A^{*2}_{\mathbf{0}}A_{\mathbf{p}}A_{-\mathbf{p}} + A^2_{\mathbf{0}}A^*_{\mathbf{p}}A^*_{-\mathbf{p}}. \tag{50}$$

To obtain the low-temperature partition function we must compute the determinant of the matrix $\frac{\partial^2 F}{\partial A_{\mathbf{p}}\partial A_{\mathbf{q}}} - \mu_0 V\delta_{\mathbf{p},\mathbf{0}}\delta_{\mathbf{q},\mathbf{0}}$. This determinant can be obtained using the Bogoliubov transformation

$$A_{\mathbf{p}} = u_p B_{\mathbf{p}} + v_p B^*_{-\mathbf{p}} \tag{51}$$

with $u_p = \frac{A_{\mathbf{0}}}{|A_{\mathbf{0}}|}\frac{1}{\sqrt{1-L_p^2}}$, $v_p = \frac{A_{\mathbf{0}}}{|A_{\mathbf{0}}|}\frac{L_p}{\sqrt{1-L_p^2}}$ and where L_p is determined by imposing the diagonalization of $F - \mu_0|A_{\mathbf{0}}|^2V$. L_p is explicitly given in eq.(B6). Is easy to show that (51) is a canonical transformation and the normalization condition of the Poisson bracket implies $|u_p|^2 - |v_p|^2 = 1$.

Expressing F in the Bogoliubov basis we obtain

$$F = V\left[\frac{g}{2}|A_{\mathbf{0}}|^4 - \mu|A_{\mathbf{0}}|^2 + \sum_{\mathbf{p}\neq\mathbf{0}}(\epsilon(p;\mu,\mu_0) - \mathbf{W}\cdot\mathbf{p})\,|B_{\mathbf{p}}|^2\right] \tag{52}$$

with the dispersion relation (see appendix B)

$$\epsilon(p;\mu,\mu_0) = \sqrt{\left(\mu + 2\mu_0 + \frac{p^2}{2m}\right)^2 - (\mu+\mu_0)^2}. \tag{53}$$

The exited modes $B_{\mathbf{p}}$ are called phonons in quantum mechanics. Here, because of classical statistics and the quadratic Hamiltonian, there is equipartition among phonon modes. Replacing the value of the chemical potential by the saddle-point $\mu = g|A_{\mathbf{0}}|^2\big|_{\rm sp}$ (with $\mu_0 =$

0), eq.(53) yields the well known Bogoliubov dispersion relation[36]. The Bogoliubov relation $\epsilon(p)$ can also be directly obtained from the GPE by expressing ψ in hydrodynamics variables, using the Madelung transformation (6) and linearizing around an homogenous density $\rho_0 = m|A_{\mathbf{0}}|^2$[26].

The partition function now trivially factorizes in independent parts $\mathcal{Z}(\beta, V, \mu, \mathbf{W}, \mathcal{N}, \mu_0) = \mathcal{Z}_0(\beta, \mu, \mu_0) \prod_{\mathbf{p}\neq\mathbf{0}} \mathcal{Z}_{\mathbf{p}}(\beta, \mu, \mathbf{W}, \mu_0)$ where

$$\mathcal{Z}_0(\beta, V, \mu, \mu_0) = \sqrt{2}\pi^3 \sqrt{\frac{V}{g\beta}} e^{\frac{V\beta(\mu+\mu_0)^2}{2g}} \quad (54)$$

$$\mathcal{Z}_{\mathbf{p}}(\beta, \mu, \mathbf{W}, \mu_0) = \frac{1}{\beta(\epsilon(p;\mu,\mu_0) - \mathbf{W}\cdot\mathbf{p})} \quad (55)$$

The total number of modes $\mathcal{N} = \sum_k 1$ and the grand canonical potential Ω are sums over all wave-numbers

$$\Omega(\beta, V, \mu, \mathbf{W}, \mathcal{N}) = -\beta^{-1}\left[\log \mathcal{Z}_0 + \sum_{\mathbf{p}\neq\mathbf{0}} \log \mathcal{Z}_{\mathbf{p}}\right] \quad (56)$$

from where all thermodynamic quantities directly follows by using the thermodynamic relation (31).

Replacing the sum by an integral the expression for the number of modes reads

$$\mathcal{N} = \int_0^{P_{\max}} \frac{p^2 V}{2\pi^2\hbar^3}\, dp = \frac{P_{\max}^3 V}{6\pi^2\hbar^3}. \quad (57)$$

Setting $\mathbf{W} = (0, 0, w)$ the integral form of eq. (56) reads

$$\begin{aligned}\Omega(\beta, V, \mu, w, \mathcal{N}) &= -\frac{V(\mu+\mu_0)^2}{2g} + \int_0^{P_{\max}}\int_{-1}^{1} \frac{p^2 V}{2\pi^2\hbar^3} \log\left(\beta\sqrt{\left(\mu + 2\mu_0 + \frac{p^2}{2m}\right)^2 - (\mu+\mu_0)^2} - \beta p w z\right)\frac{dz\, dp}{2} \\ &= -\frac{V(\mu+2\mu_0)}{2g} - \frac{P_{\max}^3 V}{6\pi^2\beta\hbar^3}\left\{\frac{2}{3} - \log\left[\beta\epsilon(P_{\max};\mu)\right] - f\left[\frac{4m\mu}{P_{\max}^2}\right]\left(1 - \frac{w^2 m}{2\mu}\right) - \frac{\mu_0}{\mu} f_0\left[\frac{4m\mu}{P_{\max}^2}\right]\right\} \quad (58)\end{aligned}$$

where in (58) the thermodynamic limit (19) of infinite volume[58] has been taken and the conditions $w^2 \ll \mu/m$, $\mu_0/\mu \ll 1$ have been used. The functions $f[z]$ and $f_0[z]$ are explicited in eqs.(B10-B11). Note that the dependence of the grand canonical potential Ω on the number of modes $\mathcal{N}$ is implicitly given by $P_{\max}$ and eq.(57). The first term in Ω is due to the condensated mode at $\mathbf{p} = 0$.

The low-temperature approximation to all thermodynamic functions is directly obtained from equation (58) by first setting $\mu_0 = 0$ and then differentiating (58), using relation (31). It is straightforward to check that both definition of the pressure in eq. (35) coincide. Furthermore the higher order moments of the density can be easily computed by taking successive derivatives of the grand canonical potential. For instance it is straightforward to show that the variance of the density ρ (see Fig.1.a) is given by

$$V^2\langle\delta\rho^2\rangle = -\beta^{-1} m^2 \frac{\partial^2\Omega}{\partial\mu^2}. \quad (59)$$

It can also be checked on the explicit expression for the entropy S (see eqs.(B9)) that, as expected for a classical system, the entropy depends by a logarithmic term on the phase-space normalization. However the function $TS + \lambda_{\mathcal{N}}\mathcal{N}$ is independent of phase-space normalization (see discussion below eq.(38)).

Finally, low-temperature expressions for the energies (8-10) and their corresponding spectra can be easily obtained using Madelung transformation (6). At low temperatures the fluctuations are smalls and $e_{\rm kin}$ depends only on ϕ and $e_{\rm q} + e_{\rm int}$ only on ρ. The total energy is thus decomposed in two non-interacting terms. Equipartition of energy between the total kinetic energy $e_{\rm kin}$ and quantum plus internal energy $e_{\rm q} + e_{\rm int}$ is thus expected at low temperature.

The next subsections will be concerned with the vanishing counterflown case $w = 0$. The states with non-zero counterflow w will be studied in details in section V.

C. λ transition and vortices

To characterize the condensation transition, we present here four temperature scans performed using SGLE (41). Three of them are at resolution of 64^3 with respectively constant chemical potential, density and pressure (using eqs.(43-44)). The fourth scan is performed at constant pressure but at a resolution of 128^3. The coherence length is fixed so that $\xi k_{\max} = 1.48$ is kept constant.

Figure 2.a displays the results of the scans. Note that the behavior at low-temperature is in good agreement with the low-temperature analytical calculations of section III B and the explicit formulae given in appendix B. Also note that the constant pressure scans at resolutions of 64^3 and 128^2 coincide for all temperatures showing that the thermodynamic limit (19) discussed in section II B is obtained at these resolutions.

Figure 2.b displays the temperatures dependence of the

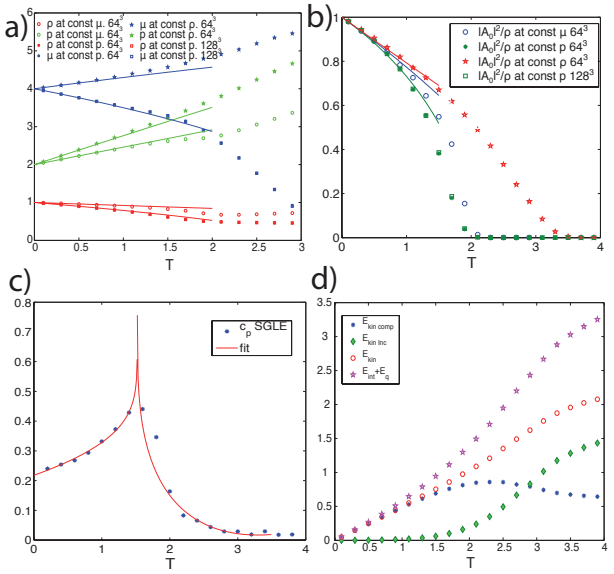

FIG. 2: a) Temperature dependence of the density ρ, pressure p and chemical potential μ for SGLE scans at constant density, pressure and chemical potential (see legend on figure). b) Temperature dependence of the condensate fraction $|A_{\mathbf{0}}|/\rho$ (same scans as in a)). c) Specific heat $c_p = \frac{\partial H}{\partial T}\big|_p$ at constant pressure and resolution 128^3 the solid line corresponds to a fit (see eq.(60)). d) Temperature dependence of the energies $e^{\rm c}_{\rm kin}$, $e^{\rm i}_{\rm kin}$, $e_{\rm kin}$ and $e_{\rm q}+e_{\rm int}$ at constant density; equipartition of energy between $e_{\rm kin}$ and $e_{\rm q}+e_{\rm int}$ is apparent at low temperatures.

condensate fraction $|A_{\mathbf{0}}|/\rho$ for the four SGLE runs. Note that the condensation transition previously obtained (in the constant density case) by microcanonical simulations in references[13,24] is reproduced and also present (at different critical temperatures) in the constant pressure and chemical potential scans.

The SGLE algorithm directly provides the temperature. It thus allows to easily obtain the specific heat from the data. Figure 2.c displays the specific heat at constant pressure $c_p = \frac{\partial H}{\partial T}\big|_p$ for the scan at resolution 128^3. As the $(w=0)$ statistic weight of distribution (21,22) corresponds to that of (standard two-component) second order phase transitions[28,29], we thus expect the condensation transition visible on Fig.2.c to be in this standard class. This point is confirmed by the solid lines in Figure 2.c that correspond to a fit with the theoretical prediction given by the renormalization group (RG)

$$c_p = \frac{A^{\pm}}{\alpha}|\tau|^{-\alpha}(1 + a_c^{\pm}|\tau|^{\Delta} + b_c^{\pm}|\tau|^{2\Delta} + \ldots) + B^{\pm} \quad (60)$$

where $\tau = \frac{T-T_\lambda}{T_\lambda}$ and the $+$ and $-$ signs refer to $T > T_\lambda$ and $T < T_\lambda$, see reference[37]. The fit was obtained in the following way: first the identification of the transition temperature T_λ is done by finding the zero of the linear interpolation of the second order difference of H. Then the three closest point to T_λ are discarded from the fit. Posteriorly, using the critical exponents $\alpha = -0.01126$ and $\Delta = 0.529$ given by the RG the data is fitted as in reference[37] over the non-universal constant. The values obtained give $A^+/A^- = 0.98$, very close to that one found to be about 1.05 in reference[37].

Finally on Fig.2.d the temperature dependence at constant density of the different energies (8-10) expressed in terms of hydrodynamical variables is displayed. Observe that the incompressible kinetic energy $E^{\rm i}_{\rm kin}$ vanishes for low temperatures $T \ll T^{\rho}_{\lambda}$, where $T^{\rho}_{\lambda} = 2.48$ is the transition temperature at constant density. This is due the disappearance of vortices, that it is also manifest in the density histograms in Fig.1. At low temperature equipartition of energy between the total kinetic energy $e_{\rm kin}$ and quantum plus internal energy $e_{\rm q} + e_{\rm int}$, as discussed at the end of section III B, is apparent on the figure.

IV. ENERGY CASCADE, PARTIAL THERMALIZATION AND VORTEX ANNIHILATION

A new mechanism of thermalization through a direct cascade of energy is studied in section IV A. Using initial conditions with mass and energy distributed at large scales, a long transient with partial thermalization of the density waves is obtained at small-scales. Vortex annihilation is observed to take place and is related to mutual friction effects. A bottleneck effect that produces spontaneous self truncation with partial thermalization and a time-evolving effective truncation wavenumber is characterized in section IV B for large dispersive effects at the maximum wavenumber of the simulation.

A. Partial thermalization

We now study the (partial) thermalization of the superfluid Taylor-Green (TG) vortex. This flow, that was first introduced in reference[6], develops from an initial condition that is prepared by a minimization procedure using the advected real Ginzburg-Landau equation (ARGLE)[6]. The nodal lines of the initial condition $\psi_{\rm TG}$ are the vortex lines of the standard TG vortex and obeys all its symmetries. Numerical integrations are performed with a symmetric pseudo-spectral code, making use of the TG symmetries to speed up the computations and optimize memory use, as described in reference[6]. We use the equivalent to 256^3 collocation points and the coherence length is set to $\xi = \sqrt{2}/80$ giving $\xi k_{\rm max} = 1.48$.

The temporal evolution of $e_{\rm kin}$, $e^{\rm i}_{\rm kin}$, $e^{\rm c}_{\rm kin}$, $e_{\rm q}+e_{\rm int}$ is displayed in Fig.3.a and the corresponding energy spectra in Fig.3.c. Observe that at $t=0$ $e^{\rm i}_{\rm kin}$ contains almost all the energy because the highly vortical initial condition. The early times ($t \leq 15$) correspond to those described, in the PDE regime of the GPE (1) previously reported

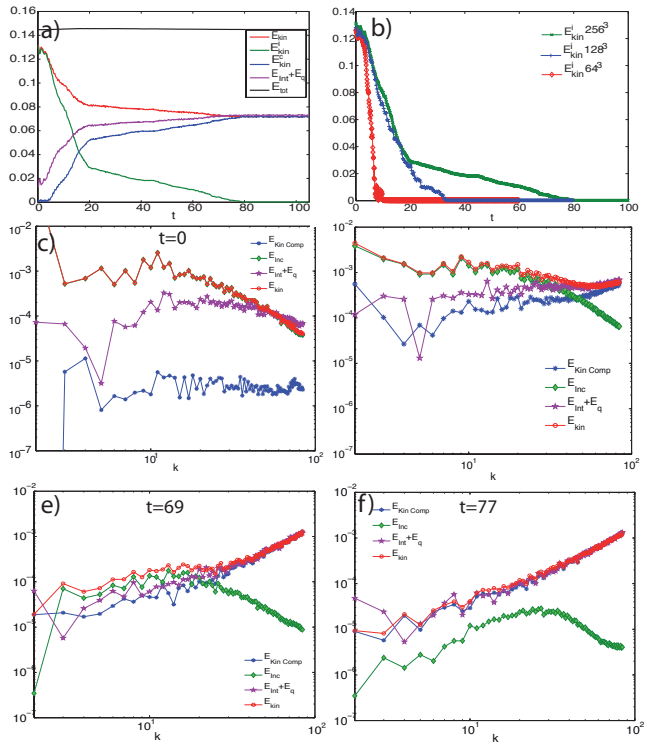

FIG. 3: a) Temporal evolution of energies $e^{\rm c}_{\rm kin}$, $e^{\rm i}_{\rm kin}$, $e_{\rm kin}$ and $e_{\rm q}+e_{\rm int}$. At large times, the incompressible energy vanishes and equipartition of energy between $e_{\rm kin}$ and $e_{\rm q}+e_{\rm int}$ is observed. b) Temporal evolution of $e^{\rm i}_{\rm kin}$ at resolution of 64^3, 128^3 and 256^3 with constant $\xi k_{\rm max}=1.48$. c-f) Energy spectra at $t=0$, 15, 69, 77 at resolution 256^3. Figure e) shows that equipartition is reached for all mode.

in[5,6]. An energy transfer from $e^{\rm i}_{\rm kin}$ to density waves is observed.

Continuing the temporal integration the spectral convergence of the GP partial differential equation is lost. The dynamics is thus now influenced by the truncation wavenumbers $k_{\rm max}$ and thermalization starts to take place. Two new regimes are observed. The first one for $20\lesssim t\lesssim 80$ corresponds to a partial thermalization at small-scales is apparent on Fig.3.d-f. Note that equipartition of $e^{\rm c}_{\rm kin}$ and $e_{\rm q}+e_{\rm int}$ starts to establish. This thermalized zone progressively extends to larger wave-numbers. During this phase $e^{\rm i}_{\rm kin}$ decrease at almost constant rate. It is apparent on Fig.3.b that this phase is delayed by increasing the resolution (at constant $\xi k_{\rm max}$).

Around $t=80$ (Fig.3.a and f) equipartition is established for each wave-number and $e^{\rm i}_{\rm kin}$ almost vanishes. The vortices thus disappear, first reconnecting into simpler structures and then decreasing in size (as can be directly observed on density visualizations, pictures not shown). Note that the annihilation of the vortices can be related to the contraction of vortex rings due to mutual friction reported in[27]. For $t>80$ the system finally reaches the thermodynamic equilibrium. The absence of vortices and the equipartition of energy between $e^{\rm c}_{\rm kin}$ and $e_{\rm q}+e_{\rm int}$ is a consequence of the low energy initial condition $\psi_{\rm TG}$ as it is apparent in the temperature scan in Fig.2.d. We have thus presented for the first time a new mechanism of thermalization through a direct cascade of energy of the TGPE similar to that of the incompressible truncated Euler equation reported in reference[18].

B. Dispersive slowdown of thermalization and bottleneck

We now turn to the study of dispersion effects on the thermalization of the TGPE dynamics and on vortex annihilation. To wit, we prepare three different initial conditions with different values of $\xi k_{\rm max}$ using the TG initial condition described in the preceding section. We fix the value of the coherence length to $\xi=\sqrt{2}/20$ and use resolutions of 64^3, 128^3 and 256^3 corresponding to $\xi k_{\rm max}=1.48$, 2.97 and 6.01 respectively. The three initial condition therefore represent the same field at different resolutions.

The temporal evolutions of $e_{\rm kin}$, $e^{\rm i}_{\rm kin}$, $e^{\rm c}_{\rm kin}$ and $e_{\rm q}+e_{\rm int}$ for the three runs (indexed by the resolution) are displayed on Fig.4.a. They are identical until $t\approx 5$ where the run of resolution 64^3 starts to lose its spectral convergence. At at $t\approx 20$ all runs appear to have thermalized on Fig.4.a. However the kinetic energy spectra on Fig.4.b shows a clear difference between the runs (the dashed line corresponds to k^2 power-law scaling). The high-wavenumber modes of the 64^3 run are thermalized. For the 128^3 run the high-wavenumbers begin to fall down and, at resolution 256^3, two zone are clearly distinguished. An intermediate thermalized range with an approximative k^2 power-law scaling is followed by a steep decay zone well before $k_{\rm max}=85$. Remark that in the 256^3 run the spectral convergence is still ensured and the (partial) thermalization is thus obtained within the GP PDE-dynamics.

The temporal evolution of $e_{\rm kin}(k)$ for the 256^3 run is displayed in Fig.4.c. The large wave-number k^3 power-law behavior at $t=0$ is an artifact of the high-k decomposition of energies in the presence of vortices (see pp. 2649-2650 of ref.[6] and[38]) and a faster decay is recovered as soon as the vortices disappear. The thermalized intermediate zone is observed to slowly extends to smaller wave-numbers. This naturally defines a *self-truncation* wave-number $k_c(t)$ where the energy spectrum starts to drastically decrease.

In order to determine $k_c(t)$ we have tested fits to $e_{\rm kin}(k)$ using two type of trial spectra with three free parameters: $e_{\rm fit\,I}(k)=A(t)k^{-n}\exp\left[-2\delta(t)k\right]$ and $e_{\rm fit\,II}(k)=A(t)k^{-n}\exp\left[-\gamma(t)k^2\right]$. The $e_{\rm fit\,II}(k)$ fit was found to work better in the sense that it both gives the correct $n=-2$ prefactor at intermediate and large times and also gives a better fit to the data at high k (data not

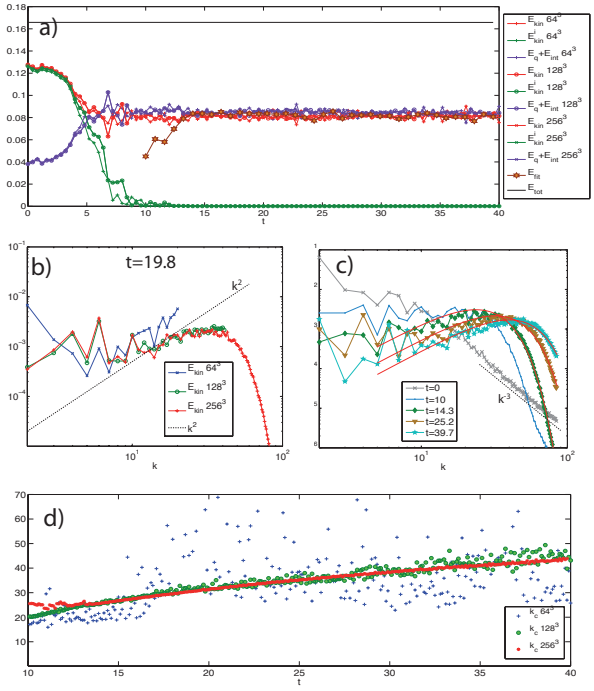

FIG. 4: a) Temporal evolution of energies (as in Fig3.a) for $\xi k_{\max} = 1.48$, 2.97 and 6.01 (resolution 64^2, 128^3 and 256^3 respectively). Yellow stars are the kinetic energy reconstructed from fit data using eq.(62). b) Kinetic energy spectrum at $t = 17.4$ for $\xi k_{\max} = 1.48$, 2.97 and 6.01; the dashed black line indicates k^2 power-law scaling. c) Temporal evolution of kinetic energy spectrum; the solid red lines correspond to fits using eq.(61) and the dashes black line indicate k^{-3} power-law scaling. d) Temporal evolution of effective self-truncation wavenumber k_c at different resolutions.

shown). Fixing the prefactor at the value $n = -2$, we finally define our working two-parameter fit as:

$$e_{\rm fit}(k,t) = A(t)k^2 e^{-\left[\left(\frac{9\pi}{16}\right)^{\frac{1}{3}}\left(\frac{k}{k_c(t)}\right)^2\right]} \quad (61)$$

$$e_{\rm fit}(t) = \int_0^{k_{\max}} e_{\rm fit}(k,t)dk. \quad (62)$$

The factor $(9\pi/16)^{1/3}$ in eq.(61) was set in order to obtain both limits $Ak_c/3$ and $Ak_{\max}/3$ from $e_{\rm fit}(t)$ when $k_{\max} \to \infty$ and $k_c \to \infty$ respectively. The fits are also displayed in Fig.4.c. They are in good agreement with the data after vortices have disappeared. The temporal evolution of $e_{\rm fit}(t)$ is displayed in Fig.4.a. It does converge to the thermalized value of the energy. Finally the temporal evolution of the self-truncation wavenumber $k_c(t)$, which seems to have a well defined limit at infinite resolution, is displayed in Fig.4.d for the three runs.

As the dynamics of modes at wave-numbers larger than k_c is weakly nonlinear, it should be amenable to a description in terms of wave turbulence theory; this could perhaps explain the slowdown of the thermalization in this zone. The new regime indicates that total thermalization is delayed when increasing the amount of dispersion (controlled by $\xi k_{\max}$) but is preceded by a partial thermalization (quasi-equilibrium up to k_c) *within* a PDE.

V. METASTABILITY OF COUNTERFLOW, MUTUAL FRICTION AND KELVIN WAVES

Counter-flow states with non-zero values of momentum generated by the new SGLE algorithm and their interaction with vortices are investigated in this section. The counter-flow states are shown to be metastable under SGLE evolution; the spontaneous nucleation of vortex ring and the corresponding Arrhenius law are characterized in section V A. Dynamical counter-flow effects are investigated in section V B using vortex rings and vortex lines patterns that are exact solutions of the GPE. Longitudinal and transverse mutual friction effects are produced and measured. An anomalous translational velocity of vortex ring is exhibited and is quantitatively related to the effect of thermally excited finite-amplitude Kelvin waves. Orders of magnitude are estimated for the corresponding effects in BEC and superfluid ^{4}He.

A. Metastability of grand canonical states with counterflow

1. *Thermodynamic limit of states with nonzero counterflow*

The counterflow states with $\mathbf{W} \neq \mathbf{0}$ are determined by thermal fluctuations around the minima of the energy F eq.(22). These minima correspond to the solution of

$$\frac{\delta F}{\delta \psi^*} = 0 = -\frac{\hbar^2}{2m}\nabla^2\psi + g\mathcal{P}_{\rm G}[|\psi|^2]\psi - \mu\psi + i\hbar\mathbf{W}\cdot\nabla\psi \quad (63)$$

that are plane-waves of the form

$$\psi(x;\mathbf{v}_{\rm s}) = g^{-\frac{1}{2}}\sqrt{\mu - m\mathbf{W}\cdot\mathbf{v}_{\rm s} + \frac{mv_{\rm s}^2}{2}}e^{-i\frac{m}{\hbar}\mathbf{v}_{\rm s}\cdot\mathbf{x}}, \quad (64)$$

where the velocity $\mathbf{v}_{\rm s}$ indexes the different solutions.

In the thermodynamic limit, the Galilean group defined by the transformations (11-14) is continuously indexed by the velocity $\mathbf{v}_{\rm s}$. All wavefunctions (64) are thus equivalent by Galilean transformation (and redefinition of the chemical potential). Under the Galilean transformation (11) the energy F is transformed as $F' = F - (m\mathbf{W}\cdot\mathbf{v}_{\rm s} - mv_{\rm s}^2/2)N + \mathbf{v}_{\rm s}\cdot\mathbf{P}$. Note that, among all the minima of F the one with $\mathbf{v}_{\rm s} = \mathbf{W}$ minimizes F'. This state corresponds to a condensate moving with uniform velocity $\mathbf{W}$. The $\mathbf{W}\cdot\mathbf{P}$ term is thus only imposing a Galilean transformation of the global minimum.

However, when working in a finite volume, the Galilean transformation is quantized (see eq. (18)) and an the

minima of F' of lowest energy corresponds to a condensate moving with the uniform velocity $\mathbf{v}_s$ closest to $\mathbf{W}$. At finite temperature and volume, when $\mathbf{W}$ is not too large, we thus have two ways to produce momentum in the system. The first one corresponds to Galilean transformations and the second one to fluctuations of the exited phonons; with the momentum of phonons imposed by the term $\mathbf{W}\cdot\mathbf{P}$ in the grand canonical distribution (21), and $\mathbf{v}_s = 0$ in (64). Metastability is thus expected when $\mathbf{W} \neq 0$ with quasi-equilibrium corresponding to condensates at different wavenumbers with an energy barrier between each of those states.

In the context of the Landau two-fluid model[1] the velocity $\mathbf{v}_s$ of the condensate corresponds to the superfluid velocity and the momentum carried by the exited phonons is written as $\mathbf{P} = \rho_n(\mathbf{v}_n - \mathbf{v}_s)$ where ρ_n and $\mathbf{v}_n$ are called the normal density and velocity respectively. The counterflow velocity defined by $\widetilde{\mathbf{W}} = \mathbf{v}_n - \mathbf{v}_s$ is a Galilean invariant.

The above discussion shows that, in general the variable $\mathbf{W}$ in the SGLE (41) corresponds to $\mathbf{W} = \mathbf{v}_n$. In the thermodynamic limit $\mathbf{W} = \mathbf{v}_s$ and there is thus no counterflow $\widetilde{\mathbf{W}} = \mathbf{v}_n - \mathbf{v}_s = \mathbf{0}$. For finite-size systems, in general $\mathbf{v}_s \neq \mathbf{W}$ and $\widetilde{\mathbf{W}} \neq \mathbf{0}$.

We thus define (when $v_s = 0$) the normal density by

$$\rho_n = \left.\frac{\partial P_z}{\partial w_z}\right|_{w_z=0}. \tag{65}$$

2. *Thermodynamics of metastable states at small temperature and small counterflow*

To validate the SGLE in the presence of counterflow two scans are performed at constant density using a resolution of 64^3 and $\xi k_{\max} = 1.48$. The condensate is set at $\mathbf{k} = 0$ in the SGLE initial data and the temperature is fixed to $T = 0.2$. This low temperature allows us to increase the value of the counterflow w_z (hereafter we set $w_x = w_y = 0$) keeping the condensate at $\mathbf{k} = 0$. The dependence of the momentum P_z on w_z is presented in Fig.5.a. The solid line corresponds to the low-temperature calculations (eq. (58) and appendix B eqs.(B9)). The second run correspond to a temperature scan (at low counterflow $w_z = .1$). The temperature dependence of ρ_n is displayed together with the low-temperature calculation on the inset of Fig.5.a.

Figure 5.a-b display histograms of P_z and $-P_z$ in physical space, both obtained at $T = 1$ with the condensate at $\mathbf{k} = 0$ but with zero and non-zero counterflow. Observe that the histograms are both centered at $P_z = 0$ but the non-zero counterflow induces an asymmetry in the statistical distribution that yields a non-zero value for the mean momentum.

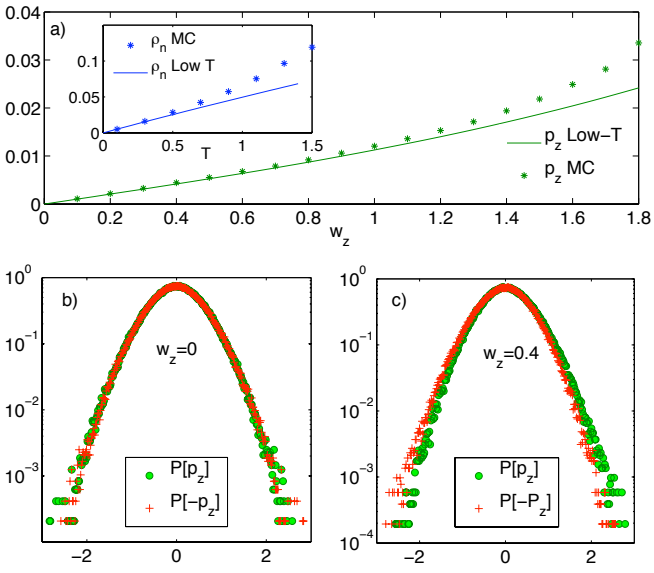

FIG. 5: Counterflow dependence of momentum P_z ($w_x = w_y = 0$). Inset: Temperature dependence of $\rho_n = \left.\frac{\partial P_z}{\partial w_z}\right|_{w_z=0}$. b) Histograms of momentum P_z and $-P_z$ (in $log-lin$) with no counterflow at $T = 1$. No asymmetry is observed. c) Histograms of momentum P_z and $-P_z$ with counterflow $w_z = .4$ at $T = 1$. An asymmetry, induced by counterflow, is apparent. Observe that both histograms are centered at $P_z = 0$.

3. *Spontaneous nucleation of vortex rings and Arrhenius law*

At temperatures and counterflow velocities large enough the stochastic process defined by the SGLE can jump between different metastable states. In this section, we show how the different states are explored, under SGLE evolution, by spontaneous nucleation of vortex rings. To wit, we present a numerical integration of SGLE at resolution 64^3 with $\xi k_{\max} = 1.48$. With this choice of parameters the velocity quantum (18) is fixed to 0.2. The temperature is set to $T = 0.775$ and the counterflow to $w_z = 0.8$. The condensate is set at $\mathbf{k} = \mathbf{0}$ in the SGLE initial data and the density is kept constant to $\rho = 1$.

The temporal evolution of the momentum P_z is displayed in Fig.6.a (right scale). Observe that the system first spends some time at the state (I) with $P_z \approx 0.05$ and that, around $t = 55$, it jumps to the state (II) with $P_z \approx 0.225$. These two metastable states correspond to quasi-equilibrium at $\mathbf{k} = \mathbf{0}$ and $\mathbf{k} = \mathbf{1}$ as is apparent in Fig.6.a (left scale) where the temporal evolution of $|A_{\mathbf{0}}|^2$ and $|A_{\mathbf{1}}|^2$ (see eq. (15)) are displayed.

To illustrate the dynamic of the condensate jump from $\mathbf{k} = \mathbf{0}$ to $\mathbf{k} = \mathbf{1}$ $3d$ visualization of the density at $t = 54.5$, $t = 56$ and $t = 60.5$ are presented on Fig.6.b. The wave-

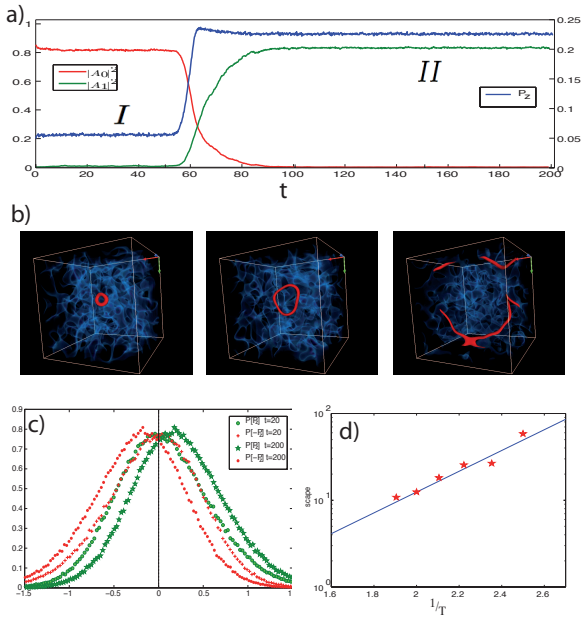

FIG. 6: a) Temporal evolution of $|A_0|^2$ and $|A_1|^2$ (left scale) under SGL dynamics. Observe that there are two *quasi*-stationary states (I and II) and the condensate makes a transition from $k = 0$ to $k = 1$. The temporal evolution of the momentum p_z is displayed in the same plot (right scale). Note that transition from one state to the other is accompanied by an increase of momentum. b) $3d$ visualization of density at $t = 54.5$, $t = 56$ and $t = 60.5$; the blue clouds corresponds to density fluctuations and the vortices are displayed as red isosurface (see colorbar on Fig.8 below). c) Histogram of momentum p_z and $-p_z$ at the two *quasi*-stationary states (I and II) in $lin - lin$ plot. d) Arrhenius law: data form SGL dynamics (points) and theoretical eq. (66) (solid line).

function ψ is first low-pass filtered and the density is then visualized using the VAPOR[59] software. At early times ($t < 50$, pictures not shown) there were no vortices in the box. At $t \approx 54$ a vortex ring is nucleated, then it increases its size under SGLE evolution until it reconnects with the neighbor rings (recall that periodic boundary condition are used). The ring finally contracts and disappears (pictures not shown) . During this evolution, the local phase defect of the ring becomes global and changes the condensate wavenumber. Histograms of momentum P_z and $-P_z$ in the two metastable states I and II are presented in Fig.6.c in a $lin - lin$ plot. Observe that both metastable states are asymmetrical as in Fig.5.c. However, I is centered at $P_z = 0$ and II at $P_z = 0.2$, respectively corresponding to the wavenumbers $\mathbf{k} = \mathbf{0}$ and $\mathbf{k} = \mathbf{1}$.

It is well known that the the escape time of a metastable quasiequilibirum is given, in general, by an Arrhenius law[39,40]

$$t_{\rm esc} \sim t_c e^{-\beta \Delta F}, \tag{66}$$

where ΔF is the activation energy of the nucleation solution and t_c is a characteristic time. Here, the nucleation solution is given by a vortex ring that satisfies $\frac{\partial F}{\partial \psi^*} = 0$. The energy barrier is thus determined by $\Delta F = H_{\rm ring}(R^*) - \mathbf{V}_{\rm ring} \cdot \mathbf{P}_{\rm ring}(R^*)$, where the analytic expressions for the energy $H_{\rm ring}$, the momentum $\mathbf{P}_{\rm ring}$ and the radius are given by

$$V_{\rm ring} = \frac{\hbar}{2m}\frac{1}{R^*}[\ln(\frac{8R^*}{\xi}) - a] \tag{67}$$

$$P^*_{\rm ring} = \frac{2\pi^2\hbar\rho_\infty}{m} R^{*2} \tag{68}$$

$$H^*_{\rm ring} = \frac{2\pi^2\hbar^2}{m^2}\rho_\infty R^*[\ln(\frac{8R^*}{\xi}) - 1 - a] \tag{69}$$

where ρ_∞ is the density at the infinity and a is a core model-depending constant with value $a = 0.615$ for the GPE vortices[4]. Formulae (67-69) and the value of a have been numerically validated in reference[41] using a Newton method[42–44].

In order to numerically check that the escape time indeed follows an Arrhenius law we now perform runs with with $\xi k_{\rm max} = 1.48$ and resolution 32^3. The counter-flow is fixed at $w = 1.4$ and the condensate is set initially at $\mathbf{k} = \mathbf{0}$ (constant density $\rho = 1$). At each fixed temperature T, several numerical integration of SGLE are performed and the escape times for the condensate to leave the wavenumber $\mathbf{k} = \mathbf{0}$ are measured. These escape times are then averaged over more than 10 realizations. Figure 6.d displays the escape time $t_{\rm esc}$ obtained in this way as a function of the inverse temperature $1/T$ in $log - lin$. The slope of the solid line is computed using the analytic formulae (67-69) of ΔF. Both, numerical and theoretical Arrhenius laws are in good agreement. It is thus possible to use the SGLE dynamics to prepare metastable states with finite value of counterflow and lifetime quantitatively given by the Arrhenius law (66).

B. Dynamical effects of finite temperature and counterflow on vortices

We now turn to the study the dynamical effects of counterflow on TGPE vortex evolution, we set up finite temperature and finite counterflow initial states that also contain vortices. Two cases are investigated: (i) vortex lines, in a perfect crystal pattern that does not produce self induced velocity and (ii) vortex rings, producing self induced velocity.

1. *Perfect crystal*

To numerically study the effect of counterflow on vortices we prepare an initial condition $\psi_{\rm cristal}$ consisting in a periodical array (of alternate sign) straight vortices similar to those used in[45] to study the scattering of first sound. The lattice (obtained with a Newton

method[42–44]) it is stationary exact solution of GPE. As the vortices are separated by a distance $d = \pi$, they can be considered isolated in the limit $\xi \ll d$. Note that this limit is obtained when the resolution is increased at constant $\xi k_{\max}$. To include temperature effect we prepare absolute equilibria $\psi_{\rm eq}$ using SGLE with the counterflow aligned with the z-axis (perpendicular to the vortices in $\psi_{crystal}$). Then the initial condition $\psi = \psi_{\rm crystal} \times \psi_{\rm eq}$ is evolved with the TGPE. Several runs were performed at different resolutions (with $\xi k_{\max} = 1.48$), temperature and counterflow values (see legend on Fig. 7.b).

Figure 7.a displays the temporal evolution of $(R_\parallel, R_\perp)$ the respectively parallel and perpendicular component of the vortex filament to the counterflow for $T = 0.5$, 1 and $w_z = 0.4$. The trajectories are obtained by first averaging

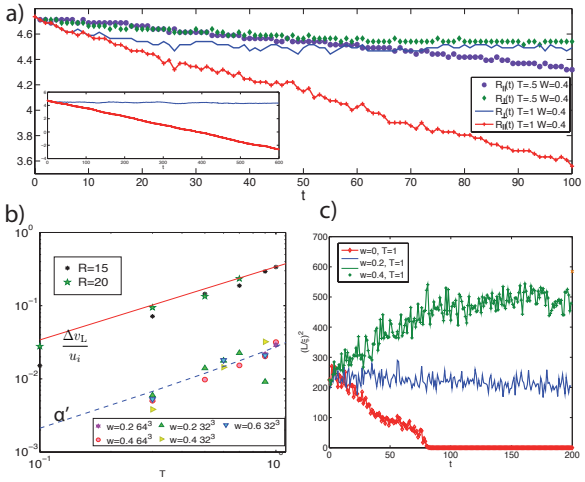

FIG. 7: a) Trajectory of a straight vortex in the crystal pattern for $T = 1$, $T = 0.5$ and $w_z = .4$. Inset: run with $T = 1$ until $t = 600$. b) Temperature dependence of the advection velocity $v_\parallel/w_z$ for the crystal and $\Delta v_L/u_i$ for the vortex rings; dashed line corresponds to to eq.(71) with $B' = 0.8334$ and solid line to the theoretical prediction (82). c) Temporal evolution of the square of the length of the vortex ring for different values of counterflow, $T = 1$ and initial radius $R = 15\xi$.

along the direction of the vortices, then the (averaged) coordinate of the vortices is found by seeking the zero of the reduced $2d$ wavefunction. Observe that the vortex, originally located at $(\frac{3\pi}{4}, \frac{3\pi}{4})$, moves in the direction of the counterflow and its velocity clearly depends on the temperature. It is apparent that a perpendicular movement is also induced at short times. This movement has two phases, the first one is related to an adaptation and makes the crystal slightly imperfect. Then the perpendicular movement almost stops (a very small slope can be observed for long time integration). The initial phase where the parallel and perpendicular motions have similar velocities lasts longer when ξ/d is decreased by increasing the resolution (data not shown). Observe that the imperfection of the crystal in the final configurations is almost equal for the two temperatures presented in Fig.7.a, but the parallel velocities are considerably different. Thus, the self-induced parallel velocity caused by the slight crystal imperfection is thus very small and not driving the longitudinal motion.

We now concentrate on the measurement of $R_\parallel$ for which the present configuration is best suited.

$R_\parallel$ has a linear behavior, that allows to directly measure the parallel velocity $v_\parallel$. The temperature dependence of $v_\parallel/w_z$ is presented on Fig.7.b for different values of w_z and d/ξ (corresponding to the different resolutions).

For superfluid vortices the standard phenomenological dynamic equation of the vortex line velocity v_L is[4]

$$\mathbf{v}_{\rm L} = \mathbf{v}_{\rm sl} + \alpha \mathbf{s}' \times (\mathbf{v}_{\rm n} - \mathbf{v}_{\rm sl}) - \alpha' \mathbf{s}' \times [\mathbf{s}' \times (\mathbf{v}_{\rm n} - \mathbf{v}_{\rm sl})], \quad (70)$$

where s' is the tangent of the vortex line, $\mathbf{v}_{\rm sl}$ is the is the local superfluid velocity that is the sum of the ambient superfluid velocity $v_{\rm s}$ and the self-induced vortex velocity $u_{\rm i}$ and $v_{\rm n} = w + v_{\rm s}$ is the normal velocity. The constants α, α' depend on the temperature. The existence of the transverse force (related to the third term of r.h.s. in Eq.70) has been subject of a large debate in the low-temperature community in the last part of the 90's[46–52] and the controversy is still not resolved. Applied to the present case, eq.(70) predicts $v_\perp = -\alpha w_z$ and $v_\parallel = \alpha' w_z$. The value of the constant α', related to the transverse force, depends on the normal density and the scattering section. It can be expressed as

$$\alpha' = B' \frac{\rho_n}{2\rho} \quad (71)$$

where B' is a order one constant[4]. A fit to the measured values of $v_\parallel/w_z$ yields $B' = 0.8334$, see fig.7b. We thus conclude that finite-temperature TGPE counterflow effects measured on $R_\parallel$ for the crystal pattern are in quantitative agreement with standard phenomenology (eq.(70)). We have seen above that the effect on $R_\perp$ is of the same order of magnitude that the one on $R_\parallel$, as long as crystal imperfection does not come into play.

2. *Vortex rings*

We now turn to study the effect of counterflow on vortex rings. The initial condition is prepared as in the previous section but with the crystal $\psi_{crystal}$ replaced by a vortex ring $\psi_{\rm ring}$, that is an exact stationary (in a co-moving frame) solution of GPE. The plane containing the vortex rings of radius R is perpendicular to the counterflow and the rings are numerically obtained by a Newton method[42–44].

In the case of vortex rings the general formula (70) yields

$$\dot{R} = -\alpha(u_i - w_z) \quad (72)$$

$$v_{\rm L} = v_{\rm s} + (1 - \alpha')u_{\rm i} + \alpha' w_z, \quad (73)$$

where u_i denotes the ring velocity at zero temperature, explicitly given by $V_{\rm ring}$ in formula (67) (replacing R^* by the corresponding radius). In the special simple case $w_z = 0$, a finite-temperature contraction of the vortex ring is predicted. This transverse effect effect was first obtained and measured by Berloff, using a finite-difference scheme version of the TGPE that exactly conserves the energy and particle number[27].

The temporal evolution of the square of the vortex length of a ring of initial radius $R = 15\xi$ at temperature $T = 1$ and counterflow $w_z = 0$, 0.2 and 0.4 is displayed on Fig.7.c. For $w = 0$, the dynamics under TGPE evolution reproduces the Berloff ring contraction[27]. The temperature dependence of the contraction obtained for $w = 0$ (data not shown) quantitatively agrees with Berloff's results. A dilatation of vortex rings is apparent on Fig.7.c for w larger than the measured vortex ring velocity $v_L = 0.23$.

However, v_L has a very strong dependence on temperature that is also present for $w = 0$. The temperature dependence of $\Delta v_L/u_i$ where $\Delta v_L = u_i - v_L$ and is displayed on Fig.7.b. We have checked that the velocity v_L directly measured at $T = 0$ is indeed given by u_i. Equation (70) predicts (in the absence of counterflow) a longitudinal velocity for the vortex ring $v_L = (1 - \alpha')u_i$. Observe that $\Delta v_L/u_i$ is one order of magnitude above the transverse mutual friction coefficient measured in the perfect crystal.

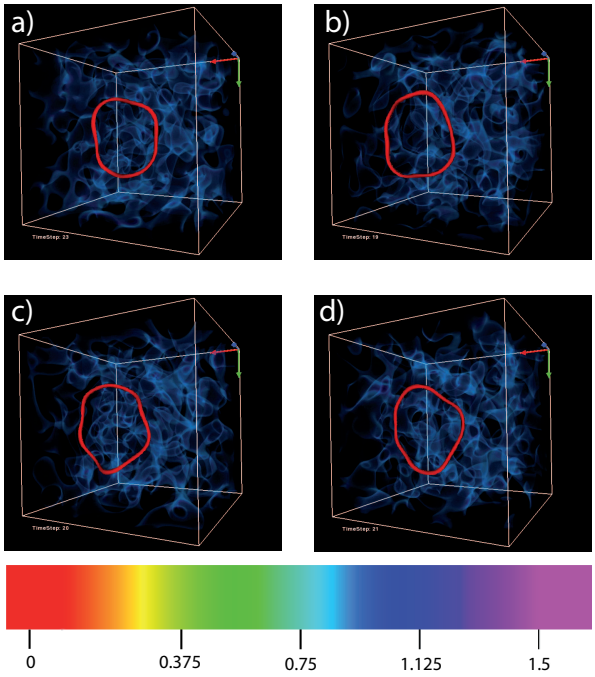

FIG. 8: $3d$ visualization of density at $t = 18$, 19, 20 and 21 at temperature $T = 1$. Blue cloud correspond to density fluctuations and a vortex ring of radius $R = 20\xi$ with thermally excited Kelvin waves is displayed in red isosurfaces

3. *Anomalous translational velocity and Kelvin waves*

In this section we relate the finite temperature slowdown to the anomalous translational velocity of vortex ring with finite-amplitude Kelvin waves reported in[53,54]. Kelvin waves are clearly observed in $3d$ visualizations of vortex rings driven by TGPE as it is apparent on fig.8 obtained in the same way that fig.6.b.

Following reference[54], Kelvin waves of amplitude A and wavelength $2\pi R/N$ on a ring of radius R are parametrized, in cylindrical coordinates r, ϕ and z, as

$$x = (R + A\cos N\phi)\cos\phi \quad (74)$$
$$y = (R + A\cos N\phi)\sin\phi \quad (75)$$
$$z = -A\sin\phi. \quad (76)$$

In the limit $N \gg 1$ the dispersion relation $\omega(k)$ of the Kelvin wave (74-76) is given by[53]

$$\omega(k) = \frac{\hbar}{2m}k^2[\ln(\frac{8R}{\xi}) - a] \quad (77)$$

where $k = N/R$ and a is the core model-depending constant in formula (67).

The anomalous translational velocity caused by an excited Kelvin wave was first reported by Kiknadze and Mamaladze[53] in the framework of the local induction approximation (LIA). The effect was then obtained and numerically characterized within the Biot-Savart equation by Barenghi et al.[54]. The anomalous translational velocity $v_{\rm a}$ of a vortex ring reads (in the limit $N \gg 1$, see eq. (26) of reference[53])

$$v_{\rm a} \approx u_{\rm i}(1 - \frac{A^2N^2}{R^2}) \quad (78)$$

where $u_i = V_{\rm ring}$ is the self-induced velocity (67) without Kelvin waves.

The variation of the energy of a vortex ring caused by a (small amplitude) Kelvin wave can be estimated as

$$\Delta E = \frac{dH}{dR}\frac{\Delta L}{2\pi} \quad (79)$$

where H is the energy given by Eq.(69) and the length variation ΔL produced by the Kelvin wave (74-76) is given, at lowest order in the amplitude A/R, by $\Delta L = \pi A^2N^2/R$. Assuming equipartition of the energy of Kelvin waves with the heat bath implies $\Delta E = k_BT$, which yields the value of A^2N^2/R^2 as function of T:

$$\frac{A^2N^2}{R^2} = \frac{m^2k_BT}{\pi^2\rho\hbar^2R(\log\frac{8R}{\xi} - a)}. \quad (80)$$

The equipartition law (80) can also be directly obtained as the classical limit of the quantum distribution computed by Bareghi *et al.*[55], up to a redefinition of the core constant model a (see eq.(25) in reference[55]).

We finally assume that the slowing down effect of each individual Kelvin wave is additive and that the waves populate all the possible modes. Kelvin waves are bending oscillations of the the quantized vortex lines, with wavenumber $k \lesssim 2\pi/\xi$. The total number of modes can thus be estimated as

$$\mathcal{N}_{\rm Kelvin} \approx 2\pi R/\xi. \tag{81}$$

Replacing A^2N^2/R^2 in eq.(78) by eq.(80) and multiplying by the total number of waves $\mathcal{N}_{\rm Kelvin}$ we obtain the following expression for the anomalous translational effect due to thermally exited Kelvin waves

$$\frac{\Delta v_L}{u_i} \equiv \frac{u_i - v_{\rm a}}{v_{\rm a}} \approx \frac{2k_B T m^2}{\pi\rho\xi\hbar^2}\frac{1}{\log\frac{8R}{\xi} - a} \tag{82}$$

The temperature dependence of the equipartition estimate (82) of the thermal slowdown is plotted on Fig.7.b (top straight line). The data obtained form the measurements of the rings velocity in the TGPE runs is in very good agreement with the estimate (82).

As discussed in[3,13]the TGPE gives a good approximation of Bose-Einstein condensate (BEC) only for the modes with high occupation number. In this sprit quantum effects on the Kelvin waves oscillations must also be taken into account to obtain the total slowing down effect in a BEC. The TGPE estimation (82) can be adapted to weakly interacting BEC by the following considerations.

At very low temperature, only a limited range of low-wavenumber Kelvin waves are in equipartition. This range is determined by the relation $k \leq k_{\rm eq}$ with $\hbar\omega(k_{\rm eq}) = k_{\rm B}T$ and the dispersion relation (77), it reads:

$$k_{\rm eq} = \sqrt{\frac{k_{\rm B}T\,2m}{\hbar^2[\ln(\frac{8R}{\xi}) - a]}}. \tag{83}$$

The coherence length ξ defined in eq. (7) can be expressed in terms of the s-wave scattering length $\tilde{a}$ defined by $g = 4\pi\tilde{a}\hbar^2/m$ and the mean inter-atomic particle distance $\ell \equiv n^{-1/3} \approx |A_0|^{-2/3}$ as

$$\xi = (8\pi n\tilde{a})^{-1/2} = \ell\frac{1}{\sqrt{8\pi}}\left(\frac{\ell}{\tilde{a}}\right)^{1/2}. \tag{84}$$

For weakly interacting BEC the coherence length thus satisfies $\xi \gg \ell$.

Using the Bose-Einstein condensation temperature of non-interacting particles (valid for $\tilde{a} \ll \ell$)[3]

$$T_\lambda = \frac{2\pi\hbar^2}{k_{\rm B}m}\left[\frac{n}{\zeta(\frac{3}{2})}\right]^{2/3} \tag{85}$$

where $\zeta(3/2) = 2.6124\ldots$, the number of Kelvin waves can be expressed as

$$k_{\rm eq} = \sqrt{\frac{4\pi\, n^{2/3}}{\zeta(\frac{3}{2})^{2/3}[\ln(\frac{8R}{\xi}) - a]}}\left(\frac{T}{T_\lambda}\right)^{1/2}. \tag{86}$$

Observe that $k_{\rm eq}$ varies from $k_{\rm eq} = 0$ at $T = 0$ to wavenumber of order $k_{\rm eq} \sim \ell^{-1}$ at T_λ and it is equal to $k_\xi = 2\pi/\xi$ at T^* defined by

$$T^* = 8\pi^2\zeta(\frac{3}{2})^{2/3}[\ln(\frac{8R}{\xi}) - a]\left(\frac{\tilde{a}}{\ell}\right)T_\lambda. \tag{87}$$

Therefore at temperatures $T^* < T < T_\lambda$ the energy of all Kelvin waves are in equipartition and equation (82) thus applies directly.

It is natural to suggest that an additional effect, caused by the quantum fluctuations of the amplitudes of Kelvin waves, will take place at low temperatures $T < T^*$. This quantum effect can be estimated by using the standard relation for the energy of the fundamental level of a harmonic oscillator $\Delta E = \hbar\omega(k)/2$. Applied to the Kelvin waves, this relation yields the k-independent quantum amplitude $A_Q^2 = m/4\pi^2R\rho$. The quantum effect can thus be estimated as the sum

$$\sum_{N=\mathcal{N}^{eq}_{\rm Kelvin}}^{\mathcal{N}_{\rm Kelvin}} \frac{A_Q^2N^2}{R^2} \sim \frac{A_Q^2{\mathcal{N}_{\rm Kelvin}}^3}{3R^2} = \frac{2m\pi}{3\rho\xi^3} = \frac{64\pi^{5/2}}{3\sqrt{2}}\left(\frac{a}{\ell}\right)^{3/2}. \tag{88}$$

The total effect is obtained superposing the thermal effect and the quantum effect and the final result is

$$\left.\frac{\Delta v_L}{u_i}\right|_{T<T^*} = \frac{64\pi^{5/2}}{3\sqrt{2}}\left(\frac{\tilde{a}}{\ell}\right)^{3/2} + \frac{(4/\sqrt{\pi})}{\zeta(\frac{3}{2})C[\frac{R}{\xi}]^{3/2}}\left(\frac{T}{T_\lambda}\right)^{3/2} \tag{89}$$

$$\left.\frac{\Delta v_L}{u_i}\right|_{T>T^*} = \frac{8\sqrt{2\pi}}{\zeta(\frac{3}{2})^{2/3}C[\frac{R}{\xi}]}\left(\frac{\tilde{a}}{\ell}\right)^{1/2}\frac{T}{T_\lambda} \tag{90}$$

where $C[R/\xi] = \log\left(\frac{8R}{\xi}\right) - a$.

In the case of superfluid Helium, where $\tilde{a} \sim \ell$, the GPE description is only expected to give qualitative predictions and, at best, order of magnitude estimates (see ref.[4]). It is thus difficult to extend the above considerations, obtained in the case of weakly interacting BEC with $\tilde{a} \ll \ell$, to Helium.

Nevertheless the results obtained above in the weakly interacting case strongly suggest the presence of new slowing down effects, not included in the usual mutual friction descriptions of Helium that predicts $\frac{\Delta v_L}{u_i} \sim \rho_n/\rho \sim (T/T_\lambda)^4$. The new effects, because of their temperature dependence (see eq. (90)), should be dominant at low-temperature.

The zero-temperature quantum slowdown is independent of the ring diameter and the finite temperature effects are stronger for small rings. Time of flight measurements of vortex rings in ^{4}He could be used to determine the translational velocity. The effect could also be studied in ultra-cold atomic gases BEC. For these systems the effect of the inhomogeneity of the superfluid should be taken into account.

VI. CONCLUSIONS

In summary our main results were obtained by making use of a stochastically forced Ginzburg-Landau equation (SGLE) that allowed us to efficiently obtain and control truncated Gross-Pitaevskii absolute equilibrium. This allowed us to show that the condensation transition observed in references[13,24,25] corresponds to a standard second-order transition described by the $\lambda - \phi^4$ theory.

We also found that thermodynamic equilibrium can be obtained by a direct energy cascade, in a way similar to that of Cichowlas et al.[18], accompanied by vortex annihilation as a prelude to final thermalization. Increasing the amount of dispersion of the system a slowdown of the energy transfer was produced inducing a partial thermalization independently of the truncation wavenumber.

Using the SGLE in the presence of a counterflow we observed that the counterflow can block the contraction of vortex rings reported by Berloff and Svistunov[27] and also induce a dilatation. We directly measured the mutual friction coefficient related to the transverse force. An unexpected result was found by immersing a vortex ring in a finite-temperature bath: a strong dependence of the translational velocity in the temperature was observed. This effect was an order of magnitude above the transverse mutual friction effect. We explained this effect by relating it to to the anomalous translational velocity due to finite amplitude Kelvin waves that was previously found by Kiknadze and Mamaladze[53] and Barenghi et al[54]. Assuming equipartition of the energy of the Kelvin waves with the heat bath yields a formula that gives a very good quantitative estimate of the numerically observed effect. This new formula also gives an experimentally-testable quantitative prediction for the thermal slowdown of vortex rings in weakly interacting Bose-Einstein condensates and superfluid ^{4}He.

The TGPE dynamics was thus found to contain many physically sound phenomenon of finite-temperature superflows. This strongly suggests the possibility to obtain the propagation of second sound waves in the TGPE. Some preliminary results support this conjecture (data not shown), however very high resolutions seem to be needed and this will be the subject of a future work.

Acknowledgments

We acknowledge useful scientific discussions with G. Düring and S. Rica. The computations were carried out at IDRIS (CNRS).

Appendix A: Conservation Laws and Dealiasing

In the standard case, for quadratic nonlinearities and quadratic invariants, the system can be correctly dealiased using the 2/3−rule that consists in truncation for wavenumber $|\mathbf{k}| < k_{\max} = N/3$, where $N/2$ is the largest wavenumber of the discrete system. With this procedure, one third of the available modes are not used. Such discrete dealiased pseudo-spectral system exactly conserve the quadratic invariant and is therefore identical to the original Galerkin truncated system.

In the TGPE case, the problem is more complicated because the equation is cubic and the invariants are quartic. Let us first recall Parseval's theorem that states $\int d^3x f(\mathbf{x}) g^*(\mathbf{x}) = V \sum_{\mathbf{k}} \hat{f}_{\mathbf{k}} \hat{g}^*_{\mathbf{k}}$, where $\hat{f}_{\mathbf{k}}$ and $\hat{g}_{\mathbf{k}}$ are the Fourier transform of f and g. This identity remains valid in truncated systems and it holds whether the functions are dealiased or not. The integration by parts formula is a consequence of Parseval's theorem:

$$\int d^3x\, f \frac{\partial g^*}{\partial x_j} \;=\; V \sum_{\mathbf{k}} -ik_j \hat{f}_{\mathbf{k}} \hat{g}^*_{\mathbf{k}} = -\int d^3x\, \frac{\partial f}{\partial x_j} g^*.$$

Remark that the product rule $(fg)' = f'g + fg'$ is only valid if the fields are dealiased.

The conservation of the total number of particles is directly obtained using the GPE (1)

$$\frac{dN}{dt} = \int d^3x (\dot{\psi}\bar{\psi} + \psi\dot{\bar{\psi}}) = \frac{i\hbar}{2m} \int d^3x (\bar{\psi}\nabla^2\psi - \psi\nabla^2\bar{\psi}) = 0.$$

where the last equality is a consequence of the Parseval identity and is thus true independently of dealiasing. Similar relations lead to the conservation of the energy H.

Using the dealiased TGPE (17) the conservation law for the momentum reads

$$\frac{dP_j}{dt} = 2g \int d^3x \left[\left(\partial_j \mathcal{P}_{\mathrm{G}}[|\psi|^2] \right) |\psi|^2 + \mathcal{P}_{\mathrm{G}}[|\psi|^2] \partial_j |\psi|^2 \right]. \tag{A1}$$

If ψ is dealiased the 2/3−rule implies that

$$\begin{aligned} \int d^3x (\mathcal{P}_{\mathrm{G}}[|\psi|^2]\bar{\psi}) \partial_j \psi \;&=\; \int d^3x \mathcal{P}_{\mathrm{G}} \left[\mathcal{P}_{\mathrm{G}}[|\psi|^2]\bar{\psi} \right] \partial_j \psi \\ \partial_j \left(\mathcal{P}_{\mathrm{G}}[|\psi|^2]\bar{\psi} \right) \;&=\; \left(\partial_j \mathcal{P}_{\mathrm{G}}[|\psi|^2] \right) \bar{\psi} + \mathcal{P}_{\mathrm{G}}[|\psi|^2] \partial_j \bar{\psi} \\ \partial_j |\psi|^2 \;&=\; \psi \partial_j \bar{\psi} + \partial_j \psi \bar{\psi}, \end{aligned}$$

it follows that $\frac{dP_j}{dt} = 0$. Without a Galerkin projector in eq. (17) the aliased field would obey $\left(|\psi|^2 \bar{\psi} \right) \partial_j \psi + \left(|\psi|^2 \psi \right) \partial_j \bar{\psi} \neq \partial_j (|\psi|^4)$ and the conservation of momentum would therefore be lost.

Conservation of N, H and $\mathbf{P}$ can be numerically checked by using absolute equilibria with non-zero momentum. The conservation of $\mathbf{P}$ is ensured only if the system is dealiased. The error of aliased runs grow up to a 50% in a few units of time and is independent of the time-step (data not shown). We thus believe that it would important to explicitly check the conservation of momentum when using finite-difference schemes, even if they exactly conserve the energy and the particle number.

Appendix B: Low-temperature calculation of thermodynamic functions

We are interested in computing the grand partition function $\mathcal{Z}$ in eq.(46) where $F = H - \mu N - \mathbf{W}\cdot\mathbf{P}$ is written in terms of Fourier amplitudes as

$$\frac{H}{V} = \sum_{\mathbf{k}} \frac{\hbar^2 k^2}{2m}|A_{\mathbf{k}}|^2 + \frac{g}{2}\sum A^*_{\mathbf{k_3}+\mathbf{k_1}} A_{\mathbf{k_2}} A^*_{\mathbf{k_4}+\mathbf{k_2}} \delta_{\mathbf{k_3},-\mathbf{k_4}} \tag{B1}$$

$$N = V\sum_{\mathbf{k}} |A_{\mathbf{k}}|^2 \tag{B2}$$

$$P_j = \sum_{\mathbf{k}} \hbar k_j |A_{\mathbf{k}}|^2 V \tag{B3}$$

where $A_{\mathbf{k}} = 0$ if $k \geq k_{\max}$ and the second sum in H is over $\mathbf{k_1}$, $\mathbf{k_2}$, $\mathbf{k_3}$, $\mathbf{k_4}$.

The saddle-point is determined by the condition $\frac{\partial F}{\partial A^*_{\mathbf{k}}} - \mu_0 A_{\mathbf{0}} V \delta_{\mathbf{k},\mathbf{0}} = 0$ which, explicitly written for $\mathbf{k} = \mathbf{0}$ and $\mathbf{k} \neq \mathbf{0}$, reads

$$(g|A_{\mathbf{0}}|^2 - \mu + \mu_0)A_{\mathbf{0}} + 2g\sum_{\mathbf{k_1}\neq\mathbf{0}} A_{\mathbf{0}}|A_{\mathbf{k_1}}|^2 + g\sum_{\mathbf{k_1},\mathbf{k_2}\neq\mathbf{0}} A_{\mathbf{k_1}} A^*_{\mathbf{k_2}-\mathbf{k_1}} A_{-\mathbf{k_2}} = 0 \tag{B4}$$

$$\frac{\hbar^2 k^2}{2m}A_{\mathbf{k}} - \mu A_{\mathbf{k}} - \hbar\mathbf{W}\cdot\mathbf{k}\, A_{\mathbf{k}} + g\sum_{\mathbf{k_1},\mathbf{k_2}\neq 0} A_{\mathbf{k_1}} A^*_{\mathbf{k_2}+\mathbf{k_1}} A_{\mathbf{k}+\mathbf{k_2}} = 0 \tag{B5}$$

from which eq.(47) follows.

To diagonalize $F = H - \mu N - \mathbf{W}\cdot\mathbf{P}$ we first apply the Bogoliubov transformation to $H - \mu N$ and then show that P is also diagonal in this basis. Replacing $B_{\mathbf{p}}$, defined by the transformation (51), in $H - \mu N$ (recall that $\mathbf{p} = \hbar\mathbf{k}$) and then imposing the diagonalization determines the coefficient L_p:

$$L_p = \frac{-2|A_{\mathbf{0}}|^2 g - \frac{p^2}{2m} + \mu + \epsilon(p)}{|A_{\mathbf{0}}|^2 g} \tag{B6}$$

where $\epsilon(p)$ is given by

$$\epsilon(p) = \sqrt{\left(2|A_{\mathbf{0}}|^2 g + \frac{p^2}{2m} - \mu\right)^2 - |A_{\mathbf{0}}|^4 g^2}. \tag{B7}$$

The dispersion relation (53) is obtained by replacing $|A_{\mathbf{0}}|^2$ by its saddle-point value eq.(47).

We now express $\mathbf{P}$ in the Bogoliubov base. Using (51) directly yields

$$|A_{\mathbf{p}}|^2 = |u_p|^2|B_{\mathbf{p}}|^2 + |v_p|^2|B_{-\mathbf{p}}|^2 + (u^*{}_p v^*{}_p B_{\mathbf{p}} B_{-\mathbf{p}} + c.c). \tag{B8}$$

Replacing eq.(B8) in the definition of $\mathbf{P}$ (B3), the last two terms vanish by symmetry and using the relation $|u_p|^2 - |v_p|^2 = 1$, the momentum (B3) reads $\mathbf{P} = \sum_{\mathbf{p}} \mathbf{p}|B_{\mathbf{p}}|^2 V$. Gathering $H - \mu N$ and $\mathbf{W}\cdot\mathbf{P}$ formula (52) is finally obtained.

The mean value of the condensate amplitude is obtained as $V\overline{|A_{\mathbf{0}}|^2} = -\left.\frac{\partial\Omega}{\partial\mu_0}\right|_{\mu_0=0}$. All the thermodynamic variables are directly generated by first putting $\mu_0 = 0$ in (58) and then by differentiation using relation (31). The fluctuations of the number of particles are computed as $\overline{\delta N^2} = -\beta^{-1}\frac{\partial^2\Omega}{\partial\mu^2}$. These quantities are explicitly listed below.

$$\begin{aligned}
\overline{|A_{\mathbf{0}}|^2} &= \frac{\mu}{g} - \frac{\mathcal{N}}{V\beta\mu} f_0\left[\frac{4m\mu}{P^2_{\max}}\right] \\
\bar{p} &= \frac{\mu^2}{2g} + \frac{\mathcal{N}}{V\beta}\left(\frac{2}{3} - f\left[\frac{4m\mu}{P^2_{\max}}\right] + \frac{2}{3}\frac{2w^2m^2}{P^2_{\max}} f'\left[\frac{4m\mu}{P^2_{\max}}\right]\right) \\
\bar{N} &= \frac{V\mu}{g} - \frac{\mathcal{N}}{\beta}\left(\frac{3}{2\mu} f\left[\frac{4m\mu}{P^2_{\max}}\right] - \frac{8w^2m^3}{P^4_{\max}} f_2\left[\frac{4m\mu}{P^2_{\max}}\right]\right) \\
S &= \mathcal{N}\left(f\left[\frac{4m\mu}{P^2_{\max}}\right](1 + \frac{2w^2m}{4\mu}) - \log\left[\frac{\beta\epsilon(P_{\max};\mu)}{e^{-\frac{5}{3}}}\right]\right) \\
\lambda_{\mathcal{N}} &= \beta^{-1}\log\left[\beta\epsilon(P_{\max};\mu)\right] - \frac{1}{3\beta}\frac{2w^2m^2}{P^2_{\max}}\frac{1}{1 + \frac{4m\mu}{P^2_{\max}}} \\
\bar{P}_z &= \frac{\mathcal{N}}{\beta}\frac{wm}{\mu} f\left[\frac{4m\mu}{P^2_{\max}}\right] + \frac{3\mathcal{N}}{10\beta}\frac{w^3m^2}{\mu^2} f_1\left[\frac{4m\mu}{P^2_{\max}}\right] \\
\overline{\delta N^2} &= \frac{V}{g\beta} + \frac{3\mathcal{N}}{4\beta^2\mu^2} f_1\left[\frac{4m\mu}{P^2_{\max}}\right],
\end{aligned} \tag{B9}$$

$$f[z] = z - z^{3/2}\cot^{-1}\left(\sqrt{z}\right) \tag{B10}$$

$$f_0[z] = 3(z + 3f[z])/4 \tag{B11}$$

$$f_1[z] = \frac{z}{z+1} - f(z) \tag{B12}$$

$$f_2[z] = \frac{d}{dz}(f[z]/z) \tag{B13}$$

The dependence of the entropy on the phase-space normalization constant is manifested by the presence of the logarithm term in S and $\lambda_{\mathcal{N}}$. Note that the function $S + \beta\lambda_{\mathcal{N}}$ is, however, completely defined. Also note that the pressure p must be computed, by definition, at constant total number of modes $\mathcal{N}$. All the thermodynamic relations discussed in section II B can be explicitly checked on the low-temperature expressions. The previous formulae have been confronted with the SGLE numerically generated data in Fig.2.a-b.

[1] L D Landau and L M Lifshitz. *Course of Theoretical Physics, Volume VI: Fluid Mechanics*. Butterworth-Heinemann, Jan 1987.

[2] W. F. Vinen. Mutual Friction in a Heat Current in Liquid Helium II. III. Theory of the Mutual Friction. *Proceedings of the Royal Society of London. Series A. Mathematical and Physical Sciences*, 242(1231):493–515, 1957.

[3] Nick P Proukakis and Brian Jackson. Finite-temperature models of bose–einstein condensation. *J. Phys. B: At. Mol. Opt. Phys.*, 41(20):203002, Oct 2008.

[4] R. J. Donnelly. *Quantized Vortices in Helium II*. Cambridge Univ. Press, 1991.

[5] C Nore, M Abid, and ME Brachet. Kolmogorov turbulence in low-temperature superflows. *Physical Review Letters*, 78(20):3896–3899, Jan 1997.

[6] C Nore, M Abid, and ME Brachet. Decaying kolmogorov turbulence in a model of superflow. *Phys. Fluids*, 9(9):2644–2669, Jan 1997.

[7] M Kobayashi and M Tsubota. Kolmogorov spectrum of superfluid turbulence: Numerical analysis of the gross-pitaevskii equation with a small-scale dissipation. *Physical Review Letters*, 94(6):065302, Jan 2005.

[8] Jeffrey Yepez, George Vahala, Linda Vahala, and Min Soe. Superfluid turbulence from quantum kelvin wave to classical kolmogorov cascades. *Physical Review Letters*, 103(8):084501, Aug 2009.

[9] M Abid, ME Brachet, J Maurer, C Nore, and P Tabeling. Experimental and numerical investigations of low-temperature superfluid turbulence. *Eur J Mech B-Fluid*, 17(4):665–675, Jan 1998.

[10] J Maurer and P Tabeling. Local investigation of superfluid turbulence. *Europhysics Letters*, 43(1):29–34, Jan 1998.

[11] G. P. Bewley, M. S. Paoletti, K. R. Sreenivasan, and D. P. Lathrop. Characterization of reconnecting vortices in superfluid helium. *PNAS*, 105(37):13707–13710, 2008.

[12] M. S. Paoletti, M. E. Fisher, K. R. Sreenivasan, and D. P. Lathrop. Velocity statistics distinguish quantum turbulence from classical turbulence. *Physical Review Letters*, 101(15):154501, 2008.

[13] MJ Davis, SA Morgan, and K Burnett. Simulations of bose fields at finite temperature. *Physical Review Letters*, 87(16):160402–160402, 2001.

[14] T.D. Lee. On some statistical properties of hydrodynamical and magneto-hydrodynamical fields. *Quart Appl Math*, 10(1):69–74, Jan 1952.

[15] R. Kraichnan. On the statistical mechanics of an adiabatically compressible fluid. *J Acoust Soc Am*, 27(3):438–441, Jan 1955.

[16] R. Kraichnan. Helical turbulence and absolute equilibrium. *Journal of Fluid Mechanics*, 59(AUG7):745–752, Jan 1973.

[17] S.A. Orszag. *Statistical Theory of Turbulence*. in, Les Houches 1973: Fluid dynamics, R. Balian and J.L. Peube eds. Gordon and Breach, New York, 1977.

[18] C Cichowlas, P Bonaiti, F Debbasch, and M Brachet. Effective dissipation and turbulence in spectrally truncated euler flows. *Physical Review Letters*, 95(26):264502, Jan 2005.

[19] W. J. T Bos and J.-P Bertoglio. Dynamics of spectrally truncated inviscid turbulence. *Phys. Fluids*, 18(7):071701, Jan 2006.

[20] G Krstulovic and M Brachet. Two-fluid model of the truncated euler equations. *Physica D: Nonlinear Phenomena*, 237(14-17):2015–2019, Aug 2008.

[21] G Krstulovic, P D Mininni, M E Brachet, and A Pouquet. Cascades, thermalization, and eddy viscosity in helical galerkin truncated euler flows. *Physical review. E*, pages 1–5, May 2009.

[22] Uriel Frisch, Susan Kurien, Rahul Pandit, Walter Pauls, Samriddhi Sankar Ray, Achim Wirth, and Jian-Zhou Zhu. Hyperviscosity, galerkin truncation, and bottlenecks in turbulence. *Physical Review Letters*, 101(14):144501, Jan 2008.

[23] G Krstulovic, C Cartes, M Brachet, and E Tirapegui. Generation and characterization of absolute equilibrium of compressible flows. *International Journal of Bifurcation and Chaos (IJBC)*, 19(10):3445–3459, 2009.

[24] C Connaughton, C Josserand, A Picozzi, Y Pomeau, and S Rica. Condensation of classical nonlinear waves. *Physical Review Letters*, 95(26):263901, Jan 2005.

[25] Antonio Picozzi Gustavo Düring and Sergio Rica. Breakdown of weak-turbulence and nonlinear wave condensation,. *Physica D*, 238(16):1524–1549, August 2009.

[26] NG Berloff and BV Svistunov. Scenario of strongly nonequilibrated bose-einstein condensation. *Physical Review A*, 66(1):013603, Jan 2002.

[27] Natalia G Berloff and Anthony J Youd. Dissipative dynamics of superfluid vortices at nonzero temperatures. *Physical Review Letters*, 99(14):4, Oct 2007.

[28] Jean Zinn-Justin. *Phase Transitions and Renormalisation Group*. Oxford University Press, USA, August 2007.

[29] Daniel J. Amit and Victor Martin-Mayor. *Field Theory; The Renormalization Group and Critical Phenomena*. World Scientific Publishing Company, June 2005.

[30] M Abid, C Huepe, S Metens, C Nore, CT Pham, LS Tuckerman, and ME BRACHET. Gross-pitaevskii dynamics of bose-einstein condensates and superfluid turbulence. *Fluid Dyn Res*, 33(5-6):509–544, Jan 2003.

[31] D. Gottlieb and S. A. Orszag. *Numerical Analysis of Spectral Methods*. SIAM, Philadelphia, 1977.

[32] L D Landau and L M Lifshitz. *Course of Theoretical Physics, Volume V: Statistical Physics (Part 1)*. Butterworth-Heinemann, Aug 1996.

[33] N. G. van. Kampen. *Stochastic processes in physics and chemistry / N.G. van Kampen*. North-Holland ; sole distributors for the USA and Canada, Elsevier North-Holland, Amsterdam ; New York : New York :, 1981.

[34] Flor Langouche, Dirk Roekaerts, and Enrique Tirapegui. *Functional integration and semiclassical expansions?* D Reidel Pub Co, Jan 1982.

[35] Jon Mathews and Robert Lee Walker. *Mathematical methods of physics*. W. A. Benjamin, 1970, Jan 1970.

[36] E M Lifshitz and L P Pitaevskii. *Course of Theoretical Physics, Volume IX: Statistical Physics (Part 2)*. Butterworth-Heinemann, Jan 1980.

[37] J Lipa, J Nissen, D Stricker, and D Swanson. Specific heat of liquid helium in zero gravity very near the lambda point. *Phys. Rev. B*, Jan 2003.

[38] Giorgio Krstulovic and Marc Brachet. Comment on "superfluid turbulence from quantum kelvin wave to classical kolmogorov cascade". [arxiv:0905.0159v1], 2009.

[39] C Huepe, S Metens, G Dewel, P Borckmans, and ME Brachet. Decay rates in attractive bose-einstein condensates.

Physical Review Letters, 82(8):1616–1619, Jan 1999.

[40] C. W. Gardiner. *Handbook of Stochastic Methods: For Physics, Chemistry and the Natural Sciences (Springer Series in Synergetics)*. Springer, November 1996.

[41] T Winiecki, JF McCann, and CS Adams. Vortex structures in dilute quantum fluids. *Europhysics Letters*, 48(5):475–481, Jan 1999.

[42] C Huepe and ME Brachet. Scaling laws for vortical nucleation solutions in a model of superflow. *PHYSICA D-NONLINEAR PHENOMENA*, 140(1-2):126–140, JUN 1 2000.

[43] Tuckerman LS, Huepe C, and Brachet ME. Numerical methods for bifurcation problems. 9:75–83, 2004.

[44] CT Pham, C Nore, and ME Brachet. Boundary layers and emitted excitations in nonlinear Schrodinger superflow past a disk. *PHYSICA D-NONLINEAR PHENOMENA*, 210(3-4):203–226, OCT 15 2005.

[45] C Nore, ME Brachet, E Cerda, and E Tirapegui. Scattering of first sound by superfluid vortices. *Physical Review Letters*, 72(16):2593–2595, Jan 1994.

[46] DJ Thouless, P Ao, and Q Niu. Transverse force on a quantized vortex in a superfluid. *Physical Review Letters*, 76(20):3758–3761, Jan 1996.

[47] GE Volovik. Transverse force on a quantized vortex in a superfluid - comment. *Physical Review Letters*, 77(22):4687–4687, Jan 1996.

[48] C Wexler. Magnus and iordanskii forces in superfluids. *Physical Review Letters*, 79(7):1321–1324, Jan 1997.

[49] HE Hall and JR Hook. Comment on "magnus and iordanskii forces in superfluids". *Physical Review Letters*, 80(19):4356–4356, Jan 1998.

[50] EB Sonin. Comment on "berry's phase and the magnus force for a vortex line in a superconductor," "transverse force on a quantized vortex in a superfluid," and "magnus and iordanskii forces in superfluids". *Physical Review Letters*, 81(19):4276–4276, Jan 1998.

[51] C Wexler, DJ Thouless, P Ao, and Q Niu. Comment on "magnus and iordanskii forces in superfluids" - wexler et al reply. *Physical Review Letters*, 80(19):4357–4357, Jan 1998.

[52] J Fuchs, G Malka, J. C Adam, F Amiranoff, S. D Baton, N Blanchot, A Héron, G Laval, J. L Miquel, P Mora, H Pépin, and C Rousseaux. Fuchs et al. reply:. *Physical Review Letters*, 81:4275, Nov 1998.

[53] L Kiknadze and Y Mamaladze. The waves on the vortex ring in He ii. *Journal of Low Temperature Physics*, 126(1-2):321–326, Jan 2002.

[54] C. F Barenghi, R Hanninen, and M Tsubota. Anomalous translational velocity of vortex ring with finite-amplitude kelvin waves. *Physical Review E*, 74(4):046303, Jan 2006.

[55] CF Barenghi, RJ Donnelly, and WF Vinen. Thermal excitation of waves on quantized vortices. *Phys Fluids*, 28(2):498–504, Jan 1985.

[56] VA Zagrebnov and JB Bru. The bogoliubov model of weakly imperfect bose gas. *Phys Rep*, 350(5-6):292–434, Jan 2001.

[57] Note that grand canonical computations avoid difficulties that are present in the canonical ensemble with the explicit conservation of the number of particles (see section 2.2 of reference[56] and references therein)

[58] The thermodynamic limit is taken over the grand canonical potential $\Omega = -\beta^{-1} \log \mathcal{Z}$ as $V \left(\lim_{V \to \infty} \frac{\Omega}{V} \right)$.

[59] http://www.vapor.ucar.edu

6.3.1 Supplementary material

Partial thermalization

We give here some $3D$ density visualization corresponding to the partial thermalization using the initial conditions of the Taylor-Green vortex.

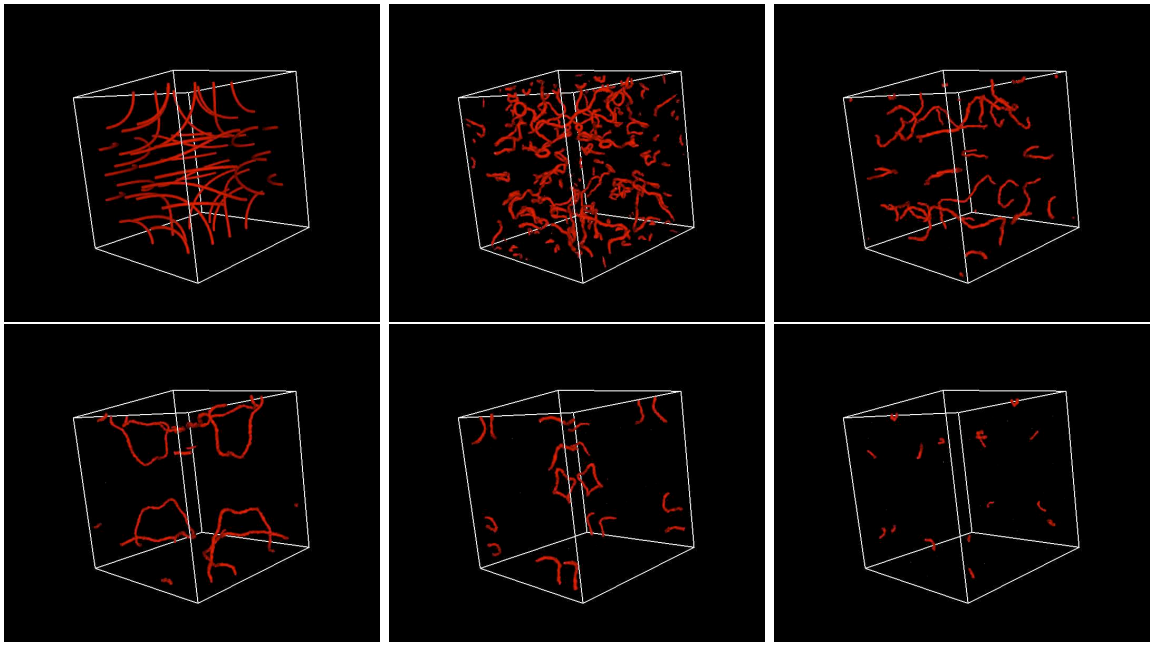

Fig. 6.2: $3d$ visualization of the density Taylor-Green vortex at $t = 0$, $t = 15$, $t = 30$, $t = 45$, $t = 60$ and $t = 75$. 256^3.

We observe that the initial condition evolves to first form a complex vortex tangle. This is the turbulent phase where Kolmogorov spectrum is found. Then vortices reconnect and form simpler structures. Finally, only some large size rings are presented that contract due to mutual friction effects.

Spontaneous nucleation under TGPE

In section V.A the metastability was explicitly observed and the dynamics under SGLE was characterized with an Arrhenius law. Due thermal fluctuations (explicitly given by the thermal bath induced by the noise $\zeta(t)$) vortex rings were spontaneous nucleated. Under the dynamics of TGPE there is no such forcing term. However the thermalized modes can play the role of a thermostat. Of course, the system is completely different because the energy, the momentum and number of particle remain constant during the evolution under TGPE while in SGLE the conjugate variable remain constant.

To study the nucleation of vortex rings under TGPE we prepare an initial condition using SGLE with 64^3 collocation points and $\rho = 1$. The temperature is set to $T = 0.8$

and the counterflow to $w = 1$. When SGLE reaches a quasi-equilibrium (at $\mathbf{k} = \mathbf{0}$) the wavefunction is saved and posteriorly used as initial condition of TGPE. Three-dimensional visualizations of the density are displayed on Fig.6.3. A vortex ring is

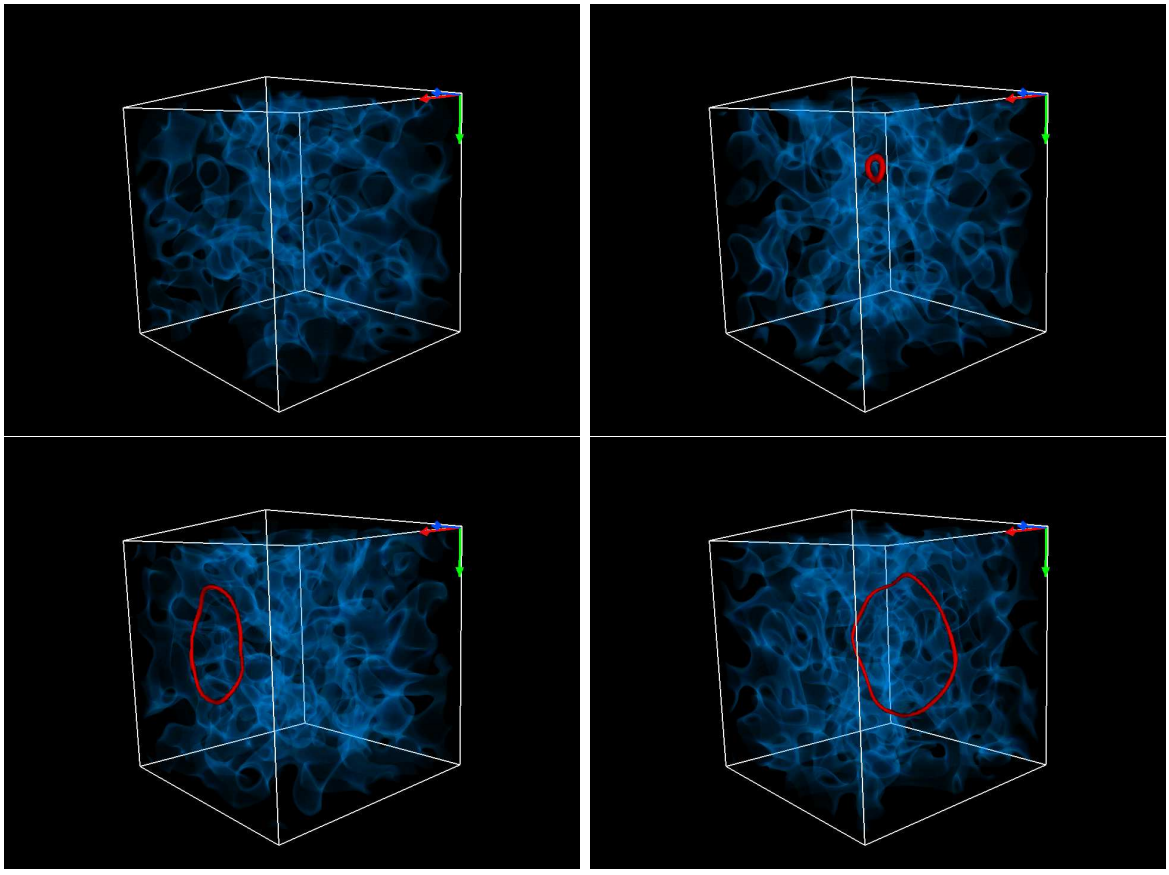

Fig. 6.3: Spontaneous nucleation under TGPE. $3d$ visualization of the density. $t = 0$, $t = 54$, $t = 114$, and $t = 228$.

nucleated near of $t \approx 50$, then it increases it size due to counterflow effects. Finally the vortex ring reaches a maximum value as observed on figure 6.4. This maximum value is explained since as the momentum depends on radius square of the ring, arbitrary large rings are not compatible with the conservation of momentum.

Dynamical effects of finite temperature and counterflow on vortices: Crystal visualizations

We present here a $3D$ visualizations of the density ρ corresponding to the dynamic evolution of a crystal (see section V.B1 of the article) for a typical run presented in figure 7.b of the article. The corresponding temporal evolution with 64^3 collocations points, $T = 1$ and $w = 0.4$ is displayed in Fig.6.5.

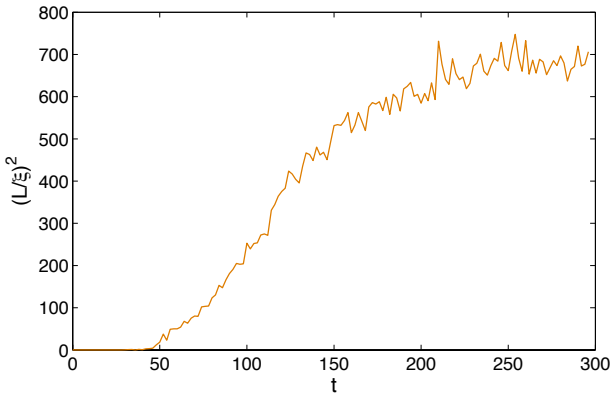

Fig. 6.4: Temporal evolution of vortex ring length square $(L/\xi)^2$. A spontaneous nucleation is observed at $t \approx 50$. 64^3 collocation points, $T = 0.775$ and $w = 1$.

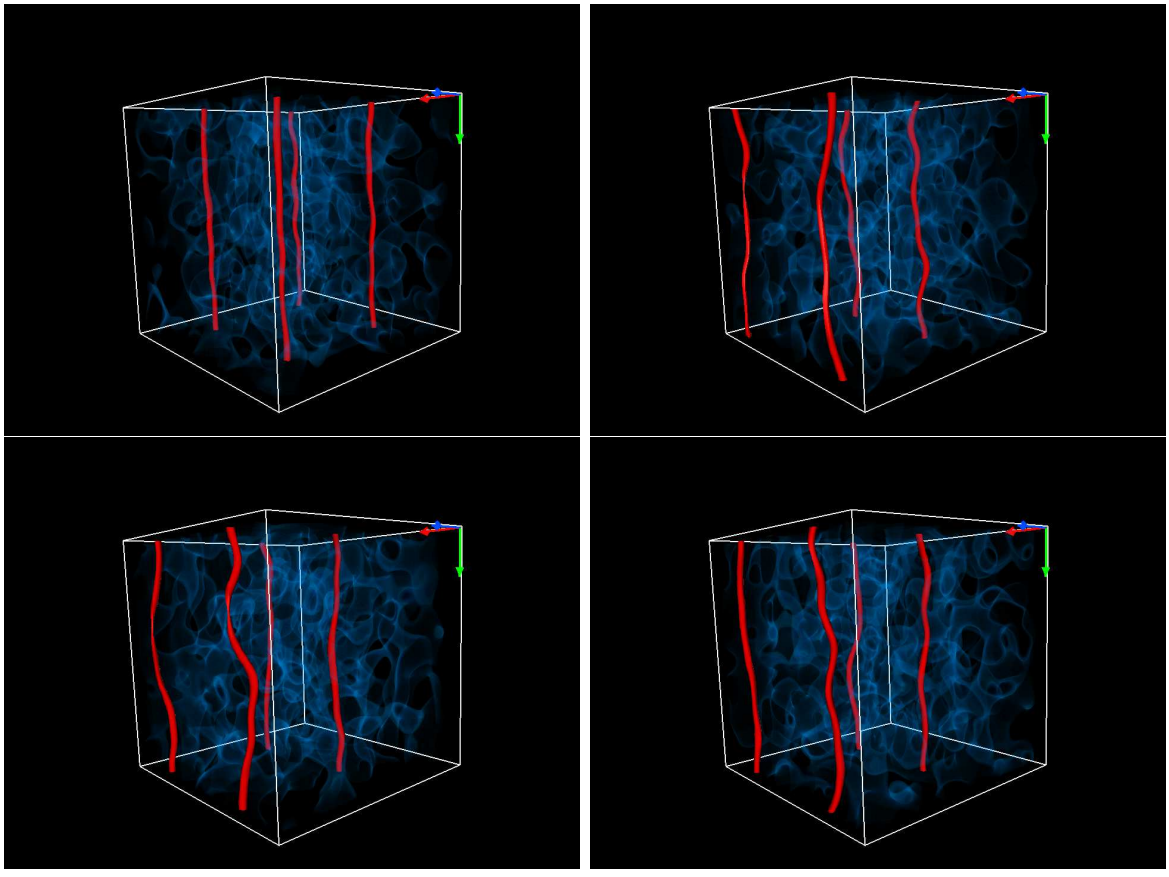

Fig. 6.5: $3d$ visualization of the density. $t = 0$, $t = 150$, $t = 160$, and $t = 165$. Kelvin waves are clearly observed in the crystal

Thermal induced Kelvin waves in a vortex ring

In section B.3 of the article, assuming equipartition of the energy of Kelvin waves with the heat bath, we determined the value of the amplitude of the waves A as function of T:

$$A^2 = \frac{m^2 k_B T}{\pi^2 \rho \hbar^2 R(\log \frac{8R}{\xi} - a)} \frac{R^2}{N^2}, \tag{6.55}$$

which allows to obtain the rms amplitude of waves as

$$A_{\rm rms} = \sqrt{\frac{m^2 k_B T R}{\pi^2 \rho \hbar^2 (\log \frac{8R}{\xi} - a)}} \left(\sum_{N=1}^{\mathcal{N}_{\rm Kelvin}} \frac{1}{N^2} \right)^{1/2} \approx \sqrt{\frac{m^2 k_B T R}{6 \rho \hbar^2 (\log \frac{8R}{\xi} - a)}}. \tag{6.56}$$

The equipartition law (6.55) can also be directly obtained as the classical limit of the quantum distribution computed by Barenghi *et al.* [100], up to a redefinition of the core constant model a (see eq.(25) in reference [100]).

The data used for the $3D$ visualization of the density allows to perform a rough measurement of the rms amplitude of the Kelvin waves. Remark that, as the density fields used for the visualization have been low-filtered, a lower value of $A_{\rm rms}$ will be obtained. We expect thus that measurements and formula (6.56) can only coincide in order of magnitudes. The coordinates of the vortex rings in a plane perpendicular to the ring are obtained by finding the minimum of a cubic interpolation of the density. The temperature dependence of $A_{\rm rms}/R$ is plotted on figure 6.6. Observe that orders

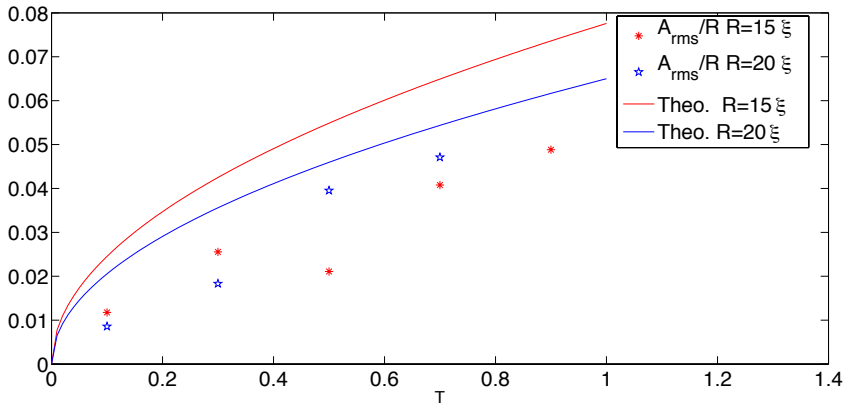

Fig. 6.6: $3d$ visualization of the density. $t = 0$, $t = 150$, $t = 160$, and $t = 165$. Kelvin waves are clearly observed in the crystal

of magnitudes are in agreement with prediction (6.56). Also observe that the largest amplitudes are of order $A_{\rm rms} \sim 0.05R$ avoiding the possibility of self-reconnection at these temperatures.

A more precise measurement of $A_{\rm rms}$ can be obtained by finding the coordinate

of the vortex ring on the complete field (not low-filtered). This can be done with high accuracy using a Newton method (see appendix B) in the same way that in the publication presented in chapter 7. Finding the coordinates of the ring during the numerical integration should permit to have a much better sampling than that used for the $3D$ visualization. We will attempt in a future work to study in detail the thermal induced Kelvin waves for different values of the vortex ring radius and higher temperatures.

7. RADIATION AND VORTEX DYNAMICS IN THE GROSS-PITAEVSKII EQUATION

In this chapter we present our publication [39], done in collaboration with Enrique Tirapegui. We studied the sound emission produced by the interaction of several vortices in a two-dimensional homogeneous system. The radiative field is explicitly obtained as a series in the Mach number M. Using this expression the total power radiated is computed. This result is then applied to a simple test case of two corotating vortices. Then, numerical simulations of two-dimensional Gross-Pitaevskii equation are performed and confronted to the theoretical predictions. The numerical data give support to the theoretical estimate of radiation.

7.1 Publication: "Radiation and vortex dynamics in the nonlinear Schrödinger equation"

As it has been discussed in previous chapter an effective dissipation is observed in conservative superfluid dynamics driven by the GPE. It has been shown [27] that the incompressible kinetic energy, that one related to the vortices, is transferred to sound waves. This process is achieved by vortex reconnection, once two filaments reconnect a cusp is produced exiting long-wavelength helical waves known as Kelvin waves. These waves subsequently decay into sound waves.

The problem of vortex reconnection is a purely three-dimensional phenomenon and to study these complicated effects from first principles present a formidable task. There exist some models, pioneered by Schwarz [101], that allows directly evaluate and consider the Kelvin waves on a vortex filament. In this article we are interested in vortex dynamics under the GPE evolution and we consider the simpler analogous problem: a two-dimensional configuration of several vortices, where the effects can be studied analytically.

Based on the acoustic approximation of GPE and assumed vortex trajectories we computed the far field and the power radiated by the moving vortex using a development in the Mach number M. One interesting fact, directly related to the non-local character of the two-dimensional Green function of the wave equation, is that the formulae depend on non-integer derivatives of the trajectories. At lower order the total radiated power depends on the 3/2-*derivative* of the trajectory instead of the 2-*derivative* that is present in three dimensions.

The theoretical prediction is then applied to a test case of two corotating vortices of frequency ω. Because of this simple configuration and simplicity of the computations an explicit series is obtained. We present here only the final results of the power radiated energy

$$\begin{aligned} J &= \frac{4\pi^2\hbar^2\omega}{m^2}\sum_{n=1}^{\infty}\sum_{m=1}^{\infty}\frac{(-M^2)^{n+m}}{(2n-1)!(2m-1)!}\sum_{l=0}^{n}\binom{2n}{l}\binom{2m}{l+m-n}(n-l)^{2(n+m)-1} \\ &= \frac{4\pi^2\hbar^2\omega}{m^2}M^4\left(1-\frac{4M^2}{3}+\frac{17M^4}{4}-\frac{157M^6}{18}+\frac{91783M^8}{4320}-\dots\right). \end{aligned} \tag{7.1}$$

This problem was also numerically studied in reference [102], they found emission of dipolar sound waves for the case of a vortex in a harmonic trap (see also [103]) and quadrupolar radiation for the corotating vortices configuration.

Finally in the publication included below some numerical simulations were performed. From the numerical point of view this was a very difficult task because radiative effects are of order M^4, at it is apparent in formula (7.1). Because of energy lost by radiation the trajectories of the rotating vortices are not closed and weakly increase their radius at each turn. We numerically measured the relative variation of the radius (of order M^4) with resolution up to 4096^2 collocation points checking carefully the conservation of energy. This computation needs long time integration (the time needed for a revolution diverges in the limit $M \to 0$). The numerical data gave support to the estimate of radiation[1].

Although the lower order term of the theoretical prediction (7.1) has been known since the 60's [104], this work is to best of our knowledge, the first clear numerical evidence supporting this prediction.

We will attempt in the future to study the sound-vortex interaction in this configuration because it has been recently observed [105] that such vortices undergo an annihilation process assisted by sound, which is the route to Bose-Einsten condensation in $2D$. It would be interesting to relate the mutual friction effects described in the previous chapter to this process.

[1] The conservation of energy was carefully checked and numerical errors are smaller than 10^{-6}.

Radiation and vortex dynamics in the nonlinear Schrödinger equation

Giorgio Krstulovic and Marc Brachet
Laboratoire de Physique Statistique de l'Ecole Normale Supérieure, CNRS and Universités Paris VI et VII, 24 Rue Lhomond, 75231 Paris, France

Enrique Tirapegui
Departamento de Física, Facultad de Ciencias Físicas y Matemáticas de la Universidad de Chile, Blanco Encalada 2008, Santiago, Chile

(Received 12 June 2008; published 1 August 2008)

Sound emission produced by the interaction of several vortices in a two-dimensional homogeneous system obeying the nonlinear Schrödinger (NLS) equation is considered. The radiation effect is explicitly computed in terms of assumed vortex motion. The results are applied to a simple test case of two corotating vortices. The prediction is compared to the result of numerical simulations of the NLS equation. The numerical data give support to the estimate of radiation.

DOI: 10.1103/PhysRevE.78.026601 PACS number(s): 05.45.Yv, 67.25.dk, 47.32.C−

I. INTRODUCTION

Strong turbulent effective dissipation has been observed to take place in inviscid and conservative systems, in the context of (compressible) low-temperature superfluid turbulence [1,2]. Vortices are thus subject to some significant dynamical dissipation mechanism. It has been suggested that sound emission from the vortices is the major decay process [3–5]. Detailed mechanisms are fully three dimensional (3D). They involve initial vortex reconnection followed by secondary excitation of long-wavelength helical waves, known as Kelvin waves, along the vortex line and their subsequent decay into sound waves [6]. It appears that evaluating these complicated 3D effects from first principles is a formidable task at the present time.

The purpose of the present paper is to compute the simpler analogous problem in two dimensions. We thus consider sound emission produced by the interaction of several vortices in a 2D homogenous system obeying the nonlinear Schrödinger (NLS) equation.

Our main result is that the far field, and thus the radiation effect can be directly computed in terms of an assumed vortex motion [see Eq. (17)]. These main formulas are then applied to the simple test case of two corotating vortices, reproducing theoretical estimates of the same test case [7,8], and the prediction is compared to the result of numerical integrations of the NLS equation.

The paper is organized as follows. In Sec. II we establish the basic proprieties of the NLS equation and recall the general expression for the field produced by moving vortices. Section III is devoted to the derivation of explicit trajectory-dependent expressions for the radiative contribution to the far field and the radiated energy flux. Section IV contains the determination of vortex trajectories by numerical solutions of the NLS and the comparison with theoretical predictions. Discussion and conclusions are finally given in Sec. V.

II. NONLINEAR SCHRÖDINGER EQUATION

We consider the nonlinear Schrodinger equation (NLSE) written with the physically relevant parameters: the coherence length ξ and the sound velocity c,

$$i\frac{\partial\psi}{\partial t}=\frac{c}{\sqrt{2}\xi}(-\xi^2\Delta\psi-\psi+|\psi|^2\psi). \tag{1}$$

This equation has Galilean invariance with the transformation $\psi(x,t)\to\psi(x-vt,t)e^{i(v\cdot x-v^2t/2)}$ and it also has a Lagrangian structure from which we can calculate an energy-momentum tensor and the conserved quantities corresponding to space-time translations [4].

We can map the NLSE to hydrodynamics equations using the Madelung transformation defined by

$$\psi(x,t)=\sqrt{\rho(x,t)}\exp\left(i\frac{\phi(x,t)}{\sqrt{2}c\xi}\right). \tag{2}$$

Replacing Eq. (2) in the NLSE (1) and separating real and imaginary parts we get

$$\frac{\partial\rho}{\partial t}+\boldsymbol{\nabla}\cdot(\rho\,\boldsymbol{\nabla}\,\phi)=0, \tag{3}$$

$$\frac{\partial\phi}{\partial t}+\frac{1}{2}(\nabla\phi)^2=c^2(1-\rho)+c^2\xi^2\frac{\Delta\sqrt{\rho}}{\sqrt{\rho}}. \tag{4}$$

We recognize here the continuity equation (3) for a fluid of density ρ and velocity $\mathbf{v}=\boldsymbol{\nabla}\phi$ and the Bernoulli equation (4), except for the last term which is usually called quantum pressure since it has no analog in standard fluid mechanics (it is proportional to $\hbar^2$ in the superfluidity context and it can be neglected when the semiclassical limit is taken).

We note that, if the function ψ has a zero, the density ρ is well defined but the phase ϕ is undefined. The existence of a zero requires the real and the imaginary parts of ψ to vanish simultaneously and consequently these kind of singularities generically appear as curves in 3D and points in 2D. These topological defects have the property that their circulation is a multiple of $4\pi\alpha$ ($\alpha=c\xi/\sqrt{2}$), and for this reason they are called *quantum vortices* in the context of superfluidity. In 2D a stationary vortex solution centered at the origin can be constructed in polar coordinates (ρ,θ) using the ansatz $\rho(r,\theta)=\rho_0(r)^2$ and $\phi(r,\theta)=2\alpha m\theta$, with $m\in\mathbb{Z}$ the vortex

charge. The function $\rho_0(r)$ satisfies the equation

$$\frac{\partial^2\rho_0}{\partial r^2}+\frac{1}{r}\frac{\partial\rho_0}{\partial r}+\frac{1}{\xi^2}\left(1-\rho_0^2-\frac{\xi^2m^2}{r^2}\right)\rho_0=0$$

with boundary conditions $\rho_0(0)=0$, $\rho_0(\infty)=1$. This equation can be solved numerically and one finds that ρ_0 is an increasing function in $[0,\infty]$. The region where the function is much smaller than 1, the core of the vortex, increases with m for fixed ξ and c.

Replacing ρ from (4) into (3) we obtain the exact equation

$$\frac{\partial^2\phi}{\partial t^2}-c^2\Delta\phi=-\frac{\partial\phi}{\partial t}\Delta\phi-\frac{\partial(\nabla\phi)^2}{\partial t}-\nabla\cdot\left(\frac{(\nabla\phi)^2}{2}\nabla\phi\right)+\frac{\partial\Gamma}{\partial t}+\nabla\cdot(\Gamma\nabla\phi)$$

where $\Gamma(\rho)=(c^2\xi^2/2)\Delta\sqrt{\rho}/\sqrt{\rho}$. Far from the vortex, the field is almost constant and we can perturb it by putting $\rho=1+2s$. If we consider long-wavelength propagative disturbances the appropriates scalings are

$$\phi=o(1),\quad s=o(\epsilon),$$

$$\frac{\partial}{\partial x_i}=o(\epsilon),\quad \frac{\partial}{\partial t}=o(\epsilon),$$

with ϵ a small parameter. We obtain:

$$\Gamma(s)=\frac{c^2\xi^2}{2}[\Delta s-s\Delta s-(\nabla s)^2+o(\epsilon^5)] \tag{5}$$

and then

$$\frac{\partial\Gamma}{\partial t}+\nabla\cdot(\Gamma\nabla\phi)=\frac{c^2\xi^2}{2}\Delta\frac{\partial s}{\partial t}+o(\epsilon^5)=-\frac{c^2\xi^2}{2}\Delta^2\phi+o(\epsilon^5).$$

Finally we find in the leading order

$$\frac{\partial^2\phi}{\partial t^2}-c^2\Delta\phi=-\frac{\partial\phi}{\partial t}\Delta\phi-\frac{\partial(\nabla\phi)^2}{\partial t}-\nabla\cdot\left(\frac{(\nabla\phi)^2}{2}\nabla\phi\right)-\frac{c^2\xi^2}{2}\Delta^2\phi. \tag{6}$$

Equation (6) was derived in [9] and it is invariant under Galilean transformations.

Near the vortex [7] and considering the asymptotic proprieties of ρ_0^2 in the core it is possible to show that

$$\frac{\partial\Gamma}{\partial t}+\nabla\cdot(\Gamma\nabla\phi)=o(\epsilon^3). \tag{7}$$

Hence, to the lowest order, the phase satisfies a wave equation with a boundary condition in its circulation:

$$\frac{1}{c^2}\frac{\partial^2\phi}{\partial t^2}=\Delta\phi, \tag{8}$$

$$\int_{\mathcal{C}}\nabla\phi\cdot d\mathbf{l}=4\pi m\alpha, \tag{9}$$

where m is an integer, $\alpha=c\xi/\sqrt{2}$, and $\mathcal{C}$ is a circuit around the center of the vortex, i.e., the point in 2D where the field vanishes.

In the case of a moving vortex of charge m, trajectory $R(t)$ and velocity $\dot{R}(t)$ it is possible to give a formal expression of the time derivative of the solution of Eqs. (8) and (9) [10]. Introducing a branch of discontinuity and using the Green function of the wave equation, this expression reads

$$\dot{\phi}(x,t)=4\pi\alpha m\epsilon_{ij}\int_{-\infty}^{\infty}dt'\dot{R}_i(t')\frac{\partial G}{\partial x^j}[x-R(t'),t-t'], \tag{10}$$

where ϵ_{ij} is the Levi-Cività symbol ($\epsilon_{12}=1=-\epsilon_{21}$, $\epsilon_{11}=\epsilon_{22}=0$) and G is the two-dimensional Green function,

$$G(x-x',t-t')=-\frac{c\,\theta(c(t-t')-|x-x'|)}{2\pi\sqrt{c^2(t-t')^2-|x-x'|^2}}. \tag{11}$$

We remark the well-known fact (Huygens principle) that in even dimensions the Green function of the wave equation does not have a local support as it is the case in odd dimensions; this implies from formula (10) that the value of $\dot{\phi}$ at a given time depends on all the past history of the vortex. Because of this we can expect nonlocal expressions in the far field.

III. FAR FIELD

We now turn to the derivation of an expression for the field far away from the center of the moving vortex (far field). This expression will allow us to characterize the radiation emitted by a vortex describing an arbitrary trajectory. Our calculation will be done in the limit of small velocities, $v\ll c$, and we shall assume that the vortex is constrained to move in a bounded domain in which case all divergence in the integrals are avoided. As we have pointed out the NLS equation can be derived from a Lagrangian from which we can construct an energy-momentum tensor and a Poynting vector S in order to calculate the energy flux. The radiation can be expressed by

$$J=\lim_{r\to\infty}\int_0^{2\pi}S\cdot\hat{\mathbf{n}}r\,d\theta. \tag{12}$$

where S at the leading order reads $S=(\partial\phi/\partial t)\nabla\phi$ [4]. In the far-field approximation $\nabla\phi\cdot\hat{\mathbf{n}}$ can be replaced by $\dot{\phi}/c$, and therefore the only nonvanishing contributions come from terms of order $O(1/\sqrt{r})$ in the time derivative of the phase.

In order to express Eq. (10) as a function of the trajectory we can formally write

$$\dot{\phi}(x,t)=4\pi\alpha m\epsilon_{ij}\frac{\partial}{\partial x^j}\int_{-\infty}^{\infty}dt'd^2y\dot{R}_i(t')\times G(x-y,t-t')\delta(y-R(t')) \tag{13}$$

and perform the δ expansion

$$\delta(y-R)=\delta(y)-R_k\frac{\partial}{\partial y_k}\delta(y)+\frac{1}{2}R_kR_l\frac{\partial}{\partial y_k\partial y_l}\delta(y)$$
$$\times\frac{1}{3!}R_kR_lR_m\frac{\partial}{\partial y_k\partial y_l\partial y_m}\delta(y)+\cdots. \quad (14)$$

To calculate the vortex-trajectory-dependent integral in Eq. (10) we define for an arbitrary function $W:\mathbb{C}\to\mathbb{C}$ and a function $f:\mathbb{R}\to\mathbb{R}^n$ the W derivative of f by

$$W\left(\beta\frac{d}{dt}\right)f(t)=\int_{-\infty}^{\infty}\frac{d\omega}{2\pi}W(\beta i\omega)\hat{f}(\omega)e^{i\omega t} \quad (15)$$

where $\hat{f}$ is the Fourier transform of f and β an arbitrary parameter.

Replacing Eq. (14) in Eq. (13) and using the definition (15) we obtain (see Appendix A for details)

$$\dot{\phi}(x,t)=2\alpha m\epsilon_{ij}\left[\partial_j\left(K_0\left(\frac{r}{c}\frac{d}{dt}\right)\dot{R}_i\right)-\partial_{jk}\left(K_0\left(\frac{r}{c}\frac{d}{dt}\right)\dot{R}_iR_k\right)\right]$$
$$+2\alpha m\epsilon_{ij}\left[\frac{1}{2}\partial_{jkl}\left(K_0\left(\frac{r}{c}\frac{d}{dt}\right)\dot{R}_iR_kR_l\right)\right.$$
$$\left.-\frac{1}{6}\partial_{jklm}\left(K_0\left(\frac{r}{c}\frac{d}{dt}\right)\dot{R}_iR_kR_lR_m\right)\right]+\cdots, \quad (16)$$

where all trajectories are evaluated at t, $\partial_{i_1i_2\cdots i_n}=\partial^n/\partial x_{i_1}\partial x_{i_2}\cdots\partial x_{i_n}$ and $K_n(z)$ is the modified Bessel function of the second kind.

When $z\to\infty$, $K_0(z)\approx\sqrt{\pi/2z}e^{-z}$ the K_0 derivative of the first term of Eq. (16) can be evaluated as

$$K_0\left(\frac{r}{c}\frac{d}{dt}\right)\dot{R}_i(t)\approx\sqrt{\frac{\pi}{2}\frac{c}{r}}\partial_{t^{-1/2}}e^{-(r/c)d/dt}\dot{R}_i(t)+o(r^{-3/2})$$
$$=\sqrt{\frac{\pi}{2}\frac{c}{r}}\partial_{t^{-1/2}}\dot{R}_i(t_r)+o(r^{-3/2})$$

where $t_r=t-r/c$ is the retarded time. Thus the radiative contribution of the two lowest orders of Eq. (16) is explicitly given by

$$\dot{\phi}(x,t)=-\alpha m\sqrt{\frac{2\pi}{r}}\epsilon_{ij}\ c^{1/2}\hat{n}_j\partial_{t^{-1/2}}\left(\frac{R_i}{c}\right)\Bigg|_{t=t_r}$$
$$-\alpha m\sqrt{\frac{2\pi}{r}}\epsilon_{ij}\ c^{1/2}\hat{n}_j\hat{n}_k\partial_{t^{3/2}}\left(\frac{\dot{R}_iR_k}{c^2}\right)\Bigg|_{t=t_r}. \quad (17)$$

We remark the important difference between this formula (17) and the radiation formulae for moving electrons in three dimensions [11]. Here one finds that in the lowest order the field depends of the $\frac{3}{2}$-*derivative* of the vortex trajectory instead of the 2-*derivative* which appears in the 3D case [12]. We also note that all the functions are evaluated at the retarded time and the fractional derivatives that appear here put in evidence the nonlocality of the 2D Green function, i.e., one must know the whole trajectory of the vortex from $t=-\infty$ to $t=t_r$ in order to calculate Eq. (17). Now using (17) together with the expression of the flux of energy (12) yields after a straightforward calculation

$$J=\frac{2m^2\alpha^2\pi^2}{c^2}|\partial_{t^{3/2}}R|^2+\frac{2m^2\alpha^2\pi^2}{c^4}\partial_{t^{3/2}}(\dot{R}_iR_j)\partial_{t^{3/2}}(\dot{R}_kR_l)N_{ijkl}, \quad (18)$$

where $N_{ijkl}=(1/\pi)\int_0^{2\pi}\epsilon^{i\gamma}\epsilon^{k\mu}n_\gamma n_j n_\mu n_l d\theta$. This explicit formula for the radiation of a moving vortex in terms of its trajectory is one of our main results.

In the case of a single uniformly rotating vortex, $R(t)=ae^{i\omega t}$, the formula can be simplified. The term $|\partial_{t^{3/2}}R|^2$ is given by

$$|\partial_{t^{3/2}}R|^2=\int_{-\infty}^{\infty}\frac{d\omega_1}{2\pi}\frac{d\omega_2}{2\pi}(i\omega_1)^{3/2}(-i\omega_2)^{3/2}$$
$$\times\hat{R}(\omega_1)\hat{R}^*(\omega_2)e^{it_r(\omega_1-\omega_2)}$$
$$=\int_{-\infty}^{\infty}\frac{d\omega_1}{2\pi}\frac{d\omega_2}{2\pi}(i\omega_1)^{3/2}(-i\omega_2)^{3/2}(a2\pi)^2e^{it_r(\omega_1-\omega_2)}$$
$$\times\delta(\omega_1-\omega)\delta(\omega_2-\omega)=a^2\omega^3,$$

and therefore the lower-order term of Eq. (18) reads

$$J=\frac{2m^2\alpha^2\pi^2}{c^2}a^2\omega^3=m^2\pi^2c^2\xi^2M^2\omega, \quad (19)$$

where we have reintroduced c and ξ and defined the Mach number $M=a\omega/c$.

We shall apply now this result to the case of two rotating vortices, separated by a distance $2a$, with the same unitary charge ($m=1$). It is well known that in the incompressible approximation the vortices will rotate in a perfect circle one around the other with a frequency $\omega=\alpha/a^2$. For two vortices the total far field produced is just the superposition of the field produced by each one, taking into account their charges which here are equal. In the case of two rotating vortices their trajectories are symmetric and then the odd power of R in Eq. (16) vanishes. Hence we get to the lowest order

$$\dot{\phi}(x,t)=-4\alpha\epsilon_{ij}\partial_{jk}\left(K_0\left(\frac{r}{c}\frac{d}{dt}\right)\dot{R}_iR_k\right)$$
$$=2\alpha a^2\omega\mathrm{Re}$$
$$\times\left\{e^{i2\omega(t-\theta)}\left[\frac{4\omega^2}{c^2}K_0''\left(i\frac{2\omega}{c}r\right)+i\frac{2\omega}{cr}K_0'\left(i\frac{2\omega}{c}r\right)\right]\right\}. \quad (20)$$

Note that the wavelength $\lambda=2\pi c/\omega$ of waves emitted by the vortex appears explicitly in formula (20) and the incompressible limit $a\ll r\ll\lambda$ is easily obtained using the asymptotic of $K_0(z)$ for small z (see Appendix A). It reads

$$\dot{\phi}=-8\alpha\omega\frac{a^2}{r^2}\cos 2(\omega t-\theta) \quad (21)$$

which is the well-known first order of the multipolar expansion [7,8]. The next orders can be obtained similarly.

The radiative far field is obtained in the limit $a\ll\lambda\ll r$ and yields, using Eq. (12), the energy lost due to radiation,

$$J = 16\pi^2\alpha^2\frac{a^4\omega^4}{c^4}\omega = 8\pi^2c^2\xi^2M^4\omega. \tag{22}$$

Note that this energy flux is very small. If we now make an energy balance between the radiated energy J and the variation of energy due to a change in the distance between the vortex, we can obtain a simple equation for the radius a. At lowest order the energy is simply $\mathcal{E}=\frac{1}{2}\int dx(\nabla\phi)^2$. For two vortices separated a distance $2a$ the interaction part of the energy, after some algebra, reads [7,8]

$$\mathcal{E}_{\text{int}} = -4\pi c^2\xi^2\ln 2a. \tag{23}$$

Thus $d\mathcal{E}_{\text{int}}/dt=-J$ leads to an evolution equation for the radius:

$$\frac{da}{dt} = \frac{\pi c\xi^5}{2\sqrt{2}}\frac{1}{a^5}. \tag{24}$$

From this equation we obtain the law $a(t)=[a_0^6+(3\pi/\sqrt{2})\xi^5ct]^{1/6}$ which shows that the vortex distance increases, but very slowly. This result was obtained in 1966 by Klyatskin [8] using a matching between a compressible, but vortex independent far field and an incompressible near field. Note that there are some misprints in the literature [7,8] which lead to erroneous values of prefactor in formula (24); see [15] for details.

Because of the very simple form of the terms in development (16) one can get $\dot{\phi}$ explicitly at any order in M. This explicit series reads (see Appendix B):

$$\dot{\phi}(x,t) = \sum_{n=1}^{\infty}\dot{\phi}_{M^{2n}}M^{2n} \tag{25}$$

with

$$\dot{\phi}_{M^{2n}}(x,t) = -4\alpha\sqrt{\frac{\pi c\omega}{r}}\frac{1}{(2n-1)!}\sum_{l=0}^{n}\binom{2n}{l}(n-l)^{2n-1/2} \times\cos\left[2(n-l)(\theta-\omega t_r)+\frac{\pi}{2}\left(2n-\frac{1}{2}\right)\right] \tag{26}$$

and it follows that the total radiated power can be expanded as

$$J = 16\pi^2\alpha^2\omega\sum_{n=1}^{\infty}\sum_{m=1}^{\infty}\frac{(-M^2)^{n+m}}{(2n-1)!(2m-1)!}\sum_{l=0}^{n}\binom{2n}{l}\binom{2m}{l+m-n} \times(n-l)^{2(n+m)-1} \tag{27}$$

$$= 16\pi^2\alpha^2M^4\omega\left(1-\frac{4M^2}{3}+\frac{17M^4}{4}-\frac{157M^6}{18} + \frac{91783M^8}{4320}-\cdots\right). \tag{28}$$

This series has a finite radius of convergence equal to $M_c=0.667$; hence we can expect that radiation effects in the NLSE will be well described by (28) only for lower values of M.

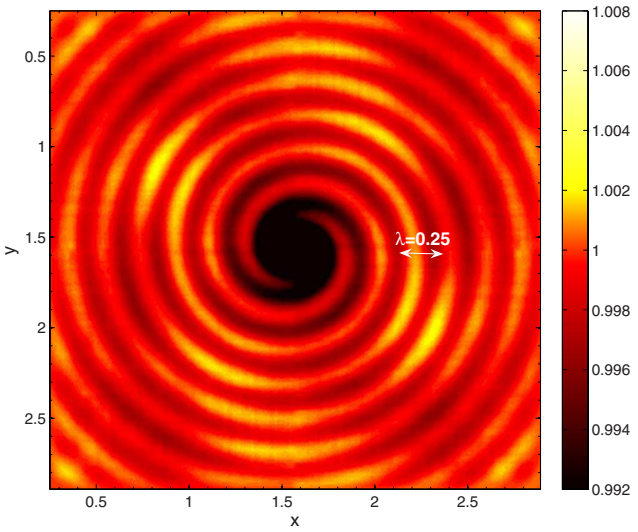

FIG. 1. (Color online) Radiation of a vortex pair with an initial separation of $2a=2.53\xi$ ($M=0.56$, $\lambda=0.2493$). Run of NLSE with absorbing boundaries (see below) using 512^2 Fourier modes.

IV. NUMERICAL DETERMINATION OF RADIATION AND VORTEX TRAJECTORIES

To numerically the integrate NLSE, we will use using standard [13] pseudospectral methods. In order to work with complex periodic fields (which must have zero total topological charge) we place the two rotating vortices within a box of mirror symmetries. Equation (1) is solved numerically using pseudospectral methods that were specially tailored to the mirror symmetries of the initial data in order to gain on both computer time and central memory storage. The corresponding Fourier pseudospectral algorithms are described in detail in Ref. [4].

The 2π-periodic fields are symmetric by reflection on the lines $x=0,\pi$ and $y=0,\pi$ that constitute the boundaries of the so-called impermeable box. We prepare an initial condition by letting a charge-2 vortex, situated at the center of the impermeable box, evolve under the Ginzburg-Landau real (GLR) dynamics [which can be easily obtained from Eq. (1) by performing a Wick rotation $\tau=it$]. The vortex then splits into two single-charge vortices and the GLR dynamics is continued until they reach a distance $2a$ (see Ref. [4] for details). These initial data are then evolved under NLS dynamics (1). The physical parameters are $c=0.0625$, $\xi=0.0177$, 0.0089, 0.0044, 0.0022, and $512^2,1024^2,2048^2,4096^2$ Fourier modes are used, respectively.

A typical result with 512^2 Fourier modes is shown on Fig. 1, where we plot the density $\rho=|\psi|^2$ and emitted waves can be clearly observed. Note that the wavelength $\lambda=c2\pi/\omega=0.2493$ is illustrated by a double arrow.

The vortex trajectories are determined by the following procedure. First a rough location is found by seeking the grid point with minimum density ρ. In a second step Newton iterations are used in order to determine the precise location of the vortex by solving the equation $\psi(x)=0$. A typical vortex trajectory obtained in this way, with an initial separation

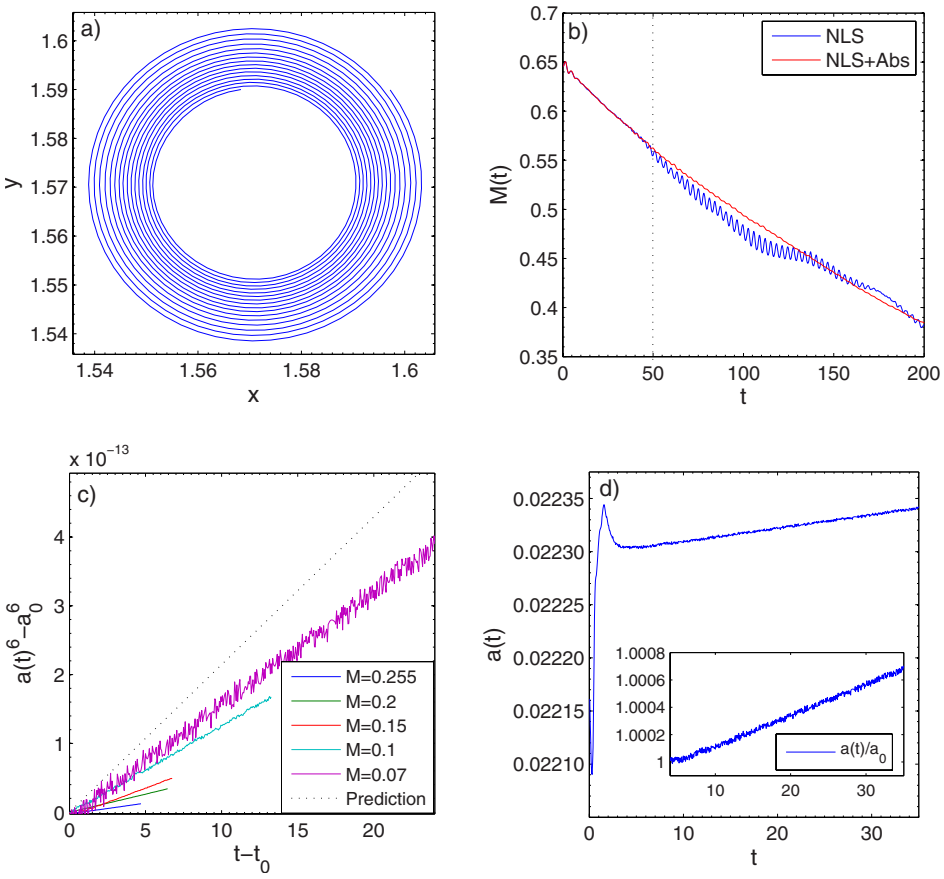

FIG. 2. (Color online) (a) Vortex trajectory with an initial separation of $2a=2.18\xi$. (b) Temporal evolution of Mach number with and without absorbing boundaries. Initial separation of $2a=2.18\xi$. (c) Temporal evolution of $a(t)^6-a_0$ for different Mach numbers. (d) Temporal evolution of $a(t)$ with Mach number $M=0.077$. Inset: Temporal evolution of $a(t)/a_0$ after the transient. (a) and (b) use 512^2 Fourier modes and (d) and (c) 4096^2.

of $2a=2.18\xi$, is plotted on Fig. 2(a). It is apparent on the figure that the vortex follows a spiral trajectory, with a very weak increase of its radius at each turn.

There are two natural time scales in the problem. The first one corresponds to the transient adaptation to the initial condition and it is of the order of the time for the wave coming from one vortex to travel to the other. Thus, an inferior bound is $t_{\rm tr}=2a/c$ depending on the original separation $2a$. The second time scale corresponds to the time taken by the waves produced by the vortices placed in neighbor impermeable cells to arrive at another cell. It can easily be estimated as $t_w=\pi/c$. In the present numerical calculations these values are $t_{\rm tr}=0.5-5$ and $t_w=50$. The temporal evolution of the Mach number $M=a\omega/c$ is plotted in Fig. 2(b); note that the transient time $t_{\rm tr}$ and the arrival of waves at $t_w=50$ (vertical dashed line) are clearly observed.

During the transient time the vortices emit a large amount of sound that significantly perturbs the vortex trajectories when it arrives at the neighbor cells, as can be seen in Fig. 2(b). In order to isolate the vortex we added absorption in the border of the cell, performing a modified GLR step between each NLS step. The GLR modified step consists in the GLR equation with the right-hand side modulated by a function that is null almost everywhere except near the border. The results of absorption are also shown in Fig. 2(b). Note that oscillations are effectively reduced without significant modification of the vortex trajectories before t_w.

In Fig. 2(c) the radius as a function of time is displayed for different initial conditions. Note that the slope increases when the Mach number M diminishes, as well as the oscillations.

Figure 2(d) displays the temporal evolution of the radius corresponding to the run with the smallest Mach number. Note that the total increase of the radius after the transient time is less than 0.08% [see inset in Fig. 2(d)]. This explains the large fluctuation in the corresponding curve in Fig. 2(c).

We now turn to the comparison of the results of the numerical integrations of the NLSE with the theoretical prediction (24). To wit, we measure the relative variation of M in a fraction β of turns of the vortex pair for each trajectory (obtained with different ξ and resolutions). This turnover time is simply $T=2\pi/\omega=2\pi\sqrt{2}a^2/c\xi$ and from the theoretical prediction (24) it follows that

$$M(\beta T)=M_0[1+24\beta\pi^2M_0^4]^{-1/6}\approx M_0(1-4\beta\pi^2M_0^4) \tag{29}$$

for M small. Note that the Mach numbers can be expressed directly using ξ and a by $M=\xi/\sqrt{2}a$.

Each initial condition obtained using GLR dynamics is evolved under the NLSE for more than a turn of the vortices. The mean value of $[1-M(\beta T)/M_0]/(4\beta\pi^2M_0^4)$ (over the NLS evolution) for different values of Mach number and resolutions is plotted in Fig. 3 The value of β is always between $1/8$ and 1. It is chosen in each case in order to obtain clear data.

The error bars shown for small Mach number in Fig. 3 are produced by the oscillation of the trajectories [see Fig. 2(c)].

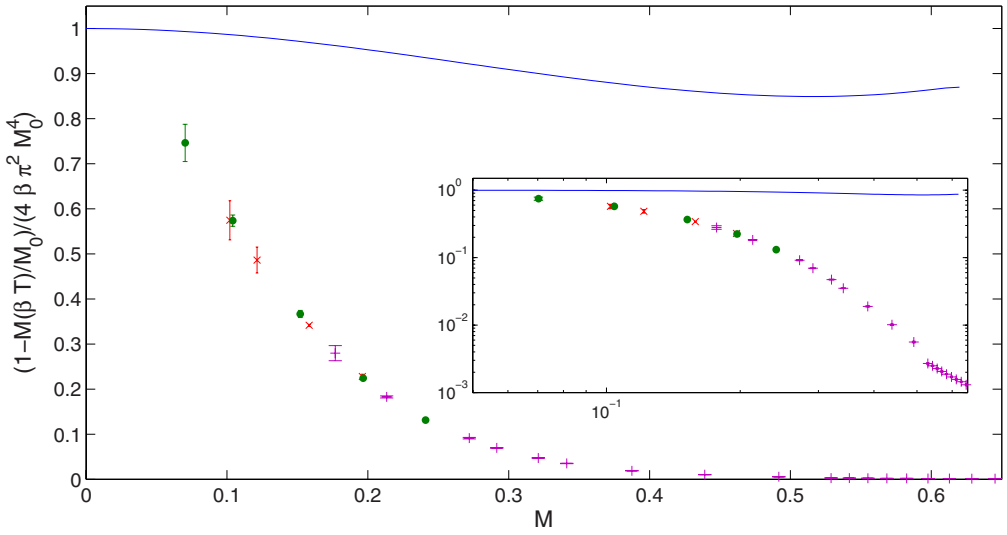

FIG. 3. (Color online) Relative variation of $[1-M(\beta T)/M_0]/(4\beta\pi^2 M_0^4)$ as a function of M. Solid line is the theoretical prediction (28), with limit 1 for $M\to 0$. Inset: same plot in log-log scale. Runs with 4096^2 (●), 2048^2, (×), and 1024^2 (+) Fourier modes.

These errors can be reduced by taking lower values of ξ at constant M, but the resolution must then be increased in order to well resolve the vortex. Thus, with a fixed resolution it is impossible to go to arbitrarily lows values of the Mach number. However, using up to 4096^2 Fourier modes, the values seem to approach well the theoretical prediction as the Mach number decreases, as is apparent in the inset of Fig. 3. On the other hand, for the computed intermediate values of M, the data are not in good agreement, even when using the high orders in M of the series (28). It is clear that at these intermediate Mach numbers the dispersive effects of the NLSE, which were not taken into account in our computation, become relevant.

V. CONCLUSION

Our main result for the radiation far field directly expressed in terms of vortex motion [Eqs. (25)–(28)] was validated by comparison with the result of numerical simulations of the NLS equation in a simple test case. The numerical data showed that the relative variation of $\Delta M/M^4$ in a fraction of turns is below the theoretical prediction at intermediate values of M. However, the data also display a clear tendency for $\Delta M/M^4$ to increase in the small Mach number limit, in a way that seems consistent with reaching the theoretical value.

ACKNOWLEDGMENTS

We acknowledge support from an ECOS/CONICYT action and one of the authors (E.T.) is grateful to the Project ACT 15 of CONICYT, Chile. The computations were carried out at IDRIS (CNRS).

APPENDIX A: FAR-FIELD CALCULATION

Formulas (13) and (14) are concerned with integrals of the type

$$\int_{-\infty}^{\infty} dt' f(t')G(x,t-t') = \int_{-\infty}^{\infty} dt' \int_{-\infty}^{\infty} \frac{d\omega}{2\pi}\hat{f}(\omega)e^{i\omega t'}G(x,t-t') = \int_{-\infty}^{\infty} \frac{d\omega}{2\pi}\hat{f}(\omega)\frac{e^{i\omega t}}{2\pi}K_0\left(i\frac{r\omega}{c}\right),$$

where $K_n(z)$ is the modified Bessel function of the second kind [14]. We can use the K_0 derivative in order to give a formal expression; hence

$$\int_{-\infty}^{\infty} dt' f(t')G(x,t-t') = \frac{1}{2\pi}K_0\left(\frac{r}{c}\frac{d}{dt}\right)f(t). \tag{A1}$$

In the last expression, the function K_0 is understood as a functional operator applied in Fourier space. We now use the series expansion around $z=\infty$ of the function K_0,

$$K_0(z) = \sqrt{\frac{\pi}{2}}e^{-z}\left(z^{-1/2} - \frac{1}{8}z^{-3/2} + \frac{9}{128}z^{-5/2} + o(z^{-7/2})\right),$$

and the fractional derivative Eq. (A1), becomes

$$K_0\left(\frac{r}{c}\frac{d}{dt}\right)f(t) = \sqrt{\frac{\pi}{2}}\left[\left(\frac{r}{c}\right)^{-1/2}\partial_{s^{-1/2}}f - \frac{1}{8}\left(\frac{r}{c}\right)^{-3/2}\partial_{s^{-3/2}}f + \frac{9}{128}\left(\frac{r}{c}\right)^{-5/2}\partial_{s^{-5/2}}f + \cdots\right]\Bigg|_{t_r}, \tag{A2}$$

where $t_r=t-r/c$. Formula (16) is directly obtained by replacing Eq. (14) in Eq. (13), using Eqs. (A1) and (A2) and noting that $\partial G/\partial y_k = -\partial G/\partial x_k$.

In order to get the multipolar expansion we write the series expansion of $K_0(z)$ for $z\approx 0$:

$$K_0(z) \approx -\ln(z) + \ln(2) - \gamma_E + \frac{1}{4}[-\ln(z) + \ln(2) - \gamma_E + 1]z^2 + o(z^4) \tag{A3}$$

with $\gamma_E = 0.572\,215\,6\ldots$ the Euler-Mascheroni constant. The multipolar expression (21) follows directly from Eqs. (20) and (A3).

APPENDIX B: SERIES EXPANSION

In this appendix we compute the series (25). Let n be an even number; from Eq. (13) it is apparent that the contribution of order M^n to the series is coming from the term

$$\dot{\phi}_{M^n} M^n = \frac{4\alpha \epsilon_{j_0 j_1}}{(n-1)!} \partial_{j_0 j_2 \ldots j_n} \left(K_0\left(\frac{r}{c}\frac{d}{dt}\right) \dot{R}_{j_1} R_{j_2} \cdots R_{j_n} \right)$$
$$= \frac{4\alpha}{c^n (n-1)!} \sqrt{\frac{\pi c}{2r}} \epsilon_{j_0 j_1} \hat{n}_{j_0} \hat{n}_{j_2} \cdots \hat{n}_{j_n} \times \partial_{t^{n-1/2}} (\dot{R}_{j_1} R_{j_2} \cdots R_{j_n}), \tag{B1}$$

where we have used that, in the radiative limit,

$$K_0\left(\frac{r}{c}\frac{d}{dt}\right) f(t) = \sqrt{\frac{\pi c}{2r}}\, \partial_{s^{-1/2}} f(s)|_{s=t_r}$$

and thus $\partial_{j_k} = -\hat{n}_{j_k} c^{-1} \partial_t$.

Let $\Gamma_k \in \mathbb{C}$ be such that $R_k = \mathrm{Re}(\Gamma_k e^{i\omega t})$; then

$$\dot{R}_{j_1} R_{j_2} \cdots R_{j_n} = \frac{1}{2^n} (i\omega \Gamma_{j_1} e^{i\omega t} - i\omega \bar{\Gamma}_{j_1} e^{-i\omega t})(\Gamma_{j_2} e^{i\omega t} + \bar{\Gamma}_{j_2} e^{-i\omega t}) \cdots (\Gamma_{j_n} e^{i\omega t} + \bar{\Gamma}_{j_n} e^{-i\omega t}),$$

$$\begin{aligned}
\dot{R}_{j_1} R_{j_2} \cdots R_{j_n} = {} & \frac{\omega}{2^n} (i\Gamma_{j_1} \Gamma_{j_2} \cdots \Gamma_{j_n} e^{in\omega t} + \text{c.c.}) \\
& + \frac{\omega}{2^n} (-i\bar{\Gamma}_{j_1} \Gamma_{j_2} \cdots \Gamma_{j_n} e^{i(n-2)\omega t} + i\Gamma_{j_1} \bar{\Gamma}_{j_2} \cdots \Gamma_{j_n} e^{i(n-2)\omega t} + \cdots + i\Gamma_{j_1} \Gamma_{j_2} \cdots \bar{\Gamma}_{j_n} e^{i(n-2)\omega t} + \text{c.c.}) \\
& + \frac{\omega}{2^n} (-i\bar{\Gamma}_{j_1} \bar{\Gamma}_{j_2} \cdots \Gamma_{j_n} e^{i(n-4)\omega t} + i\Gamma_{j_1} \bar{\Gamma}_{j_2} \bar{\Gamma}_{j_3} \cdots \Gamma_{j_n} e^{i(n-4)\omega t} + \cdots + i\Gamma_{j_1} \Gamma_{j_2} \cdots \bar{\Gamma}_{j_{n-1}} \bar{\Gamma}_{j_n} e^{i(n-4)\omega t} + \text{c.c.}) + \cdots \\
& + \frac{\omega}{2^n} (-i\bar{\Gamma}_{j_1} \bar{\Gamma}_{j_2} \cdots \bar{\Gamma}_{j_{n/2}} \Gamma_{j_{n/2+1}} \cdots \Gamma_{j_n} e^{i(n-2n/2)\omega t} + \cdots + \text{c.c.}).
\end{aligned} \tag{B2}$$

We can directly check that

$$-\epsilon_{j_0 j_1} \hat{n}_{j_0} \bar{\Gamma}_{j_1} \hat{n}_{j_2} \Gamma_{j_2} = \epsilon_{j_0 j_1} \hat{n}_{j_0} \Gamma_{j_1} \hat{n}_{j_2} \bar{\Gamma}_{j_2},$$

$$\epsilon_{j_0 j_1} \hat{n}_{j_0} \Gamma_{j_1} = iae^{-i\theta},$$

$$\hat{n}_j \Gamma_j = ae^{-i\theta},$$

$$\hat{n}_j \bar{\Gamma}_j = ae^{i\theta},$$

and thus each term inside each parenthesis in the right-hand side of Eq. (B2) has the same value. We see in (B2) that the contribution with the frequency $(n-2l)\omega$ has l terms (of the total of n) with Γ conjugate and thus $\binom{n}{l}$ ways of choosing them. Hence

$$\epsilon_{j_0 j_1} \hat{n}_{j_0} \cdots \hat{n}_{j_n} \dot{R}_{j_1} R_{j_2} \cdots R_{j_n} = -\frac{\omega a^n}{2^{n-1}} \mathrm{Re}\left[\binom{n}{0} e^{in(\omega t_r - \theta)} + \binom{n}{1} e^{i(n-2)(\omega t_r - \theta)} + \cdots + \binom{n}{\frac{n}{2}} e^{i(n-2n/2)(\omega t_r - \theta)} \right] \tag{B3}$$

$$= -\frac{\omega a^n}{2^{n-1}} \sum_{l=0}^{n/2} \binom{n}{l} \mathrm{Re}(e^{i(n-2l)(\omega t_r - \theta)}). \tag{B4}$$

From (B1) we obtain

$$\dot{\phi}_{M^n} M^n = 4\alpha \sqrt{\frac{\pi c}{2r}} \frac{\omega a^n}{2^{n-1}(n-1)!} \sum_{l=0}^{n/2} \binom{n}{l} \partial_t^{n-1/2} \mathrm{Re}(e^{i(n-2l)(\omega t_r - \theta)})$$

$$= 4\alpha \sqrt{\frac{\pi\omega c}{2r}} \left(\frac{a\omega}{c}\right)^n \frac{1}{2^{n-1}(n-1)!} \sum_{l=0}^{n/2} \binom{n}{l} (n-2l)^{n-1/2} \mathrm{Re}(i^{n-1/2} e^{i(n-2l)(\omega t_r - \theta)}) \tag{B5}$$

and finally formula (25) follows directly.

The total radiated power (28) is easily obtained by noting that

$$\int_0^{2\theta} d\theta \cos\left[(n-2l)(\omega t_r - \theta) + \frac{\pi}{2}\left(n - \frac{1}{2}\right)\right] \cos\left[(m-2k)(\omega t_r - \theta) + \frac{\pi}{2}\left(m - \frac{1}{2}\right)\right] = \pi \delta_{n-m,2l-2k} \cos\frac{\pi}{2}(n-m)$$

for all n,m,l,k integer.

[1] M. Abid, C. Huepe, S. Metens, C. T. Pham, L. S. Tuckerman, and M. Brachet, Fluid Dyn. Res. **33**, 509 (2003).

[2] M. Abid, M. Brachet, J. Maurer, C. Nore, and P. Tabeling, Eur. J. Mech. B/Fluids **17**, 665 (1998).

[3] C. Nore, M. Abid, and M. E. Brachet, Phys. Rev. Lett. **78**, 3896 (1997).

[4] C. Nore, M. Abid, and M. Brachet, Phys. Fluids **9**, 2644 (1997).

[5] S. Ogawa, M. Tsubota, and Y. Hattori, J. Phys. Soc. Jpn. **73**, 813 (2002).

[6] M. Leadbeater, T. Winiecki, D. C. Samuels, C. F. Barenghi, and C. S. Adams, Phys. Rev. Lett. **86**, 1410 (2001).

[7] R. M. Pismen, *Vortices in Nonlinear Fields* (Clarendon Press, Oxford, 1999).

[8] V. I. Klyatskin, Izv. Akad. Nauk SSSR, Mekh. Zhidk. Gaza **6**, 87 (1966).

[9] C. Nore, M.-E. Brachet, and S. Fauve, Physica D **65**, 154 (1993).

[10] F. Lund, Phys. Fluids A **1**, 1521 (1989).

[11] M.-E. Brachet and E. Tirapegui, Nuovo Cimento Soc. Ital. Fis., A **47**, 210 (1978).

[12] J. S. Schwinger, L. L. DeRaad, Jr., K. A. Milton, and W.-Y. Tsai, in *Classical Electrodynamics*, edited by J. S. Schwinger (Perseus Books, Cambridge, MA, 1998).

[13] D. Gottlieb and S. A. Orszag, *Numerical Analysis of Spectral Methods* (SIAM, Philadelphia, 1977).

[14] E. T. Whittaker and G. N. Watson, *A Course of Modern Analysis* (University Press, Cambridge, U.K., 2000).

[15] There are several misprints in the principal references of the literature [7,8] that need to be clarified in order to check that our prefactor in formula (24) is indeed correct. First, in Klyatskin [8], formula (2.11) uses the same definition of the energy as we do: $\mathcal{E}=(1/2)\int dx(\nabla\phi)^2$, but, in formula (2.12), the vortex interaction energy is two times greater than in our formula (23). This leads to a difference in a factor 1/2 from our Eq. (24) for the radius a. Second, in Pismen [7], Chap. 4, formula (4.26), the definition of the total energy is $\mathcal{E}=(1/8)\int dx(\nabla\phi)^2$, leading to a vortex interaction energy $\mathcal{E}_{\mathrm{int}}=-\pi c^2\xi^2 \ln 2a$ that is consistent with our formula (23). However, the energy flux used in [7], Chap. 4, formula (4.48) is not consistent with this definition of the interaction energy [furthermore, a factor π is also missing in formula (4.50) for J] leading to a difference of a factor $\pi/8$ from our Eq. (24) for the radius a.

8. CONCLUSIONS

In this thesis we have studied several different Fourier Galerkin-truncated conservative systems. We showed that, in a very general way, the systems relax toward the equilibrium with a rich and interesting transient. The thermalized small scales acts as thermostats generating a pseudo-dissipation at large scales.

Because of this pseudo-dissipation a Kolmogorov regime can be observed in the truncated Euler equation. This fact motivated study of the effective viscosity in the truncated Euler equation. We were able to propose a phenomenological two-fluid model of the truncated Euler equation our treatment of helical flows allowed us to observe a mixed energy and helicity cascade, followed by a Kraichnan helical absolute equilibrium. Using our previously determined eddy-viscosity we showed that the large scales of the truncated Euler flows quantitatively behave as an effective Navier-Stoke equation with a time and scale dependent viscosity.

We thus turned to the study of the $2D$ truncated Euler equation. The main difference with the $3d$ case is the presence of a direct cascade of enstrophy. This quantity plays the role of the energy in $3D$, thermalizing in equipartition at large wave-number and yielding a k^{-1} law in the inertial zone. A remarkable difference with the $3D$ situation is the absence of a dissipative zone that is probably due to a vanishing $2D$ eddy viscosity.

We the extended our study to the magnetohydrodynamic case. Similar to the $3d$ case of non magnetic flows, the direct cascade of energy leads to an energy equipartition at large wave-number. An Iroshnikov-Kraichnan $k^{-3/2}$-spectrum was observed in the inertial zone. When a strong magnetic field is applied, the Alfvén waves slowdown the nonlinear interactions and an apparent bottleneck appears in an intermediate zone before the equipartition range extends to the smallest scales. This is an interesting result because the partial thermalization zone appears while the spectral convergence is still ensured. The different scaling-laws present in the energy spectra strongly suggest to reproduce in the future, with higher resolutions, the simulations involving a strong constant magnetic field in order determine the different exponents.

We then decided to study the case of the compressible truncated Euler flows. A new algorithm allowing the construction of absolute equilibrium of spectrally truncated compressible flows was introduced. The algorithm used stochastic processes based on the Clebsch representation of the velocity field to generate density and velocity fields that followed by construction the absolute equilibrium stationary probability. This algorithm was posteriorly adapted to the truncated Gross-Pitaevskii equation.

Some preliminary results were obtained that strongly suggested the existence of

second sound waves in the compressible truncated Euler equation and TGPE dynamics. However, it was is not possible to distinguish the effect from a ballistic propagation. Note that it is not possible to increase the temperature in the compressible truncated Euler equation without changing the equation of state. The TGPE thus seems to to be a good system to look for second sound in a future detailed study. A better configuration could be obtained by studying at higher resolution (larger than 128^3) the heat propagation of a hot spot. We will perform in the future a parametric study in such a configuration by varying the temperature and the amount of dispersion of the system controlled by the value of $\xi k_{\max}$.

The second part of this thesis was devoted to the Gross-Pitaevskii equation. We studied the sound emission produced by the interaction of several vortices in a 2-d homogenous system. We obtained analytics predictions for the power radiated by moving vortices and found that the numerical simulations that we performed at very high resolution gave support to the estimate of radiation.

Studying the truncated Gross-Pitaevskii equation (TGPE) we found several astonishing results. To obtain the absolute equilibrium of this equation we introduced a stochastically forced Ginzburg-Landau equation (SGLE), that very efficiently allowed to perform temperature scans. We explicitly showed that the condensation transition observed in references [29, 30, 31] corresponds to a standard second-order transition described by the $\lambda - \phi^4$ theory.

We also showed that the thermodynamical equilibrium can be achieved by a direct energy cascade, in a way similar to Cichowlas et al.[5], but with a thermalization of sound waves at small scales, accompanied by vortex annihilation as a prelude to final thermalization. An amazing result was observed increasing the amount of dispersion of the system. A slowdown of the energy transfer was produced inducing a partial thermalization independently of the truncation wavenumber. This was the second example of a partial thermalization within the frame of a PDE reported in this thesis.

Using the SGLE in the presence of a counterflow we discovered interesting properties present in the TGPE dynamics. The counterflow can avoid and reverse the contraction of vortex ring due to mutual friction reported by Berloff and Svistunov [32]. We also observed that when the counterflow pass trough a crystal pattern it induces a collective movement in the crystal. This allowed us to directly measure the mutual friction coefficient related to the transverse force. An astonishing result was found by immersing a vortex ring in a thermic bath: a strong dependence on the temperature of the translational velocity was observed. This effect was a order of magnitude above the transverse mutual friction effect measured in the perfect crystal. We related this to the anomalous translational velocity due to finite amplitude Kelvin waves in vortex rings reported by Kiknadze and Mamaladze [33] and Barenghi et al [34]. By assuming equipartition of the energy of the Kelvin waves with the heat bath we obtained a good estimate of the observed effect and we gave a quantitative prediction for the thermal slowdown of vortex rings in He^4.

When counterflow is aligned to an ordered vortex arrays it can induce an instability called Donnelly-Glaberson. This instability was observed experimentally by Swanson

et al [106] in 1983 and numerical simulations based on Bio-Savart law performed by Tsubota et al. [107] allowed to obtain a physical visualization of the instability. We will attempt in the future to study this instability in the context of TGPE.

We thus showed that the TGPE appears as minimal model of superfluidity at finite temperature, where counterflows and mutual friction effects are naturally present. Because of the experimental technics has were recently developed allowing the visualization of vortex structures in superfluid He^4 by following solid hydrogen particles [108, 109], more and more pictures coming from experiments will be available in the future that could be confronted with visualization form TGPE and vice-versa.

APPENDIX

A. ACOUSTIC PROPAGATION OF TRUNCATED GROSS-PITAEVSKII EQUATION: A SIMPLE TWO-FLUID MODEL DERIVATION

In this appendix we derive a set of acoustic equations for the TGPE based on the Landau two-fluid model of He^4 [54] and the extended thermodynamics relations of section IIB of the article [38] presented in chapter 6. This derivation has an academical character because dissipative effects are neglected. To obtain a more realistic description a kinetic description of TGPE should be used.

The present calculations allows to overpass the difficulty that the well known formula for the second sound velocity u_2 of He^4 at $T = 0$ given by

$$u_2 = \sqrt{\frac{Ts^2\rho_s}{c_p\rho}}, \tag{A.1}$$

where s is the entropy per unit mass, becomes meaningless in a classical system because the absolute value of s is not defined.

The starting point is the conservation relations (6.7), (6.8), (6.9) and the Galileo transformation relations (6.15) - (6.20). We consider a constant number of modes $\mathcal{N}$. We also assume that the vectors $\mathbf{v}_s$ and $\mathbf{P}$ are small quantities and that all the thermodynamics quantities depend slowly on space, by a small perturbation around to an homogeneous state where a local thermodynamical equilibrium is supposed to be instantly established.

As usual in hydrodynamics, we will consider the energy and momentum per unit of volume and the chemical potential per unit of mass. Keeping the same notation with the new units the thermodynamical relation (26) of [38] in chapter 6 ($H \equiv E$, $dV = 0$ and $d\mathcal{N} = 0$) becomes

$$dE = Td(\rho s) + \mu d\rho + \mathbf{W} \cdot d\mathbf{P}, \tag{A.2}$$

where $S = V\rho s$ is the total entropy .

In the acoustic regime the conservation equations (6.7), (6.8) and the Galilean transformation relations (6.15) - (6.20) simplifies to

$$\frac{\partial \rho}{\partial t} = -\nabla \cdot \mathbf{P} \qquad \text{(A.3)} \qquad\qquad \frac{\partial \mathbf{P}}{\partial t} = -\nabla p \qquad \text{(A.6)}$$

$$\frac{\partial H}{\partial t} = -\nabla \cdot \mathbf{Q} \qquad \text{(A.4)} \qquad\qquad H = H_0 \qquad \text{(A.7)}$$

$$\mathbf{P} = \rho \mathbf{v}_\mathrm{s} + \mathbf{P}_0 \qquad \text{(A.5)} \qquad\qquad \mathbf{Q} = (H_0 + p)\mathbf{v}_\mathrm{s} + \mathbf{Q}_0 \qquad \text{(A.8)}$$

where the subindex 0 denotes that the quantities are evaluated in the referential where $\mathbf{v}_\mathrm{s} = 0$ and we implicitly assume that terms multiplying small quantities do not depend on space.

Equations (A.3-A.8) must be supplied with an equation for the superfluid velocity $\mathbf{v}_\mathrm{s}$. To wit, observe that the Bernoulli eq.(6.6) can be rewritten as

$$\frac{\partial \phi}{\partial t} = -\frac{\delta H}{\delta \rho}. \qquad \text{(A.9)}$$

First identify $\mathbf{v}_\mathrm{s} = \nabla \bar{\phi}$, where the bar stands for an ensemble average. Then, for adiabatic compressions [84] we have $\overline{\frac{\delta H}{\delta \rho}} = \left.\frac{\partial E}{\partial \rho}\right|_S$. Finally, from the thermodynamic relation (A.2) we obtain the equation

$$\frac{\partial \mathbf{v}_\mathrm{s}}{\partial t} = -\nabla \mu, \qquad \text{(A.10)}$$

just as in the Landau two-fluid model.

The link between the Landau two-fluid model and eqs.(A.3-A.10) is evident using the identifications

$$\rho = \rho_\mathrm{n} + \rho_\mathrm{s} \qquad \text{(A.11)}$$

$$\mathbf{P}_0 = \rho_\mathrm{n} (\mathbf{v}_\mathrm{n} - \mathbf{v}_\mathrm{s}) \qquad \text{(A.12)}$$

The next step is be able from the conservation equations and the thermodynamical relations to obtain the *fountain effect*. Combining the thermodynamic relations of the Gibbs potentials G and dG (equations (27) and (30) of [38] in chapter 6) we obtain

$$\rho d\mu + \frac{\mathcal{N}}{V} d\lambda_\mathcal{N} = dp - \rho s dT - \mathbf{P} \cdot d\mathbf{W}, \qquad \text{(A.13)}$$

where $S = V \rho s$. Assuming local thermodynamical equilibrium we obtain at the leading order

$$\rho \nabla \mu = \nabla p - s\rho \nabla T - \frac{\mathcal{N}}{V} \nabla \lambda_\mathcal{N}. \qquad \text{(A.14)}$$

Replacing ∇p and $\nabla \mu$ by Eqs. (A.6) and (A.10) and the momentum $\mathbf{P}$ by Eq. (A.5) and (A.12) we obtain

$$\frac{\partial \mathbf{P}_0}{\partial t} = -s\rho \nabla T - \frac{\mathcal{N}}{V} \nabla \lambda_\mathcal{N}. \qquad \text{(A.15)}$$

Defining

$$\tilde{\lambda}_{\mathcal{N}} = \frac{\lambda_{\mathcal{N}}}{T}\,, \quad s_{\text{eff}} = s + \frac{\mathcal{N}}{\rho V}\tilde{\lambda}_{\mathcal{N}} \tag{A.16}$$

equation (A.15) becomes

$$\frac{\partial \mathbf{P}_0}{\partial t} = -s_{\text{eff}}\rho\nabla T - \frac{\mathcal{N}}{V}\nabla\tilde{\lambda}_{\mathcal{N}}. \tag{A.17}$$

Note that Eq.(A.17) is well defined because s_{eff} and $\nabla\tilde{\lambda}_{\mathcal{N}}$ are uniquely determined (see the discussion at the end of sections IIB and IIIB in [38] in chapter 6). This equation is analogous to the corresponding one of Landau two-fluid model [54] (see section A.2 below).

Using definitions (A.16), the thermodynamic relation (38) of [38] in chapter 6 expressed per unit of volume reads at leading order

$$H + p - \mu\rho = T\rho\, s_{\text{eff}}. \tag{A.18}$$

To obtain an equation describing the *thermomechanical effect* we will first find an equation for the entropy flux. Using the thermodynamical relation (A.2) the energy conservation relation (A.4) and Eq.(A.8), we find at leading order reads

$$\frac{\partial H}{\partial t} = T\frac{\partial(\rho s)}{\partial t} + \mu\frac{\partial \rho}{\partial t} = -\nabla\cdot[(H_0 + p)\mathbf{v}_{\text{s}} + \mathbf{Q}_0]. \tag{A.19}$$

Using Eq.(A.3), (A.12) and the thermodynamic relation (A.18) we obtain the entropy flux equation

$$T\frac{\partial(\rho s)}{\partial t} + \nabla\cdot[T\rho\, s_{\text{eff}}\mathbf{v}_{\text{s}} + \mathbf{Q}_0 - \mu\mathbf{P}_0] = 0 \tag{A.20}$$

Defining the density q by the relation

$$\mathbf{Q}_0 - \mu\mathbf{P}_0 = qT\, s_{\text{eff}}\,(\mathbf{v}_{\text{n}} - \mathbf{v}_{\text{s}})\,, \tag{A.21}$$

and using the identity

$$\frac{\partial s_{\text{eff}}}{\partial t} = \frac{1}{\rho}\frac{\partial}{\partial t}(\rho\, s_{\text{eff}}) - \frac{s_{\text{eff}}}{\rho}\frac{\partial \rho}{\partial t}$$

together eqs. (A.3) and (A.5) we finally obtain an equation for temporal variation of s_{eff}

$$\frac{\partial s_{\text{eff}}}{\partial t} + \frac{s_{\text{eff}}(q - \rho_{\text{n}})}{\rho\rho_{\text{n}}}\nabla\cdot\mathbf{P}_0 = \frac{\mathcal{N}}{\rho V}\frac{\partial\tilde{\lambda}_{\mathcal{N}}}{\partial t}. \tag{A.22}$$

Equation (A.22) corresponds to the thermomechanical effect and together with Eq.(A.17) describe a second sound mode. Remark that it is a completely defined equation (it does not directly depend on the entropy).

To numerically study the effect predicted by eqs. (A.17) and (A.22) we prepare an initial condition using the SGLE with a space-variable temperature and chemical

potential of the form

$$T = T_0(1 + \epsilon \sin x) \quad \text{(A.23)}$$

$$\mu = \mu_0 + \mu_1 \sin x. \quad \text{(A.24)}$$

We use a resolution of 128^3, the mean temperature is fixed at $T_0 = 2$ and the mean chemical potential μ_0 is chosen in order to keep the density at $\rho = 1$. To reduce the emission of density waves the value of μ_1 is automatically adjusted to obtain a flat pressure profile. The initial condition is then evolved under the TGPE dynamics.

To visualize the x-dependent fields we average on y and z directions. The initial values of $H - \mu N$ (that is proportional to T) and P_0 are displayed on Fig.A.1.a. Observe on Fig.A.1.b that the temperature gradient induces a current P_0 according to

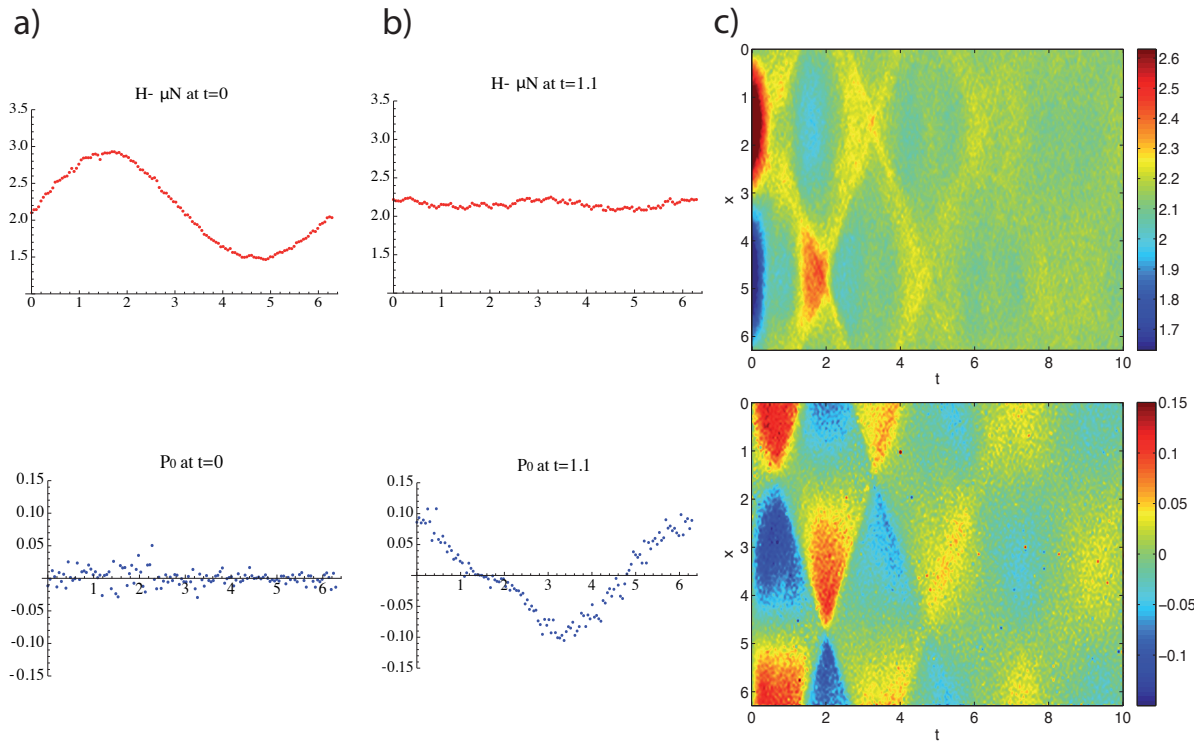

Fig. A.1: Temporal evolution of a space-modulated temperature initial condition. a-b) $H-\mu N$ and P_0 at $t = 0$ and $t = 1.1$. c) $x - t$ diagram of $H - \mu N$ (upper) and P_0 (bottom).

(A.17). Figure A.1.c displays a $x - t$ diagram of the run. Observe that the damping is considerable.

These preliminary results, that become observable at resolutions of 128^3, strongly suggest the existence of second sound waves in the TGPE dynamics. However, is not possible with this configuration to distinguish from a ballistic propagation. A better configuration could be obtained by using a Taylor-Green symmetric code, in order to

easily increase the resolution, and studying the heat propagation of a hot spot. We will attempt in the future perform a parametric study of this problem varying the temperature and the amount of dispersion of the system ($\xi k_{\max}$).

A.1 Propagation of Sound in truncated Gross-Pitaevskii equation

The generalized acoustic equations of TGPE are obtained combing Eqs.(A.3), (A.6), (A.17) and (A.22). This set of coupled equations reads

$$\frac{\partial^2 \rho}{\partial t^2} = \nabla^2 p \tag{A.25}$$

$$\frac{\partial^2 s_{\rm eff}}{\partial t^2} = \frac{s_{\rm eff}^2}{\rho_{\rm n}}(q-\rho_{\rm n})\nabla^2 T + \frac{\mathcal{N}}{\rho V}\frac{\partial^2 \tilde{\lambda}_{\mathcal{N}}}{\partial t^2} + \frac{s_{\rm eff}}{\rho_{\rm n}}\frac{\mathcal{N}}{\rho V}(q-\rho_{\rm n})\nabla^2\tilde{\lambda}_{\mathcal{N}} \tag{A.26}$$

The space varying quantities in Eqs. (A.25) and (A.26) are function of only two independent variables. The simplest choice is the chemical potential and the temperature pair. Writing

$$T = \bar{T} + \delta T \qquad \mu = \bar{\mu} + \delta\mu \tag{A.27}$$

$$\rho = \bar{\rho} + \frac{\partial \rho}{\partial T}\delta T + \frac{\partial \rho}{\partial \mu}\delta\mu \qquad p = \bar{p} + \frac{\partial p}{\partial T}\delta T + \frac{\partial p}{\partial \mu}\delta\mu \tag{A.28}$$

$$s_{\rm eff} = \bar{s}_{\rm eff} + \frac{\partial s_{\rm eff}}{\partial T}\delta T + \frac{\partial s_{\rm eff}}{\partial \mu}\delta\mu \qquad \tilde{\lambda}_{\mathcal{N}} = \bar{\tilde{\lambda}}_{\mathcal{N}} + \frac{\partial \tilde{\lambda}_{\mathcal{N}}}{\partial T}\delta T + \frac{\partial \tilde{\lambda}_{\mathcal{N}}}{\partial \mu}\delta\mu \tag{A.29}$$

where the bars denotes that the corresponding quantities are evaluated at the homogeneous value $\bar{T}$ and $\bar{\lambda}$. Replacing Eqs.(A.27) - (A.29) in Eqs.(A.25) and (A.26) leads to a set of coupled hyperbolic equations for the pair δT and $\delta\mu$ with two wave propagation velocities.

Using the low-temperature expressions obtained[1] in section IIIB in [38] in chapter 6, we obtain in the limit $T \to 0$ the two velocity u_1 and u_2

$$u_1^2 = \mu\,, \qquad u_2^2 = \mu \frac{\left[\frac{2}{3} - f\left[\frac{4m\mu}{P_{\max}^2}\right]\right]^2}{f\left[\frac{4m\mu}{P_{\max}^2}\right]}, \tag{A.30}$$

where $f[z] = z - z^{3/2}\cot^{-1}(\sqrt{z})$ is the function defined in Eq.B9 of [38] in chapter 6.

[1] The value of $\mathbf{Q_0}$ in Eq.(A.21) can be directly computed with the low-temperature calculations. The quartic term Q_k of Eq.(6.11) is evaluated by using the Wick theorem that gives the relation $\overline{\psi\psi^*\psi\partial_k\psi^*} = 2\,\overline{|\psi|^2}\;\overline{\psi\partial_k\psi}$. The value of the energy flux obtained is $\mathbf{Q_0} = \frac{2}{3}\frac{\mathcal{N}}{\beta}\mathbf{W}$ and it has been also corroborated with data form SGLE.

It is straightforward to show that

$$\lim_{x\to\infty} \frac{\left[\frac{2}{3} - f\left[x\right]\right]^2}{f\left[x\right]} = \frac{1}{3}, \tag{A.31}$$

and therefore in the limit of vanishing dispersion $\frac{P_{\max}^2}{4m\mu} \sim (\xi k_{\max})^2 \to 0$, we thus find that the quotient of the sound velocities is

$$\frac{u_2}{u_1} = \frac{1}{\sqrt{3}}. \tag{A.32}$$

This correspond to the well know zero-temperature limit of the Landau two-fluid model. Remark however that this limit is somewhat anomalous seen from the Gross-Pitaevskii equation because as ξ is the size of vortex core, that implies that vortices are not resolved by the TGPE. However, at finite values of $\xi k_{\max}$ some interesting behavior could be found. The dependence of u_2^2/u_1^2 on $\frac{4m\mu}{P_{\max}^2}$ is displayed on the left plot of figure A.2.

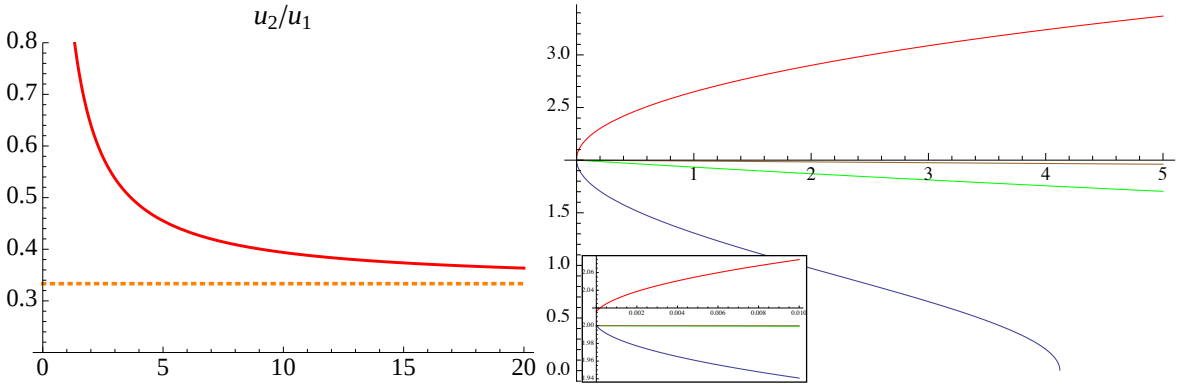

Fig. A.2: left) $(u_2/u_2)^2$ as function of $\frac{4m\mu}{P_{\max}^2}$. Orange dashed line indicates the asymptotic value 1/3. right) Temperature dependence of u_1 (blue) , u_2 (red) obtained from Eqs.(A.25) and (A.26) and $\sqrt{\frac{\partial p}{\partial \rho}}\Big|_S$ (brown), $\sqrt{\frac{\partial p}{\partial \rho}}\Big|_T$ (green). Inset: zoom at low temperature.

At finite temperature the formal expression are too large to be written here. Using the typical values used for numerical simulations in [38] (chapter 6) the temperature dependence of the velocities is shown on plot on the right of Fig.A.2.

Note that the value of first sound velocity decrease faster than $\sqrt{\frac{\partial p}{\partial \rho}}\Big|_S$ and $\sqrt{\frac{\partial p}{\partial \rho}}\Big|_T$ computed using low-temperature calculations in [38] (chapter 6).

A.2 Brief discussion on quantum statistics and two-fluid model

Suppose that in the previous section quantum statistics have been used instead of classical statistics. With quantum statistics the potential associated with the number of modes exactly vanishes: $\lambda_{\mathcal{N}} = 0$. Therefore $s_{\text{eff}} = s$. It is also possible to show, using the quantum statistics developed in section 5.4, that from the definition (A.21) we obtain $q = \rho$. Thus the eq.(A.20) for the entropy flux reduce to

$$\frac{\partial(\rho s)}{\partial t} + \nabla \cdot (\rho s \mathbf{v}_n) = 0 \tag{A.33}$$

This equation, exactly corresponds to that of two-fluid model where only the normal fluid can transport the entropy. It is the starting point of Landau's derivation of his model.

It is straightforward to show that in the $T \to 0$ limit we recover the first and second sound velocities

$$u_1^2 = \mu\,, \qquad u_2^2 = \frac{\mu}{3} \tag{A.34}$$

of the Landau's model.

We have thus shown that the Landau two-fluid model can be naturally derived from the conservation equations of GPE. This fact is simply related to the correspondence of the Gross-Pitaevskii equation to the hydrodynamics description.

B. NUMERICAL METHODS

In this appendix we give a short description of the numerical methods used in this thesis.

B.1 Fourier transform

All the numerical simulations performed in this thesis have periodical boundary conditions on the domain $[0, 2\pi]^D$. For simplicity in the present section we will consider $D = 1$. A field f can be represented by its Fourier series

$$f(x) = \sum_{k=-\infty}^{\infty} \hat{f}(k) e^{ikx} \tag{B.1}$$

where the Fourier transform is defined by

$$\hat{f}(k) = \frac{1}{2\pi} \int_0^{2\pi} f(x) e^{-ikx} dx. \tag{B.2}$$

If we have a partition of the interval $[0, 2\pi]$ with N collocation points $x_0, x_1 \ldots; x_{N_1}$ with $x_j = j\Delta x$ the discrete Fourier transform reads

$$\hat{f}_N(k) = \sum_{j=-\frac{N}{2}}^{j=\frac{N}{2}} f(x_j) e^{ik\frac{2\pi j}{N}}. \tag{B.3}$$

The wavevectors k thus take the values $-\frac{N}{2}, -\frac{N}{2}+1, \ldots, \frac{N}{2}-1$.

The Fourier transform requires $O(N)$ operations to be computed. In practice, Fourier transforms are performed by using the Fast Fourier Transform (FFT) algorithm that reduce to $O(N \log_2 N)$ the number of operations [110].

The generalization to D dimensions is straightforward.

B.2 Solving a PDE

The PDE's considered in this thesis can be written in the general form

$$\frac{\partial u}{\partial t} = Lu + NL[u] \tag{B.4}$$

where L is a linear operator and $NL[u]$ is the non-linear term of the equation.

B.2.1 Pseudo-spectral methods

In Fourier space the non-linear term $NL[u]$ in eq.(B.4) involves convolutions that are expensive to compute numerically . We thus solve the equations of the type (B.4) by using standard pseudo-spectral codes [14], that consist in evaluating the non-linear term in physical space using the FFT. This procedure reduces the computational time from $O(N^{2D})$ for the convolution in the case of quadratic nonlinearity to $O(N^D \log_2 N)$ for pseudo-spectral method.

The error of approximating a PDE by a pseudo-spectral code is $O(1/N^N)$. Thus a pseudo-spectral resolves much better a PDE than a finite difference scheme with the same resolution.

B.2.2 Dealiasing

However the gain of computational time and precision obtained by using pseudo-spectral codes generates a problem called *aliasing*. Suppose that $NL[u]$ in eq.(B.4) has a nonlinearity of order 2. The interaction of two Fourier modes k_1 and k_2 generates contribution to the wavenumber $k_1 - k_2$ and $k_1 + k_2$. By definition of the discrete Fourier transform (B.3) the wavenumbers are defined modulus N. Therefore wavenumbers satisfying $|k_1 \pm k_2| > N/2$ are considered as small wavenumbers. This situation can induces problems with the conservation laws of the PDE.

The system can be *dealiased* by the the following procedure. Suppose a nonlinearity of order m. The de-aliasing consist in reducing the Fourier space to a sub-set $(-k_{\max}, k_{\max})$ and to eliminate at each time-step the Fourier modes outside this interval. The condition that determines $k_{\max}$ is given by $mk_{\max} - N < -k_{\max}$, i.e $k_{\max} < \frac{N}{m+1}$. This is known as the $1/(m+1)$-rule [14].

With this procedure a factor $\frac{m-1}{m+1}$ of the resolution is lost. However, the Leibnitz rule for the derivative of a product is recovered. Suppose that f and g are two aliased field, we have then

$$\widehat{(fg)'}(k) = i \sum_{j+n=_{mod_N} k} k\hat{f}_N(j)\hat{g}_N(j)\hat{f}_N(j) = i \sum_{j+n=_{mod_N} k} (j+n)_{mod_N}\hat{f}_N(j)\hat{g}_N(j)\hat{f}_N(j), \tag{B.5}$$

and the sum cannot be split in two terms. If the fields are de-aliased with the 2/3-rule the sum can be separated and we recover the Leibnitz rule. Most of the conservation

laws are based on this rule and can be broken if the fields are aliased.

We have used the 2/3-rule in all our numerical schemes used in the present thesis. For the TGPE, where the non-linearity is cubic, we proposed a new scheme that needs an extra FFT for which the 2/3-rule can be used instead of the 1/2-rule. In thermalized truncated system, where the contribution of the fields is dominated by large wavenumbers, the lack of a correct de-aliasing scheme can induce considerable errors in the conservation of invariants. The TGPE presents a particularity; the energy and the number of particles is conserved even if the system is aliased. However, errors in the conservation of momentum can rise up to a 50% in a few units of time (see Appendix of article [38] in chapter 6). Figure B.1 shows the conservation of the energy, the number of particles and the momentum of the TGPE using a Runge-Kutta of order 4 (see next section). Observe that the error of the conservation of the momentum does not depends

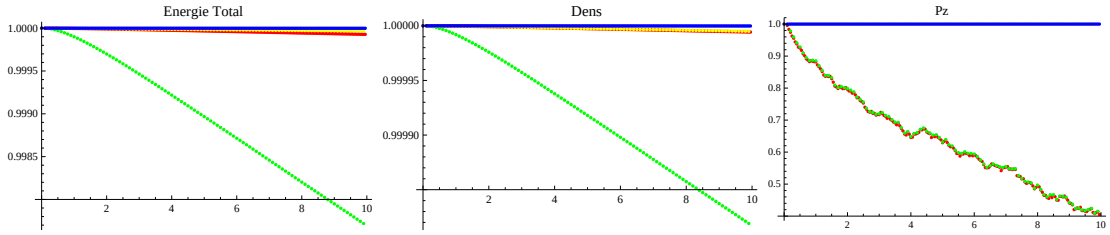

Fig. B.1: Temporal evolution of of H, N and P_z normalized by their values at $t = 0$. The colors correspond to numerical integration of the dealiased NLS (Yellow $dt = 0.5 \times 10^{-2}$ and Blue $dt = 0.25 \times 10^{-2}$) and not de-aliased (Green $dt = 0.5 \times 10^{-2}$ and Red $dt = 0.25 \times 10^{-2}$). Initial condition obtained with SGLE at $T = 1$, $w = 0.5$ and using a resolution of 32^3

on the time-step dt.

B.2.3 Time-stepping

Suppose that at $t = 0$ the value of $u_0 = u(0)$ is known. In the following we denote $t_n = n\,dt$ and $u_n = u(t_n)$. The time-stepping used in this thesis for solving equation of the type B.4 are:

- **Explicit Euler** (order $O(dt)$)

$$\begin{aligned} u_{n+1} &= u_n + Euler[u_n] \\ Euler[u_n] &= dt\,(Lu + NL[u]) \end{aligned} \tag{B.6}$$

- **Implicit Euler** (order $O(dt)$)

$$u_{n+1} = \frac{u_n + dt\,NL[u]}{1 - dtL} \tag{B.7}$$

- **Runge-Kutta** (order $O(dt^4)$)

$$\begin{aligned} u_{n+1} &= u_n + \frac{k_1}{6} + \frac{k_2}{3} + \frac{k_3}{3} + \frac{k_4}{6} + \frac{k_1}{6} \\ k_1 &= Euler[u_n] \\ k_2 &= Euler[u_n + \frac{k_2}{2}] \\ k_3 &= Euler[u_n + \frac{k_2}{2}] \\ k_4 &= Euler[u_n + k_3] \end{aligned} \tag{B.8}$$

Because a high accuracy in the conservation of invariants is needed in the study of thermalization, in all the conservative systems we used a Runge-Kutta scheme. For the stochastic algorithm we used explicit Euler and for the advected real Ginzburg-Landau equation (ARGLE) we used an Implicit Euler scheme.

B.2.4 White-noise

The space-time δ-correlated white noise used in simulations is first generated in physical space as

$$\zeta(x_i, y_j, z_k) = \sqrt{\frac{n_x n_y n_z}{dt}} \zeta_{ijk} \tag{B.9}$$

where ζ_{ijk} are independent Gaussian number [110] of zero mean and variance 1. Then the fields are transformed to Fourier space and de-aliased.

B.2.5 Taylor-Green symmetries

The symmetrical pseudo-codes are optimized in the way of references [67, 27] to take in account the symmetries of the Taylor-Green vortex: rotational of angle π around the axis $(x = z = \pi/2)$, $(y = z = \pi/2)$ and $(x = y = \pi/2)$ and mirror symmetry with respect to the planes $x = 0, \pi$, $y = 0, \pi$, $z = 0, \pi$.

Using these symmetries, the velocity field admits the following representation:

$$v_x(r,t) = \sum_{m=0}^{\infty}\sum_{n=0}^{\infty}\sum_{p=0}^{\infty} u_x(m,n,p,t) \sin mx \cos ny \cos pz \tag{B.10}$$

$$v_y(r,t) = \sum_{m=0}^{\infty}\sum_{n=0}^{\infty}\sum_{p=0}^{\infty} u_y(m,n,p,t) \cos mx \sin ny \cos pz \tag{B.11}$$

$$v_z(r,t) = \sum_{m=0}^{\infty}\sum_{n=0}^{\infty}\sum_{p=0}^{\infty} u_z(m,n,p,t) \cos mx \cos ny \sin pz \tag{B.12}$$

with $\mathbf{u}(m,n,p,t) = 0$ unless m, n, p are either all even or all odd integers. For GPE,

the symmetries imply a similar decomposition with $\cos mx \cos ny \cos pz$.

The symmetries also imply for the Fourier modes

$$u_x(m,n,p,t) = (-1)^r u_y(n,m,p,t) \quad \text{(B.13)}$$
$$u_z(m,n,p,t) = (-1)^r u_z(n,m,p,t) \quad \text{(B.14)}$$

with $r = 1$ if m, n, p are all odd and $r = 2$ if m, n, p are all even.

The relations (B.13) and (B.14) allow us to obtain v_y from v_x and v_z. The decomposition (B.10) permit to gain a factor 32 in memory storage and CPU time compared with general pseudo-spectral codes.

B.3 Newton method

In this thesis the Newton method is used in several occasions to obtain a zero of a function or a stationary state of a non-linear operator.

In general, consider a smooth unction $f : \mathbb{R}^n \to \mathbb{R}^m$ and let $\mathbf{x_0}$ be an initial guess of the problem $f(\mathbf{x}) = 0$. The Newton method consist by iteratively solving for the linear approximation of f at the precedent known point $\mathbf{x_n}$:

$$f(\mathbf{x_n} + \mathbf{h}) \approx f(\mathbf{x_n}) + Df(\mathbf{x_n})\mathbf{h} = 0 \quad \text{(B.15)}$$
$$\mathbf{x_{n+1}} = \mathbf{x_n} + \mathbf{h}. \quad \text{(B.16)}$$

It is possible to show, by using the Banach fixed point theorem, that his algorithm converge exponentially to the solution of the problem. However, in the general case $Df(\mathbf{x_n})$ is a $m \times n$ not necessarily invertible matrix. To solve (B.15) can be extremely complex and expensive in computational time.

In the particular case of $2D$ GPE studied in chapter 7, $Df(\mathbf{x_n})$ is a 2×2 invertible matrix and the system (B.15) can be explicitly solved. Choosing the initial guess $\mathbf{x_0}$ by finding the minimum of $|\psi|^2$ on the mesh, the algorithm quickly converges to the zero of ψ with an accuracy much larger than the mesh size.

B.3.1 Partial differential equations

The Newton method can be also applied to PDE's to obtain stationary states. The algorithm (B.15-B.16) applies directly by replacing the the Jacobian $Df(\mathbf{x_n})$ by the respective linearized operator.

When, this method is numerically applied, the linearized operator becomes a matrix of dimension of the order $N^D \times N^D$ and the linear system cannot be easily solved. This difficulty was technically solved by using the bi-conjugate gradient method Bi-CGSTAB [111]. The application of the Newton method to obtain stationary states (stable and unstable) of a PDE is used and explained in detail in references [112, 113, 114].

Initial guesses

The initial guess used by the Newton method to generate a vortex ring of radius R was obtained by performing some steps of ARGLE using as initial condition the function

$$\psi(x,y,z) = e^{iz}U(x,y) + 1 - U(x,y) \tag{B.17}$$

$$U(x,y) = \frac{\tanh\left(\frac{R-r}{2\xi}\right)+1}{\tanh\left(\frac{R}{2\xi}\right)+1} \tag{B.18}$$

$$r(x,y) = 2\sqrt{\cos^2\left(\frac{x}{2}\right)+\cos^2\left(\frac{y}{2}\right)}, \tag{B.19}$$

For the crystal, the initial guess was based on the Clebsh representation described in reference [27]

$$\lambda = \sqrt{2}\cos x \quad , \quad \mu = \sqrt{2}\cos y \tag{B.20}$$

$$\zeta = \lambda + i\mu \tag{B.21}$$

$$\psi(x,y,z) = \frac{\zeta}{|\zeta|}\tanh\frac{|\zeta|}{\sqrt{2}\xi}. \tag{B.22}$$

C. COMMENT ON "SUPERFLUID TURBULENCE FROM QUANTUM KELVIN WAVE TO CLASSICAL KOLMOGOROV CASCADE"

Comment on "Superfluid turbulence from quantum Kelvin wave to classical Kolmogorov cascade"

Giorgio Krstulovic[1] and Marc Brachet[1]

[1]*Laboratoire de Physique Statistique de l'Ecole Normale Supérieure, associé au CNRS et aux Universités Paris VI et VII, 24 Rue Lhomond, 75231 Paris, France*

(Dated: February 3, 2010)

PACS numbers: 47.37.+q, 03.67.Ac, 03.75.Kk, 67.25.dk

In a recent Letter [1], Yepez *et al.* performed numerical simulations of the Gross-Pitaevskii equation (GPE) using a novel unitary quantum algorithm with very high resolution. They claim to have found new power-law scalings for the incompressible kinetic energy spectrum: "...(the) solution clearly exhibits three power law regions for $E_{\rm kin}^{\rm incomp}(k)$: for small k the Kolmogorov $k^{-\frac{5}{3}}$ spectrum while for high k a Kevlin wave spectrum of k^{-3}...".

In this comment we point out that the high wavenumber k^{-3} power-law observed by Yepez *et al.* is an artifact stemming from the definition of the kinetic energy spectra and is thus not directly related to a Kelvin wave cascade. Furthermore, we clarify a confusion about the wavenumber intervals on which Kolmogorov and Kelvin wave cascades are expected to take place. Finally, we point out that the incompressible kinetic energy spectrum of the initial data chosen by Yepez *et al.* scales like k^{-1} at small wavenumbers, perhaps not the best choice to obtain a clean Kolmogorov regime.

The dynamics of a superflow is described by the GPE

$$\partial_t\psi = ic/(\sqrt{2}\xi)(\psi - |\psi|^2\psi + \xi^2\nabla^2\psi), \qquad (1)$$

where the complex field ψ is related by Madelung's transformation $\psi = \sqrt{\rho}\exp\left(i\frac{\phi}{\sqrt{2}c\xi}\right)$ to the density ρ and velocity $\vec{v} = \nabla\phi$ of the superfluid. In these formulae, ξ is the coherence length and c is the velocity of sound (for a fluid of unit mean density). The superflow is irrotational, except on the nodal lines $\psi = 0$ which are the superfluid vortices.

The GPE dynamics Eq. (1) conserves the energy that can we written as the sum (the space-integral) of three parts: the kinetic energy $\mathcal{E}_{kin} = 1/2(\sqrt{\rho}v_j)^2$, the internal energy $\mathcal{E}_{int} = (c^2/2)(\rho-1)^2$ and the quantum energy $\mathcal{E}_q = c^2\xi^2(\partial_j\sqrt{\rho})^2$. Using Parseval's theorem, one can define corresponding energy spectra: e.g. the kinetic energy spectrum $E_{kin}(k)$ as the angle-average of $\left|\frac{1}{(2\pi)^3}\int d^3r e^{ir_jk_j}\sqrt{\rho}v_j\right|^2$ [2].

The 3D angle-averaged spectrum of a smooth isolated vortex line is known to be proportional to that of the 2D axisymmetric vortex, an exact solution of Eq. (1) given by $\psi^{vort}(r) = \sqrt{\rho(r)}\exp(\pm i\varphi)$ in polar coordinates (r,φ). The corresponding velocity field $v(r) = \sqrt{2}c\xi/r$ is azimuthal and the density profile, of characteristic spatial extent ξ, verifies $\sqrt{\rho(r)} \sim r$ as $r \to 0$ and $\sqrt{\rho(r)} = 1 + O(r^{-2})$ for $r \to \infty$. Thus $\sqrt{\rho}v_j$ has a small r singular behavior of the type r^0 and behaves as r^{-1} at large r. In general for a function scaling as $g(r) \sim r^s$ the (2D) Fourier transform is $\hat{g}(k) \sim k^{-s-2}$ and the associated spectrum scales as k^{-2s-3}. Thus $E_{kin}(k)$ scales as k^{-3} for $k \gg k_\xi \sim \xi^{-1}$ and as k^{-1} for $k \ll k_\xi$. [3].

Following the above discussion, the k^{-3} power-law observed in [1] is an artifact stemming from the definition of the kinetic energy spectra and is not directly related to a Kelvin wave cascade.

Another very important scale, not discussed in the Letter [1], is the scale ℓ of the mean intervortex distance. The hydrodynamic (Kolmogorov) energy cascade is expected to end at $k_\ell \sim \ell^{-1}$ [2] and the Kelvin wave cascade to begin there, after an eventual bottleneck [4]. Note that $\ell_I \gg \ell \gg \xi$, where ℓ_I is the energy containing scale. We thus believe that nothing particularly interesting is taking place between k_ξ and the maximum wavenumber $k_{\rm max}$ of the simulation and that there is a confusion in [1] between k_ℓ and k_ξ.

Furthermore, the initial data used in [1] (see the supplementary material) is a 3D set of 12 straight vortex lines, with intervortex distance ℓ of the order of the box size. The k^{-1} scaling of the initial data $E_{kin}(k)$ thus extends down to small wavenumbers $k_I \sim \ell_I^{-1}$. This behavior of the initial data is in contrast to the Taylor-Green initial data used in [3], where destructive interferences deplete the value of $E_{kin}(k)$ in the interval for $k_I < k < k_\ell$. The initial data chosen in [1] is thus perhaps not the best choice to obtain a clean Kolmogorov regime. This might explain the high level of compressible kinetic energy in the $-5/3$ scaling zone that is apparent in the movie of the supplementary material.

We thank M. Abid and C. Nore for useful discussions.

[1] Jeffrey Yepez, George Vahala, Linda Vahala, and Min Soe. *Phys. Rev. Lett.*, 103(8):084501, 2009.

[2] C. Nore, M. Abid, and M. E. Brachet. *Phys. Rev. Lett.*, 78(20):3896–3899, May 1997.

[3] C. Nore, M. Abid, and M. E. Brachet. *Phys. of Fluids*, 9(9):2644–2669, 1997.

[4] Victor S. L'vov, Sergei V. Nazarenko, and O. Rudenko. newblock *Phys. Rev. B*, 76(2):024520, 2007.

BIBLIOGRAPHY

[1] T.D. Lee. On some statistical properties of hydrodynamical and magneto-hydrodynamical fields. *Quart Appl Math*, 10(1):69–74, Jan 1952.

[2] R. Kraichnan. Inertial ranges in two-dimensional turbulence. *Phys. Fluids*, 10(7):1417–&, Jan 1967.

[3] R. Kraichnan. Helical turbulence and absolute equilibrium. *Journal of Fluid Mechanics*, 59(7):745–752, Jan 1973.

[4] SA Orszag. Analytical theories of turbulence. *Journal of Fluid Mechanics*, 41:363–&, Jan 1970.

[5] C Cichowlas, P Bonaiti, F Debbasch, and M Brachet. Effective dissipation and turbulence in spectrally truncated Euler flows. *Physical Review Letters*, 95(26):264502, Jan 2005.

[6] W. J. T Bos and J.P. Bertoglio. Dynamics of spectrally truncated inviscid turbulence. *Phys. Fluids*, 18(7):071701, Jan 2006.

[7] S.A. Orszag. *Statistical Theory of Turbulence*. in, Les Houches 1973: Fluid dynamics, R. Balian and J.L. Peube eds. Gordon and Breach, New York, 1977.

[8] R. Kraichnan. Classical fluctuation-relaxation theorem. *Physical Review*, 113(5):1181–1182, Jan 1959.

[9] Uriel Frisch, Susan Kurien, Rahul Pandit, Walter Pauls, Samriddhi Sankar Ray, Achim Wirth, and Jian-Zhou Zhu. Hyperviscosity, Galerkin truncation, and bottlenecks in turbulence. *Physical Review Letters*, 101(14):144501, Jan 2008.

[10] G Falkovich. Bottleneck phenomenon in developed turbulence. *Phys. Fluids*, 6(4):1411–1414, Jan 1994.

[11] Y Kaneda, T Ishihara, M Yokokawa, K Itakura, and A Uno. Energy dissipation rate and energy spectrum in high resolution direct numerical simulations of turbulence in a periodic box. *Phys. Fluids*, 15(2):L21–L24, Jan 2003.

[12] W Dobler, NEL Haugen, TA Yousef, and A Brandenburg. Bottleneck effect in three-dimensional turbulence simulations. *Physical Review E*, 68(2):026304, Jan 2003.

[13] P. D Mininni, A Alexakis, and A Pouquet. Nonlocal interactions in hydrodynamic turbulence at high Reynolds numbers: The slow emergence of scaling laws. *Physical Review E*, 77(3):036306, Jan 2008.

[14] D. Gottlieb and S. A. Orszag. *Numerical Analysis of Spectral Methods*. SIAM, Philadelphia, 1977.

[15] Victor S L'vov, Sergei V Nazarenko, and Oleksii Rudenko. Bottleneck crossover between classical and quantum superfluid turbulence. *Physical Review B*, 76(2):024520, Jul 2007.

[16] JD Fournier and U Frisch. The deterministic and statistical burgers-equation. *J Mec Theor Appl*, 2(5):699–750, Jan 1983.

[17] C Bardos, S Benachour, and M Zerner. Analyticity of periodic-solutions of 2-dimensional eulers equation. *Cr Acad Sci A Math*, 282(17):995–998, Jan 1976.

[18] U Frisch, T Matsumoto, and J Bec. Singularities of Euler flow? not out of the blue! *J Stat Phys*, 113(5-6):761–781, Jan 2003.

[19] C Cichowlas and ME Brachet. Evolution of complex singularities in Kida-Pelz and Taylor-Green inviscid flows. *Fluid Dyn Res*, 36(4-6):239–248, Jan 2005.

[20] C. Cichowlas. *Equation d'Euler tronquée: de la dynamique des singularités complexes à la relaxation turbulente*. Université Pierre et Marie Curie - Paris VI, 2005.

[21] U. Frisch. *Turbulence: The Legacy of A. N.Kolmogorov*. Cambridge University Press, Cambridge, November 1995.

[22] DK Lilly. The structure, energetics and propagation of rotating convective storms .2. helicity and storm stabilization. *Journal of the Atmospheric Sciences*, 43(2):126–140, Jan 1986.

[23] P. D Mininni and A Pouquet. Helicity cascades in rotating turbulence. *Physical Review E*, 79(2):026304, Jan 2009.

[24] JJ Moreau. Constantes d'un îlot tourbillonaire en fluide parfait barotrope. *C. R. Acad. Sci. Paris*, 252:2810–2812, 1961.

[25] H Moffatt. The degree of knottedness of tangled vortex lines. *J. Fluid Mech*, 35:117–129, Jan 1969.

[26] C Nore, M Abid, and ME Brachet. Kolmogorov turbulence in low-temperature superflows. *Physical Review Letters*, 78(20):3896–3899, Jan 1997.

[27] C Nore, M Abid, and ME Brachet. Decaying Kolmogorov turbulence in a model of superflow. *Phys. Fluids*, 9(9):2644–2669, Jan 1997.

[28] Jeffrey Yepez, George Vahala, Linda Vahala, and Min Soe. Superfluid turbulence from quantum kelvin wave to classical kolmogorov cascades. *Physical Review Letters*, 103(8):084501, Aug 2009.

[29] MJ Davis, SA Morgan, and K Burnett. Simulations of Bose fields at finite temperature. *Physical Review Letters*, 87(16):160402–160402, 2001.

[30] C Connaughton, C Josserand, A Picozzi, Y Pomeau, and S Rica. Condensation of classical nonlinear waves. *Physical Review Letters*, 95(26):263901, Jan 2005.

[31] Antonio Picozzi Gustavo Düring and Sergio Rica. Breakdown of weak-turbulence and nonlinear wave condensation,. *Physica D*, 238(16):1524–1549, August 2009.

[32] Natalia G Berloff and Anthony J Youd. Dissipative dynamics of superfluid vortices at nonzero temperatures. *Physical Review Letters*, 99(14):4, Oct 2007.

[33] L Kiknadze and Y Mamaladze. The waves on the vortex ring in heii. *Journal of Low Temperature Physics*, 126(1-2):321–326, Jan 2002.

[34] C. F Barenghi, R Hanninen, and M Tsubota. Anomalous translational velocity of vortex ring with finite-amplitude Kelvin waves. *Physical Review E*, 74(4):046303, Jan 2006.

[35] G Krstulovic and M Brachet. Two-fluid model of the truncated Euler equations. *Physica D: Nonlinear Phenomena*, 237(14-17):2015–2019, Aug 2008.

[36] G. Krstulovic, P. D. Mininni, M. E. Brachet, and A. Pouquet. Cascades, thermalization, and eddy viscosity in helical Galerkin truncated Euler flows. *Physical Review E*, 79(5):056304, May 2009.

[37] G. Krstulovic, C. Cartes, M. Brachet, and E. Tirapegui. Generation and characterization of absolute equilibrium of compressible flows. *International Journal of Bifurcation and Chaos (IJBC)*, 19(10):3445–3459, 2009.

[38] Giorgio Krstulovic and Marc Brachet. Energy cascade with small-scales thermalization, counter flow metastability and anomalous velocity of vortex rings in fourier-truncated Gross-Pitaevskii equation. *To be published*, 2010.

[39] G Krstulovic, M Brachet, and E Tirapegui. Radiation and vortex dynamics in the nonlinear schrödinger equation. *Physical review. E*, Jan 2008.

[40] A.N.Kolmogorov. The local structure of turbulence in incompressible viscous fluid for very large Reynolds. *Proceedings: Mathematical and Physical Sciences*, Jan 1941.

[41] A. N.Kolmogorov. On degeneration decay of isotropic turbulence in an incompressible viscous liquid. *C. R. Acad. Sci. U.S.S.R*, **31**:538–540, 1941.

[42] A. N.Kolmogorov. Dissipation of energy in locally isotropic turbulence. *C. R. Acad. Sci. U.S.S.R*, **32**:16–18, 1941.

[43] A. N.Kolmogorov. A refinement of previous hypotheses concerning the local structure of turbulence in a viscous incompressible fluid at high Reynolds number. *J. Fluid Mech.*, **13**:82–85, 1962.

[44] R. Kraichnan. Small-scale structure of a scalar field convected by turbulence. *Phys. Fluids*, 11(5):945–&, Jan 1968.

[45] R. Kraichnan. Passive scalar: Sealing exponents and realizability. *Physical Review Letters*, 78(26):4922–4925, Jan 1997.

[46] A Brissaud, U Frisch, J Leorat, and M Lesieur. Helicity cascades in fully developed isotropic turbulence. *Phys. Fluids*, 16(8), Jan 1973.

[47] H Moffatt and A Tsinober. Helicity in laminar and turbulent flow. *Annual review of fluid mechanics*, 24:281–312, Jan 1992.

[48] ME Brachet. Direct simulation of three-dimensional turbulence in the Taylor–Green vortex. *Fluid Dyn Res*, 8:1–8, 1991.

[49] S Douady, Y Couder, and ME Brachet. Direct observation of the intermittency of intense vorticity filaments in turbulence. *Physical Review Letters*, 67(8):983–986, Jan 1991.

[50] L. F. Richardson. *Weather prediction by numerical process*. Cambridge University Press England, 1922.

[51] KR Sreenivasan. On the universality of the kolmogorov constant. *Phys. Fluids*, 7(11):2778–2784, Jan 1995.

[52] F Champagne. The fine-scale structure of the turbulent velocity field. *Journal of Fluid Mechanics*, 86(1):67–108, Jan 1978.

[53] Stephen B. Pope. *Turbulent flows*. Cambridge University Press, Cambridge, 2000.

[54] L. D. Landau and L. M. Lifshitz. *Course of Theoretical Physics, Volume VI: Fluid Mechanics*. Butterworth-Heinemann, 2 edition, January 1987.

[55] C Connaughton and S Nazarenko. Warm cascades and anomalous scaling in a diffusion model of turbulence. *Physical Review Letters*, 92(4):044501, Jan 2004.

[56] Kerson Huang. *Statistical Mechanics*. John Wiley & Sons, New York, 2 edition, 1987.

[57] M. Lesieur and D. Schertzer. Amortissement auto-similaire d'une turbulence à grand nombre de amortissement auto-similaire d'une turbulence à grand nombre de Reynolds. *J. Mécanique*, 17:609–646, 1978.

[58] C. Sulem, P.-L. Sulem, and H. Frisch. Tracing complex singularities with spectral methods. *Journal of Computational Physics*, 50:138–161, April 1983.

[59] P Mininni, A Alexakis, and A Pouquet. Large-scale flow effects, energy transfer, and self-similarity on turbulence. *Physical Review E*, Jan 2006.

[60] J Charney. The dynamics of long waves in a baroclinic westerly current. *J. Meteor*, 4(5):135–161, Jan 1947.

[61] N Weiss. The expulsion of magnetic flux by eddies. *Proceedings of the Royal Society of London. Series A*, 293(1434):310–328, Jan 1966.

[62] F Krause and G Rüdiger. On the turbulent decay of strong magnetic fields and the development of sunspot areas. *Solar Physics*, 42:107–119, Jan 1975.

[63] A Pouquet. On two-dimensional magnetohydrodynamic turbulence. *Journal of Fluid Mechanics*, 88:1–16, 1978.

[64] SA Orszag and CM Tang. Small-scale structure of two-dimensional magnetohydrodynamic turbulence. *Journal of Fluid Mechanics*, 90(1):129–143, 1979.

[65] Uriel Frisch, A Pouquet, PL Sulem, and M Meneguzzi. The dynamics of two-dimensional ideal mhd. *J Mec Theor Appl*, pages 191–216, Jan 1983.

[66] U Frisch and PL Sulem. Numerical-simulation of the inverse cascade in two-dimensional turbulence. *Phys. Fluids*, 27(8):1921–1923, Jan 1984.

[67] ME Brachet, M Meneguzzi, and PL Sulem. Small-scale dynamics of high-Reynolds-number two-dimensional turbulence. *Physical Review Letters*, 57(6):683–686, Jan 1986.

[68] H. Politano, A. Pouquet, and PL. Sulem. Inertial ranges and resistive instabilities in two-dimensional magnetohydrodynamic turbulence. *Phys Fluids B-Plasma*, 1(12):2330–2339, Jan 1989.

[69] Y Couder. Two-dimensional grid turbulence in a thin liquid film. *Journal de Physique Lettres*, 45:353–360, Jan 1984.

[70] J Sommeria. Experimental study of the two-dimensional inverse energy cascade in a square box. *Journal of Fluid Mechanics*, 170:139–168, Jan 1986.

[71] O Cardoso, D Marteau, and P Tabeling. Quantitative experimental study of the free decay of quasi-two-dimensional turbulence. *Physical Review E*, 49(1):454–461, Jan 1994.

[72] H Kellay and W Goldburg. Two-dimensional turbulence: a review of some recent experiments. *Reports on Progress in Physics*, 65:845–894, Jan 2002.

[73] Galtier, S Nazarenko, A Newell, and A Pouquet. A weak turbulence theory for incompressible magnetohydrodynamics. *Journal of Plasma Physics*, 63(5):447–488, Jan 2000.

[74] R Kraichnan and D Montgomery. Two-dimensional turbulence. *Reports on Progress in Physics*, 43:547–619, Jan 1980.

[75] HA Rose. Eddy diffusivity, eddy noise and subgrid-scale modelling. *Journal of Fluid Mechanics*, 81:719–734, 1977.

[76] PS Iroshnikov. Turbulence of a conducting fluid in a strong magnetic field. *Sov. Astron*, 7:566–571, 1964.

[77] R. Kraichnan. Inertial-range spectrum of hydromagnetic turbulence. *Phys. Fluids*, 8(7):1385–&, Jan 1965.

[78] P Goldreich and S Sridhar. Toward a theory of interstellar turbulence. 2: Strong alfvenic turbulence. *The Astrophysical Journal*, 438(2):763–775, Jan 1995.

[79] D Fyfe and D Montgomery. High-beta turbulence in 2-dimensional magnetohydrodynamics. *Journal of Plasma Physics*, 16(OCT):181–191, Jan 1976.

[80] E Fermi, J Pasta, and S Ulam. Studies of nonlinear problems. *LASL Report LA-1940*, Jan 1955.

[81] R. Kraichnan. On the statistical mechanics of an adiabatically compressible fluid. *J Acoust Soc Am*, 27(3):438–441, Jan 1955.

[82] S. D. Mobbs. Variational principles for perfect and dissipative fluid flows. *Proc. R. Soc. Lond.A*, 381(1781):457–468, 1982.

[83] Walter Greiner, Ludwig Neise, and Horst Stöcker. *Thermodynamics and statistical mechanics*. Springer, Jan 2001.

[84] L. D. Landau and L. M. Lifshitz. *Course of Theoretical Physics, Volume V: Statistical Physics (Part 1)*. Butterworth-Heinemann, August 1996.

[85] E. M. Lifshitz and L. P. Pitaevskii. *Course of Theoretical Physics, Volume IX: Statistical Physics (Part 2)*. Butterworth-Heinemann, January 1980.

[86] VA Zagrebnov and JB Bru. The bogoliubov model of weakly imperfect bose gas. *Phys Rep*, 350(5-6):292–434, Jan 2001.

[87] EP Gross. Hydrodynamics of a superfluid condensate. *J Math Phys*, 4(2):195–&, Jan 1963.

[88] VL Ginzburg and LP PitaevskiiI. On the theory of superfluidity. *Sov Phys Jetp-Ussr*, 7(5):858–861, Jan 1958.

[89] L. D. Landau and L. M. Lifshitz. *Course of Theoretical Physics, Volume I: Mechanics*. Butterworth-Heinemann, 3rd edition, January 1976.

[90] Nick P Proukakis and Brian Jackson. Finite-temperature models of bose–einstein condensation. *J. Phys. B: At. Mol. Opt. Phys.*, 41(20):203002, Oct 2008.

[91] M Abid, ME Brachet, J Maurer, C Nore, and P Tabeling. Experimental and numerical investigations of low-temperature superfluid turbulence. *Eur J Mech B-Fluid*, 17(4):665–675, Jan 1998.

[92] J Maurer and P Tabeling. Local investigation of superfluid turbulence. *Europhysics Letters*, 43(1):29–34, Jan 1998.

[93] M Kobayashi and M Tsubota. Kolmogorov spectrum of superfluid turbulence: Numerical analysis of the Gross-Pitaevskii equation with a small-scale dissipation. *Physical Review Letters*, 94(6):065302, Jan 2005.

[94] R. J. Donnelly. *Quantized Vortices in Helium II*. Cambridge Univ. Press, 1991.

[95] E Kozik and B Svistunov. Kelvin-wave cascade and decay of superfluid turbulence. *Physical Review Letters*, 92(3):035301, Jan 2004.

[96] S Nazarenko. Kelvin wave turbulence generated by vortex reconnections. *Jetp Lett+*, 84(11):585–587, Jan 2007.

[97] Victor S L'vov and Sergey Nazarenko. Spectrum of Kelvin-wave turbulence in superfluids. *arXiv*, nlin.CD, Jan 2009.

[98] Nick P Proukakis and Brian Jackson. Finite-temperature models of bose-einstein condensation. *J Phys B-At Mol Opt*, 41(20):203002, Jan 2008.

[99] B Jackson, N. P Proukakis, C. F Barenghi, and E Zaremba. Finite-temperature vortex dynamics in bose-einstein condensates. *Physical Review A*, 79(5):053615, Jan 2009.

[100] CF Barenghi, RJ Donnelly, and WF Vinen. Thermal excitation of waves on quantized vortices. *Phys Fluids*, 28(2):498–504, Jan 1985.

[101] K W Schwarz. Three-dimensional vortex dynamics in superfluid He^4: Line-line and line-boundary interactions. *Phys. Rev. B*, 31(9):5782–5804, May 1985.

[102] CF Barenghi, NG Parker, NP Proukakis, and CS Adams. Decay of quantised vorticity by sound emission. *J Low Temp Phys*, 138(3-4):629–634, Jan 2005.

[103] N. G. Parker, N. P. Proukakis, C. F. Barenghi, and C. S. Adams. Controlled vortex-sound interactions in atomic bose-einstein condensates. *Phys. Rev. Lett.*, 92(16):160403, Apr 2004.

[104] V I Klyatskin. Sound radiation by a system of vortices, izv. *AN SSSR Mekhanika Zhidkosti i Gza*, (1):87–92, 1966.

[105] Sergey Nazarenko and Miguel Onorato. Freely decaying turbulence and bose-einstein condensation in gross-pitaevski model. *Journal of Low Temperature Physics*, 146(1-2):31–46, Jan 2007.

[106] CE Swanson, CF Barenghi, and RJ Donnelly. Rotation of a tangle of quantized vortex lines in He-ii. *Physical Review Letters*, 50(3):190–193, Jan 1983.

[107] M Tsubota, T Araki, and CF Barenghi. Rotating superfluid turbulence. *Physical Review Letters*, 90(20):205301, 2003.

[108] Gregory P Bewley, Daniel P Lathrop, and Katepalli R Sreenivasan. Superfluid helium - visualization of quantized vortices. *Nature*, 441(7093):588–588, Jan 2006.

[109] Gregory P Bewley, K. R Sreenivasan, and Daniel P Lathrop. Particles for tracing turbulent liquid helium. *Exp Fluids*, 44(6):887–896, Jan 2008.

[110] William H. Press, Brian P. Flannery, Saul A. Teukolsky, and William T. Vetterling. *Numerical Recipes in FORTRAN 77: The Art of Scientific Computing (v. 1)*. Cambridge University Press, 2 edition, September 1992.

[111] H. A. van der Vorst. Bi-cgstab: A fast and smoothly converging variant of bi-cg for the solution of nonsymmetric linear systems. *SIAM Journal on Scientific and Statistical Computing*, 13(2):631–644, 1992.

[112] C Huepe and ME Brachet. Scaling laws for vortical nucleation solutions in a model of superflow. *PHYSICA D-NONLINEAR PHENOMENA*, 140(1-2):126–140, JUN 1 2000.

[113] Tuckerman LS, Huepe C, and Brachet ME. Numerical methods for bifurcation problems. 9:75–83, 2004.

[114] CT Pham, C Nore, and ME Brachet. Boundary layers and emitted excitations in nonlinear Schrodinger superflow past a disk. *PHYSICA D-NONLINEAR PHENOMENA*, 210(3-4):203–226, OCT 15 2005.

RÉSUMÉ:

Cette thèse regroupe des études portant sur la dynamique de relaxation de différents systèmes conservatifs ayant tous une troncature de Galerkin sur les modes de Fourier. On montre que, de façon très générale, ces systèmes relaxent lentement vers l'équilibre thermodynamique avec une thermalisation partielle à petite échelle qui induit une dissipation effective à grande échelle, tout en conservant les invariants globaux.

La première partie de ce travail est consacrée à l'étude de la viscosité effective dans l'équation d'Euler incompressible tronquée. L'utilisation des méthodes de Monte-Carlo et de la théorie EDQNM permet la construction d'un modèle à deux fluides de ce système. Cette étude est ensuite généralisée au cas des écoulements hélicitaires. La dynamique de relaxation des écoulements décrits par les équations de la magnétohydrodynamique et des fluides compressibles tronqués est finalement caractérisée.

Dans une deuxième partie, nous généralisons l'étude de la thermalisation au cas de l'équation de Gross-Pitaevski tronquée. On trouve que des effets existant dans les superfluides à température finie, comme la friction mutuelle et le "counterflow", sont naturellement présents dans ce modèle. On propose ainsi l'équation de Gross-Pitaevskii tronquée comme un modèle simple et riche de la dynamique superfluide à température finie.

La radiation produite par le mouvement de vortex ponctuels décrits par l'équation de Gross-Pitevskii 2D est finalement caractérisée analytiquement et numériquement.

MOTS-CLÉS: Euler tronquée, magnétohydrodynamique, thermalisation, viscosité effective, Gross-Pitaevskii,troncature de Galerkin, friction mutuelle, turbulence.

ABSTRACT:

In this thesis several different Fourier Galerkin-truncated conservative systems are studied. It is shown that, in a very general way, these systems relax toward the thermodynamic equilibrium with a small-scale thermalization that induces an effective dissipation at large scales while conserving the global invariants.

The first part of this work is concerned with the study of the effective viscosity of the truncated Euler equation, making use of the EDQNM closure theory and Monte-Carlo methods. We propose a two-fluid model of the system and this work is extended to the case of helical flows. The relaxation dynamics described by the two-dimensional truncated magnetohydrodynamics equations and three-dimensional compressible fluids is then characterized.

In a second part, a generalization of the previous study to the truncated Gross-Pitaevski equation is given. Finite-temperature effects that are present in superfluids, such as mutual friction and counterflow, are found to be naturally included in the truncated Gross-Pitaevski equation. This system thus appears as simple and rich model of superfluidity at finite temperature.

Finally, the radiation produced by moving point Gross-Pitaevskii vortices is studied analytically and numerically.

KEYWORDS: Truncated Euler, magnetohydrodynamics, thermalization, effective viscosity, Gross-Pitaevskii, Galerkin truncation, mutual friction, turbulence.